

Molecular attachment to oxidised (100) CVD diamond surfaces

Michael William Anderson MChem, AMRSC

Thesis submitted for the Degree of Doctor of Philosophy

Heriot-Watt University,
School of Engineering and Physical Sciences

February 2010

The copyright in this thesis is owned by the author. Any quotation from the thesis or use of any of the information contained in it must acknowledge the thesis as the source of the quotation or information.

Abstract

The unique bulk and surface properties of diamond coupled with the development of CVD techniques to produce wide area, high quality thin film single crystal diamond films make it an attractive substrate to fulfil the demanding requirements of future device fabrication. Methods by which to modify the diamond surface with an organic functional group, either to impart some property of the organic species to the diamond surface, or to modify the properties of the diamond substrate, are required.

Commercial CVD single crystal (100) diamond substrates have been treated by hydrogen plasma to maximise the (100) terrace width and provide high quality surfaces. Thermal oxidation, under controlled conditions, introduced one complete monolayer of oxygen to the (100) diamond surface. The majority of the oxygen was present in a carbonyl-like configuration. Studies of the (100) diamond surface morphology after extended periods suggested oxidation took place by anisotropic etching of steps present on the (100) diamond surface and caused eventual roughening of the surface.

A small organic ketone, 2-adamantanone, was used as a molecular mimic of the oxidised (100) diamond surface due to its structural similarity to a small section of the surface. Kinetic studies elucidated the mechanism of reversible imine formation by nucleophilic attack of amines upon 2-adamantanone. Variation from the standard literature reaction mechanism was attributed to steric hindrance around the carbonyl group in 2-adamantanone, and best conditions under which to attempt extension of the reaction to the structurally hindered carbonyl-functional (100) diamond surface were established.

The fluorinated amine 4-trifluoromethylbenzylamine has been introduced to the oxidised (100) diamond surface. Covalent binding of 4-trifluoromethylbenzylamine to the (100) diamond surface via an imine bond was strongly supported by XPS evidence. Reductive amination of oxidised (100) diamond introduced 4-trifluoromethylbenzylamine to the diamond surface which could not be removed by washing in water, consistent with in-situ reduction of the imine bond to a water stable amine linkage.

Acknowledgements

Completion of this work could not have been achieved without the advice, assistance and support of many people, to all of whom I am very grateful. I would like to thank my supervisor, Professor Phillip John, for the initial concept behind the work, for his continued enthusiasm and for his invaluable advice. The assistance and camaraderie of current and former members of the 'Diamond Group' was very much appreciated, in particular I would like to thank Prof. John Wilson, Dr Neil Polwart, Dr Fraser Gray and Dr Jae-Kap Lee. During the course of this work I supervised a number of students and it would be remiss not to mention Dr Olivier Pauvert, Miss Joanne Curran and Miss Victoria Speedie. As part of an undergraduate project Mr Anthony Purdie and Miss Vikki Anderson carried out synthetic procedures reported here.

Without access to a range of techniques and instrumentation this study would not have been possible. I am very grateful of everyone who trained and assisted me in new techniques and aided in the analysis of results. I am indebted to Dr Graham Beamson and Dr Danny Law (NCESS, Daresbury), Mrs Marian Millar, Mr Gerry Smith and Dr Georgina Rosair (EPS, Heriot-Watt University) and Mr Alan Jackson (Thermo Fisher Scientific). I would like to thank Mr Iain Drummond (EPS, Heriot-Watt University) for always having an effective solution, and usually a simple and elegant one, and my thanks also go to Mr Ian Scullion and Dr Jack Davidson (EPS, Heriot-Watt University).

I would like to acknowledge Heriot-Watt University, School of Engineering and Physical Sciences for allocating me an EPSRC Doctoral Training Award.

On a personal note, I owe huge thanks to my family; to my parents, Marion and Russell, for their continued encouragement and unswerving support, and also to my sister Christine, an excellent experimental chemist, Craig and Natalie.

Contents

Abstract	ii
Acknowledgements.....	iii
Contents	iv
1 – Introduction	1
2 – Modification of (100) diamond surfaces.....	4
2.1 Introduction.....	4
2.1.1 The surface structure of diamond.....	5
2.1.2 Hydrogen etching of (100) diamond	8
2.1.3 Oxidative etching of (100) diamond	15
2.2 Experimental.....	23
2.2.1 Diamond substrates	23
2.2.2 X-ray diffraction (XRD).....	23
2.2.3 Hydrogen plasma treatment.....	27
2.2.4 Thermal Oxidation	30
2.2.5 Optical microscopy.....	32
2.2.6 Scanning electron microscopy (SEM).....	32
2.2.7 Atomic force microscopy (AFM).....	32
2.2.8 X-ray photoelectron spectroscopy (XPS).....	36
2.3 Results and Discussion.....	39
2.3.1 Determination of diamond plate crystallographic information.....	39
2.3.2 In-situ monitoring of species present in a hydrogen plasma.	43
2.3.3 Hydrogen plasma exposure of (100) single crystal diamond surfaces.....	44
2.3.4 Thermal oxidation of the (100) single crystal diamond surface.	49
2.3.5 Oxidative etching of the (100) single crystal diamond surface.	65
2.4 Conclusions.....	74
3 – Reactions of amines with the diamondoid molecule 2-adamantanone.	78
3.1 Introduction.....	78
3.1.1 Diamondoids	78
3.1.2 Modelling the reactions of oxidised diamond surfaces.	81
3.1.3 Reactions of ketones.....	82
3.1.4 Imine formation.....	84

3.1.5 Reduction of imines.....	92
3.1.6 Chemical kinetics and mechanism.....	93
3.2 Experimental.....	94
3.2.1 Synthesis of 2-adamantanone derivatives.....	95
3.2.2 Chemical kinetic studies by FTIR.....	96
3.2.3 Chemical kinetic simulations.....	99
3.3 Results and Discussion.....	100
3.3.1 Derivatives of 2-adamantanone.....	100
3.3.2 Kinetic study of imine formation reactions involving 2-adamantanone.	104
3.3.4 Determination of observed rate constant.....	108
3.3.5 Variation of rate with amine.....	112
3.3.6 Variation of rate with pH.....	114
3.3.7 Effect of solvent on rate.....	116
3.3.8 Computational modelling.....	117
3.3.3 Rate of imine formation.....	122
3.3.9 Discussion of imine formation from 2-adamantanone.....	123
3.3.10 Reductive amination.....	129
3.4 Conclusions.....	131
4 – Introduction of an amine to oxidised (100) CVD diamond surfaces.....	135
4.1 Introduction.....	135
4.1.1 Reactions with radical species.....	136
4.1.2 Cycloaddition reactions.....	138
4.1.3 Attachment of alkenes to hydrogenated diamond.....	140
4.1.4 Reaction with silane coupling agents.....	141
4.1.5 Reactions analogous to synthetic organic procedures.....	142
4.1.6 Imine formation.....	144
4.2 Experimental.....	147
4.2.1 X-ray Photoelectron Spectroscopy (XPS).....	148
4.2.2 Hydrogen termination.....	148
4.2.3 Thermal oxidation.....	149
4.2.4 Surface attachment and washing experiments.....	149
4.2.5 Room temperature immersion experiments.....	150
4.2.6 Elevated temperature immersion experiments.....	151
4.2.7 Reductive amination and washing experiment.....	152
4.2.8 Control experiments on oxidised (100) diamond surfaces.....	152

4.2.9 Control experiments on hydrogenated (100) diamond surfaces	153
4.3 Results and discussion.....	154
4.3.1 Introduction of a fluorinated amine to (100) CVD diamond surfaces	154
4.3.2 Quantifying the level of fluorinated amine on (100) diamond surfaces.....	157
4.3.3 Nature of the bonding between 4-trifluoromethylbenzylamine and (100) diamond.....	162
4.3.4 Kinetics of attachment at room temperature.....	170
4.3.5 Attachment at elevated temperature	175
4.3.6 Reductive amination.....	179
4.4 Conclusions.....	181
5 – Summary and conclusions.....	185
6 – Future work	190
References	192

1 – Introduction

The rapid rate of technological advancement since the Second World War has had a great effect on the way we live our lives. Advances in microelectronics have made integrated circuits and computing power ubiquitous and begun a great drive for miniaturisation¹. Continued scientific and technological development will be required throughout the 21st century to address problems such as global warming, dwindling fossil fuel supplies and a rising world population. These problems themselves argue for careful use of finite resources and so the trend for miniaturisation can be expected to continue, with thin film materials and their surface science playing an essential role.

Chemical vapour deposition of diamond has advanced such that nanocrystalline^{2, 3}, polycrystalline^{4, 5} and single crystal^{6, 7} films can be reliably grown. The quality of single crystal CVD diamond is such that deposited films may have lower defect densities than natural single crystal diamond⁸. In addition to its extreme bulk properties such as its hardness, thermal conductivity and refractive index, exploitation of diamond in thin film form is attractive due to its interesting surface properties.

Naturally an inert, insulating material, diamond is stable in most environments, including biological media⁹⁻¹¹, making it a suitable substrate material for the manufacture of a range of devices. The ability to control the electronic properties of diamond surfaces widens the potential for it to be used in electronic devices. Diamond can be made semiconducting by the inclusion of dopant atoms such as boron in the lattice structure and hydrogen terminated diamond displays a surface conductivity effect¹²⁻¹⁵ which is not observed on oxidised diamond surfaces. Despite the chemical stability generally displayed by diamond it is possible to chemically modify diamond surfaces by carefully selecting suitable conditions. Hydrogen terminated surfaces can undertake radical processes such as the photochemical attachment of alkenes described by Strother et al.¹⁶ but greater reactivity may be introduced to diamond surfaces by oxidising treatments which replace the surface hydrogen by oxygen.

Surface functionalisation or organic modification of substrate surfaces involves depositing a layer of organic molecules on the surface to impart some property of the organic species, such as an optical response or chemical sensing capability, to the substrate. The potential to couple organic molecules to diamond surfaces via stable covalent bonds to carbon makes diamond an attractive substrate for organic modification. In sensor and array applications (e.g. so-called bio-chips), stability issues with the organic molecule – substrate interface have been experienced with other substrate materials such as silicon, glass and gold¹⁷. Additionally, diamond could perform an active role in signal transduction rather than merely acting as a passive support for probe molecules. Heteroepitaxy of diamond films on silicon substrates could allow their incorporation into standard silicon chip electronics or the electrical properties of diamond could be exploited to allow signal transduction by free-standing diamond substrates themselves. Organically modified diamond films could allow fabrication of integrated chip-based sensors with molecular recognition carried out by the organic functionality and signal processing within the diamond substrate.

To achieve the potential benefits offered by diamond as a substrate material it is necessary to develop routine, reproducible methods by which organic molecules may be reliably and controllably tethered to the surface. Approaches to diamond surface functionalisation have been reported in the literature on diamond powders and nano, poly and single crystalline substrates. The diamond substrates functionalised are not always well characterised and a clear mechanistic understanding of the chemical reactions occurring on the diamond surface is lacking for most approaches. Without an understanding of the fundamental surface reactions occurring, optimisation and extension of attachment methodologies is hampered. Photochemical attachment of alkenes to functionalise hydrogen terminated diamond has been routinely reported in the literature^{16, 18-22}. To exploit the full potential of diamond films for device fabrication, complementary methods by which to functionalise oxidised diamond are required.

This thesis demonstrates a novel approach to the organic functionalisation of diamond. Covalent coupling of a fluorinated amine to a well characterised, oxidised, single crystal (100) diamond surface has been achieved and the nature of the chemical reactions occurring on the diamond surface probed. The results are consistent with the formation of an imine by reaction of the fluorinated amine with carbonyl-like groups on the (100) diamond surface.

Suitable reactivity must be introduced to diamond surfaces to allow organic modification. Chapter 2 describes hydrogen plasma treatment of single crystal (100) diamond substrates to reduce the roughness and improve the quality of the (100) surface. Subsequent thermal oxidation is revealed, by in-depth XPS characterisation, to have introduced a monolayer of oxygen to the diamond surface; the majority of which is doubly bonded to carbon in a carbonyl-like, 'on-top' configuration. Microscopic analysis of the (100) diamond surface following exposure to oxygen at elevated temperature allows the mechanism of oxidation to be investigated.

In chapter 3 the well known solution phase condensation reaction of a ketone and an amine to form an imine is investigated for the ketone 2-adamantanone; a molecular mimic of the oxidised (100) diamond surface. The effect on the reaction mechanism of steric hindrance around the carbonyl group is elucidated and suitable reaction conditions to achieve imine formation determined. Reduction of the hydrolysable imine product to a stable amine has been investigated.

In chapter 4 a fluorinated amine is reacted, under conditions utilised in chapter 3, with the oxidised (100) diamond surface, characterised in chapter 2 as mainly terminated with carbonyl-like oxygen functional groups. Experiments to characterise the nature of the bonding between the amine and (100) diamond surface are consistent with the formation of a hydrolysable imine bond. Similar experiments carried out after attempted reduction of the imine to an amine are consistent with the creation of a water-stable linkage.

2 – Modification of (100) diamond surfaces.

2.1 Introduction

Critical to understanding any reaction occurring on a solid substrate is a well defined and understood surface structure. The structure of the surface dictates the participating chemistry and the results of any surface process which subsequently occurs.

The surface structure of diamond crystals can vary depending on the orientation with which the surface truncates the diamond lattice, any surface reconstruction and chemical functionality. Despite this, the only chemical functionality present on any hydrogen terminated diamond surface is carbon – hydrogen bonds. Although these can be induced to take part in radical processes, which has been exploited in some diamond functionalisation approaches, they are generally rather unreactive and give rise to the recognised chemical stability of diamond in a wide range of environments. More reactivity may be imparted to diamond surfaces by oxidising treatments which replace the surface hydrogen by oxygen. The configurations adopted by oxygen depend on the structure of the diamond surface. Only on the low index (100) diamond surface may oxygen adopt a configuration in which it forms a double bond to a surface carbon atom, to give a carbonyl-like moiety, analogous to ketone molecules in organic chemistry. In organic chemistry, ketones may undergo reaction with nucleophiles to form a new covalent bond. Surface carbonyl groups may therefore provide suitable reactivity by which to introduce organic molecules to diamond surfaces.

An attempt to functionalise the diamond surface via a reaction analogous to nucleophilic attack on a ketone would appear to be best served by a diamond surface on which the number of carbonyl-like moieties were maximised. Intuitively, a $>C=O$ terminated atomically flat (100) surface would appear to fulfil this criterion. This chapter describes experiments in which hydrogen plasma treatment was utilised to effect smoothing of the (100) diamond surface and oxidation to terminate the surface with carbonyl-like

moieties was undertaken. The effect of oxidation on the morphology of the (100) diamond surface was also investigated.

2.1.1 The surface structure of diamond

The simplest diamond surfaces are obtained by cleaving the lattice along the low index Miller planes, (100), (110) or (111). Figure 1 indicates the geometric position of these planes relative to one another as viewed orthogonal to a (100) surface.

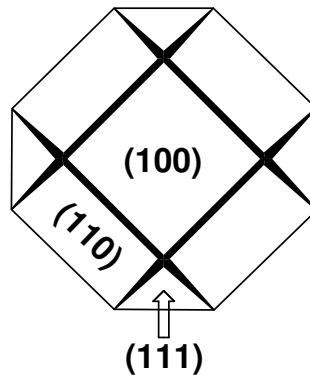


Figure 1 – The geometric relationship between the low index faces of diamond.

The low index planes dissect the diamond unit cell as shown below in Figure 2. If the diamond lattice is truncated along these planes then surface carbon atoms are left with unpaired electrons or ‘dangling bonds’ which are no longer fully bound to other carbon atoms within the bulk lattice. The surfaces obtained when the carbon atom valencies are satisfied by bonding to hydrogen are shown in Figure 3. Each carbon atom on the surface of (110) and (111) diamond faces has only one unpaired electron but carbon atoms on the surface of (100) diamond have two unpaired bonding sites per atom.

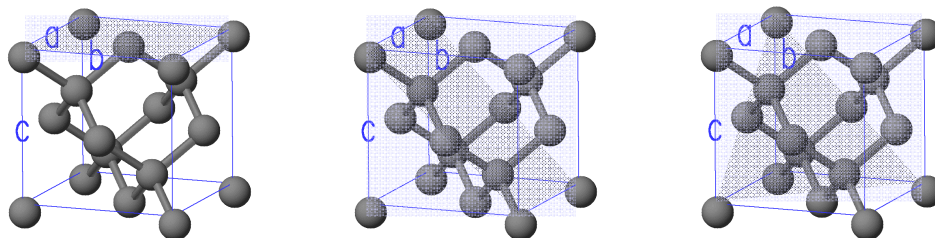


Figure 2 – The unit cell of diamond dissected by; from left to right, a (100), (110) and (111) plane. Reused with permission from reference 23.

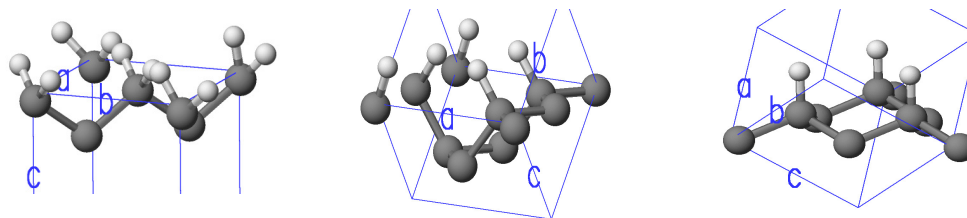


Figure 3 – The hydrogen terminated surfaces obtained upon truncating the diamond unit cell along, from left to right, a (100), (110 and (111) plane. Reused with permission from reference 23.

The dihydride terminated structure of (100) surfaces, shown in Figure 3, reconstructs by dimer formation to give a 2x1 monohydride terminated structure, shown schematically in Figure 4. Unreconstructed (100) diamond surfaces comprise zigzag chains of carbon atoms running parallel to the $\langle 110 \rangle$ direction, in which every second atom in the chain is a surface atom. The bulk crystal can be viewed as comprising similar zigzag chains, parallel to $\langle 110 \rangle$, which alternate by ninety degrees for each atomic layer. Terraces on the hydrogenated (100):H 2x1 reconstructed surface comprise rows of dimers running parallel to the $\langle 110 \rangle$ direction. Where single monolayer height steps occur, the dimer rows on the adjacent terrace occur at an angle of ninety degrees to those on the terrace above, due to the direction of the zigzag carbon atom chains.

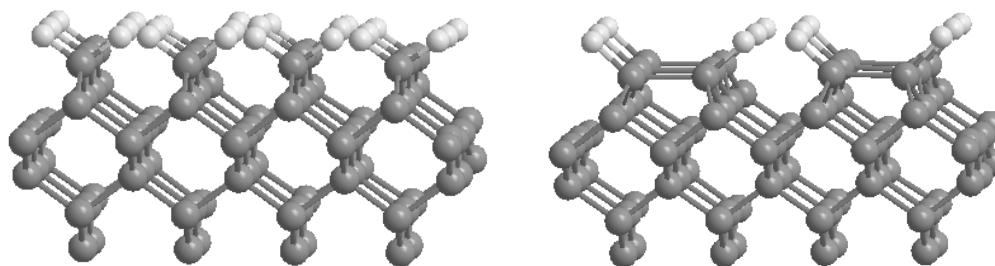


Figure 4 – Possible surface configurations of (100) diamond. Left - the unreconstructed 1x1 dihydride structure. Right – The reconstructed 2x1 monohydride structure.

Terraces of dimer rows on 2 x 1 reconstructed (100):H diamond are bounded by steps. Steps can vary from single steps with a height of 0.9 \AA , the distance between adjacent (100) atomic planes in diamond, through double-height steps to macro-scale bunched steps. Steps can run parallel to the dimer rows of the terrace they truncate as is the case for an S_A type step, shown in Figure 5. This geometry gives rise to straight steps,

running parallel to a dimer row. Steps running perpendicular to the dimer rows, such as the S_B type step shown in Figure 5, often give ‘ragged’ step edges with each dimer row being truncated at a different position. These features have been observed experimentally by STM²⁴ as shown in Figure 6.

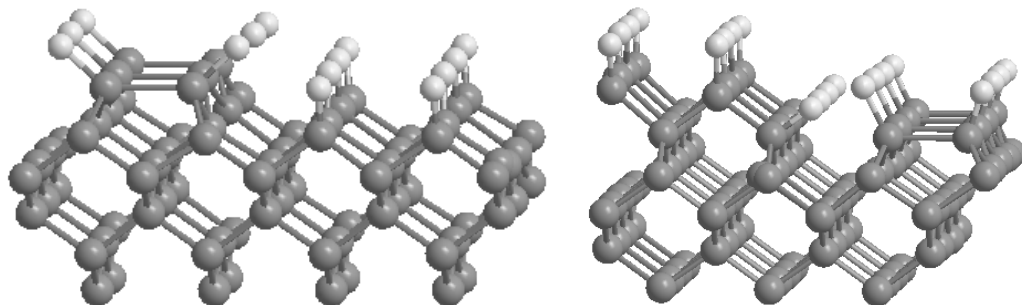


Figure 5 – Single-layer steps on the 2x1 reconstructed hydrogen terminated (100) diamond surface. On the left an S_A step runs parallel to the dimer row on the top atomic layer. Dimer rows on the lower terrace run perpendicular to this. On the right an S_B step runs perpendicular to the dimer rows on the top atomic layer. The visible dimer row on the lower terrace is oriented perpendicular to those on the layer above.

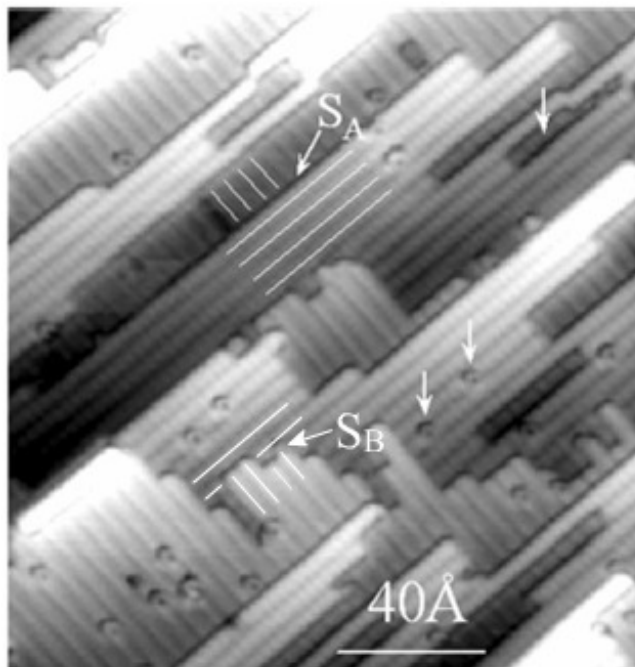


Figure 6 - Scanning tunneling microscope (STM) image of a (100) diamond 2x1:H reconstructed surface clearly showing a straight S_A step and ragged S_B step. The white lines highlight the dimer rows around each step. The dimer rows on adjacent atomic levels run at 90° to each other. Reproduced from reference 24.

Termination of perfect theoretical diamond surfaces by a monolayer of hydrogen results in the monohydride (111), (110) and dihydride (100) surfaces shown in Figure 3 above. On (111) and (110) surfaces, where each surface carbon atom has three bonds to the lattice structure, terminating with oxygen can only give rise to functionality where each surface carbon atom forms one bond to oxygen, i.e. the surface may be terminated with –OH or –OR groups or with oxygen atoms bound in a ‘bridging’ ether-like configuration where valency restrictions imply that only one bond can form with each of two adjacent surface carbon atoms. On the (100) diamond surface where each surface carbon atom is capable of forming two bonds to the lattice carbon atoms, the additional possibility exists that an oxygen atom may form a double bond to a single surface carbon atom to give an ‘on-top’ carbonyl-like configuration. The alternative bridging and on-top configurations of an oxygen terminated (100) diamond surface are shown in Figure 7.

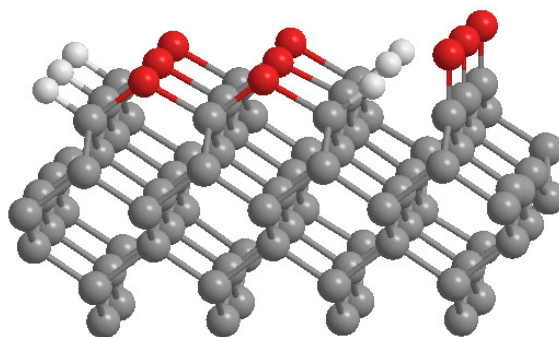


Figure 7 – Possible configurations of oxygen terminated (100) diamond. In the ether-like or bridging configuration one oxygen atom forms a single bond with two adjacent surface carbon atoms. In the carbonyl-like or ‘on-top’ configuration an oxygen atom forms a double bond with each surface carbon atom.

2.1.2 Hydrogen etching of (100) diamond

The surface of diamond appears to be inert to molecular hydrogen whereas exposure to atomic hydrogen causes etching of the diamond surface. Molecular hydrogen does not thermally decompose to atomic hydrogen significantly at temperatures less than around 2000 K, at which temperature diamond spontaneously graphitises²⁵. For this reason etching studies of diamond by hydrogen require activation of the hydrogen, usually by hot filament or plasma, to generate hydrogen atoms or ions²⁵. The effects caused by the

impingement of activated hydrogen on a diamond surface have been the subject of extensive research²⁶⁻³¹, not least because of the importance attributed to hydrogen in the growth of CVD diamond. During the deposition of diamond, hydrogen is believed to play a vital role such as etching non-diamond species, stabilizing the growth surface and assisting in the formation of faceted films³²⁻³⁸. A detailed understanding of the role of hydrogen requires studies on well defined low index planes of diamond. The genesis of the diamond i.e. natural, high pressure high temperature (HPHT) or CVD, the quality of the substrate, the crystal face exposed to the hydrogen flux, the misorientation angle of the crystal, the substrate temperature and the partial pressure of hydrogen and any other gases present could potentially affect the hydrogen etching process.

The present research, which forms the basis of this thesis, was carried out on nominally (100) diamond surfaces. The diamond (100) surface has been more widely studied than the other commonly observed growth surfaces as high quality single crystal films are easier to achieve on this surface²⁸. For these reasons the results discussed here are limited to (100) surfaces subject to activated hydrogen exposure.

The misorientation or miscut angle of a (100) diamond film is the angle between the actual surface plane and the {100} crystal planes. The morphology of the surface obtained after hydrogen etching depends on the miscut angle of the substrate. When etched in a hydrogen plasma at 1300°C, Lee and Badzian^{28, 29} found that (100) diamond films grown from type Ib HPHT substrates with a low misorientation angle resulted in a pitted, rough surface while substrates with a higher miscut angle yielded smoother surfaces with a lower density of etch pits. The etch pits developed were square sided with stepped side faces and edges running parallel to the $\langle 110 \rangle$ directions²⁹. A substrate with a misorientation angle of 3.5° demonstrated fewer etch pits than one with a 0.1° miscut but also had macro-steps running across the entire surface, parallel to $\langle 110 \rangle$ directions. The macro-steps were aligned in a direction consistent with the surface misorientation of the sample. A substrate with an 11° miscut demonstrated similar steps parallel to $\langle 110 \rangle$ directions and had the lowest density of etch pits. From these results it was rationalised that (100) diamond was etched by migration of steps along $\langle 110 \rangle$ ²⁹. The steps could originate either from the surface misorientation of the sample or from the creation of etch pits.

Etch pits on diamond surfaces usually develop from lattice defects such as point defects and dislocations. Indeed, hydrogen plasma etching has been utilised as a tool to reveal defects in diamond films and thus measure their areal density³⁰. Bonds to carbon atoms adjacent to defects may be more strained than bonds remote from defects. Strained atoms have a higher surface free energy than their unstrained counterparts and are therefore more susceptible to etching^{30, 31}. Etching of the strained atoms creates a step in the surface atomic layer and preferential etching of steps can extend the etched area. Since dislocations run through the bulk lattice, strained atoms below the surface layer are exposed and subsequently etched and the pit propagates deeper into the diamond. Lee and Badzian²⁹ measured etch pit densities of the order of $1 \times 10^7 \text{ cm}^{-2}$ ($0.1 \mu\text{m}^{-2}$). Regions of approximately $150 \mu\text{m}^2$ were analysed by scanning electron microscopy and the images obtained were dominated by etch pits. Examination of the areas between the etch pits gives an indication of the etching process undergone by high quality, defect free (100) diamond films. In these regions steps running across the surface, parallel to $\langle 110 \rangle$ directions, were observed.

Watanabe et al.^{32, 34} studied the mechanism of hydrogen plasma etching of (100) diamond by using atomic force microscopy to analyse the effect on the substrate surface morphology. The type Ib HPHT substrates studied by Watanabe et al.^{32, 34} were mechanically polished prior to use. The polishing had imparted a pattern of peaks and troughs separated by about 200 nm and a similar periodic pattern on a smaller scale of around 20nm. After hydrogen etching a 0.1° misoriented film for 1 hour at 800°C the AFM image obtained showed an atomically flat surface with terraces ~ 35 nm wide and double atomic height steps running parallel to $\langle 110 \rangle$. AFM analysis of a substrate miscut by 2.9° from (100) after hydrogen etching revealed that the smaller periodic pattern had been removed but the larger one remained and round etch pits had appeared. The circular etch pits had a diameter of 20 – 60 nm and depth of 0.5 – 1.5 nm: their genesis was not speculated upon. The results of this study were rationalised in terms of anisotropic etching of diamond by atomic hydrogen, where step edges are etched preferentially to terrace atoms. The explanation is represented in Figure 8. On substrates with low misorientation angles the migration of steps due to etching can remove protuberances standing proud of the surface, causing a smoothing effect and creating wide flat terraces on the surface. Hydrogen etching of substrates with a high misorientation angle causes migration of steps in a direction towards the bulk crystal.

This effect does not remove surface features in the same way so does not provide a smoothing effect or maximise the terrace widths.

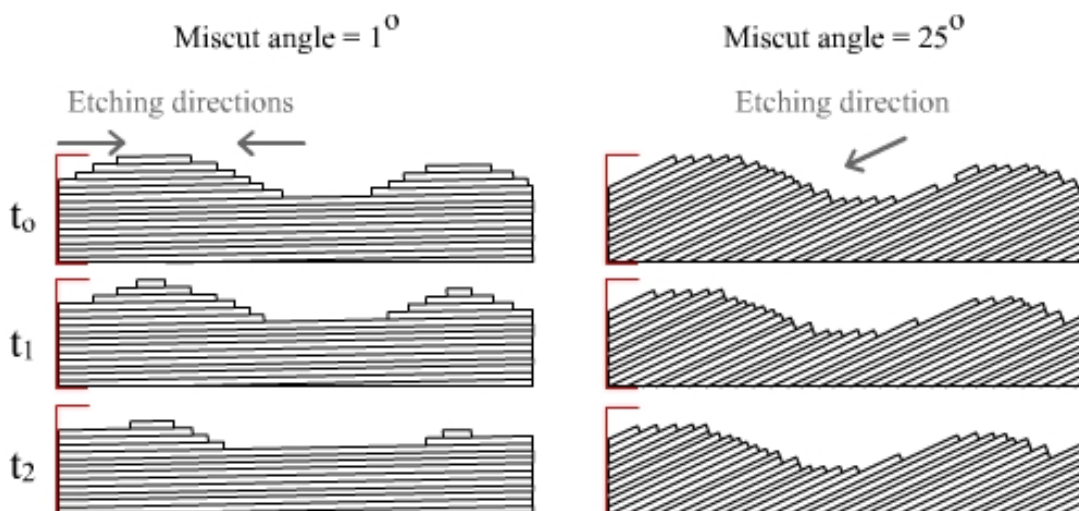


Figure 8 – Representation of the effect of miscut angle on the resultant diamond surface after hydrogen etching. Parallel black lines represent (100) crystal planes. On the left, with a low miscut angle, surface features are etched back until they are removed creating wide terraces. On the right a high miscut angle means whole atomic layers are not removed in the same way and a surface smoothing does not result.

The steps observed by Watanabe et al.^{32, 34} on substrates with a low misorientation from (100) were double the atomic step height in diamond and their observation would require the resolution provided by atomic force microscopy. As steps migrate during growth or etching it is possible for variation to occur in step velocities causing some steps to ‘catch-up’ with those in front. This causes step-bunching and increases the step height between terraces. As an increasing number of steps bunch together the step height can become macro-scale and may be observable by lower resolution techniques such as SEM or optical microscopy. The ridges observed by Lee and Badzian^{28, 29}, running parallel to $\langle 110 \rangle$ across the substrate, are likely to be steps sufficiently macro-bunched to be visible by SEM and their appearance is in good agreement with the explanation of Watanabe et al.^{32, 34}. On low miscut surfaces a low step density means steps are separated by wide terraces. If a step became pinned the steps behind would have to be etched for a long time before reaching the pinned step and forming a macrostep. On high miscut angle surfaces the step density is high and terraces separating steps are narrow. In this case if one step becomes pinned those behind it will rapidly catch up building a macrostep. On high miscut surfaces, where Watanabe et al.^{32, 34} observed, by AFM, a rough, stepped surface, Lee and Badzian^{28, 29} observed

macrosteps by SEM after 1 hour of hydrogen etching. On low miscut samples Watanabe et al.^{32, 34} observed atomically smooth surfaces with wide terraces and a low step density whilst Lee and Badzian^{28, 29} did not observe macrosteps by SEM after 1 hour of etching.

Step bunching of diamond was investigated by de Theije et al.³⁹ by incorporating ammonia into the gas mixture used to grow homoepitaxial diamond. Step-bunching was not observed without ammonia in the growth mixture. Films grown in the presence of nitrogen demonstrated step bunching visible by optical microscopy. The requirement of the nitrogen impurity provided strong evidence to support Frank's theory⁴⁰ of impurity-induced step bunching. Frank's arguments can be applied equally well to crystal growth or etching and states that the progress of a step across a terrace is inhibited by a flux of impurities upon that terrace. When a step does manage to pass an impurity a clean surface is created, deactivating the impurity. Assuming a constant impurity flux, an impurity concentration gradient develops across a growing terrace, with the minimum concentration just behind a moving step. This implies that steps or bunches on high step density surfaces, such as those with a high miscut angle, should have a low impurity concentration ahead and advance rapidly. Steps on surfaces with wide terraces and low step density, such as those found on low miscut angle surfaces, will have a higher impurity concentration ahead and advance less quickly. In CVD diamond growth in the presence of nitrogen the observed pinning effect by nitrogen is explained by de Theije et al.³⁹ in terms of the different reactivity of carbon and nitrogen atoms on a growing surface. Carbon atoms present on the surface of a growing terrace will generally be terminated by hydrogen, which can be extracted to leave a reactive site on which attachment of a growth species could occur. Nitrogen atoms bound into a terrace and sp^3 hybridised have a lone electron pair in place of an abstractable hydrogen atom. This stable structure makes it much more difficult for carbon growth species to bind to the nitrogen atom and allow an impinging step to progress past that atomic site. While this step is pinned by the nitrogen impurity, other steps behind it may catch up creating a step-bunch or macro-step. When the step does manage to migrate past that point the nitrogen impurity is overgrown and hence does not have the same inhibiting effect on subsequent steps which pass that point. In its simplest embodiment Frank's model of step bunching treats steps as 1-dimensional. Experimentally de Theije et al.³⁹ observed that advancing step edges did not necessarily remain straight. Experimentally this suggests that only a local segment of step may be pinned by an impurity while

remote regions of the step may be able to continue to propagate. A mathematical 2-dimensional model based on Frank's mechanism developed by Kandel and Weeks^{41, 42} was used by de Theije et al.³⁹ and good agreement was found between the shape of the step edges observed experimentally and those predicted by the model.³⁹

At this point an aside on the effect of nitrogen on the growth rate of (100) diamond surfaces is timely. The above explanation for the appearance of bunched steps on the surface of (100) diamond films grown with nitrogen present in the growth mixture demonstrates that surface nitrogen inhibits the growth of diamond surfaces by a step-flow mode. This appears to contradict the well-known observation^{39, 43-48} that addition of nitrogen to the growth mixture enhances the rate of growth of (100) oriented diamond films. The reason for these two apparently contradictory observations is the difference in effect between surface and sub-surface nitrogen. Whilst a surface substitutional nitrogen atom is less likely to react with growth species than the equivalent carbon site (due to its lone electron pair in place of an abstractable hydrogen atom), once the atom has been overgrown Frauenheim et al.⁴⁷ suggest that electron density from the lone pair can be donated into a σ^* antibonding orbital of a reconstructed dimer bond on the (2x1) surface above. This causes the bond to weaken and lengthen and activates it towards addition of growth species. Upon binding of a growth species it is proposed that the charge from the nitrogen lone pair can migrate to an adjacent dimer bond and catalyse further growth, causing the increase in growth rate observed in the presence of nitrogen. Hence the observations of step-bunched (100) surfaces and enhanced (100) film growth rates are due to different effects of incorporated nitrogen and are not mutually exclusive.

The temperature dependence of the surface morphology resulting from hydrogen etching of single crystal diamond was studied by Stallcup and Perez³⁷ on films with surfaces misoriented by less than 1° from (100). Diamond films were grown on single crystal substrates by hot-filament CVD at a substrate temperature of 900°C , and doped with boron to provide sufficient conductivity for scanning tunneling microscope (STM) analysis. Films were exposed to activated hydrogen in the same reactor at substrate temperatures of 200, 500 and 900°C for 5 minutes and, to avoid contamination, transferred under vacuum to the ultra-high vacuum (UHV) STM analysis chamber. Samples exposed to hydrogen at 200°C gave atomically rough surfaces with a maximum (2x1) terrace area of around 6 nm^2 . No clear step direction was observed. It was noted that the surface observed was in keeping with an isotropically etched surface,

where all surface atoms have an equal probability of removal. Surfaces etched at 500°C gave wider areas of (2x1) reconstructed terraces (around 100 nm²) on which rough S_A and S_B steps could both be observed indicating etching took place both parallel and perpendicular to dimer rows. Single layer vacancy islands were also present, where several consecutive dimers in the midst of terraces had been removed. These vacancy islands were on average over twice as long in the direction of the dimer row as perpendicular to it. This indicates that whilst surface atoms in the midst of terraces can be removed by etching at 500°C, once the vacancy has been created preferential etching of S_B steps occurs. These surfaces also demonstrated square etch pits with (111) faces. The density of these pits was of the order of 1 x 10¹¹ cm⁻² and they were initially attributed to dislocation defects. However a later publication³¹ emphasised their density was several orders of magnitude higher than would be expected and attributed the formation of pits to etching perpendicular to the surface as well as a parallel direction. It was believed this was due to sterically strained (2x1) dihydride reconstructed regions, whose strain made them susceptible to etching. The presence of such regions was believed to be a function of the etch temperature of 500°C as lower temperatures would not surmount the activation barrier for dihydride formation and at higher temperature dihydrides would be unstable relative to monohydride moieties. Etching at 1000°C gave wide smooth (2x1) terraces of around 350 nm². Smooth S_A steps and rough S_B steps were observed. Some S_B steps had been etched back completely to give double height S_A steps. These results indicate that, at 1000°C, hydrogen etching of (100) diamond is highly anisotropic with etching along dimer rows at S_B steps occurring at a much faster rate than etching perpendicular to dimer rows at S_A steps.

The results of Stallcup et al.³⁷ indicate that the anisotropy of hydrogen etching of (100) diamond surfaces increases with temperature through 200°C, 500°C and 1000°C. At 500°C and 1000°C preferential etching of atoms at step edges appears to occur over etching of atoms incorporated in terraces. At 1000°C a preference for etching of S_B over S_A steps is also evident. The etching studies carried out by Lee and Badzian^{28, 29} were performed at 1300°C and the step-bunching observed is consistent with an anisotropic etching mechanism. Watanabe et al.^{32, 34} etched their substrates at a lower temperature of 800°C but the wide smooth terraces reported are also explained by preferentially etching of step edges. Indeed, the double atomic step heights reported could be due to preferential etching of S_B steps over S_A steps, as observed by Stallcup et al.³⁷ at 1000°C, such that every second terrace has been entirely removed.

2.1.3 Oxidative etching of (100) diamond

Compared to hydrogen, the diamond surface is relatively susceptible to reaction and etching with oxygen. Oxidation of the surface has been the cause attributed to an increase in hydrophilicity of diamond surfaces after heating to temperatures of 200°C and above in dry molecular oxygen⁴⁹. Etching by molecular oxygen can be effected at lower temperatures and etches faster than with hydrogen. However similar to hydrogen, the effects of oxygen exposure on diamond surfaces can depend on a variety of factors such as the substrate origin, exposed crystallographic facets, temperature and duration of exposure and the nature of the oxidising medium.

For practical and research applications a number of different diamond oxidation methods have been developed and utilised. Wet chemical oxidising agents, such as molten KNO₃ or a mixture of boiling H₂SO₄ and CrO₃ (so called chromic acid) can be used to chemically oxidise diamond. However with any such wet etchant systems the surface processes and the resultant effect on the substrate may be complex. For example, when metal containing compounds are employed there is considerable potential for contamination of the diamond which may require removal by other means, which may have their own effect on the substrate.

Electrochemical oxidation can be used to introduce oxygen functionality to diamond by applying a potential to conducting diamond electrodes in an oxidising medium such as dilute acid. A range of oxygen functionalities, including hydroxyl, ether, carbonyl and carboxyl^{50, 51}, have been introduced by this approach. However the requirement for boron doping to allow electrical conduction precludes this approach from being attempted with the undoped, non-conducting single crystal samples used in this study. A relatively new twist is to electrochemically oxidise hydrogenated diamond in air using an atomic force microscope tip. In this procedure, a positive voltage applied to the sample surface allows anodic oxidation of the diamond via adsorbed water which acts as an electrolyte between the diamond substrate and the AFM tip⁵². The oxidation imparted by this technique is localised to the area under the AFM tip which offers the ability to pattern the diamond surface with oxidised features of very narrow linewidth, down to around 60 nm in width⁵². The potential for patterning diamond surfaces

without recourse to standard lithographic techniques could be hugely advantageous for device and sensor applications. However, whilst the presence of oxygen has been evidenced by Auger electron spectroscopy⁵² and inferred from changes in conductivity⁵³, wettability⁵⁴ and Kelvin probe response⁵⁵, better understanding of the nature of the oxygen moieties present on different diamond faces would be required in order to allow further functionalisation with external agents.

Oxygen treatments in plasma reactors have been widely used to modify diamond substrates. Plasma processes can modify the surface properties of diamond substrates by the incorporation of oxygen^{56, 57} but in plasma systems oxygen can also be used to etch significant quantities of carbon in order to pattern the substrate⁵⁸⁻⁶⁰. For this reason, plasma processing is often utilised in research into the use of diamond for engineering applications. Whilst plasma processing is a very effective method for oxygen etching of diamond it is not ideally suited to developing a fundamental understanding of the oxidation processes occurring on the diamond surface. One problem is the sheer variety of designs of plasma systems; microwave^{56, 57}, radio-frequency⁶⁰, inductively coupled⁵⁹ and electron cyclotron⁵⁸ plasmas have all been utilised in oxygen treatments of diamond substrates. Operational parameters can vary significantly between systems. For example, a bias of varying magnitude may be applied to the substrate and a range of gas mixtures may be used. Pure oxygen, oxygen/hydrogen mixtures and oxygen/argon mixtures have all been employed. In addition, where the aim is to etch a pattern into diamond substrates, metal patterns may be deposited on the surface to act as lithographic masks. These can be sputtered across the diamond surface by the plasma^{58, 60}, as can metal filaments in hot filament systems⁶¹, and introduce further complications in understanding the surface processes taking place. The etching process under plasma conditions is a combination of physical sputtering⁶¹ and chemical etching⁶². Physical sputtering can potentially be caused by bombardment of the surface with any species present in the plasma with sufficient kinetic energy. Chemical etching may be attributed to oxygen, which in the plasma will be present in a variety of ground and electronically excited atomic and molecular forms making the chemical mechanism of etching difficult to elucidate. In systems where hydrogen is present this may contribute to the etching and further complicate the situation.

Studies of diamond oxidation more suited to elucidating the oxidation mechanism have been carried out by dosing the diamond surface with activated oxygen⁶³⁻⁶⁶. By passing molecular oxygen over iridium filaments heated to 1100 – 1300°C the oxygen can be activated without significantly heating the diamond substrate. The nature of the oxygen species generated has not been conclusively demonstrated but has been described as electronically excited molecular oxygen⁶⁵ and translationally, rotationally and vibrationally excited molecular oxygen with, possibly, traces of atomic oxygen⁶³. Distinct experiments utilizing atomic oxygen only have also been carried out by Foord et al⁶⁵. Some studies have been carried on well defined single crystal (100) surfaces^{63, 64}, others on randomly oriented polycrystalline diamond⁶⁵, whilst others do not report the exposed crystal faces⁶⁶. The nature of the active oxygen species and the diamond planes leave ambiguities. However, reports of such work concern themselves far more with the surface chemistry, discussing the surface moieties formed and species desorbed, than literature on plasma processing of diamond and as such provide a better route to a mechanistic understanding of diamond oxidation.

It has been shown⁶⁵ that the rate of reactivity of the diamond surface with oxygen increases from heated molecular oxygen through electronically excited molecular oxygen to atomic oxygen and depends on whether the surface is bare or hydrogen terminated. Thermal desorption spectra were recorded in order to examine the stability of the oxidised surfaces⁶⁵ and demonstrated that the atomic oxygen formed surface was least thermally stable and the surface formed by reaction with thermal oxygen most stable. Desorption of CO and CO₂ were both observed, the relative ratio depending on the method of preparation of the oxidised surface⁶⁵. Following oxidation by exposure to activated oxygen, undefined diamond facets which were bare or not fully hydrogenated prior to exposure gave rise to carbonyl, hydroxyl and ether-like surface groups as identified by high resolution electron energy loss (HREEL) spectroscopy⁶⁶. Undefined surfaces which had been fully hydrogenated by external MPCVD prior to oxidation by activated oxygen showed similar HREEL results. However, the authors correlated these with electron stimulated desorption (ESD) results and concluded that the lack of O⁻ electron stimulated desorption, at incident energies of less than 10 eV, indicated ether-like groupings were not formed on these surfaces by this oxidation method⁶⁶. On well defined (100) natural diamond plates, oxidation by exposure of the unheated substrate to activated oxygen resulted in an initially rapid uptake of oxygen, slowing as the oxygen coverage tended towards a full monolayer⁶³. Carbonyl, hydroxyl and bridging ether

groups on the diamond surface were identified by HREEL spectroscopy with the hydroxyl concentration decreasing as the oxygen coverage increased and bridging ether groups dominating over carbonyl at saturation coverage⁶³. On exposure of the (100) diamond substrate to activated oxygen while heating to nearly 700°C, the initial observations and surface groupings were similar to those on unheated substrates. However the increased substrate temperature promoted desorption of oxygen species simultaneously with adsorption resulting in lower peak oxygen coverages⁶⁴. The desorption of CO and CO₂ caused roughening of the (100) diamond surface and, at higher oxygen coverages, higher carbonyl to ether ratios were observed on the heated substrates than the unheated ones⁶⁴.

Thermal oxidation studies on well defined diamond surfaces have revealed morphological changes which take place with increasing temperature and provided an insight into the surface processes. A significant contribution was made by de Theije et al.⁶⁷⁻⁶⁹ who studied the effect of oxidation on single crystal {100} and {111} surfaces in 1 atmosphere of 10% oxygen in argon with and without water vapour at substrate temperatures of 700°C – 900°C. Oxidation of (100) diamond was found to take place by step etching due to stabilisation of terrace atoms by oxygen chemisorption⁶⁷.

A range of (100) single crystal substrates; type Ia natural, type IIa natural and type Ib synthetic (whether CVD or HPHT is not clear), polished to within 1° of the exact (100) orientation (polishing method not described), were exposed to dry oxygen at 700°C and above^{67, 69}. Step etching gave rise to square well-defined etch pits. Two types of etch pit were identified. Relatively large pits with sides steeply inclined by 6 - 15° were found to correlate to the density and distribution of dislocations. The creation of high energy surface sites at dislocations was therefore assumed to account for their presence. The orientation of the edges of steeper pits was observed to vary with temperature. Above 750°C the steep pits had edges aligned along <110> but below around 750°C a switch to <100> edges was observed for some pits. The change in orientation was attributed⁶⁷ to stabilisation of (100) structures by oxygen, below 750°C, which allowed (100) 'walls' to build up and induce rotation of the etch pit sides. Smaller, shallower pits inclined by 2 – 5° were observed in areas between the larger pits. Their density did not correlate with the dislocation densities of samples so their presence was attributed to agglomerated impurities or submicron inclusions in the diamond samples⁶⁷. The edges

of the shallow pits were aligned along $\langle 110 \rangle$ consistently throughout the oxidation temperature range studied.

Oxidation experiments carried out in oxygen containing water vapour revealed that the presence of water vapour retarded the rate of oxidative etching and prevented formation of pits with edges aligned along $\langle 100 \rangle$ at lower etching temperature⁶⁷. Pit edges were aligned along $\langle 110 \rangle$ at all oxidation temperatures when water vapour was present.

Pehrson et al.⁷⁰ exposed hydrogenated natural single crystal (100) diamond to very low pressures of oxygen ($2 \times 10^{-6} - 5 \times 10^{-5}$ Torr) at temperatures from room temperature to 1000°C. In this very low oxygen regime, their findings suggested that oxidation of diamond terrace atoms only took place at or close to the temperature of hydrogen desorption ($> 950^\circ\text{C}$) and that below this temperature the mechanism was consistent with oxygen dissociation only at step edges. This effect occurred even on plasma polished non-miscut substrates which scanning tunnelling microscopy (STM) and low energy electron diffraction (LEED) had demonstrated consisted of atomically smooth terraces and single layer steps. The surface morphology of substrates, particularly the surface roughness, therefore dictates the susceptibility to oxidation and etching. Rougher substrates with more steps and carbon atoms bound in atypical configurations provide more sites for oxygen dissociation and facilitate oxidation. This is consistent with prior observations that areas of inferior crystalline quality were more susceptible to oxidation than higher quality regions⁷¹.

Using the same oxidation apparatus as used in this study Polwart et al.^{23, 72} noted that oxidative etching of polycrystalline diamond crystallites, described as atomically smooth, occurred without any roughening of the surface as measured by AFM ($R_a \sim 6$ nm). The oxidative etching was proposed to have occurred by a layer-by-layer mechanism⁷². This observation is not inconsistent with the step etching mechanism described above. If atomic steps exist on crystallite surfaces, oxidation at the step sites may cause layer removal without promoting etching into the bulk of the crystallite at any particular point, leaving the surface roughness unaffected. Even on a perfect atomically flat (100) diamond surface without even single layer height steps present, serendipitous removal of one carbon atom as CO or CO₂ from a sufficiently heated diamond substrate would create step sites at the adjacent carbon atoms and step etching would allow single layer removal.

Knowledge of the oxygen species formed on (100) diamond surfaces, and how these change with temperature, is critical to an understanding of the surface processes which take place on oxidised diamond. The oxygen moieties introduced by oxidation stabilise terrace atoms and therefore induce the step-wise mechanism of oxidative etching which leads to morphological changes and etch pit formation. Oxygen species formed at atypical atom sites such as step edges must be capable of desorbing as carbon monoxide or carbon dioxide as the surface oxidises. Furthermore, any attempts to further functionalise the (100) diamond surface via chemisorption may occur via reaction with the oxygen moieties formed during oxidation. Early FTIR studies⁷³ performed to elucidate the oxygen termination of diamond powders revealed ether and carboxyl-like bands which could be assigned to cyclic ether or ester groups and cyclic ketone, lactone or carboxylic acid respectively. An increase in intensity of the carbonyl stretching band with temperature indicated changes in termination, favouring carbonyl containing groups at high temperatures⁷³. The plethora of crystal faces presented to the oxidising environment by diamond powders will provide suitable sites for a multitude of oxygen functionalities to coexist. On well-defined single crystal substrates a uniform surface limits the type of oxygen functional groups which may be formed. On a (100) diamond terrace, surface atoms have two unsatisfied bonds which may participate in bonding to oxygen which precludes formation of carboxylic acid, ester or lactone higher oxidation states. Terrace carbon atoms on (100) diamond surfaces may participate in two bridging (ether-like) single bonds or in an on-top (carbonyl-like) double bond. On initially hydrogen terminated surfaces, oxygen groupings may be present together with hydrogen atoms on surface atoms and in the presence of water vapour, hydroxyl termination could also occur.

The conditions under which bridging ether or on-top carbonyl is the favoured oxygen configuration on (100) diamond has posed an interesting question in the literature. STM studies of hydrogenated boron-doped (100) CVD diamond⁷⁴ oxidised at less than 400°C indicated the oxidation mechanism involved formation of bridging ether structures at every second monohydride dimer row, to form a 4 x 1 superstructure. Continued oxidation caused insertion to occur into the remaining dimers to give a fully oxidised surface with a bridging structure. This agreed well with LEED analysis of boron-doped single crystal diamond oxidised at similar temperatures⁷⁵. Unfortunately the study could not be extended to view the effect of increased temperature on the oxygen

configuration as oxidation at increased temperature produced diamond too insulating to allow STM analysis. Following oxidation at higher temperatures ($> 500^{\circ}\text{C}$) the presence of carbonyl-like oxygen on (100) polycrystalline diamond crystallites was suggested by John et al.⁷⁶ based on the FTIR identification of the carbonyl stretching frequency $\nu_s(\text{C}=\text{O})$ at 1731 cm^{-1} . Quantum mechanical calculations⁷⁷ found that the ether structure was slightly more stable than the carbonyl one albeit with a very small energy barrier between interconversion. Molecular dynamics calculations⁷⁸ also found there was little energy difference between the two sites and indicated that the two forms should co-exist at around 300°C but suggested that above this temperature the carbonyl groups are thermodynamically favoured⁷⁷.

An oxidation mechanism which accounts for the formation of both bridging and on-top oxygen structures was proposed by Ando et al.⁷⁹ from the results of quantum mechanical calculations. On a diamond (100):H 2×1 surface, ether groups are formed by insertion of oxygen into the monohydride dimer bond to give a H-C-O-C-H structure. As this occurs at adjacent sites on parallel dimer rows, the steric repulsion between hydrogen atoms increases and facilitates desorption of hydrogen with re-formation of the dimer bond to give an epoxy structure. Facile absorption of oxygen at the epoxy group results in on-top carbonyl termination. This route to carbonyl termination was found to be energetically more favourable than oxygen abstraction of two H atoms giving water and bare dimer structures with subsequent attachment of molecular oxygen.

To account for oxidation of (100) diamond in an oxygen atmosphere a mechanism is required which accounts for desorption of CO or CO_2 and re-formation of the oxidised surface without requiring to pass through the (2×1) monohydride surface. Such a mechanism could be concluded from the results of the molecular dynamics calculations carried out by Skokov et al.⁷⁸ and is shown in Figure 9. From a C(100):O (1×1) diamond surface terminated entirely with on-top carbonyl structures, thermal desorption of a carbonyl group as CO leaves two adjacent radical sites on the surface (step i). Once around half of the surface oxygen has been lost by this process there is sufficient flexibility for the radical sites to form bare surface dimers and there can be a reconstruction from (1×1) to a (2×1) surface (step ii). Molecular oxygen approaches the reformed (100) (2×1) dimers and can add across the double bond by dissociation to

form a C(100):O (1 x 1) carbonyl terminated surface (steps iii to vi). Dissociation of CO and absorption of molecular oxygen allows the process to continue layer by layer.

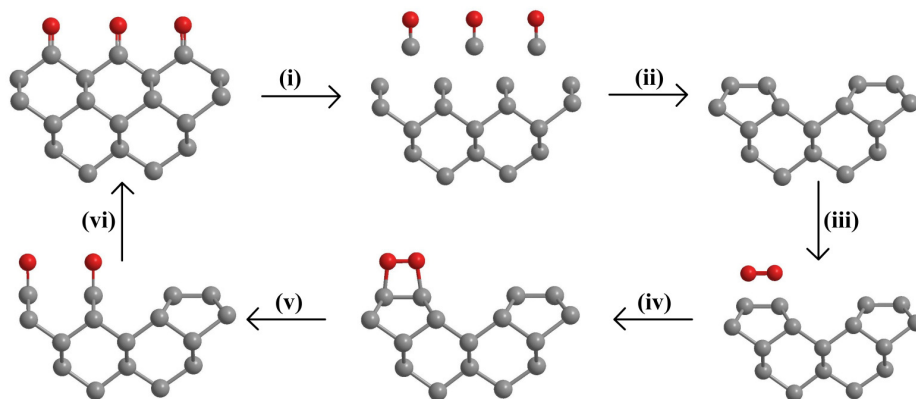


Figure 9 – Representation of the mechanism of (100) diamond oxidation proposed by Skokov et al.⁷⁸

It is not difficult to imagine an extension of the Skokov et al. mechanism⁷⁸ to a ‘real’ (100) diamond surface incorporating steps and defect sites. Such carbon atoms in such atypical configurations have increased surface energy over carbon atoms bound in ideal terrace configurations. Preferential dissociation of CO from atypical sites and subsequent facile loss of adjacent carbonyl groups, as proposed by John et al.⁷², would lead to etching of individual diamond layers and result in the step etching mechanism of (100) diamond observed experimentally.

2.2 Experimental

2.2.1 *Diamond substrates*

The CVD single crystal diamond samples used in the work reported in this thesis were purchased from Apollo Diamond Inc. and homoepitaxially grown by microwave plasma enhanced chemical vapour deposition (MPECVD) on single crystal diamond substrates. The nitrogen impurity level, determined by infra-red spectroscopy, was consistent with Type IIa quality diamond. The sample specification requested undoped 4 x 4 x 0.5 mm free-standing (100) plates with misorientation of 0° or 1°. The samples supplied were undoped 4 x 4 x ~0.2 mm free standing plates. No documentation was supplied to indicate the Miller indices of the crystal faces or the misorientation angle of the surface.

2.2.2 *X-ray diffraction (XRD)*

Determination of crystal edge direction

To identify the crystallographic directions along which the edges of the (100) single crystal diamond plates had been cut, an X-ray diffraction experiment was carried out using Mo K_α radiation at room temperature. The full 4 mm square diamond plate was too large to be mounted in the X-ray diffractometer, it was therefore cleaved into several pieces and a suitably sized section was used. This section was mounted on the end of a glass capillary on a fine wire ‘cryoloop’ in a Bruker Nonius Kappa Apex II X8 CCD diffractometer. The mounted sample was then aligned on a goniometer head such that it was in the geometric centre of the diffractometer and a series of omega scans carried out to collect intensity data for a unit cell determination. Whilst these scans were being carried out a video of the rotating sample was recorded. Once the unit cell had been identified, the diffractometer software (Apex2 version 2.1, Bruker AXS, Madison Wisconsin 2006) allowed face indexing of the crystal by relating crystal faces visible in video frames to crystal planes derived from the unit cell information. One of

the indexed faces had formed part of one side of the original plate and thus allowed crystallographic directions to be assigned to all faces of the original plate.

Determination of misorientation angle

The customer specified requirements for the single crystal diamond plates purchased from Apollo Diamond Inc. were that their top surfaces have a misorientation angle of either 0° or 1° from (100). The measurement of crystal miscut angles is usually carried out by accurate determination of rocking curves by high resolution X-ray diffraction⁸⁰ or by changes in rocking curve width⁸¹ or position⁸² if the X-ray diffractometry is carried out at glancing incidence. Lacking access to the facilities to carry out such experiments an XRD experiment was envisaged by the author that could allow an indication of the miscut angle of the received samples to be determined.

Analysis of the Cambridge Structural Database⁸³ revealed that the (400) reflection of diamond is observed at a 2θ value of 119.64° ⁸⁴ and the (400) reflection of silicon at 69.20° ⁸⁵. Using this information an experiment was conceived to attempt measurement of the misorientation angle of the (100) diamond plates using the facilities available and is shown diagrammatically in Figure 10. The rationale for the experiment is as follows. If a (100) oriented polished silicon sample with no miscut and a (100) diamond plate, also with no miscut, were placed in intimate contact, face to face, then the (100) planes of both materials would be parallel to each other. In an XRD experiment where the two materials were mounted together in this configuration, diffraction from the Si (400) planes would be observed with the detector at a 2θ angle of 69.20° and when the angle between the incident X-ray beam and the (100) planes, θ , is 34.60° . To detect diffraction from the diamond (400) planes; the detector should be shifted to a 2θ angle of 119.64° and the sample is required to be rotated such that the angle between the incident beam and the (100) planes, θ , is 59.82° . Having detected the Si (400) peak, it is known that the angle between the (100) planes (of both silicon and diamond) and the incident beam is already 34.60° , therefore to move the diamond (400) planes into the diffraction condition only requires a further rotation of the sample through $(59.82 - 34.60) = 25.22^\circ$. The angle through which the sample is rotated in the plane containing the X-ray source and detector is defined as Ω . If neither of the silicon or diamond faces in intimate contact with each other are misorientated from (100) then following

detection of the diffraction peak from Si (400) a rotation in Ω of 25.22° should allow detection of the diamond (400) diffraction peak.

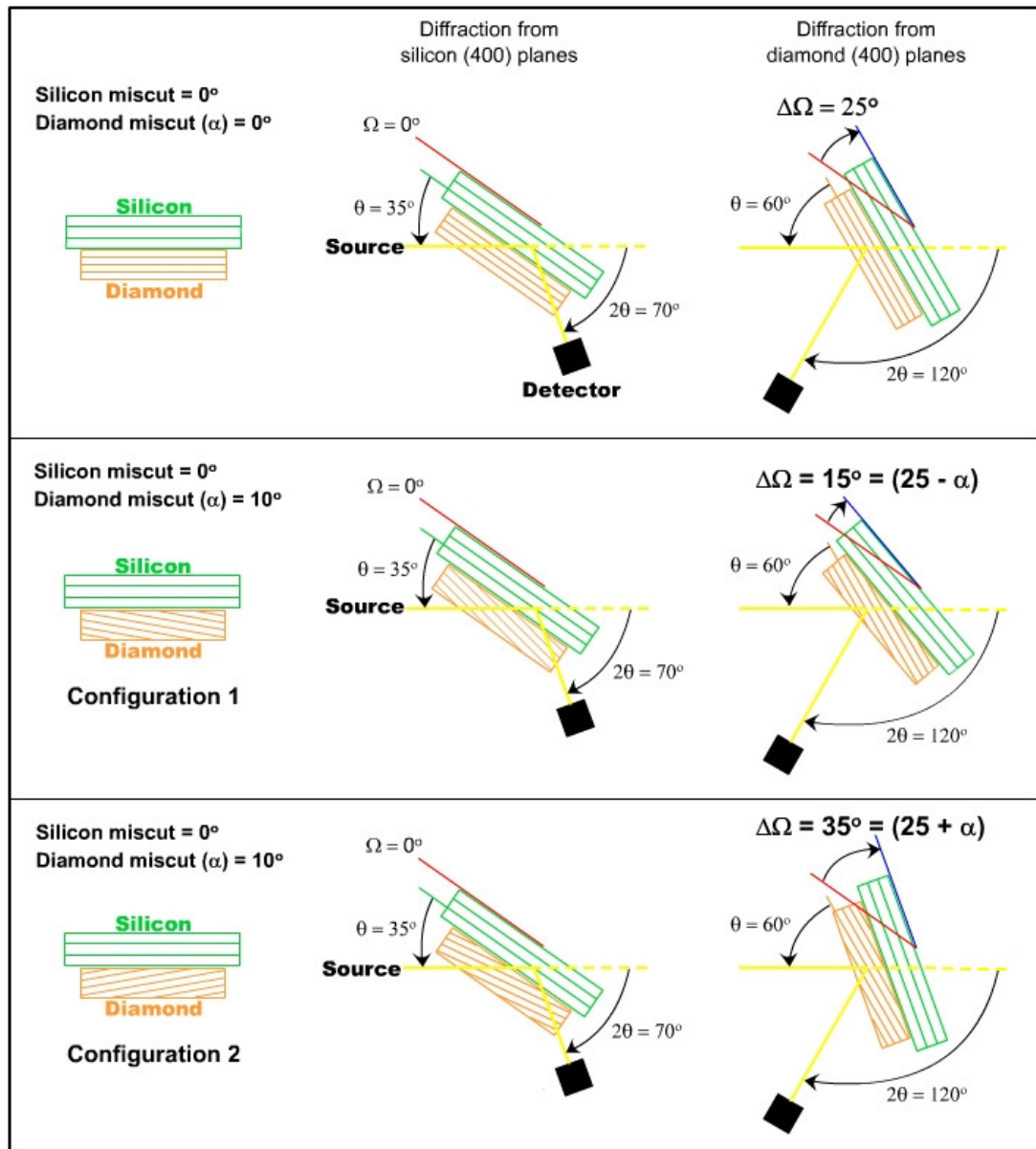


Figure 10 – The experiment envisaged to determine the miscut angle of (100) single crystal diamond plates. Using the Ω angle of the silicon (400) reflection as a reference the angle through which the sample must be rotated, in Ω , to observe the diamond (400) reflection is affected by the miscut of the diamond surface.

If the diamond surface in contact with the silicon was misoriented from (100) by α degrees while the silicon still had no miscut, the angle in Ω through which the sample required to be rotated to move from the Si (400) to the diamond (400) diffraction condition would be modified, becoming $25.22 \pm \alpha^\circ$, as is shown in Figure 10. For each (100) diamond face for which the miscut is to be determined if two experiments are carried out between which the diamond sample is rotated through 180° on the surface normal then the two $\Delta\Omega$ values corresponding to $(25.22 + \alpha^\circ)$ and $(25.22 - \alpha^\circ)$ should be obtained. The misorientation angle of the diamond surface from (100) is then given by subtracting these two values and dividing the result by 2.

A section of a (100) silicon wafer (Compart) with miscut specified as $0 \pm 1^\circ$ was obtained. Along with the (100) single crystal diamond plate the silicon wafer section was sonicated in deionised water and hexane (Fisher, laboratory reagent grade) and dried in a stream of oxygen-free nitrogen to remove any debris from the surfaces. The diamond was then placed against the silicon with the face of which the miscut was to be measured in intimate contact with the polished silicon surface. The two were mounted in this configuration, corresponding to configuration 1 in Figure 10, on a glass capillary using low melting wax and mounted in a Bruker P4 sealed tube four circle X-ray diffractometer using a graphite monochromator and Cu K_α radiation of 1.5418 \AA wavelength. Initially the silicon wafer was positioned centrally in the beam and the detector position limited between 2θ values of 68.5° and 70.5° to identify the silicon (400) line. The sample was free to be rotated around three axes until reflections from Si (400) were observed. The sample position was then corrected slightly to centralise the diamond plate in the beam and the detector position varied in the range 115.0° to 124.0° in 2θ . Again the sample was rotated around three axes until the diamond (400) line was identified. Once any reflection had been detected the diffractometer entered a 'centring' routine which adjusted the four axes (three sample axes and detector position) by small amounts to maximise the signal reaching the detector. Once the angles at which both lines were detected were recorded, the diamond plate was de-mounted and rotated through 180° to the surface normal of the silicon to achieve configuration 2 in Figure 10, in which any miscut on the diamond surface acts in the opposite direction to configuration 1. The experiment was then repeated.

2.2.3 Hydrogen plasma treatment

All hydrogen plasma etching was carried out in the 1kW microwave plasma enhanced chemical vapour deposition (MPECVD) apparatus designed and built at Heriot-Watt University which has been described in detail elsewhere⁸⁶. A system schematic is shown in Figure 11. For reasons of safety and continuous operation the apparatus is computer controlled. The system uses chambers of stainless steel and copper gasket technology to provide UHV integrity and comprises a deposition chamber and load-lock chamber separated by a pneumatic gate valve. The load-lock can be isolated and vented to atmosphere to allow samples to be hand loaded, if necessary, on molybdenum sample holders. A pumping system of a turbomolecular pump (Balzers) backed by a rotary pump (Edwards), capable of 1×10^{-7} mbar, is used to evacuate the load-lock. The deposition chamber is pumped by a trapped oil diffusion pump (Edwards) backed by rotary pump (Edwards) to a base pressure of around 1×10^{-8} mbar. Gas pressures were monitored by means of Pirani and Penning gauges (Edwards) in the loadlock and by a Penning gauge (MKS) and capacitance manometer (MKS) in the deposition chamber. Upon opening the load-lock gate valve, samples can be transferred into, or removed from, the deposition chamber by means of a transfer arm. This design means the deposition chamber itself need never be vented to atmosphere.

In the spherical deposition chamber, sample holders are placed upon a molybdenum capped platen with water-cooled stainless steel sides. The platen encases a serpentine graphite resistive heating element used as a substrate heater which is flushed with argon prior to heating to prevent its degradation. Having isolated the chamber from the high vacuum pumping system, process gases are admitted to the chamber via computer-controlled mass flow controllers (MKS) and a dynamic flow established by use of a second pumping system comprising a rotary pump and Roots blower booster (Edwards) capable of operating under a relatively high gas flow rate. An automated throttle valve (MKS) in the pumping line is used to control the pressure of process gases in the deposition chamber in the range 10 – 100 mbar. Microwave energy of 2.45 GHz is generated by a 1 kW magnetron (Phillips) and transferred via a rectangular waveguide into a cylindrical cavity defined by a perforated metal mesh inside the deposition chamber. Once ignited, a ball plasma sits at the bottom of this mesh cylinder, just above the substrate and remote from the walls of the chamber to prevent potential sputtering and contamination.

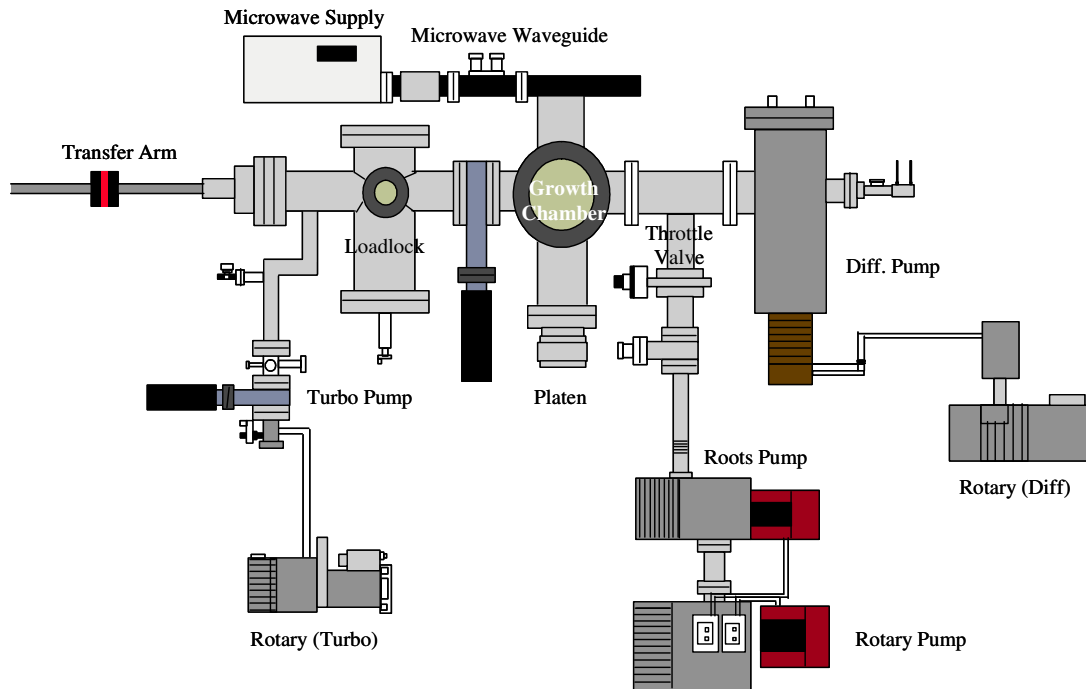


Figure 11 – Schematic of the Heriot-Watt 1kW MPECVD system highlighting the main system components. Reused with permission from reference 23.

An integral quadrupole mass spectrometer is provided (not shown on schematic) to allow monitoring of stable species present in the process gas mixture. Gases downstream of the plasma region are pumped through a needle valve by a turbomolecular pump (Balzers) backed by a small rotary pump (Edwards) to reduce the relatively high process gas pressure to a level suitable for analysis by the quadrupole mass spectrometer head. This system was recommissioned for this study and used to check the integrity of the vacuum system and to analyse for the presence of carbon species in the gas phase either from etching of the diamond substrate or desorption of carbon species present on the walls of the chamber.

The deposition chamber was designed with mesh covered quartz viewing windows which allowed manual observation to take place, but also allows non-invasive monitoring techniques to study the plasma processes. Optical emission spectroscopy (OES) and laser interferometry have previously been utilised but were not used in the study reported here. A two – wavelength pyrometer (Micron 303, wavelengths = 1.17 μm and 1.25 μm) was used to attempt to determine the substrate temperature. The pyrometer was mounted at an angle of 70° to the substrate normal and focussed on the

surface of the sample as accurately as possible given the small size of the diamond plates used in this study (4 x 4 mm).

The computer control is provided by an in-house written HP Basic program running on a Hewlett Packard 9000 series computer. Two Microlink units provide the interface between the computer and the majority of the system components. The computer provides the operator with control over mass flow controllers, valves in gas and pumping lines, most pumping units (not those associated with the mass spectrometer), the platen heater and microwave power supply. Checks are also carried out to ensure sensible operator input to prevent unsafe conditions. Computer controlled gas pressure, cooling water flow and exhaust gas flow alarms ensure safe operation and cause the system to move to a safe condition on occurrence of an unexpected event.

The conditions adopted for hydrogen etching experiments on the Apollo Diamond (100) single crystal substrates were based on those established previously on the MPECVD apparatus described above for hydrogen etching of (100) polycrystalline films²³. With the sample in place, the platen heater operating at 70% of its full power, a hydrogen gas (Linde, 99.999%) pressure of around 22 torr and hydrogen gas flow of 500 sccm, the microwave power input was slowly increased until a plasma was ignited. If the plasma did not auto-ignite before the input microwave power reached 220 W the position of the mechanical cover protecting the front viewing port was adjusted slightly, affecting the electric field sufficiently to cause ignition of a plasma. The gas pressure and microwave power were increased in increments of approximately 2 torr/min and 50 W/min respectively to 35 torr and 500 W. The plasma was allowed to stabilise before the hydrogen gas flow was increased at a rate of 100 sccm/min to 999 sccm, the maximum possible on the mass flow controller. The high gas flow rate was used to minimise the residence time of species in the deposition chamber in an attempt to limit re-deposition of any etched carbonaceous species. Under these conditions the temperature measured by two – wavelength pyrometry was $710 \pm 50^{\circ}\text{C}$. A photograph of the system in operation can be seen in Figure 12.

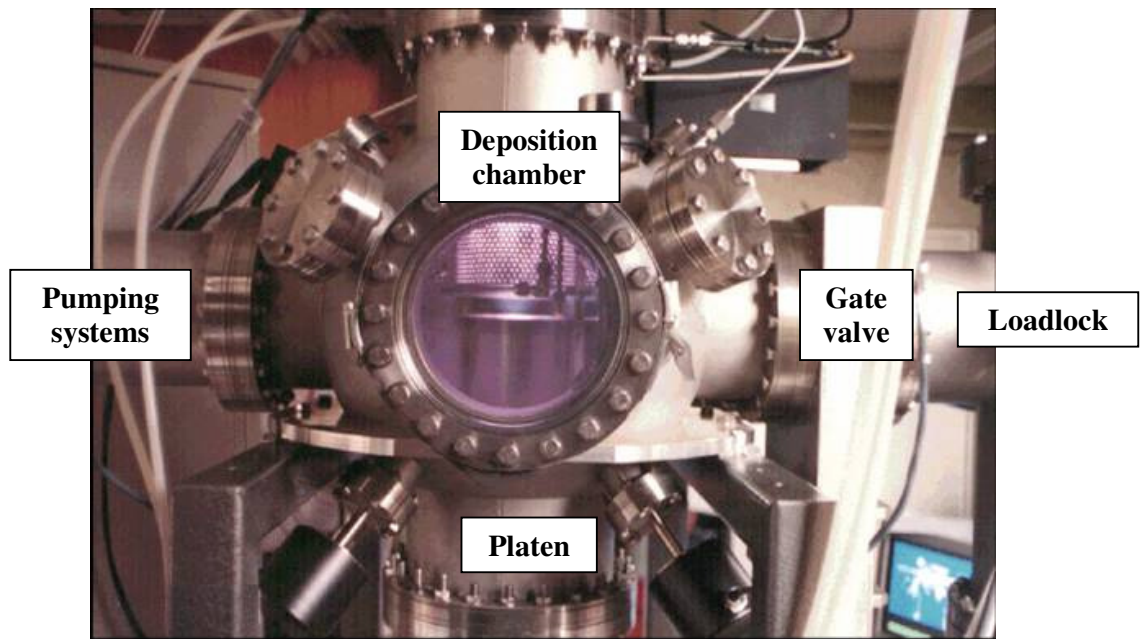


Figure 12 – Photograph of the Heriot – Watt MPECVD system in operation. The purple glow visible in the window of the deposition chamber is due to a hydrogen plasma. The cylindrical metal mesh extending the microwave cavity into the deposition chamber from above can clearly be seen. Note this photograph has been taken from the reverse of the apparatus so the configuration appears reversed to that shown in Figure 11. The monitor of the controlling computer can be seen in the bottom right hand corner.

Each of the two large (100) faces of the single crystal diamond plate were subject to hydrogen plasma treatment for a total of 12 hours and removed after 1, 2, 4, 8 and 12 hours for analysis. To terminate a plasma treatment the gas pressure and microwave power were reduced at approximately 2 torr/min and 50 W/min to 22 torr and 220 W respectively then the microwave power slowly reduced to zero, extinguishing the plasma. The sample was left under flowing hydrogen for 15 minutes before the gas flow and pumping were slowly reduced to zero leaving a static H₂ fill of around 22 torr in the chamber. The power to the platen heater was slowly reduced to zero and the sample allowed to cool for several hours, prior to transfer back to the loadlock, venting to the atmosphere and removal from the apparatus.⁸⁷

2.2.4 Thermal Oxidation

Oxidation of (100) single crystal diamond substrates was carried out in a purpose built stainless steel vacuum chamber containing a resistively heated block. The chamber was pumped by a rotary – turbomolecular pump combination (Peiffer-Baltzers TPU 050)

capable of providing a base pressure of 1×10^{-6} mbar. Vacuum pressure was monitored with a Penning gauge (Edwards 8). Oxygen gas (BOC 99.6%) was passed over zeolite A molecular sieves and passes into the chamber by means of a needle valve welded into the side of the chamber. Gas pressure in the chamber was monitored by the voltage output from a strain gauge manometer (Bell and Howell 327) calibrated to the Penning gauge at high vacuum and an external mercury barometer at atmospheric pressure. The temperature of the resistively heated block was controlled by a digital temperature controller (Eurotherm 127) and monitored by means of an internal K type thermocouple and in this set-up was capable of heating samples to over 600°C. Sample temperatures were measured by a second K type thermocouple positioned such that it was in intimate contact with the sample surface and monitored with a two wavelength pyrometer (Micron 303, wavelengths = 1.17 μm and 1.25 μm). The thermocouple was calibrated against the pyrometer up to 640°C.

With the chamber open to atmosphere, samples were loaded through a de-mountable quartz window directly onto the resistively heated block. The thermocouple was positioned and the chamber resealed and evacuated. Once base pressure had been reached and recorded, oxygen was let into the chamber to a pressure somewhat lower than that desired to allow for expansion of the gas on heating. Heating was then initiated. As the substrate reached the desired temperature of around 600°C the gas pressure in the chamber could be adjusted by bleeding small quantities of gas in through the needle valve or out through the pump. The exact pressure and substrate temperature were then noted and the sample exposed to these conditions for a period of time. Once the required time period had elapsed the oxygen gas was pumped out of the chamber and the sample cooled under vacuum with the intention of 'freezing-in' the oxygen configuration imparted by high temperature oxidation and not allowing further oxidation to occur at lower temperatures as the sample cooled. On opening the chamber to the vacuum pump the chamber pressure dropped from one atmosphere to $\sim 1 \times 10^{-2}$ mbar within 2 minutes and achieved $< 1 \times 10^{-5}$ mbar within 15 minutes. Once the sample had cooled to room temperature the chamber was let up to atmospheric pressure with air, the quartz window released and the sample removed.

2.2.5 Optical microscopy

Following thermal oxidation the single crystal diamond substrate was examined using a Nikon Optiphot optical microscope. The instrument was fitted with Watec DC10.5 mono CCD camera which could be used to capture the microscope image as a digital image. Supplying information on the microscope lens used into the image analysis software (Aquinto a4iDocu) allowed scale bars to be appended to each image and the data saved to file.

2.2.6 Scanning electron microscopy (SEM)

High magnification scanning electron microscopy was carried out, when required, on a Hitachi S-2700 scanning electron microscope (SEM). The instrument was operated in back-scattered electron mode with an electron excitation voltage of 10 kV which provided images of suitable clarity. The instrument was equipped with a thermal printer on which electron micrograph images could be captured.

2.2.7 Atomic force microscopy (AFM)

Non-contact mode analysis of samples after hydrogen plasma treatment

A Topometrix TMX 2000 Explorer Scanning Probe Microscope (SPM) in non-contact mode was used to investigate the surface topography of (100) single crystal diamond faces following exposure to a hydrogen plasma. In non-contact mode the AFM tip is held at a suitable distance above the sample surface such that attractive long-range Van der Waals forces exist between the silicon tip and sample surface. The cantilever is vibrated at its resonant frequency. Interactions between the tip and the surface affect the vibration frequency of the cantilever. A feedback loop is used to adjust the cantilever height and allow the vibration frequency to remain constant and the cantilever height can therefore be used to generate high-resolution atomic force microscopy (AFM) images. Images obtained in this way were further analysed in the proprietary

TMX 2000 data analysis software to obtain values for the surface roughness as both the R_a , average roughness, and rms, root mean square roughness. Generally scans were recorded over an area of $20 \times 20 \mu\text{m}$ though areas up to $100 \times 100 \mu\text{m}$ were possible.

In order to observe changes effected upon the (100) diamond surface by the hydrogen plasma it was desirable to have a means of analysing the same area of sample after each exposure. Previous diamond AFM studies, carried out in the research group on this instrument, had been performed on polycrystalline diamond where repeat analyses could be carried out by identifying a unique group of crystallites. This was not possible on the single crystal diamond used in this study. Instead the author, with the assistance of technical engineering personnel, devised a sample stage comprising a vacuum chuck mounted on two translation stages, the movement of each being controlled manually by means of a micrometer gauge. The translation stages were fixed one on top of the other, orientated at 90° to allow translation in the x and y directions. The sample was placed against two stops on the vacuum chuck and held in place by means of an external vacuum. With the sample mounted the stage was placed under the cantilever of the AFM in a known orientation. The sample could be translated until the tip of the cantilever appeared to be over one corner of the sample when viewed through the AFM camera attachment. By locating the cantilever tip over the same corner each time the sample was to be imaged and adjusting the micrometers on the translation stage by a fixed distance, the same point on the surface should have been arrived at prior to each analysis. One complication of this approach was that the AFM camera did not view the sample from directly over the cantilever tip but at 45° . Therefore to 'dead-reckon' back to the same point on the sample surface required the cantilever tip to be the same height above the diamond surface prior to each analysis. Operation of the translation stage was always carried out by the author but all AFM operations, including adjusting the height of the cantilever above the surface were carried out by the technician in charge of the instrument. Although it is believed analysis has been carried out repeatedly on the same area, it cannot be guaranteed that the cantilever was at exactly the same height prior to each analysis and therefore there may be slight spatial variation in the $20 \times 20 \mu\text{m}$ area imaged in successive experiments.

Samples were analysed as removed from the CVD apparatus unless advised by the operator in charge of the AFM that dust was present on the surface and cleaning was required. The cleaning procedure used involved sonication of the sample in acetone

(Fisher, reagent grade) for 5 minutes, decanting of the acetone, transfer of the sample into a fresh beaker of methanol (Fisher, reagent grade), sonication for 5 minutes, decanting of methanol, transfer of sample to a fresh beaker of deionised water, sonication for 5 minutes and drying in a stream of oxygen free nitrogen (OFN). On occasion, when this procedure did not successfully remove all debris, the surface was wiped with a piece of lens tissue soaked in acetone, then a piece soaked in methanol and finally a piece soaked in deionised water. Drying was again effected by a stream of OFN.

Contact mode analysis of samples after oxygen treatment

The AFM analyses carried out on single crystal (100) diamond samples following exposure to oxygen at elevated temperature were performed using a different AFM instrument, but of the same make and model (Topometrix TMX 2000 Explorer) as that used for the analysis of samples after hydrogen exposure. This instrument was operated by the author after training from, and with the assistance of, the technician responsible for the instrument. The area of the surface analysed after each oxygen treatment was identified by a unique deep polishing groove instead of 'dead-reckoning' back to the same area analysed after hydrogen treatments. This arrangement allowed data to be gathered more rapidly after each exposure to oxygen and with greater confidence in the reproducibility of the analysed area and images produced. However use of this instrument was restricted to operating in contact mode only. In contact mode a greater force is applied to the cantilever which forces the AFM tip towards the sample surface until it feels a repulsive force due to electrostatic repulsion between the electron clouds of atoms in the sample and the tip. At the distances involved the tip is in physical contact with the sample surface and can physically affect the surface or conversely the tip can itself be affected by the sample. The AFM was operated in constant force mode, meaning that the height of the cantilever is adjusted by a feedback loop in order to keep the force between the tip and surface constant. In this way high resolution images are obtained from the variation in height of the cantilever.

Samples were analysed directly as removed from the thermal oxidation apparatus, since debris was never evident on the surface and cleaning was not required. During data analysis a levelling step was used to correct for any divergence between the plane of the

sample surface and the scanning plane. This was performed by fitting the two dimensional image data to a second order equation:

$$Z = aX^2 + bY^2 + cXY + dX + eY + f \quad (1)$$

Where Z refers to the cantilever height at the point where the scanning head is positioned at (X,Y) along the x and y axes. This levelling routine was recommended since it provided the lowest order levelling which gave appropriate results. In fits to lower order equations extremely high or low points in the image could be seen to skew the surrounding data.

A complication of using contact mode AFM on the extremely hard diamond substrates was erosion of the silicon nitride AFM tip. The sharp point became worn down to a square-ended pyramid. Since the image collected in AFM is a function of both the substrate surface and the scanning tip, this wear manifested itself in the images obtained by making each surface feature appear square shaped. This effect can be seen in Figure 13. In Figure 13 A the image appears to be made up of many similar, repeating squares approximately $2 \mu\text{m}$ wide which have their top edges parallel to the direction in which the AFM tip is scanned. In Figure 13 B the sample has been rotated through 45° , as can be seen from the change in orientation of the prominent trench feature. The image again appears to be made up of the same repeating square features however these have not changed orientation with the sample, instead they have remained parallel to the direction of tip scanning. This indicates that the square effect is imparted by the AFM tip and not the sample. The reason for this can be seen in Figure 13 C where an SEM image of the tip used to collect Figure 13 A and B is shown. By comparison with Figure 13 D where an SEM image of a brand new AFM tip is shown, it can be seen that the used tip has been worn down to a square end instead of a sharp tip by contact with the diamond substrate. In addition to being worn down to a smooth flat end, a large square chunk has also been removed from the centre of the smoothed AFM tip, leaving a recess. On closer inspection of Figure 13 A and B, the square features in the AFM image can be seen to have a corresponding dark spot in their centre.

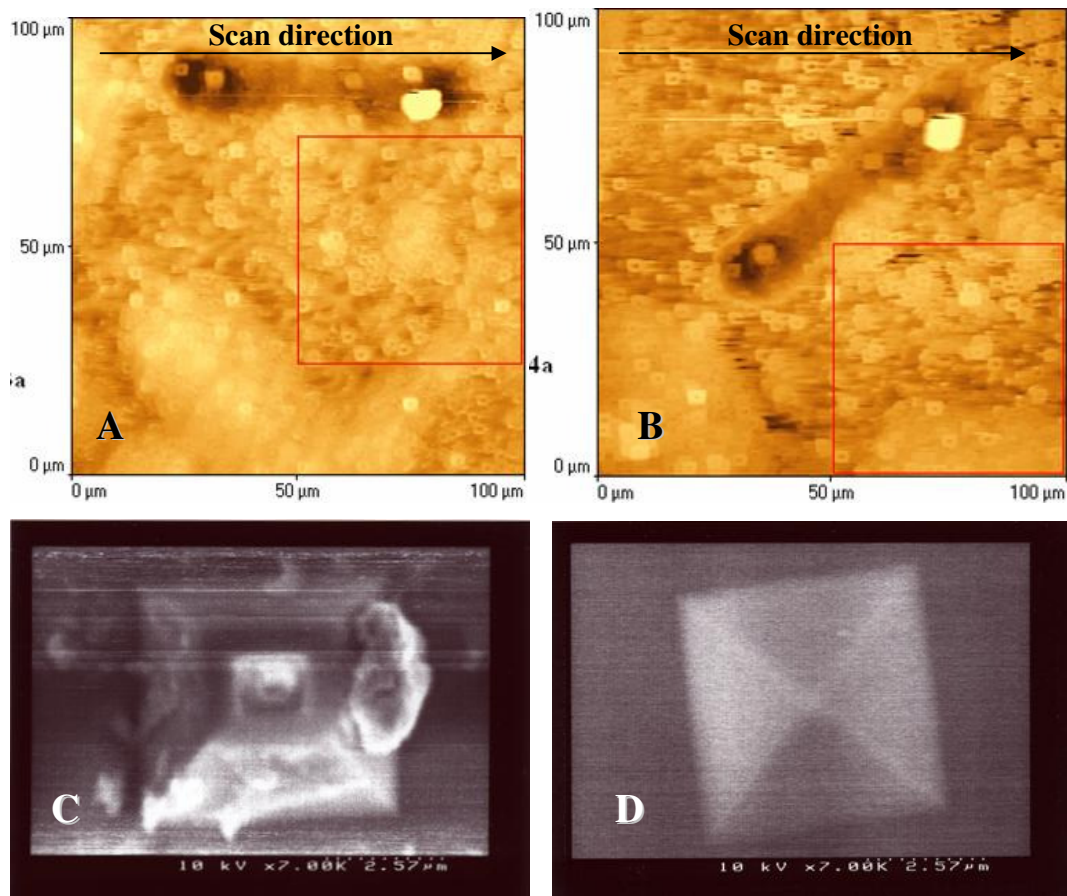


Figure 13 – AFM tip wear caused by contact mode analysis of diamond. A – an AFM image collected with a worn tip. B – The same surface area analysed with the same tip after rotating the sample through 45°. C – SEM of the worn tip used to collect the images in A and B. D – An unused AFM tip.

Care was therefore exercised when interpreting AFM data collected in contact mode on single crystal (100) diamond substrates after thermal oxidation. Comparison with optical microscope images of the same area proved a good check that surface features observed were real and not AFM tip artifacts but the effect of tip wear had to be considered when taking other measures of the AFM data, such as roughness measurements.

2.2.8 X-ray photoelectron spectroscopy (XPS)

X-ray photoelectron spectroscopic analysis of (100) single crystal diamond substrates was carried out at the National Centre for Electron Spectroscopy and Surface Analysis

(NCESS) in the Daresbury Laboratory, UK. The design and operation of the Scienta ESCA300 spectrometer in use at NCESS has been fully published in literature⁸⁸ along with detail of data interpretation and representative polymer spectra. Only a summary of the instrumental operation and detail pertinent to the analysis of the samples at hand will be included here.

Al K_{α} (1486.7 eV) X-rays are generated by impingement of an electron beam onto an aluminium band on the rim of a water-cooled titanium alloy rotating anode. The X-rays, generated with a range of trajectories, are focussed onto the sample by a monochromator consisting of seven toroidally bent α -quartz (1010) crystals, projecting an X-ray line approximately 6 x 0.5 mm with an energy spread of approximately 0.26 eV onto the sample. The anode, monochromator and sample chamber are separated by metal foils which prevent transmission of spuriously generated electrons.

Electrons ejected from the sample are collected by a multi-element electron lens which can be operated in two modes. Using only the main lens electrons are accepted from the whole area of sample under the X-ray line giving high electron transmission but poor spatial resolution (approximately 500 μm). The inclusion of a pre-lens before the main lens reduces the sample area from which electrons are gathered, reducing the electron transmission but increasing the spatial resolution of the instrument to approximately 25 μm . In this work the whole of the diamond sample surface was treated similarly and spatial analysis was not required. For this reason the pre-lens was never used, maximising the electron signal reaching the detector and allowing shorter data collection times. From the lens, electrons pass through a slit-aperture pair into a hemispherical electron analyser which is operated at one, from a range, of available pre-set pass energies. The overall spectrometer resolution is a convolution of the X-ray line-width (~ 0.26 eV) and the hemispherical analyser resolution which is dependant on the pass energy and slit width. The slit width could be varied by means of a manual carousel between values of 0.2 and 4.0 mm. Slit widths of 0.8 mm and 1.9 mm were used to acquire spectra on diamond surfaces. A wider slit provides greater electron transmission and poorer resolution and was used for survey scans over the entire energy range to identify elements present whereas the narrower slit width could be used to provide greater resolution for region scans over particular core lines. A constant pass energy of 150 eV was used to acquire spectra. In conjunction with the narrower slit this meant the spectrometer resolution was mainly limited by the X-ray line-width.

Electrons leaving the analyser are detected on a multichannel detector utilising a CCD TV camera. Each electron striking the detector generates a flash of light several pixels wide but a correcting calibration means recorded spectra reflect the true accumulated counts data.

Prior to analysis in the spectrometer, samples were mounted on sample stubs (VG ESCALAB Mk II). Rigid inflexible samples like the diamond plates would usually be mounted onto the metal stub with double-sided tape. Since these samples were irreplaceable and too precious to risk damaging or contaminating with adhesive, they were instead mounted onto a stub with an attached small metal clip which trapped the sample against the stub. Due to the small size of the diamond plates (4 mm x 4 mm) they were mounted, as far as possible, such that the length of the X-ray line would lie along the diagonal of the sample in order to maximise the diamond signal. Despite these precautions, however, it was not possible to exclude the possibility of recording signals from the metal stub or clip. The samples were loaded into the spectrometer via a turbomolecular pumped fast-entry loadlock onto a rack and pinion railway. This railway extends from the loadlock, through a preparation chamber, unused in this work, into the analysis chamber where the sample is transferred to a high precision XYZ stage. Sample transfer is provided by 'wobble' sticks. The sample stage can be rotated around an axis perpendicular to the electron lens axis, allowing experiments to be carried out at varied electron take-off angles. Electron take-off angles (TOA) between 90 and 15 degrees were utilised for analysis of diamond surfaces although due to the small size of the sample and the presence of the retaining clip, sample alignment in the X-ray beam became more difficult with decreasing take-off angle.

Loss of photoelectrons from insulating substrates can cause charging of the sample. This charging manifests itself by both shifting peaks to higher binding energy and affecting the peak shapes. To compensate for charging, the Scienta ESCA300 is fitted with an electron flood gun (VSW EG2). A real-time photoelectron signal can be observed on a television screen linked to the detector CCD camera and the flood gun settings varied till the peak position is as expected. Peak heights were maximised and widths minimised. Use was regularly made of the flood gun for analysis of diamond samples, and was particularly required for oxidised samples which are known to be insulating.

2.3 Results and Discussion

2.3.1 Determination of diamond plate crystallographic information

An optical microscope image of one of the 4 x 4 mm single crystal (100) diamond plates is shown in Figure 14. The plate as received from the supplier is shown on the left. The plate was cleaved into several pieces to facilitate analysis, the approximate pieces obtained after cleaving are shown on the right of Figure 14.

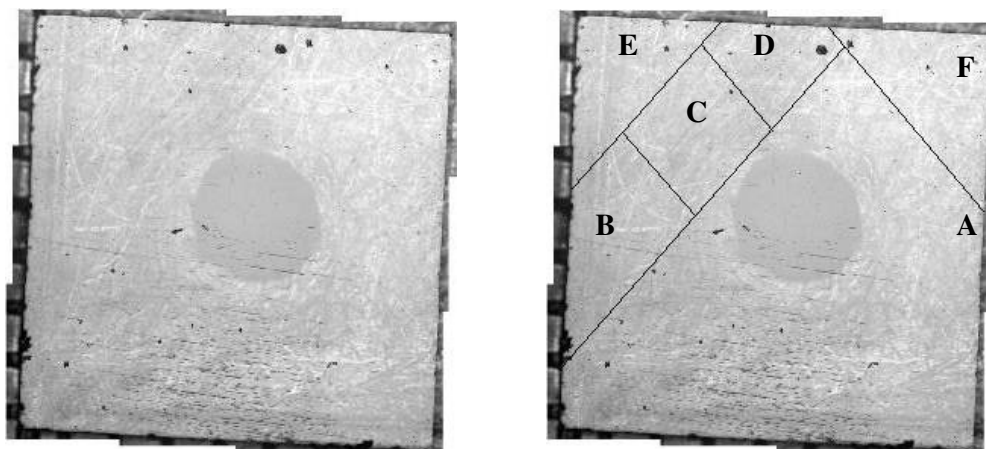


Figure 14 – Optical microscope image of a single crystal (100) diamond plate. On the left is the plate as received. The image on the right indicates the approximate pieces the plate was cleaved into to allow XRD analysis.

The section labelled D in Figure 14 was the piece used for face indexing and assigning of Miller indices as it was the smallest section and most suitable for mounting in the XRD. Since section D shared one identifiable edge with the crystal edge it was suitable for identifying the crystallographic direction of the edges of the supplied plate. Figure 15 shows a screenshot from the Apex II XRD analysis software which allowed the crystal faces to be identified and, following determination of the diamond unit cell, assigned to crystallographic directions.



Figure 15 – Apex II XRD software screenshot showing the crystal planes assigned to the faces of the crystal fragment used in the experiment. The highlighted face forms part of one edge of the original plate, allowing the crystallographic planes to be assigned.

Unfortunately even section D was a somewhat larger crystal than routinely used in the X-ray diffractometer and it was not possible to fit all crystal faces on-screen at once. However the top face of section D can easily be seen dominating Figure 15 and has been identified as a (100) face, confirming that the top and bottom faces of the supplied plate are indeed (100) surfaces. The crystal face which was originally part of the cut-edge of the diamond plate is being viewed edge-on in the bottom left hand corner of the image, emphasised by the red box. It has been assigned the (00 $\bar{1}$) Miller index, and is the highlighted assignment in the list at the right-hand side of the screenshot. This assignment identifies that, by nature of the relationship of the crystal planes, the four sides of the diamond plate are (100) diamond faces and therefore (110) planes run diagonally across the sample.

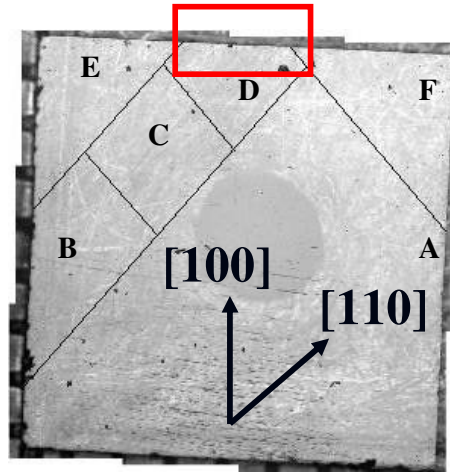


Figure 16 – The (100) diamond plate. The highlighted edge is that shown in Figure 15 and allows the crystallographic directions to be assigned.

The largest section of the cleaved diamond plate, labelled A in Figure 16, was used to determine the misorientation of the surface from the (100) plane by XRD. The miscut measured was that running from top to bottom of the diamond plate as it is oriented in Figure 16. During the experiment the crystal was allowed to rotate within a range of angles on each axis allowing more than one equivalent plane, (400), ($\bar{4}00$) and so on, to be identified. The value of Ω at which the maximum diffraction intensity from equivalent Si (400) planes was observed had small variations for each of these equivalent planes. Additionally, due to the incremental program and centring routine used by the diffractometer to identify diffraction peaks, the same plane was occasionally centred more than once. The values of Ω determined for the same plane from repeat identifications had a similar variation to that found between Ω values for equivalent places, indicating a limitation in accuracy of this experimental approach. Table 1 gives the experimental Ω values as an average value for all equivalent planes identified with standard deviations and provides a comparison with the theoretical values. Whilst the absolute Ω values for each peak could vary with the position in which the crystal was originally mounted, the difference in Ω ($\Delta\Omega$) between the Si (400) and diamond (400) peaks should provide information on the miscut of the diamond sample.

Configuration 1 and 2 in Table 1 refer to the orientation of the diamond plate with respect to rotation around its surface normal. In configuration 2 it is rotated 180° relative to configuration 1. Performing the two complimentary experiments should

result in one $\Delta\Omega$ solution equal to $(25.22 + \text{miscut})$ and one equal to $(25.22 - \text{miscut})$. Theoretically, the value of the diamond surface miscut from (100) is equal to half the difference between the two experimental $\Delta\Omega$ values. Calculating the miscut in this way and treating the uncertainty associated with each value gives a miscut of $0.1^\circ \pm 0.6^\circ$. However, the uncertainty in both experimental values is much greater than the difference between them and therefore, within the accuracy of the experiment, the two $\Delta\Omega$ values determined are the same. The miscut value determined from this experiment can only be quoted as $0^\circ \pm 1^\circ$.

	$\Omega_{\text{Si (400)}} / ^\circ$	$\Omega_{\text{D (400)}} / ^\circ$	$\Delta\Omega = (\Omega_{\text{D (400)}} - \Omega_{\text{Si (400)}}) / ^\circ$
Theory	34.60	59.82	25.22
Configuration 1	34.7 ± 0.6	58.2 ± 0.5	23.5 ± 0.8
Configuration 2	34.9 ± 0.7	58.2 ± 0.6	23.3 ± 0.9

Table 1 – The theoretical and experimentally determined values for Ω , the sample rotation in the plane of the X-ray source and detector when the Si (400) and diamond (400) diffraction peaks were observed. Experimental values are given as the average of all equivalent planes identified with standard deviations.

The specification requested of the manufacturer for the diamond plates was for a miscut of either 0° or 1° ; to distinguish between the two required the experiment to be able to accurately determine differences of less than one degree. As shown above, the uncertainty introduced by the diffractometer ($\pm 1^\circ$) and the tolerance on the manufacturer specification for the silicon wafer miscut ($\pm 1^\circ$ from (100)) are of the same order of magnitude as the result to be determined. This experiment is not of sufficient accuracy to clearly distinguish between diamond surfaces misoriented from (100) by 0° and 1° and can serve only to indicate that the sample studied is not misoriented significantly more than 1° from (100).

It is very interesting to note that both $\Delta\Omega$ results obtained are lower than the theoretical value of 25.22. If a miscut existed on the silicon surface which was significantly more than that on the diamond surface it would dominate the results obtained, any small change in $\Delta\Omega$ between configuration 1 and 2 caused by rotation of the diamond would be insignificant against the effect of the silicon miscut. In effect the experiment would be reversed and the position of the diamond (400) peak would be used as a reference to

measure the miscut from (100) of the silicon surface. Since the silicon was not rotated around the surface normal between experiments the effect of the silicon miscut would be in the same direction in both cases, giving either $(25.22 + \text{miscut})$ or $(25.22 - \text{miscut})$ from both experimental configurations. It is possible that the $\Delta\Omega$ values obtained (23.3° and 23.5°) both correspond to $(25.22 - \text{miscut})$ results caused by the situation described above. Calculating a miscut value from the average of the two results gives a silicon miscut of $1.8 \pm 0.6^\circ$ from (100). While this value is greater than the tolerance allowed by the manufacturer ($0 \pm 1^\circ$), it is of the correct order of magnitude. It is possible that a miscut on the surface of the (100) silicon wafer used as the reference in the experiment is the reason that both $\Delta\Omega$ values obtained are less than expected if neither the silicon or the diamond surfaces were miscut from (100).

2.3.2 In-situ monitoring of species present in a hydrogen plasma.

In-situ mass spectrometry was used to monitor the species present during hydrogen plasma exposure of (100) single crystal diamond plates. The positive ion mass spectrum shown in Figure 17 is representative of the spectra obtained by sampling the process gases downstream of the hydrogen plasma during hydrogen etching of (100) diamond plates. Peaks were observed at masses of 14, 15 and 16 Daltons which correspond to the masses of CH_2 , CH_3 and CH_4 respectively indicating that the chamber environment is not entirely free of carbon. These peaks were also observed when no diamond sample was present in the plasma chamber therefore their likely cause is etching of carbonaceous species from the stainless steel walls of the high vacuum apparatus. The mass spectrometer was initially re-commissioned to check the integrity of the vacuum system. No peaks indicating the presence of water vapour or O_2 were observed and the vacuum seal during experiments was believed to be sound.

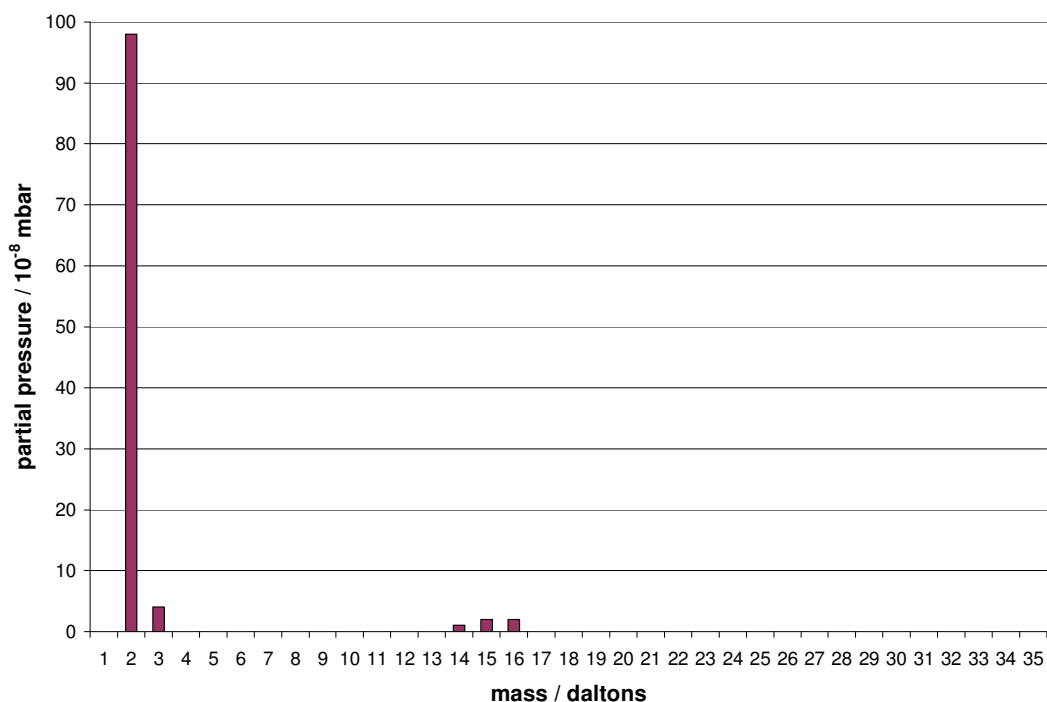


Figure 17 – Mass spectrum showing mass of species detected downstream of hydrogen plasma etching (100) diamond.

2.3.3 Hydrogen plasma exposure of (100) single crystal diamond surfaces

AFM analysis was carried out upon the (100) single crystal diamond plate as it was received from the supplier, that is, before any treatment had been carried out which could affect the surface morphology. The image obtained from one (100) face, shown in Figure 18A, reveals grooves consistent with those observed after mechanical polishing of diamond as observed by Watanabe et al³⁴. The results of polishing diamond are strongly dependent on the direction of polishing relative to the diamond crystal planes⁸⁹. ‘Hard’ and ‘soft’ polishing directions result. Polishing diamond in a hard direction results in very low material removal rates and can damage the polishing wheel. Polishing in soft directions results in much larger material removal rates and imparts a ridged pattern to the diamond surface⁹⁰. On (100) surfaces hard directions are parallel to <110> directions and soft directions parallel to <100>. These observations were rationalised by van Bouwelen and van Enkevort⁹¹. In <110> directions the diamond lattice comprises zig-zag chains of covalently bound carbon atoms. If a polishing force is applied in this direction, the force is parallel to this strongly bonded

chain of atoms and material removal is difficult. Applying a polishing force such that its component along the strongly bound zig-zag C-C chains is minimised coincides with the $\langle 100 \rangle$ direction on a (100) surface and so material removal is easiest in this direction. The direction of the polishing grooves observed in Figure 18A should be parallel to $\langle 100 \rangle$. The orientation arbitrarily chosen to mount the sample under the AFM cantilever was with the top edge of the plate approximately parallel to the scanning direction of the AFM, meaning $\langle 100 \rangle$ directions run approximately up and down and left to right across the images shown in Figure 18. The direction of the grooves in Figure 18A appears to be consistent with the $\langle 100 \rangle$ direction as determined by XRD and suggests the cause of the grooves is likely to be mechanical polishing of the sample in a soft direction. This image was obtained prior to the design and construction of the AFM sample stage so was obtained on a different area of the surface than the other images shown in Figure 18. The other images in Figure 18 show one region of the (100) face after different periods of exposure to the hydrogen plasma.

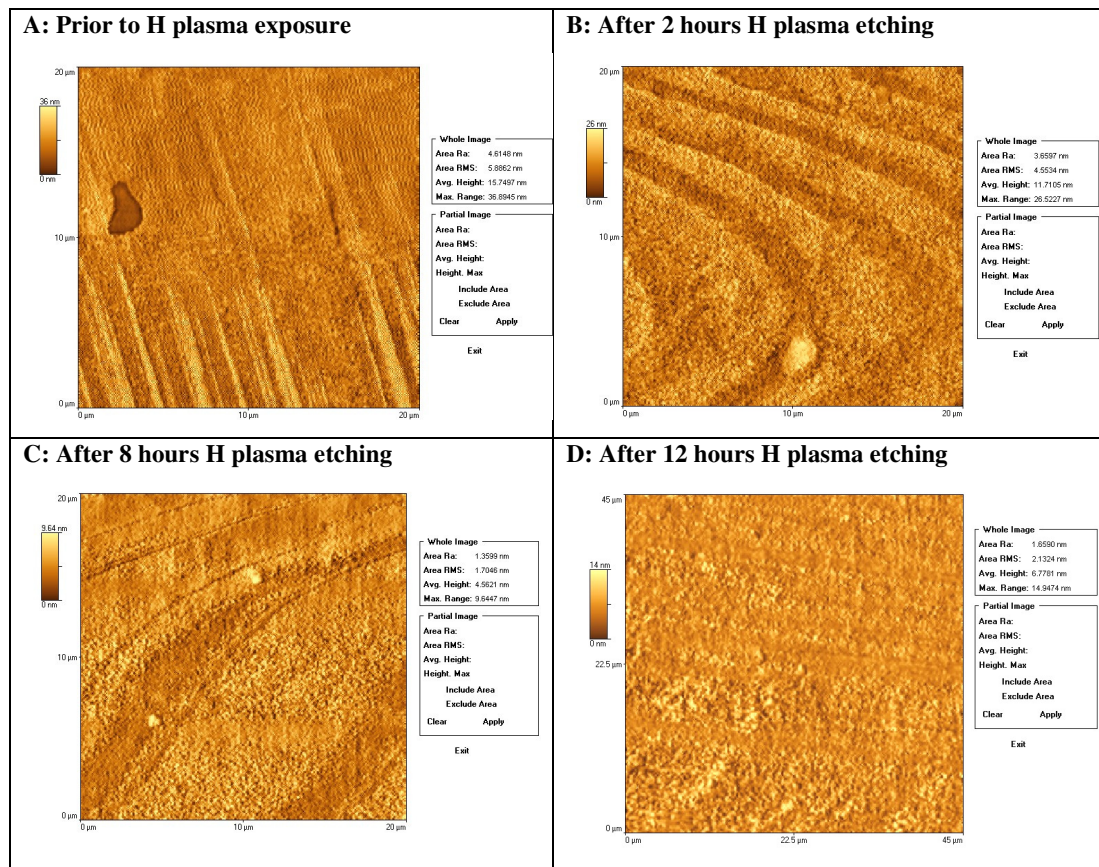


Figure 18 – AFM images of the surface of (100) single crystal diamond recorded after different periods of exposure to a hydrogen plasma.

There are no polishing ridges evident in the AFM image obtained of the surface after 2 hours exposure to the hydrogen plasma, Figure 18B. Instead curved features 5 – 10 μm wide are present, the nature of these features is unknown and unfortunately since the AFM prior to etching was not recorded over the same area it is impossible to say if they were present on the sample as received or if they have been formed by exposure to the plasma. The features were no longer present in the AFM recorded after 4 hours exposure to the plasma (not shown) which was rather featureless. After 8 hours exposure the image shown in Figure 18C was obtained, the height gradient mapped by colour indicates some bands of the surface of slightly lower height than the rest. Figure 18D shows the surface morphology obtained after 12 hours exposure to the hydrogen plasma. The surface appears very uniform with no obvious features. The absence of any recognizable feature appearing in each AFM image meant it was not possible to confirm that exactly the same area of the single crystal diamond surface was analysed each time.

It is noteworthy that a paper⁹² published since this experiment was carried out reported evidence indicating the presence of a 1 nanometre thick layer of non-diamond material on the surface of diamond after exposure to a hydrogen plasma at 800°C for periods as short as 5 minutes, in ultra-clean deposition chambers. The non-diamond layer was scraped aside by a contact AFM tip to reveal the clean diamond surface underneath. Non-contact AFM images obtained with the non-diamond film in place have bands across the image, suggesting regions of diamond of lower height than the surrounding areas, similar to the banding evident across Figure 18C. The non-diamond film also causes a noisier image to be obtained than the diamond substrate alone provides. All AFM analysis carried out in this work to investigate the effect of hydrogen plasma treatment on the surface of (100) single crystal diamond was carried out in non-contact mode. It would have been extremely interesting to investigate if sharper images could have been obtained by scanning a contact AFM tip over the sample surface.

The most noticeable feature of the AFM analysis was the trend for the surface roughness (whether measured by R_a or RMS) to decrease as the duration of exposure to the hydrogen plasma increased. The surface roughness, measured as the R_a value determined over a 400 μm^2 area, is plotted against time in Figure 19.

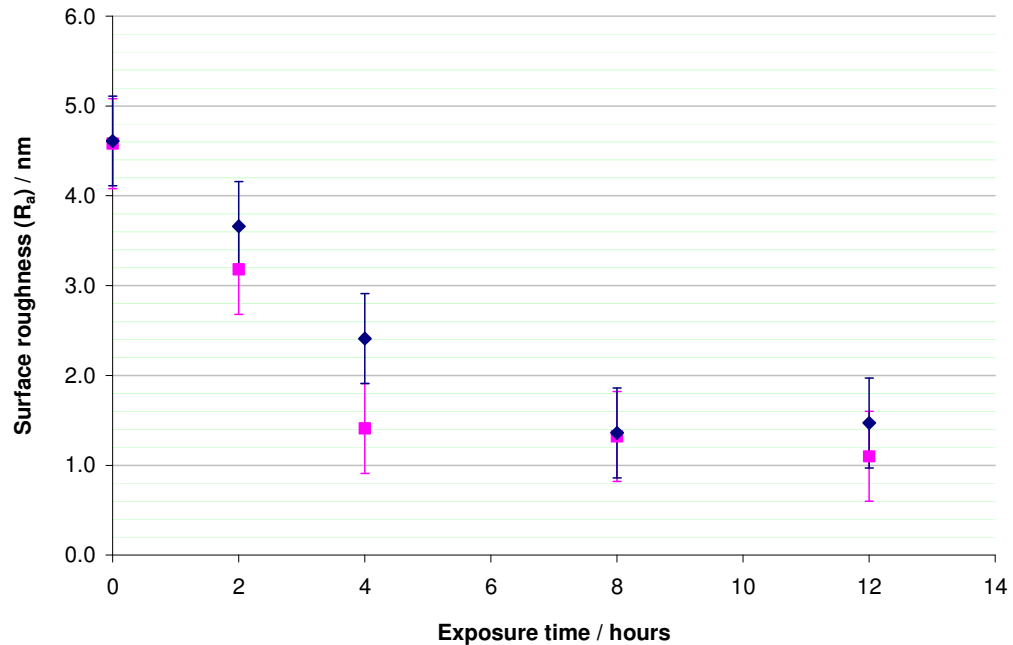


Figure 19 – Graph showing the surface roughness (R_a) of the (100) faces of a single crystal diamond plate with time of exposure to a hydrogen plasma. Side 1 (♦) and side 2 (■)

The two sets of data presented in Figure 19 correspond to the two main (100) faces of the diamond plate ('top' and 'bottom' faces). The roughness was taken as the R_a value generated by the Topometrix analysis software over the whole area of 1 image, and was not the average of repeated readings. As can be seen from the $45 \times 45 \mu\text{m}$ image in Figure 18D, after 12 hours exposure to the plasma a wider area of the surface of side 1 was analysed. The R_a values obtained from different $400 \mu\text{m}$ areas of the surface in this wider region varied by up to 0.5 nm . This value was used to estimate the uncertainty in all the R_a values determined. The error bars in Figure 19 represent $R_a \pm 0.5 \text{ nm}$. The trend observed in Figure 19 shows that the (100) surfaces studied became smoother as their time of exposure to the hydrogen plasma increased. The surface roughness decreases at a greater rate in the first few hours of etching before decreasing at longer etch times and the roughness tends to a value of $1.0 - 1.5 \text{ nm}$ after around 10 - 12 hours. This surface roughness is an order of magnitude larger than the height of single atomic steps on the (100) diamond surface. The AFM images obtained after 12 hours of etching, exemplified in Figure 18D, do not resolve any features indicative of single, double or bunched steps on the surface. Experimentally, the AFM instrument was not set up for atomic-scale imaging. While it was mounted on a vibration-damping floating

table it was otherwise open to a general laboratory atmosphere. To attempt atomic scale imaging a minimum of a clean-room set up with filtered air and acoustic hood would be essential. It seems likely that an R_a value on the order of 1 nm may well represent the limit of resolution of the instrument, under these experimental conditions, rather than some limit to the smoothness possible on the diamond surface.

The observed smoothing of (100) diamond surfaces is in keeping with the theory of anisotropic etching by activated hydrogen of a diamond surface which is slightly misoriented from (100). The smoothing mechanism in operation in this case cannot, however, be concluded from the data presented here. The AFM data are insufficiently resolved to detect any steps on the diamond surface and, so, smoothing by step etching of surface features over time cannot be established. Deposition of carbonaceous species cannot be ruled out since the mass spectrometer indicated the presence of carbon species in the gas mixture downstream of the plasma. This carbon is likely to be material etched from the walls of the reactor by the plasma since the signals were present when no diamond sample was present in the chamber. Under standard growth conditions, with relatively high methane concentration, deposition on (100) diamond with a low miscut causes roughening of the surface by nucleation of unepitaxial crystallites and growth hillocks on terraces^{38, 93}. However, Watanabe et al^{34, 38} showed that deposition on such surfaces under low methane concentrations, CH_4/H_2 ratio < 0.15%, resulted in atomically smooth films. That this was genuinely a growth effect was established by measuring the step height between a masked and unmasked area following deposition⁹⁴.

The intent of these experiments was to use anisotropic etching of diamond by hydrogen to smooth the as-received single crystal diamond surface, to improve the quality of the (100) surface. Whether the dominant surface process occurring is anisotropic etching, re-deposition of etched carbon or some other process, the AFM data strongly demonstrates that a smoothing effect has been achieved. Features standing proud of the surface, which will have non-(100) faceted sides, have either been etched back or overgrown to provide a smoother, high quality (100) surface. While it has not been possible to demonstrate an atomically smooth surface it seems likely that the minimum surface roughness of around 1 nm measured by AFM may represent a limitation in resolution of the instrument under these experimental conditions. More sensitive equipment and a lower level of background 'noise' would have been required to pursue

these experiments further. Smooth, high quality (100) diamond surfaces were believed to have been produced, providing suitable substrates on which to pursue the introduction of >C=O moieties, to generate a surface which could ultimately be functionalised by nucleophilic attack under ambient conditions.

2.3.4 Thermal oxidation of the (100) single crystal diamond surface.

Following exposure to a hydrogen plasma for 12 hours, the (100) diamond surface was interrogated by XPS and the resulting spectrum, shown in Figure 20, is consistent with a hydrogen terminated carbon substrate. Since XPS is insensitive to hydrogen, the only peaks expected were those due to carbon and a sharp peak at 285 eV, due to electrons ejected from the carbon 1s orbital, dominates. A peak around 1223 eV due to carbon Auger electrons is also present. An oxygen 1s peak is just visible above the spectrum noise at 532 eV. This oxygen signal could be due to oxygen groups terminating a small proportion of the (100) diamond substrate or it could be due to trace contamination by oxygen-containing species, such as water, deposited on the diamond surface between hydrogen exposure and XPS analysis which have not been completely desorbed by the UHV analysis environment.

In order to provide carbonyl-like reactivity on the (100) diamond surface, and potentially exploit this reactivity to tether organic molecules, it is necessary to introduce oxygen onto the surface. Heating the hydrogenated surface, analysed in Figure 20, to 640°C in 930 mbar of O₂ for 8 minutes produces an oxygenated surface as demonstrated by the XPS spectrum shown in Figure 21. Following heating in oxygen, the C 1s peak again dominates the XPS spectrum but a significant O 1s peak can be observed at 532 eV indicating an increase of oxygen on the surface. An oxygen Auger peak can also be observed at around 974 eV.

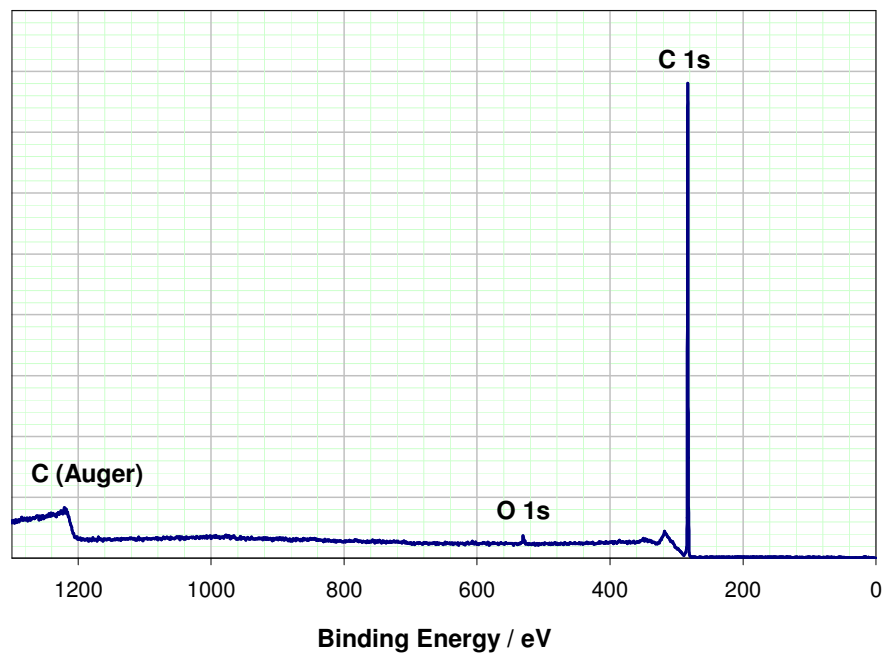


Figure 20 – The wide scan XPS spectrum obtained from the (100) diamond surface after 12 hours exposure to a hydrogen plasma.

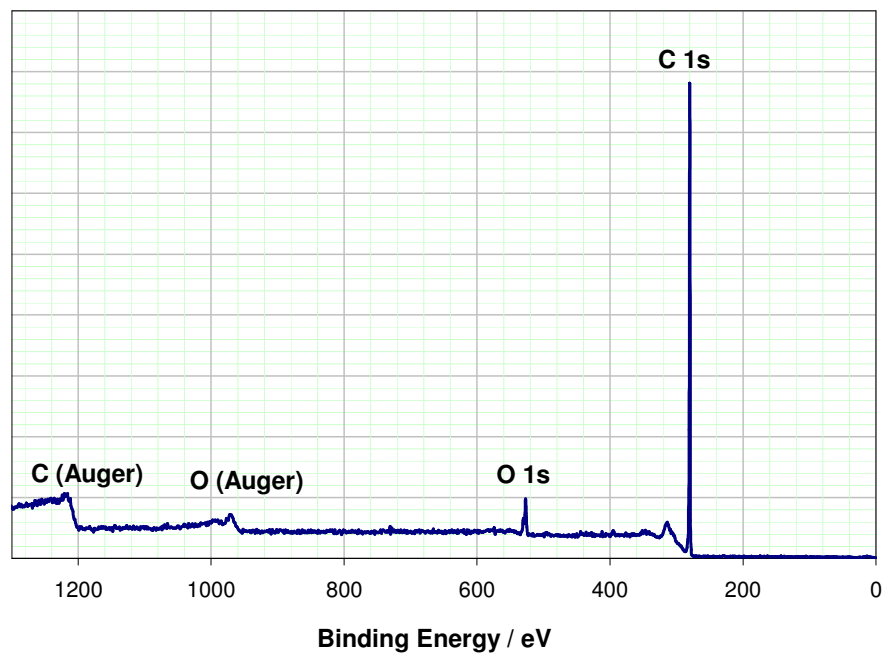


Figure 21 – The wide scan XPS spectrum resulting from analysis of a (100) diamond surface exposed to 1 atmosphere of oxygen at 600°C for 30 mins.

High resolution scans over the spectral regions of the C 1s and O 1s peaks allowed high resolution spectra and accurate peak-shapes to be obtained. Areas under XPS peaks provide information on the relative concentrations of elements present within the analysis depth. Electrons generated from different elements and different orbitals have different sensitivities to analysis by XPS so peak areas must be corrected for the sensitivity of photoelectrons from the particular orbital. Relative sensitivity factors determined on the NCESS Scienta ESCA300 for carbon and oxygen are provided in Table 2. The area under each photoelectron peak, corrected by the appropriate relative sensitivity factor, is proportional to the concentration of that element within the analysis depth.

Photoelectron	Relative sensitivity factor (RSF)
Carbon 1s	1.00
Oxygen 1s	2.80

Table 2 – Relative sensitivity factors for carbon and oxygen determined on the NCESS Scienta ESCA300 X-ray photoelectron spectrometer.

To establish if oxygen was introduced on the sample surface or in the bulk of the (100) diamond sample, the substrate was analysed at several electron take-off angles. The take-off angle (TOA) is the angle between the substrate surface and the electron analyser in the X-ray spectrometer. When this angle is small XPS is most surface sensitive and at 90° the technique probes some depth into the bulk of the sample so the relative signal from a surface layer is minimised. The data in both Figure 20 and Figure 21 were recorded with a take-off angle of 90°. Figure 22 shows the relative oxygen signal at each take-off angle studied, where:

$I_{O\ 1s}$ = the area under the O 1s photoelectron peak

$I_{C\ 1s}$ = the area under the C 1s photoelectron peak

$RSF_{O\ 1s}$ = the relative sensitivity factor for O 1s photoelectrons

$RSF_{C\ 1s}$ = the relative sensitivity factor for C 1s photoelectrons

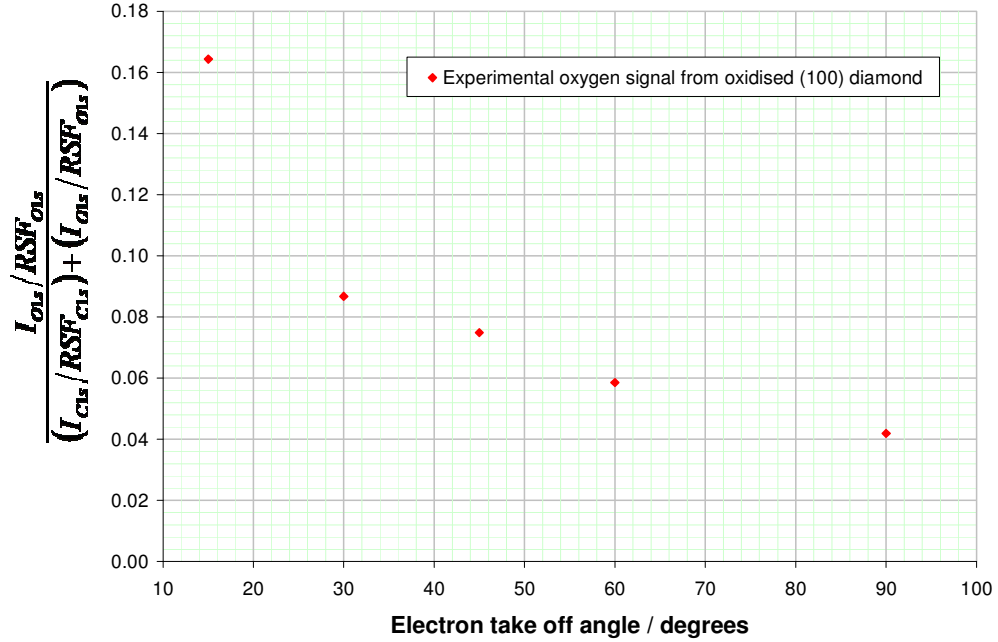


Figure 22 – Shows how the proportion of the overall XPS signal due to oxygen varies with electron take-off angle.

Figure 22 demonstrates a clear trend with an increasing contribution from oxygen to the overall signal as the take-off angle decreases. This is consistent with oxygen being present on the surface of the diamond and not distributed homogeneously throughout the diamond lattice. Thermal oxidation of a single crystal diamond would be expected to only introduce oxygen at or near the surface and not incorporate it into the bulk lattice.

Quantitative analysis of XPS data is not trivial. However, it is desirable to quantify the oxygen levels on (100) diamond surfaces. Considering a fractional monolayer of oxygen atoms on a diamond surface; the intensity (I_{O1s}) of the O 1s signal in the XPS spectrum can be written as⁹⁵:

$$I_{O1s} = K A N_A^O T_{O1s} \sigma_{O1s} \quad (2)$$

where:

K = instrumental factors

A = area sampled by the XPS experiment

N_A^O = the number of oxygen atoms per unit area on the diamond surface

T_{O1s} = the transmission of the XP spectrometer at the energy of O 1s electrons

σ_{O1s} = O 1s photoionisation cross section

if it is assumed that there is no attenuation of the O 1s signal by the oxygen monolayer itself.

The intensity (I_{C1s}) of the C 1s signal from the diamond substrate can be written as:

$$I_{C1s} = K A N_V^C T_{C1s} \sigma_{C1s} \int_0^\infty \left\{ e^{\frac{-z}{\lambda_C(E_{C1s}) \cos \theta}} \right\} dz \quad (3)$$

where:

K and A have the meanings defined for equation (2)

T_{C1s} = the transmission of the XP spectrometer at the energy of C 1s electrons

σ_{C1s} = C 1s photoionisation cross section

N_V^C = the number of carbon atoms per unit volume in diamond.

z = depth into the diamond substrate

θ = the analysis angle (90 – TOA)

$\lambda_C(E_{C1s})$ = attenuation length of C 1s electrons in diamond.

The integral term provides the total signal from the whole diamond depth, allowing for the exponential signal decay with depth. It is assumed that there is no attenuation of the C 1s signal by the oxygen monolayer.

The C 1s signal intensity, by solving equation (3) is therefore:

$$I_{C1s} = K A N_V^C T_{C1s} \sigma_{C1s} \lambda_C(E_{C1s}) \cos \theta \quad (4)$$

The ratio of the O 1s to C 1s signal is:

$$\frac{I_{O1s}}{I_{C1s}} = \frac{K A N_A^O T_{O1s} \sigma_{O1s}}{K A N_V^C T_{C1s} \sigma_{C1s} \lambda_C(E_{C1s}) \cos \theta} \quad (5)$$

Rearranging gives:

$$\frac{I_{O1s}}{I_{C1s}} = \frac{N_A^O}{N_V^C} \frac{T_{O1s} \sigma_{O1s}}{T_{C1s} \sigma_{C1s}} \frac{1}{\lambda_C(E_{C1s}) \cos \theta} \quad (6)$$

N_A^C = the number of carbon atoms per unit area on the diamond surface; considering the top layer of carbon atoms (i.e. the top 0.089 nm⁹³) on a (100) diamond surface. This is also the theoretical number of sites per unit area where attachment of oxygen atoms is possible.

Introducing this to equation (6) as $\frac{N_A^O}{N_A^C}$ gives:

$$\frac{I_{O1s}}{I_{C1s}} = \frac{N_A^O}{N_A^C} \frac{N_A^C}{N_V^C} \frac{T_{O1s} \sigma_{O1s}}{T_{C1s} \sigma_{C1s}} \frac{1}{\lambda_C(E_{C1s}) \cos \theta} \quad (7)$$

where $\frac{N_A^O}{N_A^C}$, the ratio of the number of oxygen atoms per unit area to the number of possible sites for oxygen atom attachment per unit area, is the fractional oxygen monolayer coverage (Φ).

and $\frac{N_A^C}{N_V^C}$, the number of carbon atoms per unit area divided by the number of carbon atoms per unit volume, is the thickness of a diamond monolayer (d).

$\frac{T_{O1s} \sigma_{O1s}}{T_{C1s} \sigma_{C1s}}$ can be taken as the ratio of the relative sensitivity factors $\frac{RSF_{O1s}}{RSF_{C1s}}$.

Equation (7) can therefore be re-written as:

$$\frac{I_{O1s}}{I_{C1s}} = \Phi \frac{RSF_{O1s}}{RSF_{C1s}} \frac{d}{\lambda_C(E_{C1s}) \cos \theta} \quad (8)$$

By rearranging, the fractional monolayer coverage of oxygen on a (100) diamond surface is given by⁹⁵:

$$\Phi = \frac{I_{O1s}/RSF_{O1s}}{I_{C1s}/RSF_{C1s}} \frac{\lambda_C(E_{C1s}) \cos \theta}{d} \quad (9)$$

To solve equation (9), in addition to the measured C 1s and O 1s XPS signal intensities and tabulated relative sensitivity factors, values for the thickness of a diamond monolayer (d) and the attenuation length of a C 1s electron in diamond are required. The value of d may be taken as 0.089 nm, the monoatomic step height on the surface of (100) diamond⁹³. Values of electron attenuation length are routinely provided by electron inelastic mean free path (IMFP) values⁹⁶ in chemical analysis of surfaces by electron spectroscopic techniques.

Empirical equations exist which allow calculation of IMFP values, for example the TPP-2M equation derived by Tanuma et al⁹⁷, the G-1 equation developed by Gries⁹⁸ and a set of equations published by Seah and Dench⁹⁶. These provide approximations which are a ‘best-fit’ to IMFP values calculated from experimental data and can be used to estimate IMFP values in materials where no experimental data exists. After publication of these predictive equations, the electron IMFP in diamond was calculated directly from optical experimental data by Tanuma et al⁹⁹ and confirmed by elastic peak electron spectroscopy and Monte Carlo simulations¹⁰⁰. This experimentally determined value and those estimated by the three empirical equations are shown in Table 3 for electron energies as close as possible to 1202 eV, corresponding to the kinetic energy of electrons ejected from the C 1s orbital (Excitation energy – binding energy = kinetic energy, 1486.7 eV – 284.5 eV = 1202.2 eV).

Method	IMFP / nm
Seah et al equation set ^{96, 101}	1.07
G-1 equation ^{98, 102}	1.18
TPP-2M equation ⁹⁹	3.30
Experimentally determined ^{99, 100}	1.88

Table 3 – IMFP values of electrons of E = 1200 eV in diamond by various methods.

It can be seen in Table 3 that the IMFP values estimated by the three empirical equations do not give good agreement with the experimentally determined value. Tanuma et al⁹⁹ investigated the discrepancy between the experimental IMFP and the value predicted by their TPP-2M equation and concluded that it highlighted a limitation of their model. The IMFP value of 1.88 nm provides a value for the electron attenuation length in diamond which can be used in equation (9). Having defined suitable values

for the constants d and λ , the experimentally measured C 1s and O 1s signals at each take off angle can be used to calculate the fractional monolayer coverage of oxygen on the oxidised (100) diamond surface from equation (9). The monolayer coverage values (Φ) thus determined are given in Table 4.

TOA / °	Φ / monolayers
90	0.92
60	1.14
45	1.21
30	1.00
15	1.08
Average \pm Standard deviation = 1.07 \pm 0.11 monolayers	

Table 4 – Values of the fractional monolayer coverage (Φ) of oxygen on oxidised (100) diamond, determined at various electron take-off angles. The average value and standard deviation are also shown.

The relative intensity of the O 1s and C1s XPS signals detected from an oxidised (100) diamond substrate appear to be consistent with the formation of close to one complete oxygen monolayer on the (100) diamond surface. The values obtained from the data gathered at different electron take-off angles show some scatter. This can be represented by the average value and standard deviation. This variation may be due to experimental error or may reflect the difficulty in being absolutely consistent when applying baselines to C 1s and O 1s peaks in order to be able to measure the peak areas.

An additional source of error occurred in the derivation of equation (9) when it was assumed that the oxygen monolayer did not attenuate either the O 1s or C 1s signal. An estimation of the error introduced by this assumption can be made. When a thickness of material (d) attenuates the signal from a substrate beneath the measured substrate signal is given by:^{103, 104}

$$I = I^{\infty} e^{\left(\frac{-d}{\lambda \cos \theta}\right)} \quad (10)$$

where:

I = the attenuated signal from the substrate

I^∞ = the signal from the substrate if no attenuation took place

d = the thickness of material causing attenuation

θ = the analysis angle (90 – TOA)

λ = the electron attenuation length

The experimentally measured C 1s and O 1s intensities are attenuated by the oxygen overlayer and therefore provide values of I . For simplicity, the derivation of equation (9) assumed that the measured intensities give I^∞ , the signal when no attenuation occurs. Table 5 indicates that when $d = 0.089$ nm and $\lambda = 1.88$ nm, there is a discrepancy of 5 – 17% between I and I^∞ depending on the electron take-off angle.

TOA / °	Θ / °	I/I^∞	% Error
90	0	0.95	5
60	30	0.95	5
45	45	0.94	6
30	60	0.91	9
15	75	0.83	17

Table 5 – The error introduced by neglecting attenuation by the oxygen overlayer in derivation of equation (9) at electron take-off angles used experimentally.

The dependence of equation (10) on analysis angle means that the error introduced by the simplifying assumptions in equation (9) increases as the electron take-off angle decreases. The largest error of 17% is introduced when C 1s and O 1s intensities are measured at 15° TOA. If an error of 17% exists on both the C 1s and O 1s signals, combining this by summation in quadrature results in an error of 24% being introduced to the fractional monolayer coverage (Φ) value. The error caused by neglecting XPS signal attenuation by oxygen is therefore much larger than the error introduced by experimental factors or baseline consistency. The fractional monolayer coverage of oxygen on an oxidised (100) diamond substrate is more reasonably described as 1.07 ± 0.26 monolayers. It should be noted, however, that the largest source of error may be the value chosen for the electron attenuation length. Here the experimentally determined inelastic mean free path length in diamond has been adopted despite widely

differing values being predicted by empirical equations. Additionally, while inelastic mean free path values are routinely used to provide values of attenuation length in surface analysis, differences exist in the definitions of the two terms, meaning the use of the IMFP value in equation (9) may introduce a discrepancy from the true situation.

The high-resolution spectra collected revealed detail in the shape of the C 1s and O 1s peaks. The binding energy of a core electron in an atom is affected by the chemical environment of the atom. Neighbouring chemical groups which decrease the valence electron density around an atom cause the core electrons to experience a greater effective nuclear charge and a shift to higher binding energy will be observed in the spectrum. For example, a C 1s photoelectron from a carbon atom bound to two adjacent carbon atoms and one, more electronegative, oxygen atom will display a higher binding energy than a photoelectron from a carbon atom bound to four adjacent carbon atoms. It is therefore possible to de-convolute high-resolution XPS peaks into component peaks and hence gain information on the chemical environments of atoms in the substrate.

Peak fitting of C 1s peak shapes obtained by analysis of hydrogenated and oxidised (100) diamond was performed by fitting a number of component peaks using software supplied by the XPS manufacturer¹⁰⁵. This required defining a linear or Shirley background function for the peak, introducing a specific number of component peaks and allowing the software to iteratively optimise the attributes of the component peaks until a least squares best fit to the data was achieved. For each component peak a number of parameters; peak position, width (FWHM), area, symmetry and Gaussian-Lorentzian mix, were specified and could be fixed or allowed to vary within the optimisation routine. The theory of X-ray photoelectron spectra peak shapes and the fitting thereof are discussed in detail in a range of books^{88, 104, 106} and papers¹⁰⁷⁻¹¹⁰ and so the fundamental physical effects which the peak-fitting parameters attempt to model will not be discussed in detail here. However, since these parameters are inputs to a purely mathematical fitting routine, it is necessary to ensure that chemically 'sensible' values or ranges are adopted in order for the resulting component peaks to be chemically meaningful. The number of peaks and their approximate positions was estimated from component peaks previously identified in literature on hydrogenated and oxidised diamond surfaces, as illustrated in Table 6. Peak widths and areas were estimated from the shape of the convoluted envelope. The range of allowed values for the peak asymmetry parameter and Gaussian-Lorentzian mix were ≤ 0.20 and ≥ 0.70

respectively. These were adopted having been identified as physically reasonable by Beamson and Briggs⁸⁸ over the fitting of many core line envelopes obtained experimentally on the same instrument used in this study.

For hydrogenated (100) diamond, analysed at both 90° and 30° take off angles, it was found that a good fit to the shape of the C 1s envelope could be obtained by fitting only two peaks, the main bulk peak and one shifted by 0.4 eV to higher binding energy. Such a peak has previously been observed on diamond and assigned to hydrocarbon-like carbon atoms terminated with hydrogen on the diamond surface.^{111,112}

C=O (carbonyl)	C-O (ether)	C-H (hydrocarbon)	C=C (graphitic)	Reference
+ 1.8 – 2.4	+ 0.8 – 1.6	+ 0.5 – 0.7	- 0.6 – 1.0	23
+ 2.6 – 2.9	+ 1.2 – 1.6	-	- 1.7	113
+ 3.6	+ 1.2 – 1.9	+ 0.5	- 1.3	114
+ 2.2	+ 1.1	+ 0.4	- 0.8	This work

Table 6 – Ranges or values of binding energy shift, in eV relative to the bulk C 1s peak, assigned to fitted component C 1s peaks in various XPS studies of diamond.

Achieving a fit to C 1s envelopes obtained from oxidised (100) single-crystal diamond, at both 90° and 15° take off angles, required three component peaks in addition to the bulk C 1s peak. The chemical shifts, relative to the bulk peak, of these component peaks, denoted carbonyl, ether and graphitic, are detailed in Table 6. The ‘hydrocarbon’ peak could not be reliably fitted under C 1s peaks obtained from oxidised (100) diamond surfaces, consistent with the removal of all hydrogen from the surface and its replacement by a monolayer of oxygen. Two peaks shifted to higher binding energy were required on oxidised diamond surfaces. Consistent with previous assignments on diamond^{23, 113, 114}, the peak shifted 1.1 eV from the bulk peak was ascribed to surface carbon atoms bound to three adjacent carbon atoms and with a single bond to an ether-like bridging oxygen. The peak shifted 2.2 eV from the bulk peak was assigned to surface carbon atoms bound to two adjacent carbon atoms and double bonded in a carbonyl-like configuration to an oxygen atom. The shape of the C 1s core line envelope observed on oxidised (100) single crystal diamond did not suggest the

presence of peaks due to carbon bonded in a carboxyl-like configuration (i.e. to two oxygen atoms) and such a component peak could not be reasonably included in the fit.

On oxidised surfaces, fitting of one peak shifted by 0.8 eV to lower binding energy than the bulk C 1s component was required. Peaks shifted to lower binding energy than the bulk peak have been previously observed upon annealing of hydrogenated diamond surfaces.^{111, 112, 115} Upon annealing above 900°C a peak at around -1 eV (relative to the bulk carbon peak) was attributed to π -bonded atoms on the reconstructed (2 x 1) dimer surface. At increased temperatures the peak shifted still further to lower binding energy and has been attributed to the onset of graphitisation of the diamond surface.^{112, 115} Peaks shifted to low binding energy of the bulk C 1s peak have also been observed in spectra of diamond surfaces oxidised by plasma treatment.^{114, 116} Whilst not fully understood or explained these have been attributed to defects, possibly related to the onset of graphitisation of the diamond surface¹¹⁴. Figure 24 demonstrates that a significant ‘graphitic’ peak was observed following thermal oxidation of the (100) diamond substrate. Some surface carbon atoms, such as those at step edges, may not be fully coordinated and therefore may give rise to this peak.

The component peaks resulting from curve fitting of the C 1s envelope obtained by analysis of hydrogenated and oxidised (100) single crystal diamond in this study are categorised in Table 6. The same descriptors are used to label the peaks in Figure 23 and Figure 24 which show expanded regions at the base of the C 1s peak obtained (at TOA = 90°) from hydrogen and oxygen terminated surfaces respectively, and the fitted component peaks in each case. In Figure 24 the area under the carbonyl and ether peaks represents the proportion of oxygen which has been incorporated into the diamond surface in an on-top, carbonyl-like and bridging, ether-like configuration. The ratio of the peak areas indicates that 64% of the diamond surface is covered with carbonyl-like groups and 36% with bridging oxygen moieties. The high resolution C 1s envelope obtained from the oxidised surface at an electron take-off angle of 15° was analysed in a similar fashion and the area under the carbonyl component peak indicated that 68% of the (100) diamond surface was terminated with carbonyl oxygen. Such an analysis was not undertaken at each electron take-off angle to allow an estimation of the error introduced into the result by experimental factors and peak fitting however the data provides compelling evidence that around two thirds of the oxidised (100) diamond surface is terminated with carbonyl-like groups.

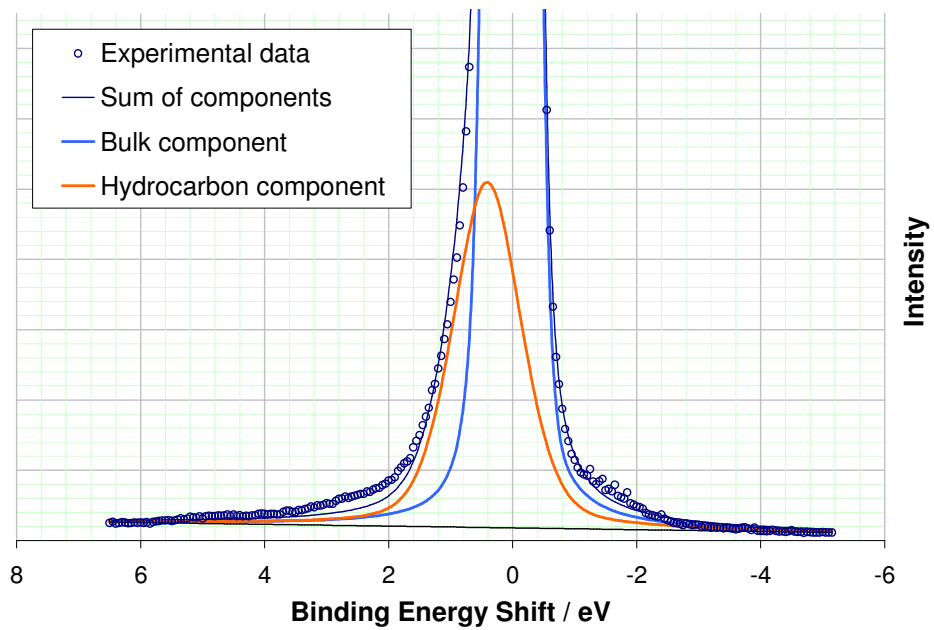


Figure 23 – The experimental C 1s envelope and fitted component peaks obtained from analysis of a hydrogenated (100) diamond surface at TOA = 90°. Binding energy shifts are quoted relative to the position of the bulk carbon peak.

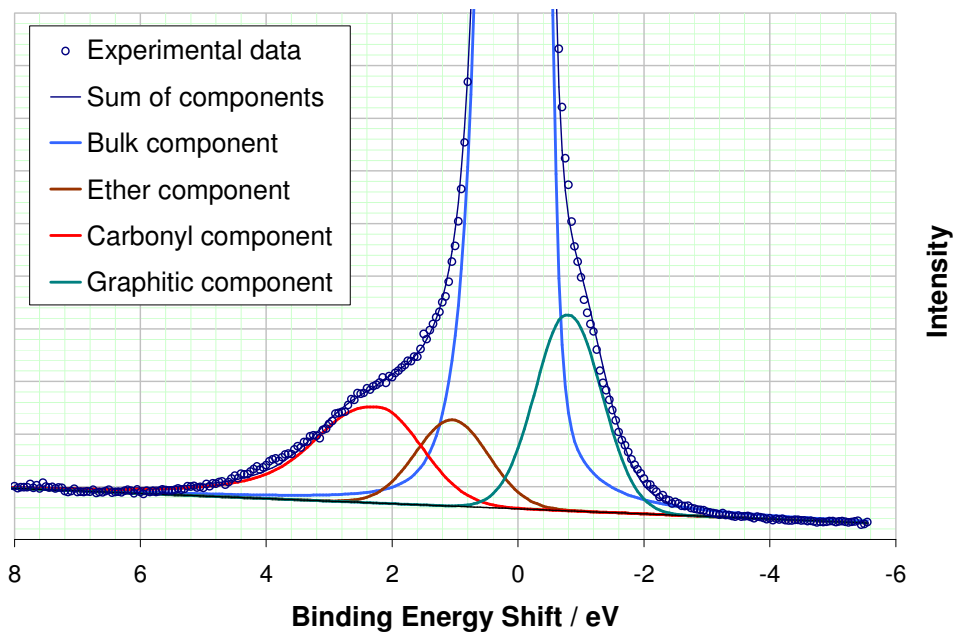


Figure 24 – The experimental C 1s envelope and fitted component peaks obtained from analysis of an oxidised (100) diamond surface at TOA = 90°. Binding energy shifts are quoted relative to the position of the bulk carbon peak.

The ultimate aim of the experiments was to generate a diamond surface capable of reacting with amine reagents in a reaction analogous with nucleophilic attack on a ketone. To achieve this, the maximum number of carbonyl groups on the diamond surface was desired. Peak fitting of the C 1s band envelope indicates that around two-thirds of the diamond surface has been successfully terminated with 'on-top' oxygen in a carbonyl configuration. When dealing with data derived from peak fitting however, one must be aware of the limitations of the approach. The requirement to produce a chemically meaningful result by careful choice of parameters, ranges and limits inevitably means the approach is strongly susceptible to subjective influence. In an attempt to test the veracity of the conclusion that the majority of oxygen on the diamond surface is bound in a carbonyl configuration, high-resolution scans of the O 1s region were analysed. While this region of X-ray photoelectron spectra obtained from diamond is much less well studied than the C 1s region, differences may still be evident if oxygen is present in a variety of chemical environments.

The shape of the O 1s envelope obtained by XPS analysis of an oxidised single crystal (100) diamond substrate at an electron take off angle of 90° is shown in Figure 25. The envelope clearly comprises at least two component photoelectron peaks. It is most likely that the two dominant O 1s component peaks are due to electron emission from oxygen bound in an ether configuration and oxygen bound in a carbonyl configuration on the (100) diamond surface. Unfortunately binding energy shifts of oxygen atoms on diamond surfaces have not been published. Despite this omission, such shifts are quoted in analyses of organic polymers and on other carbonaceous substrates and a selection are shown in Table 7. It is clear that peaks due to photoelectron emission from oxygen bound in a carbonyl group generally occur at a lower binding energy than those due to oxygen bound in ether groupings. The binding energy shift between the two peaks varies from around only 0.32 eV in aliphatic polymers to around 2.0 eV in aromatic polymers and graphite. The binding energy shift observed on oxidised (100) single crystal diamond in this work is 3.7 eV which is notably higher than that observed on the other substrates. It may be that some particular property of the highly regular diamond surface gives rise to a large binding energy shift between peaks due to oxygen functionalities. In order to establish definitively the origin of, and relationship between, the two peaks identified in Figure 25 further investigation would be required. However, as the data in Table 7 suggests peaks due to carbonyl-group oxygen appear at lower

binding energy than peaks due to ether-linkage oxygen atoms, it is possible to infer that the component peaks in Figure 25 are due to oxygen present in these two groupings on the diamond surface.

Substrate	C-O-C (ether)	C=O (carbonyl)	Reference
Aliphatic polymers	532.83 – 532.47	532.37 – 532.30	88
Aromatic polymers	533.45 – 532.98	531.25	88
Carbon fibre	533.4 – 532.2	531.6 – 531.2	117
Graphite	533.1	531.3	118
Diamond	531.8	528.1	This work

Table 7 - Ranges or values of binding energy, in eV, assigned to ether and carbonyl O 1s component peaks in various studies of oxygen containing carbonaceous substrates.

Peaks were fitted to the O 1s envelope by the same routine used for C 1s peak fitting; the number, position, width and area of peaks were estimated from the convoluted envelope and the range of allowed values for the peak asymmetry parameter and Gaussian-Lorentzian mix were ≤ 0.20 and ≥ 0.70 respectively.

Figure 25 shows the high resolution O 1s envelope obtained on analysis of the oxidised (100) diamond surface at 90° electron take-off angle and the peaks resulting from peak fitting. The area under the low binding energy O 1s peak, attributed to carbonyl oxygen, makes up 72% of the total O 1s peak, indicating that 72% of the diamond surface may be terminated with carbonyl-like groups. Curve fitting of the C 1s peak in the same spectrum suggested 64% of the diamond surface was carbonyl terminated. Fitting the O 1s peak obtained with an electron take off angle of 15° in the same way and comparing the area under each peak suggested as much as 87% of the (100) diamond surface was terminated with carbonyl groups. Peak fitting and analysis of the O 1s peak was not carried out at other electron take-off angles therefore an indication of the error in the values obtained for the proportion of oxygen bound in a carbonyl configuration could not be estimated. However, analysis of O 1s peaks obtained at 90° and 15° take-off angles suggest that at least two thirds of the oxygen present on the oxidised (100) diamond surface is present in an on-top, carbonyl-like configuration.

However an alternative explanation for the presence of two peaks in the high resolution O 1s envelope obtained on analysing oxidised (100) diamond should also be considered. One of the peaks identified may be due to oxygen chemisorbed to the diamond surface and the other may result from detection of physisorbed water, or methanol solvent, on the surface.

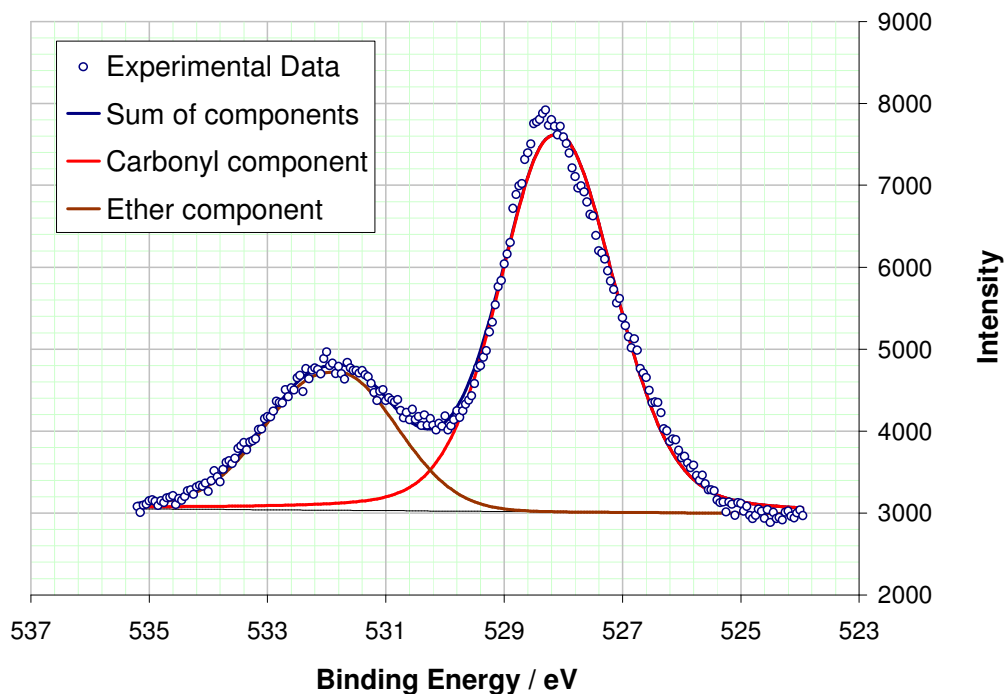


Figure 25 - The experimental O 1s envelope and fitted component peaks obtained from analysis of an oxidised (100) diamond surface at TOA = 90°.

The XPS data obtained from (100) single crystal diamond substrates confirm that oxidation at 640°C under 930 mbar O₂ for 8 minutes terminates the surface with a monolayer of oxygen. The data further suggests that around two thirds of the surface is terminated with carbonyl-like ‘on-top’ oxygen and the remainder with ether-like ‘bridging’ oxygen atoms. The results of curve fitting the C 1s and O 1s peaks agree sufficiently well to give confidence in the results obtained from curve fitting.

2.3.5 Oxidative etching of the (100) single crystal diamond surface.

Exposure of the 'as received' (100) diamond plate to a hydrogen plasma smoothed it and produced a high quality (100) surface. Oxidation of the (100) single crystal diamond at a substrate temperature of 640 °C under 930 mbar of O₂ for 8 minutes was sufficient to terminate the surface with oxygen as clearly demonstrated by the XPS evidence. The purpose of the oxidation step was to introduce the maximum concentration of carbonyl groupings which could act as reactive sites for nucleophilic coupling agents such as amines.

To investigate whether the (100) diamond surface morphology was affected by prolonged oxidation, a (100) single crystal diamond sample was exposed to the oxidising environment for an extended period and the sample surface periodically interrogated by optical microscopy and AFM. SEM analysis was attempted but high resolution images could not be obtained due to the insulating nature of the oxidised diamond. A deep groove or trench in the diamond surface, presumably imparted by polishing after manufacture by the supplier, was used as a marker for collection of the optical microscope and AFM images over the same area. In this way the morphological changes of the same area of (100) diamond could be observed with etching time. Figure 26 shows the area of (100) diamond surface interrogated relative to the crystal planes and the optical microscope images of the surface obtained after different periods of exposure to gaseous O₂ at 600°C.

The optical microscope images shown in Figure 26 (A-E) reveal an area of the (100) diamond surface approximately 300 x 200 μm. In image Figure 26 A it is clear that the surface is not atomically smooth over the whole of that area. In addition to the deep polishing groove used to repeatedly identify the area, a linear feature is clear running at approximately 45° from the corner of the polishing groove to the top right hand corner of the image and a number of small black spots can be seen across the image indicating imperfections in or below the (100) diamond surface. Between these features, however, wide uniform areas are revealed at this magnification.

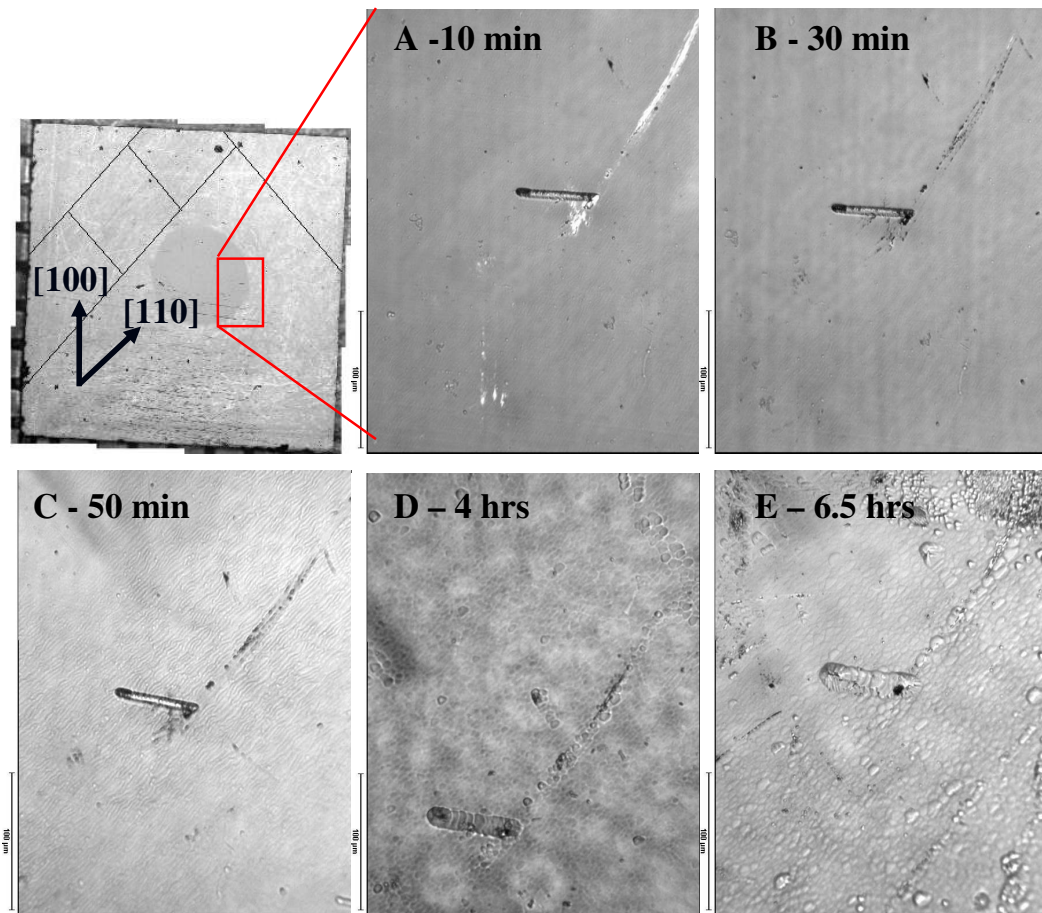


Figure 26 – Optical microscope images of the (100) single crystal diamond surface. The first image shows the whole of the sample surface, indicating the direction of the crystal planes and the approximate region shown at greater magnification in the other images. Images A-E show the same region of the substrate following exposure to 1 atmosphere of oxygen at 600°C for the cumulative time indicated on each image. The scale bar beside images A-E represents 100µm in each case.

After 50 minutes of exposure to the oxidising environment the whole area of the microscope image (Figure 26 C) can be seen to be covered with ridges running diagonally across the image from bottom left to top right. The direction of the ridges appears to be coincident with the [110] direction, although locally each ridge is not perfectly straight but instead has a wave-like appearance. Closer inspection of the images collected at shorter exposure times reveals some evidence of ridges, even in image Figure 26 A where evidence of faint ridges can be seen in the areas between more prominent features. After exposure to the oxidising environment for longer periods the (100) diamond surface morphology changed. In images Figure 26 D and E the ridge structure has broken up to give what appear to be shallow pits arranged in a regular, ‘brick work’ structure across the whole surface. The general appearance of the surface

is of rectangular pits with their long edges running from the bottom left to the top right of the images consistent with the direction of the ridges. Close inspection of individual pits reveals that, just as the ridges were not perfectly straight, the pits are not exactly rectangular in shape.

After each period of oxidation, images of the (100) diamond surface were collected by contact mode atomic force microscopy. These images were gathered from the same area of the surface photographed with the optical microscope by navigating back to the unique surface groove. Figure 27 shows images of the surface collected after each oxidation period. In each case, image (i) shows a 100 x 100 μm area of the surface containing the polishing groove and image (ii) a 20 x 20 μm image collected as closely as possible from the same region of the surface each time.

Figure 27 – A(ii) confirms that grooves running diagonally across the sample in the direction of [110] were evident on the (100) diamond surface after the shortest period of exposure to the oxidising environment. The grooved features become more prominent as the oxidation time increases through 30 to 50 minutes (Figure 27 – B and C).

After significantly increasing the oxidation time to 4 hours it became very difficult to obtain clear AFM images of the diamond surface and it can be seen that Figure 27 – D(i) and Figure 27 – D(ii) provide little information on the morphology of the surface. It was after this period of oxidation that optical microscopy revealed the broken pitted structure of the (100) diamond surface. At this time the appearance of many small square features across AFM images indicated problems with wear of the AFM tip introducing artefacts in the collected image as highlighted in the experimental section. The image in Figure 27 – E(i) was obtained following oxidation of the surface for 6.5 hours with a new AFM tip and so should provide an accurate representation of the surface morphology. The surface roughness value ($R_a = 57 \text{ nm}$) is significantly higher than those obtained from Figure 27 – A(i) to C(i) ($R_a \sim 20 \text{ nm}$) and indicates that oxidation for extended periods has caused roughening of the surface. Evidence for the abrasive nature of the diamond surface in this state was confirmed by Figure 27 - E(ii). This was obtained using the same new AFM tip as Figure 27 – E(i) however several scans of the surface had been carried out in between times which had been sufficient to wear the sharp tip down to a flat square end and introduce the regular square artefacts present in Figure 27 - E(ii).

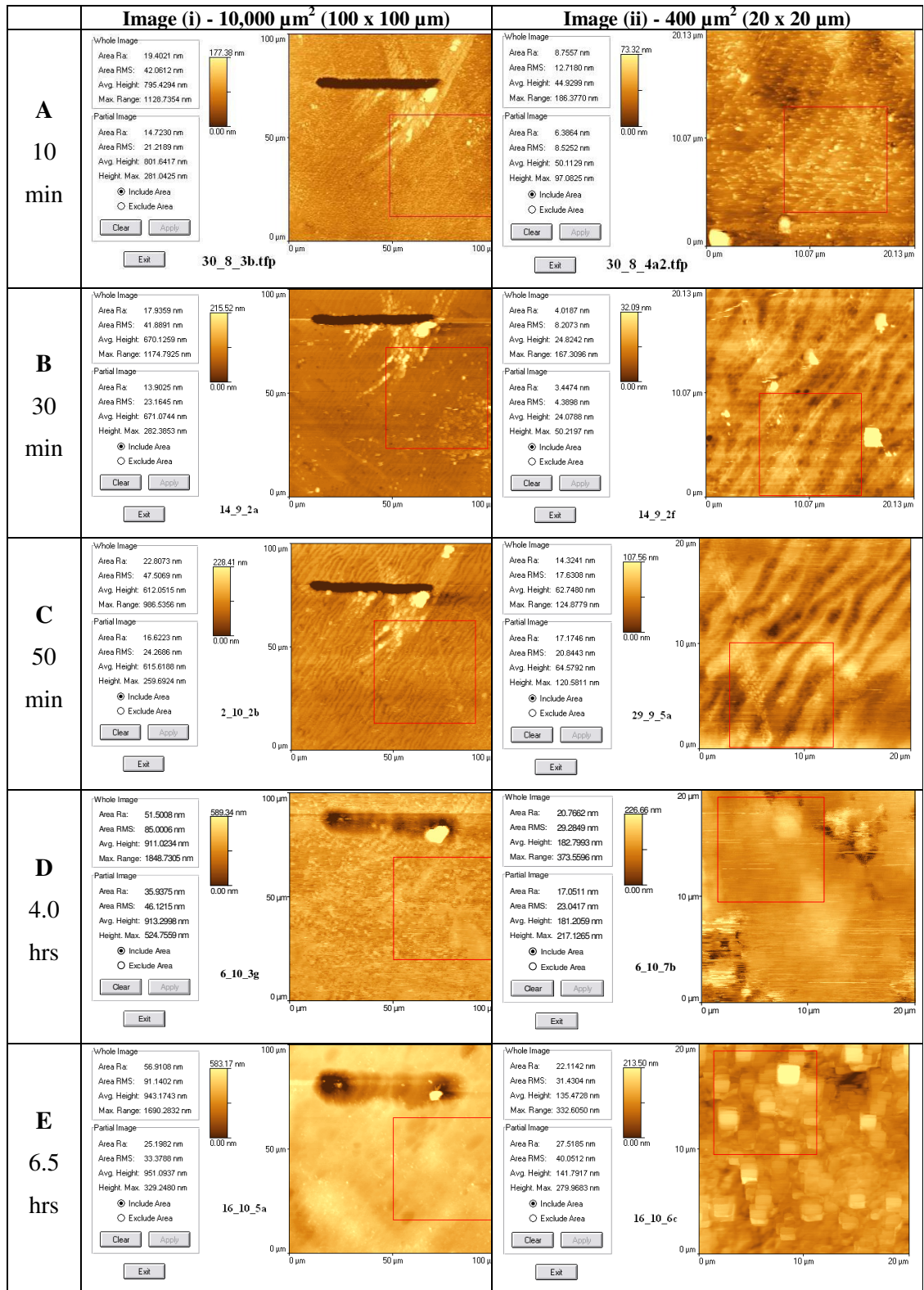


Figure 27 - AFM images of the (100) diamond surface after increasing duration of oxidation. Image (i) shows a 100 x 100 μm area of the surface containing the polishing groove. Image (ii) shows a 20 x 20 μm image collected as closely as possible from the same region of the surface each time

An increase in roughness of the (100) diamond surface with oxidation time, evidenced by the AFM data, is consistent with the surface morphology change observed by optical microscopy. In addition to the clear increase in size of the polishing groove used to identify the analysis area, roughening indicates that under the oxidation conditions used (600 °C, 1 atm, O₂) material is removed from the (100) diamond surface by oxidative etching.

Ridges, very similar in appearance to those observed in this study, have resulted from step-flow growth or hydrogen etching of (100) diamond substrates with miscut angles of around 1.5° to 3.5°^{29, 38, 39}. From the experimental reports and theoretical calculations highlighted earlier a strong argument can be made that the thermal oxidation of (100) diamond surfaces occurs by an anisotropic step mechanism. Oxygen stabilisation of terrace atoms results in etching occurring preferentially at defects and surface sites such as steps. Steps on (100) diamond tend to occur parallel to the <100> direction^{39, 119}. It therefore seems likely that the observed ridges, aligned in a [110] direction on an oxidised (100) diamond substrate, result from oxidation of <100> steps on the (100) surface.

Under the experimental conditions used the atomic force microscope was not expected to have sufficient resolution to identify single or double atomic height steps on the (100) diamond substrate. In order for the steps to become sufficiently large to be detected by the AFM and observed by optical microscopy, bunching of steps to form macro-steps must have occurred. Performing a line analysis of AFM data perpendicular to the ridge length direction reveals a cross-section through the AFM image which can be used to determine ridge heights and the inter-ridge distance. Figure 28 shows example line analyses of 20 x 20 µm scans made in the same region of the surface following etching of 10, 30 and 50 minutes. In each case the blue line on the AFM image at the right shows the line of data being analysed. The two images at the left show the height profile of the surface along that line. The markers along the line indicate the points between which the distances and heights are measured. For each of the three line analyses, the upper left image has the markers positioned to measure the trough to trough distance between steps and the distances are quantified in the adjacent blue box. The lower left image in each case has the markers positioned to measure the peak to trough height of the steps, again quantified in the adjacent blue box.

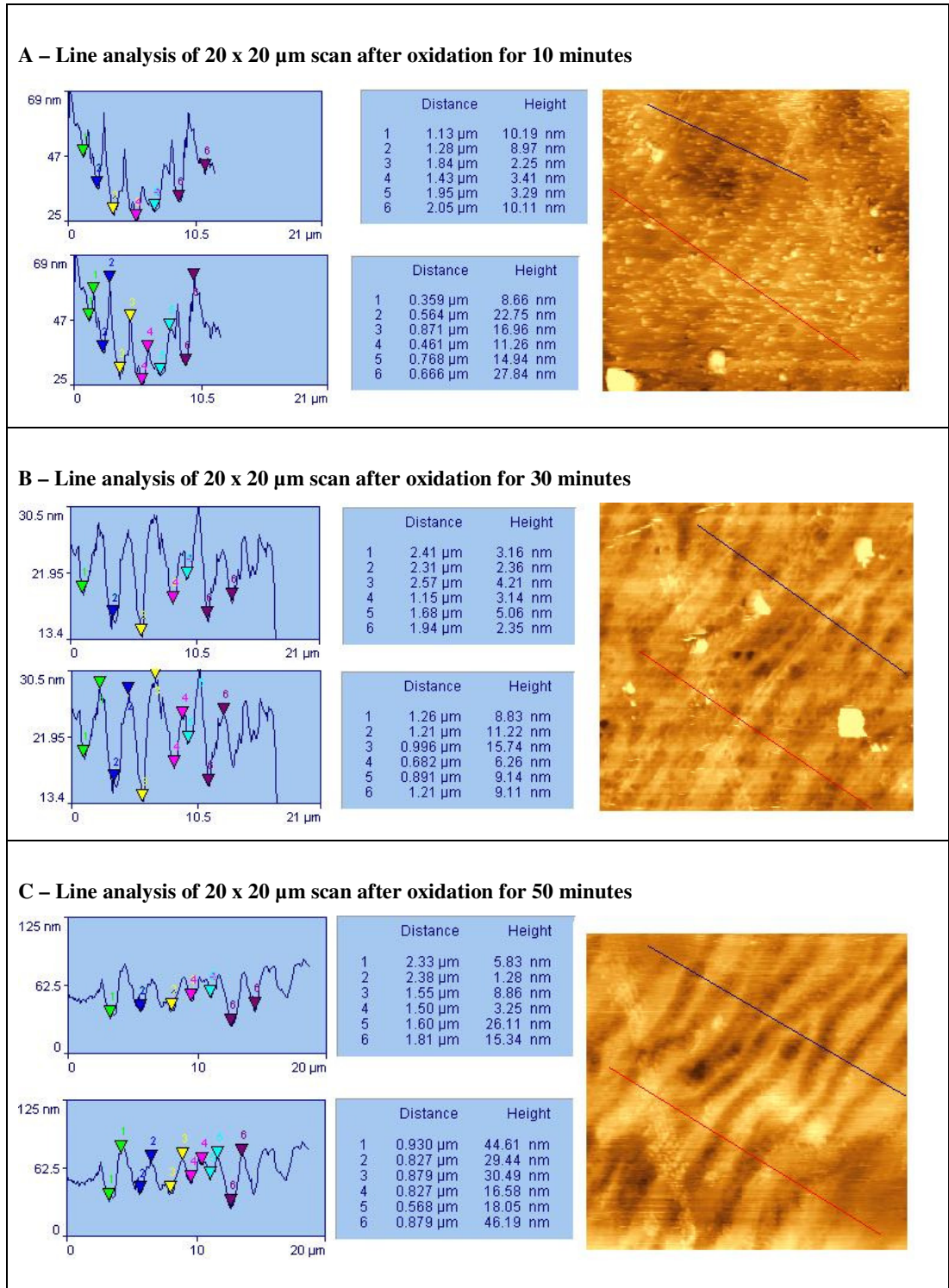


Figure 28 – 20 x 20 μm AFM scans of the (100) diamond substrate after periods of oxidation. The blue line on each image is analysed to give trough-trough distances between ridges (upper line scan and data in each image) and ridge heights (lower line scan and data) from approximately the same area of sample after each oxidation period.

It is clear from Figure 28 that step heights and terrace widths are not uniform even within each image. This is to be expected however as, by its very nature, step bunching requires migrating steps to encounter, be pinned by and eventually overcome impurities in the terrace in front of them. A heterogeneous distribution of impurities in the diamond crystal and variations in the time each step may take to pass an impurity will result in a very non-uniform surface. To identify if any general trend may be observed in the evolution of the steps with time the average step height and terrace width from each image in Figure 28 are shown below in Table 8. While there does not seem to be a significant change in the terrace widths after longer periods of etching the average step height from this very limited data set does appear to increase after 50 minutes of etching. An increase in step height with time could be explained by more steps migrating across the surface and becoming pinned by a macrostep, further building the step height. The ridges became distinctly more noticeable in both AFM analysis and optical microscope images after the etch time was increased from 30 to 50 minutes which agrees well with the measured increase in step height.

Etch time	Average terrace width (trough – trough distance) / μm	Average step height (peak – trough height) / nm	Calculated miscut / degrees
10 minutes	1.61 ± 0.38	17.1 ± 7.2	0.61
30 minutes	2.01 ± 0.53	10.1 ± 3.2	0.29
50 minutes	1.86 ± 0.40	30.9 ± 12.6	0.95

Table 8 – Average terrace widths and step heights calculated from the data measured in Figure 28. Calculated surface misorientation angle from (100) from the averaged data.

Unfortunately the angle by which the crystal surface was misoriented from (100) (the miscut angle) was not known accurately (the specifications requested of the manufacturer were for crystals of 0° or 1°). XRD analysis of the crystal was not sufficiently precise to specify the miscut angle and could only indicate that it was less than 1° misoriented from (100). With known step heights and terrace widths it is a matter of simple trigonometry to determine the miscut angle which these suggest. Miscut angles were therefore calculated from the averaged step height and terrace width data and are shown in the last column of Table 8. With the caveats that only one line

analysis has been carried out per image and the averages are taken over a very small number of steps when the oxidative etching is, by its nature, a non-uniform process, it is still interesting to note that the calculated miscut angles all fall between 0° and 1° , in complete agreement with the XRD results.

That the steps observed on oxidatively etched (100) diamond are ‘wave-like’ and not perfectly straight is to be expected. Steps observed on surfaces generated by step growth or etching processes are often not straight. A detailed model of step migration was developed by de Theije et. al³⁹ which could allow theoretical step shapes to develop and gave good agreement with the non-linear shape of steps on their experimentally produced samples. A detailed understanding of step propagation was not the intention of this work. On a simple level however, when one section of a step becomes pinned by an impurity remote sections of the step, still open to attack by growth or etching species, may propagate past that point destroying the linearity of the step. For (100) diamond it is particularly easy to imagine individual sections of S_B steps being able to migrate independently of their adjacent segments.

It is clear in Figure 26 D and E that after etching for several hours the stepped morphology of the (100) surface has given way to a different morphology. After several hours the surface appears to comprise many small shallow pits with their long edges running in the same direction as the steps lay but with clear features running perpendicular to this giving a ‘brick-work’ like structure. Some etch pits were evident, particularly in regions which were clearly not flat in the early images, such as the ‘streak’ to the top right of the optical microscope photographs in Figure 26. Figure 29 shows an AFM image of this region following 6.5 hours of oxidative etching. The deep etch pits visible here may result from dislocations or other defects in the crystal structure. Unfortunately due to the problems of AFM tip wear closer inspection was not possible.

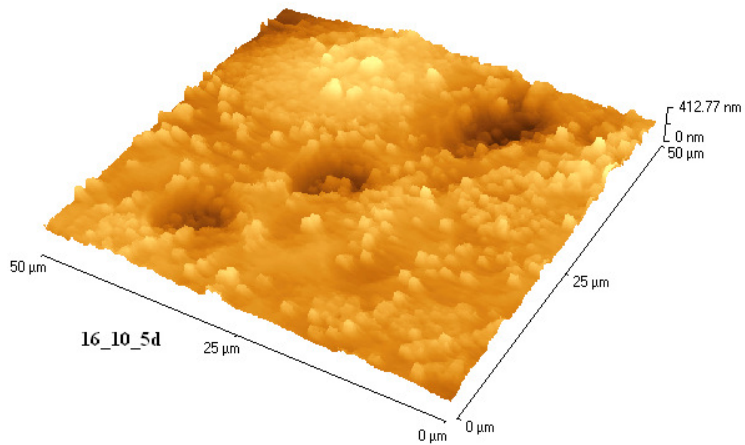


Figure 29 – 3D AFM image showing presence of etch pits on surface following 6.5 hours oxidative etching.

Such marked etch pits, however, are not representative of the shallow pits which cover the bulk of the surface and can be clearly seen in Figure 26 D and E and Figure 27 – E(i). Between larger etch pits attributed to crystal dislocations, de Theije et al.⁶⁹ found that the surface of an oxidatively etched (100) diamond was covered with small pits. These were assumed to have been introduced by agglomerated impurities or submicron inclusions in the crystal.

The pit-like features formed at long etch times in this study appear to bear too much similarity to the stepped surface which preceded them to be attributed to some alternative cause. It is instead proposed here that the pit-like features are formed by intersection of two perpendicular sets of $\langle 110 \rangle$ steps. Just as a (100) diamond crystal miscut in one $\langle 110 \rangle$ direction from (100) has an associated set of steps running across the crystal, a crystal which was miscut from (100) in two perpendicular $\langle 110 \rangle$ directions would have two sets of $\langle 110 \rangle$ steps running perpendicular to each other across the surface of the crystal. If one miscut was more significant than the other more steps and narrower terraces would exist in this direction. As the (100) surface was oxidatively etched, steps would bunch more rapidly in the direction with the higher miscut and one set of macro bunched steps would become visible. This would give rise to images like those obtained in this study after 10, 30 and 50 minutes oxidative etching. Over time, continued etching and step bunching would allow the steps associated with the lower miscut to reach a macro-height and be optically detected. At this time images of the surface would reveal two perpendicular sets of macro-steps breaking the (100)

surface up into a collection of small theoretically rectangular terraces each bounded on two sides by 'step-down' steps and by 'step-up' steps on the other two sides. Due to the non-linear nature of step propagation already discussed the shape of such features would not be uniformly rectangular.

It is proposed here that relatively defect free low miscut (100) diamond etches via the steps present on the surface. In the presence of two perpendicular miscuts this step etching causes a 'brick-work' like morphology to develop where terraces are bounded by perpendicular $\langle 100 \rangle$ steps.

2.4 Conclusions

X-ray diffraction was used to assign the faces of a single crystal diamond sample to crystallographic planes. All faces of the diamond plate were confirmed as (100) faces. The misorientation angle of the crystal surface from (100) was investigated by a novel XRD experiment conceived by the author. The diamond surface was placed in intimate contact with a (100) silicon surface and the angle through which it was required to rotate the sample to move between the Si (400) reflection and the diamond (400) reflection was measured. Deviation from the theoretical value of 25.22° indicated a miscut on either the diamond or silicon surface, or both. Variation in the exact angle reported by the spectrometer when centring repeatedly on one crystallographic plane introduced an uncertainty of almost one degree and the silicon wafer used as a reference was specified as misoriented by $0 \pm 1^\circ$. The experiment suggested any miscut of the diamond surface from (100) was small but due to the uncertainties present could only specify the misorientation angle as $0 \pm 1^\circ$. The specification requested from the manufacturer was for diamond plates misoriented from (100) by either 0° or 1° . Since no documentation was supplied to indicate the miscut of the supplied crystals this experiment was able to confirm that the crystals had a miscut in the region of that requested but not provide an accurate measurement of the miscut to less than one degree.

Smoothing of the (100) single crystal diamond surfaces was carried out by exposing the substrates to a hydrogen plasma with the surface roughness measured periodically by AFM. In situ mass spectrometry of the gas mix present just downstream from the hydrogen plasma did not detect any water vapour or O₂ but indicated the presence of hydrogen and small quantities of materials with m/z 14, 15 and 16 attributed to CH₂, CH₃, and CH₄. The carbonaceous species could be due to material etched from the diamond substrate or from the plasma chamber walls but introduced the possibility of re-deposition of carbonaceous material. AFM analysis indicated that the hydrogen plasma treatment smoothed the (100) diamond surface. The measured surface roughness (R_a) decreased from around 4.5 nm, tending to a limit of around 1.0 nm after 8 – 12 hours exposure to the plasma. No significant features such as etch pits or bunched steps were observed in the AFM images produced after 12 hours plasma exposure. The measured R_a value of 1.0 nm was an order of magnitude greater than the monoatomic step height on (100) diamond. It seems reasonable to assume that the minimum R_a value represents the limit of detection of the AFM instrument in the experimental set-up and not a limitation in the smoothness of the diamond surface which could be achieved. The mechanism of smoothing could not be elucidated from the data collected. Anisotropic etching of slightly misoriented (100) diamond by activated hydrogen would result in smoother (100) surfaces. However deposition on low miscut (100) surfaces under very low carbon concentrations has also been shown to result in smooth films^{34, 38}.

On a rough (100) diamond surface, side-walls of surface features may have non-(100) character. Smoothing the surface as far as possible by hydrogen plasma treatment produced a higher quality (100) surface. Of the low index planes of diamond, only (100) surfaces are capable of adopting carbonyl-like C=O termination on oxidation. The smooth (100) surfaces prepared therefore provided optimised substrates on which to attempt to introduce a maximum quantity of carbonyl-like C=O functionality to the diamond surface.

Exposure of hydrogenated (100) diamond surfaces to 930 mbar of O₂ gas at 640°C for 8 minutes introduced oxygen at or near the surface of the diamond which was detected by XPS analysis. The level of oxygen introduced to the (100) diamond surface by thermal oxidation was quantified based on the areas under the O 1s and C 1s peaks in high resolution XPS scans. Quantification required use of a value for the thickness of a

diamond monolayer which was taken as 0.089 nm, the single step height on a (100) diamond surface⁹³ and a value for the attenuation length of C 1s electrons in diamond, for which the experimentally determined inelastic mean free path of C 1s electrons in diamond, 1.88 nm⁹⁹, was adopted. Attenuation of the C 1s and O 1s signals by the oxygen overlayer was assumed to be negligible in the derivation of the quantification expression. This could introduce an error in the calculated monolayer coverage of up to 24%, which was greater than the experimental variation observed from repeated measurements of one oxidised surface. 24% therefore represented an estimation of the total uncertainty in any calculated oxygen monolayer coverage. Thermal oxidation of hydrogenated (100) diamond at 640°C introduced 1.07 ± 0.26 monolayers of oxygen to the diamond surface, consistent with oxygen termination of the whole (100) diamond surface with oxygen.

High resolution XPS spectra revealed detail in the shape of the C 1s peak obtained from (100) diamond. Deconvolution of the C 1s peak obtained from oxidised (100) diamond by fitting of component peaks allowed information to be obtained on the chemical environment of surface carbon atoms. Fitted peaks were based on literature parameters determined to be physically reasonable⁸⁸ with shifts in-keeping with previous XPS studies of diamond^{23, 113, 114} and peak widths and areas estimated from the shape of the convoluted envelope in order to provide a chemically meaningful result. The C 1s peak from oxidised (100) diamond was fitted to four peaks; one from the bulk diamond, one to lower binding energy than the bulk peak which has been observed in other studies^{112, 114, 115} and without full explanation been attributed to carbon atoms which are not fully coordinated or to graphitic carbon from the onset of graphitisation of the diamond, one attributed to carbon bonded to oxygen in a bridging ether-like configuration and one attributed to surface carbon atoms bound in a carbonyl-like 'on-top' configuration with oxygen. The relative area under peaks fitted to the carbonyl-like component was around twice that of the area under fitted peaks attributed to ether-like groups indicating that around twice as many >C=O groups existed on the surface as ether-like groups. This suggests that under the oxidation conditions used almost two thirds of the (100) diamond surface was terminated with carbonyl-like groups.

Examination of high resolution O 1s XPS scans of oxidised (100) diamond revealed two distinct and partially resolved peaks. In-keeping with the analysis of high resolution C 1s peaks it seems likely that these are due to ether-like oxygen and carbonyl-like oxygen

on the oxidised (100) diamond surface. Oxygen peak shifts have not been published on (100) diamond surfaces but peak shifts of oxygen groups in polymer systems have, where ether oxygen is shifted to higher binding energy than carbonyl oxygen. The two oxygen peaks were assigned to ether and carbonyl oxygen on this basis. The relative areas under each peak indicated that carbonyl oxygen may account for more than the two-thirds of a monolayer suggested by peak fitting of C 1s envelopes. Thermal oxidation of smooth hydrogen terminated (100) diamond surfaces was shown to be a suitable method by which to prepare (100) diamond surfaces with a high concentration of carbonyl-like oxygen functionality on the surface. Carbonyl functional (100) diamond surfaces provide suitable substrates with which to investigate the immobilisation of amines on the diamond surface by formation of an imine bond between the amine reagent and surface bound carbonyl group.

AFM and optical microscopy have been used to study the effect of thermal oxidation on the morphology of the (100) diamond surface over time. The dimensions of a polishing defect in the diamond crystal clearly increased with oxidation time which indicated oxidative etching of the (100) diamond surface had taken place. Ridges running across the diamond surface, which appeared to be collinear with $\langle 110 \rangle$, were evident even after short oxidation times. After longer periods of oxidation the ridged morphology broke up into a 'brick-work' like pattern, which consisted of small, individual pits with edges along $\langle 110 \rangle$ directions. The formation of ridges and later the 'brick-work' structure can be explained by anisotropic oxidative etching of steps on the (100) diamond surface. Steps on (100) diamond surfaces lie along $\langle 110 \rangle$ directions. Ridges were attributed to macro-bunching of steps present on the diamond surface due to a slight miscut from (100) in one direction. The 'brick-work' structure was attributed to the presence of a second, smaller miscut existing on the diamond surface in a direction perpendicular to the first. This would give rise to a second set of steps on the surface, perpendicular to the first. With a smaller miscut it would take longer for macro bunched steps to become visible by AFM or optical microscopy but these would appear after continued oxidation, running perpendicular to the initial ridges and breaking the surface up into small rectangular terraces bounded on two sides by step-up steps and on two sides by step-down steps. Roughening of the (100) diamond surface by oxidative etching indicated that to produce a well characterised carbonyl terminated flat (100) diamond surface from smoothed hydrogen terminated (100) diamond, the oxidation time should be as short as possible.

3 – Reactions of amines with the diamondoid molecule 2-adamantanone.

3.1 Introduction

Diamond surfaces can be made more amenable to organic modification by the introduction of reactive oxygen functional groups onto the surface. Carbonyl-like groups have been introduced to the (100) surface of single crystal diamond by thermal oxidation. The reactivity of carbonyl groups is exploited in organic chemistry by reacting them with nucleophiles to create new covalent bonds between molecules. If similar reactions can be achieved on the (100) diamond surface they will provide a route to functionalising the surface of oxidised diamond. The ketone 2-adamantanone is a cage molecule containing a carbonyl group and has the same structure as a tiny fragment of the oxidised (100) diamond surface. It is amenable to provide analogous reactions to those on an oxidised diamond surface because it has a low molecular weight, is soluble in common solvents and can be easily handled by standard synthetic organic procedures. 2-adamantanone has been used as a molecular mimic of the oxidised (100) diamond surface to investigate the formation of imine products by nucleophilic attack of amines. The steric impact of the cage structure around the carbonyl group creating hindrance to amine attack has been identified, a problem which can be expected to be significant on a (100) diamond surface.

3.1.1 Diamondoids

On viewing a section of an extended diamond lattice, it is possible to identify a cage-like repeating unit composed of ten carbon atoms. Saturating this unit with hydrogen gives the molecule tricyclo[3.3.1.1(3,7)]decane, commonly known as adamantane, molecular formula $C_{10}H_{16}$. It is possible to envisage repeatedly fusing adamantane cages together to build up a series of hydrocarbon molecules whose chemical formulae are given by $C_{(4n+6)}H_{(4n+12)}$ with $n = 1, 2, 3, \dots$ and whose carbon skeletons are superimposable on the diamond lattice. This series of ‘adamantalogues’ are known as diamondoid molecules¹²⁰. Members of the series containing up to three cage units,

shown in Figure 30 are referred to as the lower diamondoids. Tetramantane and larger molecules are referred to as the higher diamondoids.

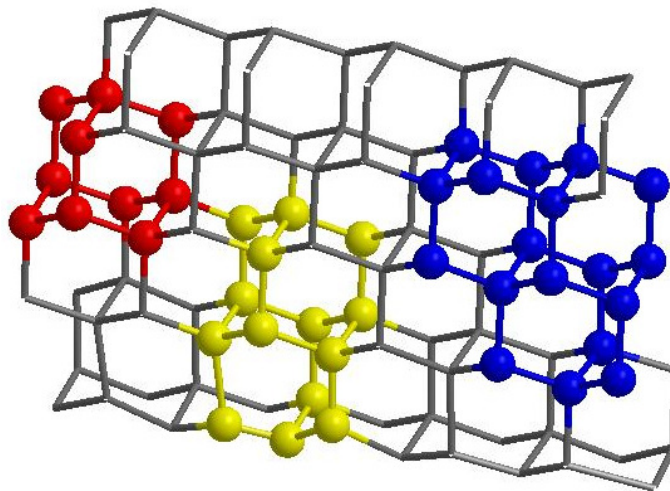


Figure 30 – Section of the diamond lattice with the cage structures of the lower diamondoids highlighted. Adamantane in red, diamantane in yellow and triamantane in blue.

Crystalline adamantane was first isolated from petroleum in 1933 but only in minute amounts. Initial efforts to synthesise the molecule met with limited success and very small yields. However, in 1957, Schleyer serendipitously discovered a synthesis of adamantane in better yield by a Lewis acid catalysed isomerism of endo-tetrahydrodicyclopentadiene¹²¹. A similar template method was employed to synthesise diamantane and triamantane; the second and third diamondoid in the series. Synthesis of higher diamondoids by this approach proved problematic. As the number of fused adamantane cages in the molecule increases to four or more, different isomers become possible and the increasing structural complexity magnifies the synthetic difficulties¹²¹. Of the higher diamondoids, only one tetramantane isomer has been synthesised¹²². Synthesis of substituted lower diamondoids is also possible by the rearrangement synthesis approach¹²³. Additionally, it is possible to generate bridgehead carbocations, directly from the parent hydrocarbon, which can undertake a range of electrophilic derivatisation reactions¹²⁴. A wide variety of substituted adamantanes are now commercially available and have found utility in disparate fields. 1-aminoadamantane or amantadine has been found to have pharmaceutical benefits in the treatment of Parkinson's syndrome and as an anti-viral agent to battle influenza¹²⁵. Military research has uncovered 1,3,5,7-tetranitroadamantane in the search for more powerful but stable

explosives¹²⁵ and other derivatives have been used in the synthesis of high temperature polymers¹²⁰.

The range of diamondoids known was increased significantly by the recent report of the isolation of higher diamondoid molecules from petroleum samples¹²⁰. The discovery of molecules from tetramantane, containing 4 adamantane cages, to undecamantane, 11 adamantane cages, with dimensions of around 1 – 2 nm means diamond structures are known on all length scales from adamantane through lower and higher diamondoids, nano-crystalline and polycrystalline diamond to single crystals. As the number of cages increases through the higher diamondoids an increasing variety of structures are possible within each family. Tetramantane is the first structure for which isomers are possible; some of which display chirality. Due to the many different ways of face-fusing five adamantane cages, different molecular weights are possible for members of the pentamantane family, meaning not all members of the same family are necessarily isomers. The variety of shapes adopted by higher diamondoids includes; rod-like where the cages all stack one above the other, disk like in the case of cyclohexamantane and even helical screw-shaped. These higher diamondoids and functionalised analogues are currently the subject of further research¹²⁶.

Diamondoid Properties

In the very lowest diamondoids all carbon atoms are terminated by hydrogen. Only in triamantane does the first fully bulk diamond-like carbon, bonded to four other carbon atoms appear. It seems likely that the properties of the diamondoids would tend more towards bulk diamond on ascending the series. Calculations have shown that the bond lengths and angles in diamondoids up to 10 cages in size are very similar to those found in bulk diamond¹²⁷ and so the strength and rigidity derived from the fused-cage structure are retained even in the lowest diamondoids. The stability of the sp³ bonded carbon arrangement means that derivatisation reactions undergone by diamondoids involve the substitution of a hydrogen atom on the surface rather than cleavage of carbon-carbon bonds. Like diamond the diamondoids also display excellent thermal stability. This feature was exploited in the isolation of the higher diamondoids as pyrolysis was utilised to remove less thermally stable species present¹²⁰. Diamondoids have been found to be insulating. Calculation and measurement, by X-ray spectroscopy, of the HOMO – LUMO gap suggests that it is largest for adamantane and

decreases to approximately the bulk diamond bandgap of around 5.5 eV for the pentamantanes and hexamantanes¹²⁸.

In contrast to the Raman spectrum of high quality bulk diamond, which shows a single sharp peak at 1332 cm^{-1} due to the interpenetrated face-centred cubic Bravais lattices vibrating in opposite directions, the Raman spectra of diamondoid molecules show several sharp discrete peaks attributed to breathing modes, cage deformations, C-C stretching modes and C-H bending modes within the molecules¹²⁹. It would be expected that with increasing diamondoid size the Raman spectra would tend to that of bulk diamond, or at a particular fragment size a switch over from molecular to bulk behaviour would be observed. Diamondoids up to pentamantanes studied to date still display discrete peaks¹²⁹, indicating that they are some way from adopting completely the structural properties of bulk diamond. Infra-red spectra of diamondoid molecules identify the surface carbon – hydrogen bonds present¹³⁰, not generally observed in bulk diamond, which is to be expected given the increased surface to volume ratio of the molecules.

3.1.2 Modelling the reactions of oxidised diamond surfaces.

The properties of diamondoids outlined above suggest that it is valid to consider them ‘molecular’ diamonds. They provide a pathway of increasing complexity into the extended diamond structure and are extremely attractive for building an understanding of diamond behaviour. The solubility of adamantanes in common solvents provides the opportunity to study the reactivity of a simple model of the diamond surface by standard solution chemistry techniques. In order to model the reactions of an oxidised surface it is required to utilise an adamantane containing some reactive oxygen group which can be readily introduced onto the diamond surface. The molecule 2-adamantanone is available in gram quantities at relatively low cost and, in the same way that adamantane is the smallest repeating cage unit in the diamond lattice, it is the smallest repeating cage identifiable on a (100) diamond surface terminated with carbon – oxygen double bonds, Figure 31.

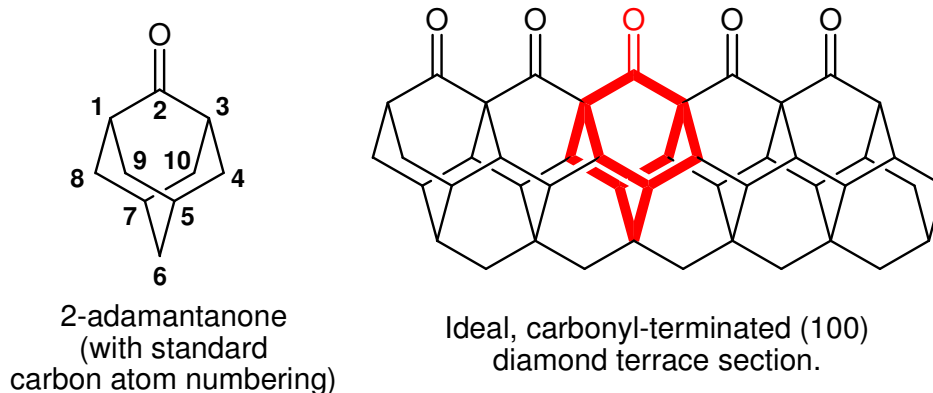


Figure 31 – Section of (100) diamond terrace terminated with ‘on-top’ oxygen, emphasising the 2-adamantanone like repeat units.

Faceted (100) polycrystalline diamond films, shown by XPS to be terminated with both on-top and bridging oxygen groups, have been analysed by diffuse reflectance infrared Fourier transform (DRIFT) spectroscopy⁷⁶. A distinct band was observed at 1731 cm^{-1} which is similar to the wavenumber at which the $>\text{C}=\text{O}$ stretching mode occurs in 2-adamantanone¹³¹. The band at 1731 cm^{-1} was therefore assigned to the stretching mode of a carbonyl group, $\nu_s(\text{C}=\text{O})$, on the diamond surface. Comparison of $\nu_s(\text{C}=\text{O})$ on diamond with various ketone compounds suggested it was indicative of a carbonyl group present as part of an unstrained six-membered ring system⁷⁶. Carbonyl terminated (100) diamond is therefore expected to be susceptible to reactions undergone by ketones containing unstrained six-membered rings. 2-adamantanone is an ideal model ketone for this system. The hindered ring structure could even begin to approximate the steric considerations relevant to reactions on an oxygenated diamond surface.

3.1.3 Reactions of ketones.

Ketones undergo a variety of chemical reactions^{132, 133}. Due to steric and other reasons some may not be feasible for attaching molecules to the oxygenated diamond surface. For example, formation of aldol products and halogenation can occur by removal of a proton from the carbon adjacent to the carbonyl group. However, it can be seen in Figure 31 that on a fully oxygenated diamond surface there are no α -hydrogen atoms present. In Norrish reactions the bond between the carbonyl carbon and α -carbon is

cleaved photochemically to give radical intermediates¹³². Due to the rigid lattice structure in diamond the radical sites would be held in very close proximity and recombination would be expected to be considerably more rapid than any other competing process. Oxidation and reduction of the carbonyl group merely generate different functional groups, which still require further reaction to couple an organic molecule to the diamond surface. The most attractive class of carbonyl reactions which can be used for binding another reagent directly are nucleophilic addition reactions. The charge distribution in the carbonyl group means the carbonyl carbon is slightly electron deficient and therefore susceptible to attack from nucleophilic species.

Finiels and Geneste have tabulated¹³⁴ the reactivity with nucleophiles of a series of ketones, including 2-adamantanone, relative to cyclohexanone. Selected data from this table are reproduced in Table 9. 2-adamantanone is more reactive than acetone, which seems counter-intuitive as the cage structure around the carbonyl group seems likely to provide steric hindrance to the approach of nucleophiles.

	Finiels and Geneste ¹³⁴	Brown <i>et al.</i> ^{135, 136}	
	$\log \frac{k}{k_o} = B$	$k \times 10^4$ / L mol ⁻¹ s ⁻¹	(B)
Cyclobutanone	0.09	264	(0.21)
Cyclohexanone	0.00	161	(0.00)
2-Adamantanone	-0.46	-	-
Cycloheptanone	-0.95	1.02	(-2.20)
Cyclopentanone	-1.18	7.01	(-1.36)
Acetone	-1.19	15.10	(-1.03)

Table 9 – Reactivity series of ketones. Finiels and Geneste data¹³⁴, tabulated as the logarithm of the rate constant relative to the rate constant of cyclohexanone (B). Brown *et al.* data^{135, 136} showing rate constants of ketone reduction by sodium borohydride and (B) the rate constants converted to the logarithm of rate constant relative to the rate constant of reduction of cyclohexanone.

Finiels and Geneste¹³⁴ derived their reactivity data from reactions of each ketone with five different nucleophiles, including hydroxylamine. Unfortunately reaction conditions are not quoted in the publication¹³⁴. Although the authors believe the ketone reactivity

is independent of nucleophile, the mechanism of reaction in each of the five different cases is not necessarily straightforward and the rate determining step may not be identical. Ketone reactivities have also been determined by reduction with sodium borohydride^{135, 136}. Reductions of different ketones were carried out under the same conditions and the rate determining step is believed to be initial addition of borohydride to the ketone in each case. Unfortunately 2-adamantanone was not included in this study. However it does give rise to a different order of reactivity for some of the same ketones used in Finiels and Geneste's study. Rate constant data^{135, 136} are shown in Table 9, the logarithm of the rate of reduction relative to the rate of reduction of cyclohexanone has also been tabulated to facilitate comparison. Notably, in this study, acetone is found to be more reactive relative to other ketones.

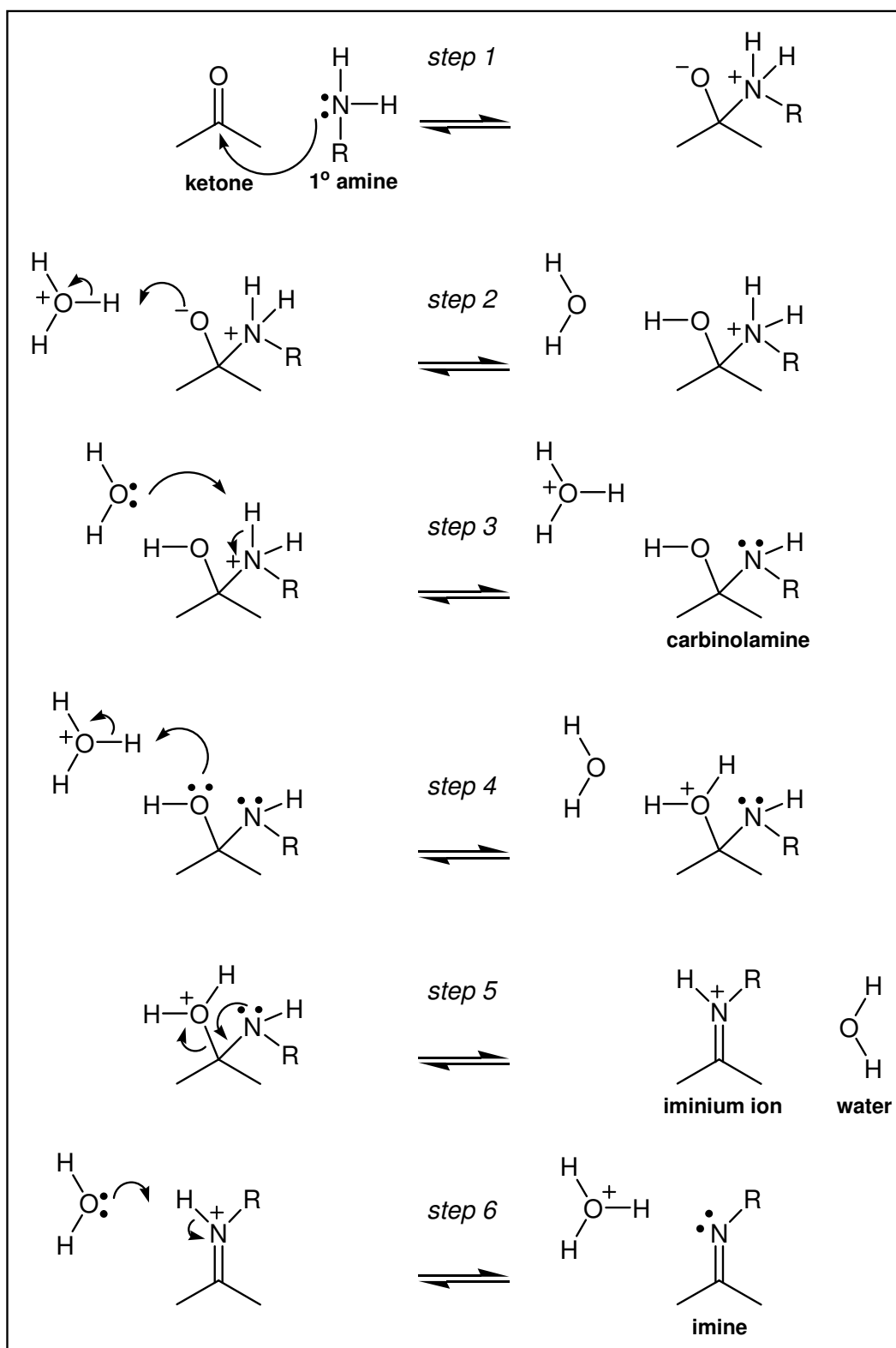
The carbonyl group in ketones undergoes nucleophilic attack from a range of nucleophiles to produce a variety of different products. Some of these reactions form new carbon – carbon bonds. For example in the Wittig reaction, reaction of a phosphorous ylide ($R_2C^-P^+R_3$) with a ketone results in the formation of an alkene. Grignard reagents ($R-MgX$) produce an alcohol in which the alkyl group has been transferred to the carbonyl carbon of the ketone. Both of these reactions require the preparation of specialised reagents. Ideal nucleophilic reagents for functionalisation of diamond surfaces should be readily available and offer a range of organic functionality which could be used for further processing once coupled to the diamond surface. Amines offer such advantages and couple to ketones via a carbon – nitrogen linkage. A plethora of organic molecules are available which incorporate nucleophilic amine moieties in addition to other functionalities. The ubiquitous nature of amino acids in biological systems would suggest they could be one 'linker' motif suitable for exploitation. Diamines, which could be further functionalised by reaction with carboxylic acids to give amide bonds, offer another promising route to the functionalisation of diamond surfaces.

3.1.4 Imine formation

The reversible reaction between ketones and primary amines to form imines is well known in synthetic organic chemistry and is an important biological reaction¹³⁷. Imines are involved in the isomerisation of retinal, found in the retina of the eye and feature in

the mechanism by which the enzyme amino acid racemase interconverts optical isomers of amino acids. The mechanism of imine formation has been elucidated by measurement of reaction rates, particularly in reactions utilising hydroxylamine and semicarbazide as the nucleophilic reagents^{87, 138-141}. The mechanism has been extended to encompass reaction of other amine reagents though subtleties exist depending on the specific reagents and reaction conditions.

A general mechanism for the imine formation reaction, broken down into six elementary steps, is shown in Scheme 1. Overall a condensation reaction takes place forming an imine in an addition – elimination process. In step 1 of this mechanism the electron lone pair localised on the amine nitrogen atom undertakes nucleophilic attack on the electron deficient carbon atom of the carbonyl bond. The carbonyl π -bond is broken and electron density is localised on the oxygen atom to form a zwitterionic adduct. In steps 2 and 3 protonation of the negatively charged oxygen atom occurs and a proton is lost from the positively charged nitrogen atom in an overall proton transfer process to form a carbinolamine intermediate. The carbinolamine can undergo dehydration to give an imine. In acidic and neutral media this can occur, as shown in Scheme 1, by protonation of the carbinolamine hydroxyl group in step 4 then dehydration and simultaneous formation of a carbon – nitrogen π -bond by the nitrogen lone pair, giving a positively charged iminium ion, as in step 5. Loss of a proton from the iminium ion yields the imine product.



Scheme 1 – Elementary steps involved in the mechanism of imine formation by reaction of a ketone with a primary amine.

For reactions of primary amines with aldehydes or ketones the reversible process outlined in Scheme 1 dominates and competing processes are not widely reported. Alternative products observed in reactions of amines with simple aldehydes and have been identified as oligomer or polymeric products resulting from further reactions of carbinolamines or imines¹⁴². For example, reaction of ammonia with acetaldehyde gives rise to a cyclic trimeric triazine product^{143, 144} and formaldehyde reacts with ammonia to form the tetrameric hexamethylenetetramine,¹⁴² which coincidentally has an adamantane-like shape. Many higher molecular weight aldehydes give monomeric imine products, from both aliphatic and aromatic aldehydes and amines¹⁴². Polymerisation reactions do not seem to be observed when the carbonyl reagent is a ketone. Chudek et al¹⁴⁴ carried out extensive NMR studies on reacting mixtures and did not report the formation of any oligomeric or polymeric species for the reaction of acetone and ammonia although the triazine oligomer product of acetaldehyde and ammonia was observed. Only the expected carbinolamine intermediate was formed during the reaction of ammonia with a series of simple aliphatic ketones. The observation of the carbinolamine in solution provides further evidence of its formation as a reaction intermediate in addition to the cases where it is sufficiently stable to be isolated. Isolated carbinolamine intermediates include a series of hydroxymethylamines from reactions of formaldehyde, and the carbinolamines from reaction of benzaldehyde with p-nitroaniline and 2,4,6- trinitrobenzaldehyde with aniline¹⁴².

Imine products are frequently unstable, easily hydrolysed to the starting materials, and difficult to isolate. If the reactant ketone or amine is aromatic, giving a product with an aromatic ring attached to the carbon or nitrogen of the C=N bond, the imine is stabilised by the ring and more readily isolated. Such imines are known as Schiff bases. Imines are also stabilised by hydroxyl groups or groups where a second nitrogen is bound to the nitrogen of the imine bond. This gives rise to the formation of oximes, semicarbazones and hydrazones as derivatives for the identification of aldehydes or ketones when reacted with hydroxylamine, semicarbazide and hydrazines respectively, as the stable products are readily isolated.

The rate of imine forming reactions exhibits a distinct dependence on pH^{138-141, 145, 146}. A classic example is the rate maximum observed by Jencks in the reaction between hydroxylamine and acetone¹³⁹. A maximum in the rate occurs at slightly acidic pH with the rate becoming greatly reduced at both lower and higher pH, as shown in Figure 32.

In addition, on the basic pH side of this maximum it was observed that the rate of formation of oxime product was not equal to that of ketone consumption, indicating the formation of an equilibrium concentration of carbinolamine intermediate. Jencks identified¹³⁹ that the rate determining step at neutral pH was the elimination of water. Since this step is catalysed by acid (step 4 in Scheme 1) increasing the acidity increases the reaction rate. The rate achieves a plateau instead of continuing to increase with acidity as the protonated amine is not an effective nucleophile. Under acidic conditions where $\text{pH} < \text{pK}_a$ of the conjugate acid of the amine, basic amine nucleophiles will be present mainly in their unreactive protonated form. Under these conditions the concentration of free amine present is sufficiently small that the first step in the mechanism in Scheme 1 i.e. nucleophilic attack by free amine becomes the rate determining step. Once this is the case, further increasing the acidity reduces the concentration of free amine present and, correspondingly, the overall reaction rate. The switch to rate limiting addition causes a change from an equilibrium concentration of carbinolamine intermediate to a steady state concentration. In turn, under these conditions the rate of oxime formation becomes equal to the rate of carbonyl consumption.

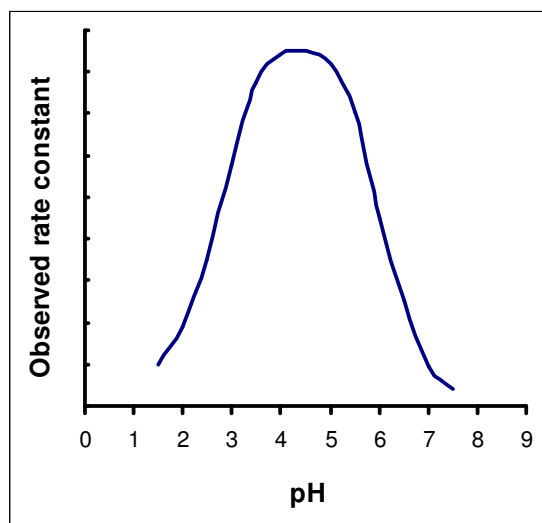
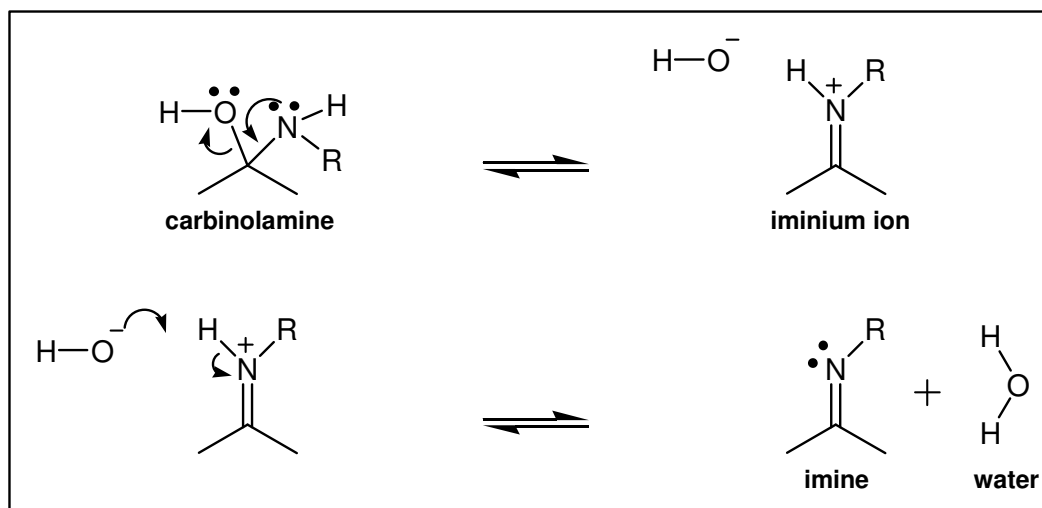


Figure 32 – Representation of the variation in reaction rate with pH observed by Jencks for the reaction between hydroxylamine and acetone. Reproduced from reference 139.

Hydroxylamine ($\text{pK}_a = 5.94$)¹⁴⁷ provides an example of the reaction of a relatively strongly basic amine. The mechanism of imine formation from strongly basic amines¹³² can operate in three different ways depending on the pH at which the reaction is carried

out. At strongly acidic pH nucleophilic attack of the amine on the carbonyl functional group is rate limiting due to the small concentration of free base present. At weakly acidic and neutral pH the concentration of free base is sufficiently large to increase the rate of the addition step and dehydration (step 5 of Scheme 1) becomes rate limiting. At alkaline pH the mechanism is dominated by hydroxide ion in the solution. The addition step is fast as the amine is unprotonated and proton transfer occurs to generate the carbinolamine intermediate. Under these conditions the rate determining elimination from the carbinolamine occurs with hydroxide ion, not water, as the leaving group¹⁴⁸ as shown in Scheme 2. This reaction generates an iminium ion which undergoes proton abstraction to generate the imine product. Loss of the hydroxide ion from the carbinolamine is uncatalysed so increasing the basicity of the solution has no effect on the reaction rate.



Scheme 2 – Mechanism of dehydration from carbinolamines formed from strongly basic amines, under alkaline conditions.

The mechanism for reactions involving more weakly basic amines such as semicarbazide or aromatic aniline derivatives is similar but reaction is aided by a catalyst¹³². Electron withdrawing substituents which reduce the basicity of the nitrogen lone pair inhibit the initial nucleophilic attack on the electrophilic carbon of the carbonyl bond but also retard dehydration where the lone pair again acts in a nucleophilic manner, forming the carbon – nitrogen π -bond (step 5 in Scheme 1), aiding ejection of the leaving group. For weakly basic amines a rate maximum is still observed at acidic pH. At pH values below this maximum the rate determining nucleophilic

addition step, step 1 in Scheme 1, is assisted by some degree of acid catalysis. Protonation of the carbonyl oxygen increases the electron deficiency and hence electrophilicity of the carbonyl carbon. The other steps operate in a similar fashion to the more basic amines. At pH values above that at which the rate maximum is observed the dehydration step is rate limiting and the nucleophilic addition remains uncatalysed as for basic amines. Base catalysis of the dehydration step, however, is possible. A basic molecule can abstract the proton attached to nitrogen in the carbinolamine and assist in expulsion of hydroxide ion⁸⁷.

Two extreme conditions exist¹⁴⁹ under which the rate limiting addition step may occur. Extremely weak nucleophiles would require complete protonation of the carbonyl before addition occurred. Strong bases can add directly to form a zwitterionic species, as shown in Scheme 1, before protonation of the oxygen atom. Between the two extremes a concerted process occurs in which both steps occur concurrently. Most amines generally fall within this range, with the degree of concerted reaction tending more to one extreme or the other depending on the basicity of the amine. Similarly, under alkaline conditions, dehydration will be base catalysed for weakly nucleophilic amines but less so for stronger bases.

Different structure – reactivity relationships have been observed depending on whether addition or dehydration is the rate determining step. A classic method of identifying the effect of substrate structure on reactivity utilises the equations proposed by Hammett¹³².

$$\log \frac{K}{K_o} = \rho\sigma \quad \text{and} \quad \log \frac{k}{k_o} = \rho\sigma \quad (11) \text{ and } (12)$$

Hammett observed that the rate constant, *k*, and equilibrium constant, *K*, for the ionisation of substituted benzoic acids varied with the nature of the substituent. By relating the constants from substituted acids (*k*, *K*) to the constants for unsubstituted benzoic acid (*k*_o, *K*_o) he proposed that a relationship existed which depended on an empirical constant for the reaction under study, ρ , and an empirical substituent constant, σ . The values of σ are now known for a wide variety of groups¹⁵⁰ and reflect the electronic influence of the substituent. The substituents are generally bound to a reacting group via an aromatic ring so their electronic influence can be transmitted to the reactive site via the π -system, whilst keeping them physically distant to minimise

steric effects. If it is found that plotting the rate or equilibrium constants for a series of substituted molecules involved in a reaction against substituent constant values, σ , gives a straight line then the gradient of the line gives ρ , the reaction constant for the specified reaction. A positive value of ρ indicates that electron withdrawing substituents increase the rate or equilibrium constant. Conversely a negative ρ value indicates that electron donating groups increase the magnitude of the rate or equilibrium constants.

Anderson and Jencks⁸⁷ applied the Hammett methodology to semicarbazone formation from a series of substituted benzaldehydes. At acidic pH, when nucleophilic addition is rate limiting, the observed rate constant was linearly related to σ . The positive gradient of the line indicated a rate increase with electron withdrawing substituents. This was rationalised by Anderson and Jencks⁸⁷ in terms of removal of electron density from the aldehyde carbonyl carbon atom by the electron withdrawing group, making it more susceptible to nucleophilic attack and facilitating the addition step in the mechanism, as shown in Figure 33.

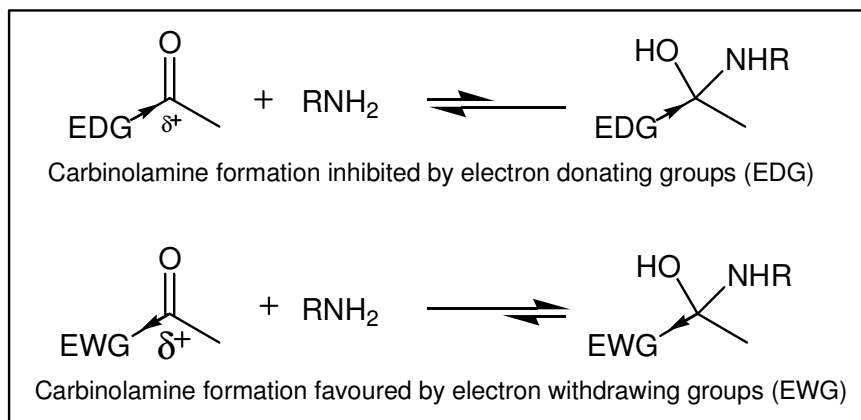


Figure 33 – Substituent effects affecting nucleophilic addition of an amine to an aldehyde or ketone. The size of the δ^+ on the carbonyl carbon of the aldehyde or ketone is intended to reflect the magnitude of the charge localised upon it.

At neutral pH, with the dehydration step rate limiting, it was found that a similar plot of observed rate constant against σ gave a straight line whose gradient was virtually zero. This indicated that the nature of the benzaldehyde substituent had little or no effect on the overall rate of reaction when dehydration was rate limiting. The reason for this was revealed by separately plotting the equilibrium constant for carbinolamine formation and the rate constant for dehydration against σ . A plot of the equilibrium constant for carbinolamine formation against σ had a positive gradient, favouring formation of the

carbinolamine when an electron withdrawing group was present, as shown in Figure 33. A plot of the rate constant for dehydration against σ gave a straight line of negative gradient, meaning dehydration was inhibited by the presence of an electron withdrawing group, as shown in Figure 34. Carbinolamine dehydration is inhibited by electron withdrawing groups as they further destabilise the iminium ion formed. Since the rate of dehydration depends on the concentration of carbinolamine (increased by electron withdrawing groups) and the rate constant for dehydration (decreased by electron withdrawing groups), under conditions where dehydration is rate limiting, substituents have two opposing effects of similar magnitude and therefore little effect on the overall observed rate of reaction⁸⁷.

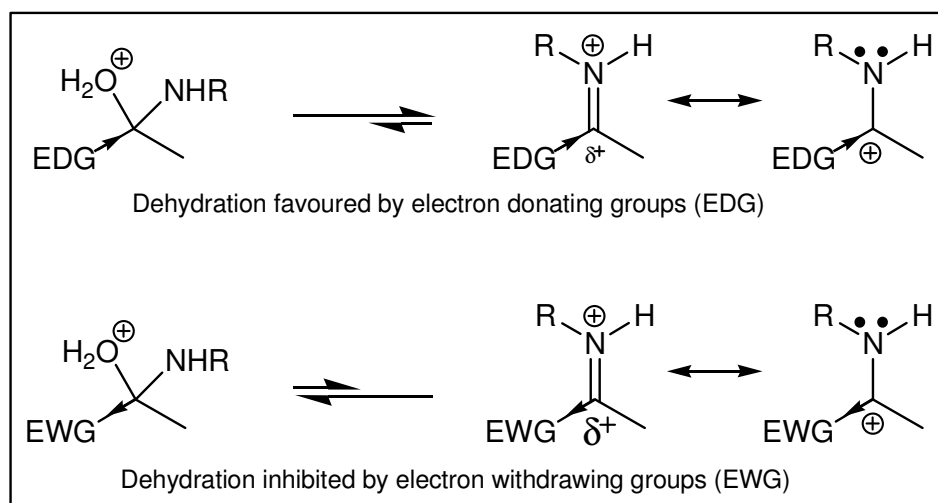


Figure 34 – Substituent effects affecting the dehydration of a carbinolamine. The size of the δ^+ on the carbonyl carbon of the aldehyde or ketone is intended to reflect the magnitude of the charge localised upon it.

3.1.5 Reduction of imines.

Due to the reversible nature of the condensation reaction between amines and ketones, the imine bond is susceptible to hydrolysis. Diamond offers great promise as a substrate for use in wide ranging and extreme conditions. In devices utilising derivatised diamond surfaces the hydrolysis of the imine bond in the presence of water vapour would be detrimental. Fortunately reduction of an imine ($R_2C=NR'$) bond to an amine ($R_2HC-NHR'$) is relatively straightforward and the carbon–nitrogen single bond formed offers far greater stability under a wide variety of conditions.

Metal hydride reagents such as lithium aluminium hydride and sodium borohydride are commonly used to effect reductions in organic chemistry. These reagents reduce aldehydes and ketones to alcohols as well as imines to secondary amines. However a more selective reagent, sodium cyanoborohydride, displays negligible reactivity to ketones under neutral conditions¹⁵¹. Sodium cyanoborohydride is therefore commonly used at neutral and slightly basic pH to effect selective reduction of imines formed from ketones (and aldehydes). The reducing agent can be present during imination and will reduce the imine to a secondary amine as it is formed. This 'one-pot' reaction is known as reductive amination¹⁵¹.

The mechanism of metal hydride reduction is complex. The metal cation plays an important role and affects the reduction rate. In the reduction of cyclohexanone by sodium cyanoborohydride, three equivalents of carbonyl compound were consumed per equivalent of reducing agent¹⁵¹ providing evidence that all the hydrogen in the anion is available to react. The nature of the solvent may also affect the reaction through solvent exchange with alkoxide groups in the boron complex¹³⁵ or by facilitating aggregation of the reducing agent¹⁵¹. The basic process involved is the transfer of hydride ion to the π -bonded carbon atom. It is convenient to consider the process as a nucleophilic hydride attack at the carbon atom of the imine moiety. The nitrogen atom can subsequently abstract a proton from the surrounding environment.

3.1.6 Chemical kinetics and mechanism.

Kinetic studies of the rates of chemical reactions and the factors upon which they depend can yield information on the reaction mechanism. Determination of a relationship between the reaction rate and some variable, such as concentration, temperature or pH, can allow an empirical rate law to be constructed. In conjunction with other experimental observations it may be possible to interpret rate laws mechanistically.

The rate of a chemical reaction can be expressed as the rate of change in concentration of any reactant or product involved in the reaction. The rate constant or rate coefficient, k , for the reaction is numerically equal to the rate when all reagents are present in unit

concentrations. An example of a rate law depending in an n'th order fashion on a reactant A is:

$$\text{Rate} = -d[A]/dt = k [A]^n. \quad (13)$$

The dependence of rate constant on temperature follows the Arrhenius Law:

$$k = Ae^{-E_a/RT} \quad (14)$$

in which A is the frequency or pre-exponential factor for the reaction. The term $e^{-E_a/RT}$ is the Boltzmann fraction of collisions with sufficient energy to surmount the activation energy, E_a , to form an activated complex. The rate constant k therefore identifies the fraction of collisions which have the correct orientation and sufficient energy to form products. The rate constant therefore governs the reaction rate; the reactant concentration terms affect the number of molecules available to react and so the frequency of collisions¹⁵².

Determination of rate constants is possible by a variety of methods. The most commonly utilised is the method of integration. A differential rate equation is selected to describe the reaction under study. The experimental data may then be fitted to the integrated form of this rate equation, usually by rearranging the integrated rate equation into a linear form. If a straight line is obtained then the order of reaction is confirmed and the rate constant can be determined. If the integrated equation for a particular order, n, is not linear another differential equation must be selected and the process repeated¹⁵².

3.2 Experimental

2-Adamantanone (99%), sodium cyanoborohydride (95%) and the amines benzylamine (99%), 4-trifluoromethylbenzylamine (97%), 3-phenylpropylamine (98%) and aniline (99%) were purchased from Aldrich and used as received without further purification. Hydroxylamine and semicarbazide were supplied as the hydrochloride (both 97%) and ethylamine and ammonia as 2.0 mol L⁻¹ solutions in methanol also from Aldrich. All

solvents were obtained from Fisher Chemicals and of laboratory reagent grade. HCl (~1.25 mol L⁻¹ in methanol) was purchased from Fluka Chemical Company.

Low resolution electron impact (EI) mass spectra were obtained on a Kratos Concept 1S spectrometer and electrospray mass spectra on a Finnigan MAT LCQ Classic instrument with a flow of 3 μL min⁻¹ and a spray voltage of 5 kV using a heated capillary at 180°C. Nuclear magnetic resonance (NMR) spectra were obtained on a Bruker AC200 spectrometer. ¹H NMR spectra were recorded at 200 MHz and ¹³C NMR spectra at 50 MHz. Chemical shift data are given in parts per million (δ in ppm) and s, m, and quat. designate singlet, multiplet and quaternary signals respectively. Elemental analyses were performed using an Exeter CE-440 elemental analyser. Measurement of pH was carried out using a BDH Gelplas combination electrode and Jenway 3310 pH meter with temperature compensation via a temperature probe.

3.2.1 Synthesis of 2-adamantanone derivatives.

Small scale syntheses were undertaken of three derivatives of 2-adamantanone to investigate whether, despite its hindered cage-like structure, it displayed the expected ketone reactivity. The syntheses were carried out by Mr Anthony Purdie and Miss Vikki Anderson as part of an undergraduate project under the guidance and supervision of the author.

*Oxime synthesis*¹⁵³

A solution of 0.51g of hydroxylamine hydrochloride (7.4 mmol) and 0.85g sodium acetate trihydrate (4.6 mmol) in methanol (5 cm³) was prepared. To this solution 1.09 g of 2-adamantanone (7.2 mmoles) was added and the solution heated on a water bath for 10 minutes before cooling in ice. The precipitate which formed was collected by filtration, washed in ice water and recrystallised from methylated spirits to give 0.63 g (3.8 mmoles, 53 %) of product, mp 168-172°C. Mass spectrum: m/z 165. Calc. for C₁₀H₁₅NO 165.23. Elemental analysis: C, 72.60; H, 9.29; N, 8.53. Calc. for C₁₀H₁₅NO C, 72.69; H, 9.15; N, 8.48. ¹³C NMR (CDCl₃) δ 166.9 (quat.); 38.6 (2 x CH₂); 37.4 (2 x CH₂) 36.3 (CH₂); 36.1 (CH); 28.4 (CH); 27.5 (2 x CH). ¹H NMR (CDCl₃) δ 7.0 (s, 1 H); 3.6 (s, 1 H); 2.6 (s, 1H); 1.7 – 2.1 (m, broad, 12 H).

*Semicarbazone synthesis*¹⁵³

To a solution of 0.50 g semicarbazide hydrochloride (4.5 mmol) and 0.81 g sodium acetate trihydrate (4.4 mmol) in water (5 cm³), 0.67 g 2-adamantanone (4.5 mmol) was added and the solution heated on a water bath for 10 minutes before cooling in ice. The product was recrystallised from acetone to afford 0.31 g (1.5 mmol, 33 %), mp 240-243°C. Mass spectrum: m/z 207. Calc. for C₁₁H₁₇N₃O 207.27. Elemental analysis: C, 63.78; H, 8.31; N, 20.26. Calc. for C₁₁H₁₇N₃O C, 63.74; H, 8.27; N, 20.27. ¹³C NMR (CDCl₃) δ 160.5 (quat.); 158.1 (quat.); 39.6 (CH); 39.0 (2 x CH₂); 37.5 (2 x CH₂); 36.3 (CH₂); 30.7 (CH); 27.8 ppm (2 x CH). ¹H NMR (CDCl₃) δ 7.3 (s, 1 H); 2.8 (s, 1 H); 2.5 (s, 1 H); 1.6 – 2.0 (m, broad, 14 H).

*Reductive amination with ethylamine*¹⁵¹

To 30 ml of 2.0 mol L⁻¹ ethylamine (60 mmol) was added 4 ml of 5 mol L⁻¹ HCl-methanol (20 mmol), 0.64 g of sodium cyanoborohydride (10 mmoles) and 1.50 g of 2-adamantanone (10 mmol). The solution was stirred at 20°C for 72 hours before being worked up. Concentrated HCl was added to reduce the pH to < 2 and the methanol removed by rotary evaporation. The residue was taken up in water (10 ml) and extracted with three 20 ml portions of diethyl ether. The pH of the aqueous layer was increased to pH > 10 by the addition of solid potassium hydroxide, then the solution saturated with NaCl and extracted with a further five 15 ml portions of diethyl ether. The ether portions were combined, dried with magnesium sulphate, filtered and the solvent removed by rotary evaporation to afford 1.11 g (6.2 x 10⁻³ moles, 62 %) of an impure yellow oil. Mass spectrum: m/z 179, 178, 177. Calc. for C₁₂H₂₁N 179.36. Calc. for C₁₂H₁₉N 177.35. Elemental analysis: C, 78.73; H, 11.15, N, 9.31. Calc. for C₁₂H₂₁N C, 80.38; H, 11.81; N, 7.81. Calc. for C₁₂H₁₉N C, 81.27; H, 10.80; N, 7.93. ¹³C NMR (CDCl₃) Ascribed to 2° Amine – δ 61.0 (CH); 40.5 (CH₂); 37.4 (CH₂); 34.0 (2 x CH); 30.7 (2 x CH₂); 29.8 (2 x CH₂); 27.2 (2 x CH); 15.2 (CH₃). Ascribed to imine – δ 46.4 (CH₂); 37.1 (2 x CH₂); 36.9 (CH₂); 33.9 (2 x CH₂); 31.4 (CH); 27.0 (CH); 26.3 (CH); 26.0 (CH); 14.8 (CH₃).

3.2.2 Chemical kinetic studies by FTIR.

All infrared spectroscopic investigations were carried out on a Nicolet 510P FTIR spectrometer, controlled via the supplied Nicolet PCIR software interface. Custom

written procedures allowed automated collection of a number of spectra with a specified delay between each. Spectra were converted from the spectrometer format into the international standard JCAMP-DX ASCII format by a freeware computer program and from there processed in Microsoft Excel using Visual Basic macros written by Dr Neil Polwart²³ and modified by the author to improve the numerical analysis.

Samples were analysed in an attenuated total reflectance (ATR) solution cell which was mounted in an adapted variable angle ATR accessory (Specac). Silicon was selected as a suitable ATR prism material since it is infrared transparent over the wavelength range of interest, inert to the reagents under study and non-toxic. The ATR cell consisted of a single crystal silicon trapezoid (50 x 20 x 2 mm) clamped between two stainless steel plates, with a PTFE gasket between each side of the crystal and each metal plate to create a reaction volume. The stainless steel plates contained luer-lock filling ports and channels which allowed the voids to be filled with solution from a standard syringe. The channels had been designed such that voids could be filled ‘bottom-up’ to ensure all air was expelled and achieve a consistency of solution volume and hence path length between experiments. Filling ports were capped with PTFE plugs once the cell had been filled. The ATR solution cell and accessory are shown in Figure 35. The ATR crystal was designed to allow 25 internal reflections along its length when light entered at 45° to the entrance face, the variable angle accessory was therefore set to 45°. The rotation and tilt of each accessory mirror was iteratively adjusted until the maximum signal was achieved at the spectrometer detector.

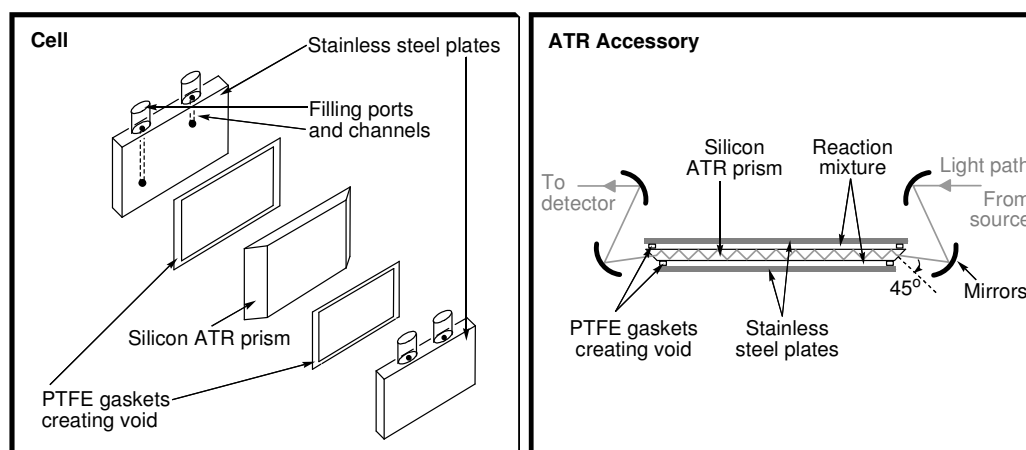


Figure 35 – Construction of cell and layout of ATR accessory for analysis of reacting mixtures.

Stock solutions of 2-adamantanone and sodium cyanoborohydride were made up by weighing the required mass into a volumetric flask and making up to the mark with solvent. Stock amine solutions were produced by pipetting the required volume into a volumetric flask and making up to the mark with solvent. 2-adamantanone 0.7 mol L⁻¹ stock solutions were diluted to give solutions ranging from 0.1 – 0.6 mol L⁻¹ to allow the construction of Beer – Lambert plots in different solvents. Reaction mixtures were made up by pipetting the appropriate volume of each stock solution into a glass sample bottle. Generally amine solutions were pipetted into solutions of 2-adamantanone or 2-adamantanone and sodium cyanoborohydride to initiate reaction and the start time of the reaction noted when half of the total required volume of amine solution had been added. Typical reagent concentrations in reaction mixtures were; 0.60, 0.45 or 0.30 mol L⁻¹ 2-adamantanone, 0.30 mol L⁻¹ amine reagent and, when present, 0.30 mol L⁻¹ sodium cyanoborohydride. When solutions required pH adjustment, the volume of acidic or basic methanol added to the reaction mixture was noted and the effect of this dilution on reagent concentrations noted. Acidic methanol was purchased as HCl in methanol; basic methanol was made by dissolving solid potassium hydroxide in methanol.

After reaction had been initiated by addition of amine reagent the reaction mixture was thoroughly mixed by agitation then drawn into a clean glass syringe and transferred expediently into the ATR cell in the spectrometer. The automated data collection procedure was initiated to record spectra at pre-determined intervals over a period of time. These were recorded against a background spectrum of the empty ATR cell. The spectrometer gain could be adjusted to maximise the signal at the detector whilst avoiding saturation. Resolution was set at 2 cm⁻¹ and 128 scans were carried out to achieve good signal to noise. The spectrometer automatic correlation function excluded any scans deviating significantly from the others in their set. Despite this some sets of time-resolved spectra contained occasional spurious spectra which gave markedly different absorbances from their neighbours. Over time this problem was observed to worsen and in conjunction with Thermo-Electron engineers was identified as a ‘slow’ detector. Replacement of the detector resolved this issue and the erroneous spectra could be justifiably excluded from processing. The ATR crystal, cell and stock solutions were stored in the spectrometer prior to use to minimise any temperature change when analysis began. The spectrometer temperature was 23 ± 3 °C. Whilst generally constant throughout daytime the spectrometer temperature was observed to decrease as the ambient temperature dropped overnight. To combat this effect the

spectrometer environment was heated overnight when analysis was in progress. However lack of effective thermostatic control meant fluctuations were observed in data collected over several days.

3.2.3 Chemical kinetic simulations

All chemical kinetic simulations were carried out using the Chemical Kinetics Simulator, CKS, v1.01 (IBM) freely available for download¹⁵⁴. This is a stochastic simulation package in which the user enters a mechanism as a number of simple steps with rate constants for each step and initial reagent concentrations. The software models a small but adequate number of molecules and distributes these between the various species defined depending on the initial concentrations specified. The probability of each step occurring is taken to be proportional to its instantaneous rate, calculated from the rate constant for that step and the concentration of its reactants. The software randomly selects between the probability weighted steps and a reaction event occurs which changes the concentrations of some species depending on the stoichiometry defined. The probabilities of each step are updated to reflect the new concentrations. The software then calculates the step in time which will occur before the next event, then selects again between the probability weighted steps to initiate the next event. This process repeats until terminated by software settings or the user and produces concentration against time data for all species involved in the mechanism.

The simple algorithm employed by the stochastic model allows relatively large simulations to be carried out on personal computers. All calculations were performed on a laptop computer with an Intel Centrino 1.50 GHz processor under Windows XP. Simulations generally took less than one minute to run. The CKS default number of particles was sufficient to model the system and pressure, temperature and volume were kept constant throughout the simulation.

3.3 Results and Discussion

3.3.1 Derivatives of 2-adamantanone.

It is generally accepted that the reaction of a ketone with hydroxylamine or semicarbazide produces an oxime or semicarbazone respectively and reductive amination with a primary amine produces a secondary amine^{133, 155}. Expected products of such reactions with the ketone 2-adamantanone are shown in Figure 36. The syntheses were carried out using standard procedures and the products characterised by electron-impact mass spectrometry, nuclear magnetic resonance (NMR) spectroscopy and carbon, hydrogen, nitrogen (CHN) elemental analysis.

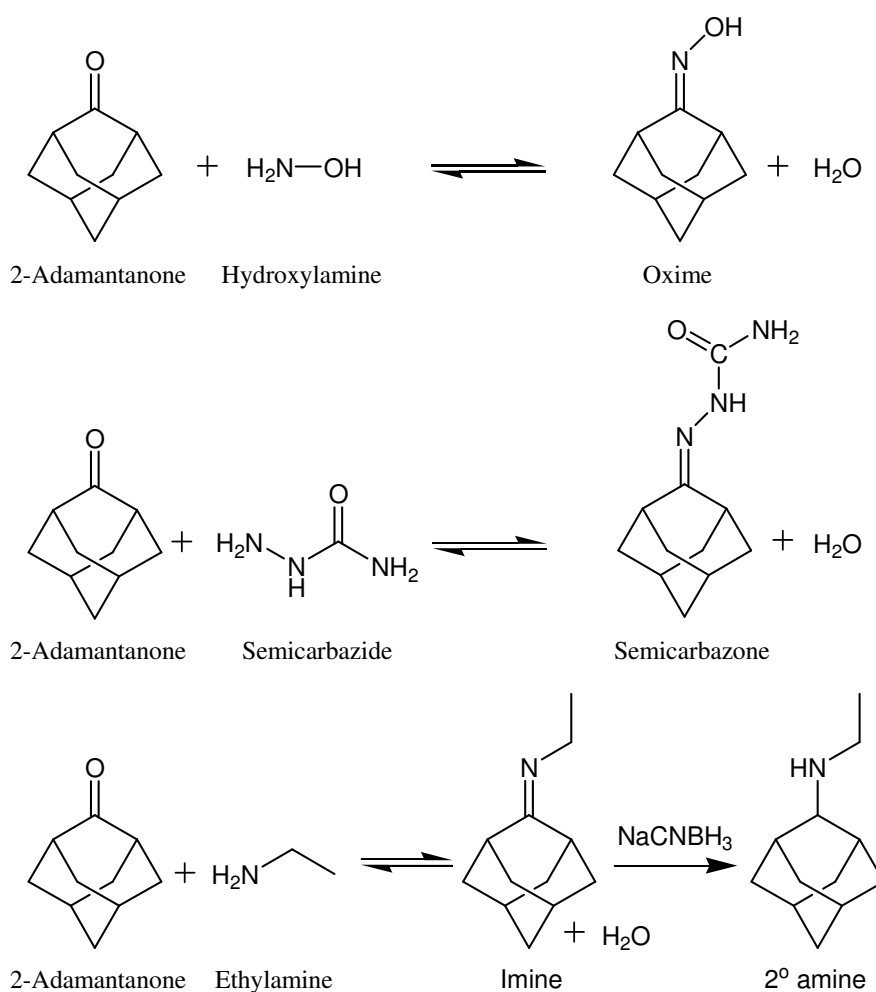


Figure 36 – Derivatisation reactions of 2-adamantanone.

Oxime Characterisation

The analytical data obtained from the product of the reaction between 2-adamantanone and hydroxylamine is consistent with the formation of the oxime 2-oximidoadamantane. The oxime molecular weight is calculated as $165.23 \text{ g}\cdot\text{mol}^{-1}$ and the low resolution mass spectrum of the product showed a molecular ion at m/z 165. Elemental analysis showed very good agreement with the predicted structure as shown in Table 10. ^{13}C NMR analysis of 2-adamantanone shows a quaternary carbon signal at 219 ppm, from the carbonyl carbon¹⁵⁶, and only four signals from the other nine carbon atoms due to the symmetry of the molecule. In the spectrum of the oxime product the quaternary carbon has shifted to 167 ppm, a decreased quaternary shift of around 55 ppm, which would be expected on conversion of a ketone to an oxime,¹⁵³ and is observed in similar compounds¹⁵⁷. There are also six signals from the remaining carbon atoms as the asymmetry around the nitrogen atom and the lack of rotation around the carbon – nitrogen π -bond destroys the symmetry of the adamantane cage. ^1H NMR shows the appearance of a signal at 7.0 ppm attributed to the hydroxyl proton.

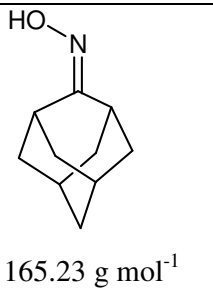
 165.23 g mol ⁻¹	Molecular Formula: C ₁₀ H ₁₅ NO			
		% C	% H	% N
	Theoretical	72.69	9.15	8.48
	Observed	72.60	9.29	8.53

Table 10 – Comparison of elemental analysis data with theoretical prediction for 2-oximidoadamantane.

Semicarbazone Characterisation

Analysis of the product of the reaction between 2-adamantanone and semicarbazide also confirms the isolation of pure semicarbazone product. The molecular ion identified at m/z 207 by mass spectrometry agrees with the molecular weight of the expected product and is confirmed by the elemental analysis, as shown in Table 11. ^{13}C NMR of the product shows two quaternary carbon peaks in the 160 ppm region. One was assigned to the carbon of the imine functional group and the other assigned to the amide carbon

of the semicarbazide. The loss of symmetry on derivatisation causes more aliphatic carbon signals to be observed than in the pure 2-adamantanone spectrum.

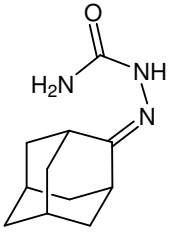
 207.27 g mol ⁻¹	Molecular Formula: C ₁₁ H ₁₇ N ₃ O			
		% C	% H	% N
	Theoretical	63.74	8.27	20.27
	Observed	63.78	8.31	20.26

Table 11 – Comparison of elemental analysis data with theoretical prediction for the semicarbazone product of 2-adamantanone.

Secondary amine characterisation

Characterisation of the product of the reductive amination between 2-adamantanone and ethylamine with sodium cyanoborohydride suggested that pure secondary amine *N*-ethyladamantan-2-amine had not been isolated. Analysis suggested the imine intermediate shown in Figure 36 was also present. Low resolution mass spectrometry gave a spectrum which contained peaks at *m/z* 177, 178 and 179. The secondary amine product has a molecular weight of 179.36 g mol⁻¹ and the imine intermediate has a molecular weight of 177.28 g mol⁻¹. The peak at *m/z* 178 may be due to a protonated form of the imine intermediate being formed during the ionisation process. Peaks attributed to protonated imines have been observed previously during similar studies²³.

Elemental analysis of the reductive amination product, shown in Table 12, does not show as good agreement with the calculated composition as the oxime and semicarbazone products. The ¹³C NMR spectrum of the product contains a peak at 61 ppm from carbon bonded to a single hydrogen atom. A peak at the latter chemical shift was not observed in any of the previous spectra of 2-adamantanone, the oxime or the semicarbazide. By comparison with similar secondary amine products^{158, 159} this peak is attributed to the carbon atom, labelled 2 in the diagram in Table 12, which has been reduced from a quaternary carbon in the imine. The peak at 61 ppm indicated the desired secondary amine product had been synthesised. Small but significant peaks in the range 10 – 50 ppm, where peaks from aliphatic carbon atoms generally occur, were indicative of the imine 2-adamantylideneethanamine, shown in Figure 36. This

suggests that imine intermediate which has not been reduced to 2-ethyladamantamine is present in significant quantity. A quaternary carbon signal from the imine intermediate was not observed in the 160 ppm region of the ^{13}C spectrum. ^{13}C signals from quaternary carbons are generally small so this peak may have been undetectable in the spectral noise.

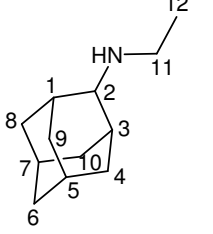
 $179.36 \text{ g mol}^{-1}$	Molecular Formula: $\text{C}_{12}\text{H}_{21}\text{N}$			
		% C	% H	% N
	Theoretical	80.38	11.81	7.81
	Observed	78.73	11.15	9.31

Table 12 – Comparison of the elemental analysis data with theoretical prediction for 2-ethyladamantamine, the reductive amination product between 2-adamantanone and ethylamine.

The outcome of these experiments demonstrated that 2-adamantanone undergoes nucleophilic attack by a primary amine to form a product containing an imine functional group. Reduction of the imine by sodium cyanoborohydride resulted in the formation of a secondary amine although a pure product was not obtained.

The stoichiometry of the reaction indicates that formation of one mole of imine requires reaction of one mole of adamantanone and one mole of ketone. The reduction process is more complex. Borch et al.¹⁵¹ identified in reductive amination reactions of several ketones, including tricyclic norbornanone, that one mole of sodium cyanoborohydride was capable of reducing three moles of imine. Experiments were not carried out to determine if this was the case in reductive amination reactions of 2-adamantanone. In the reductive amination reaction of 2-adamantanone to form 2-ethyladamantamine, sodium cyanoborohydride and 2-adamantanone were present in equimolar quantities. The reducing agent was, therefore, not present in a large excess and the reaction time allowed may not have been sufficient to effect complete reduction of the imine intermediate to 2-ethyladamantamine.

3.3.2 Kinetic study of imine formation reactions involving 2-adamantanone.

FTIR spectra of 2-adamantanone in methanol solution displayed an intense peak at 1703 cm^{-1} with additional smaller peaks or shoulders at 1679 , 1723 and 1733 cm^{-1} . Similar patterns of peaks around 1700 cm^{-1} have previously been identified and attributed to the stretching mode of the carbonyl group, $\nu_s(\text{C}=\text{O})$, in 2-adamantanone^{131, 160}. For solutions of pure 2-adamantanone in methanol the peak intensity of the 1703 cm^{-1} and related bands did not change over several hours duration.

Series of infra-red spectra recorded over several days revealed spectral drift and the appearance of water vapour peaks due to humidity changes. To compare spectra, the peak intensities were measured relative to a linear baseline between two points. The points selected were suitably removed from the wavenumber range of interest to be unaffected by any changes in the intensity of reagent peaks. Similarly, the intensity of a water vapour peak in each spectrum was monitored and used to eliminate the effect of varying environmental water vapour on the spectrum. The relative intensity of the solvent baseline points was monitored to ensure solvent did not evaporate from the reaction cell during experiments and thus affect the peak intensities of the reactants or products.

Figure 37 shows superimposed FTIR spectra of 2-adamantanone and ethylamine in methanol. The intensity of the $\nu_s(\text{C}=\text{O})$ band of 2-adamantanone decreased with time as a new peak at around 1660 cm^{-1} evolved.

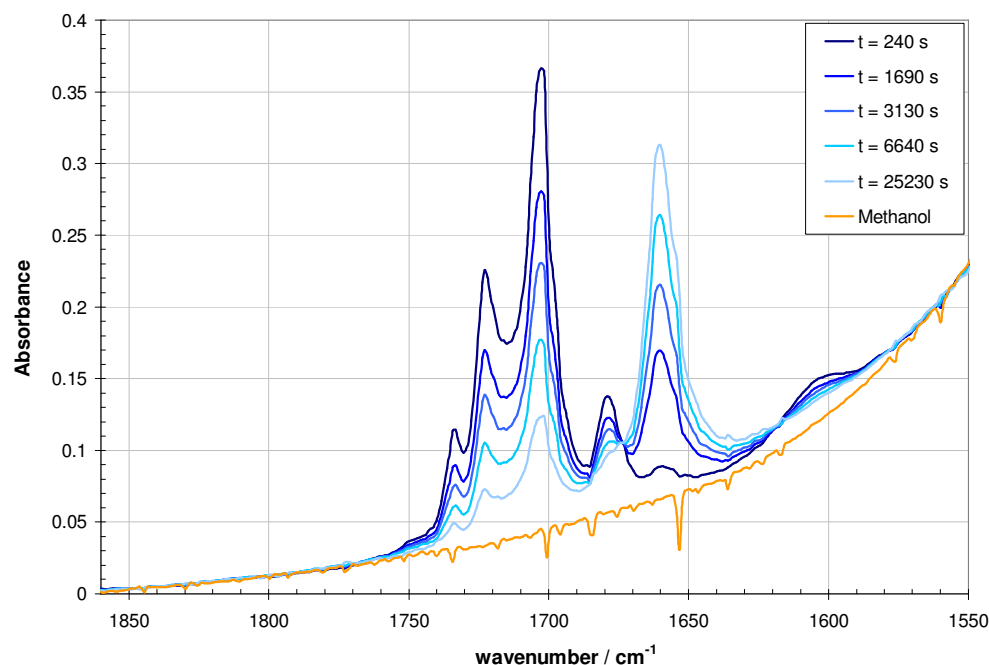


Figure 37 – Infrared spectra showing the time evolution for the reaction of 2-adamantanone and ethylamine. The $\nu_s(\text{C}=\text{O})$ band with maximum at 1702 cm^{-1} decreases and the band at 1659 cm^{-1} , assigned to $\nu_s(\text{C}=\text{N})$, increases. $T = 23 \pm 3\text{ }^\circ\text{C}$.

The reaction of 2-adamantanone and ethylamine formed a product which does not contain a carbonyl group. The new band occurs at a wavenumber consistent with an imine stretching mode $\nu_s(\text{C}=\text{N})$ ¹⁵³. The reaction of 2-adamantanone and ethylamine forming the imine *N*-ethyladamantan-2-imine (IUPAC name *N*-(tricyclo[3.3.1.1.3,7]dec-2-ylidene)ethanamine) is exemplary and provides the data for the supporting figures. The peak observed at 1660 cm^{-1} could arise from one of the reaction products, water or the corresponding imine. Solutions of liquid water in methanol show an absorption band centred at 1644 cm^{-1} arising from a bending vibration¹⁶¹. However the latter band is very broad, extending from $\sim 1610 - 1750\text{ cm}^{-1}$ which is dissimilar to the peak observed at 1660 cm^{-1} in Figure 37. Additionally, the feature appearing at 1660 cm^{-1} is an order of magnitude too intense to be due to absorption by water. A 2.0 mol L^{-1} solution of water in methanol is required to give an absorbance of the order seen in Figure 37. The maximum product concentration, due to the limiting reactant concentration, is 0.3 mol L^{-1} . Peaks associated with stretching modes of C=N bonds are regularly reported in the range $1620 - 1700\text{ cm}^{-1}$ without being described as broad^{153, 157, 158, 162}. The absorption band occurring at $\sim 1660\text{ cm}^{-1}$ is therefore ascribed to stretching of the C=N bond, $\nu_s(\text{C}=\text{N})$, in the corresponding imine.

The progress of reaction between 2-adamantanone and amine reagents was followed by incrementally recording a series of infra-red spectra over a suitable time period. The absorbance of the peaks due to the C=O and C=N stretching modes in each spectrum is shown as a function of time in Figure 38.

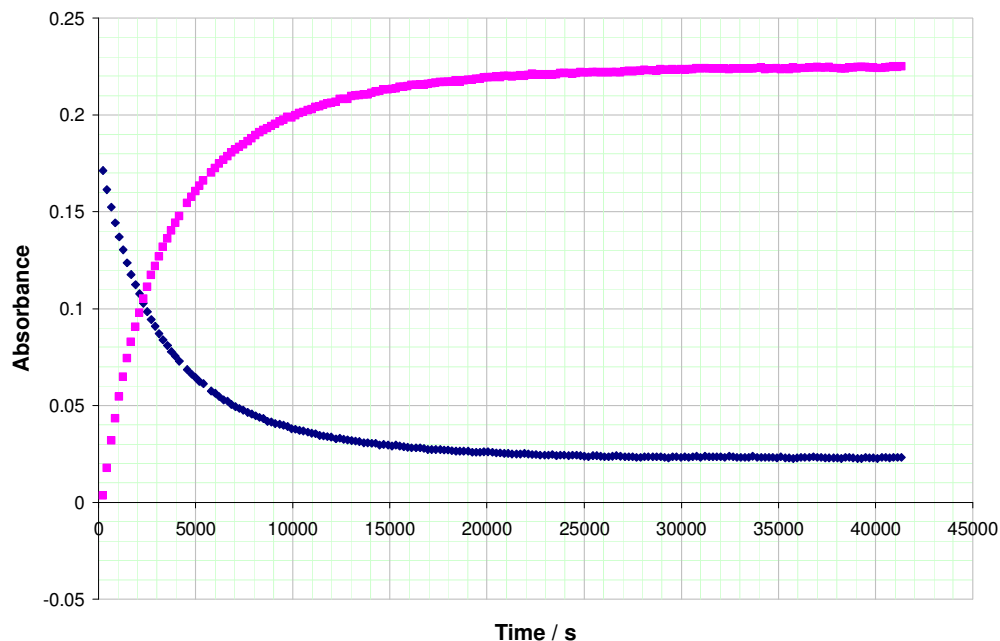


Figure 38 – Time dependence of the absorbance of $\nu_s(\text{C}=\text{O})$ (♦), and $\nu_s(\text{C}=\text{N})$, (■) at 23 ± 3 °C.

The absorbance of the $\nu_s(\text{C}=\text{O})$ peak was related to the concentration of 2-adamantanone by a Beer-Lambert relationship. A Beer-Lambert plot was constructed by plotting the $\nu_s(\text{C}=\text{O})$ peak intensity against concentration for solutions of 2-adamantanone in methanol from 0.1 to 0.7 mol L⁻¹. The Beer-Lambert plot was linear (a slightly negative intercept was observed which related to the difference between the adopted linear baseline and curved shape of the methanol envelope). The variation in 2-adamantanone concentration with time is shown in Figure 40 as the reaction attains equilibrium.

The amines in this work were generally aliphatic so the imines resulting from their reaction with 2-adamantanone are not Schiff bases and are difficult to isolate. Therefore, imine solutions of known concentration were not made up in order to construct a Beer-Lambert plot for each imine. Instead the assumption was made that the

imine concentration at equilibrium was equal to the concentration of 2-adamantanone consumed between the start of the reaction and equilibrium. This is shown in Figure 39 where a_0 and b_0 represent the initial 2-adamantanone and amine concentrations respectively and x_e represents the equilibrium concentration of imine and of water.

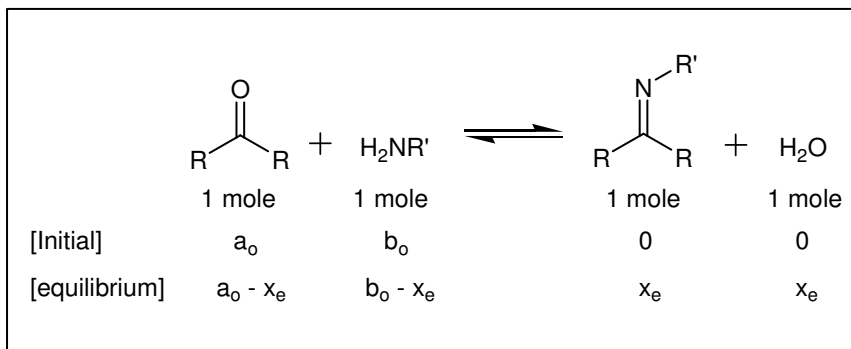


Figure 39 – The anticipated stoichiometry of imine formation and the assumption made that the equilibrium imine concentration is equal to the difference between the initial and equilibrium concentration of 2-adamantanone.

The intensity of the C=N stretching peak at equilibrium was plotted against the assumed equilibrium imine concentration. This point and the origin, where the $\nu_s(\text{C}=\text{N})$ intensity is zero when no imine is present, allowed a linear Beer-Lambert plot for the imine to be constructed. The intensity of the C=N stretch was measured in each infrared spectrum recorded over the course of the reaction, as shown in Figure 38, and related to the concentration of imine via this Beer-Lambert plot. Figure 40 shows the variation in imine concentration over the course of a reaction between 2-adamantanone and ethylamine, which attains equilibrium.

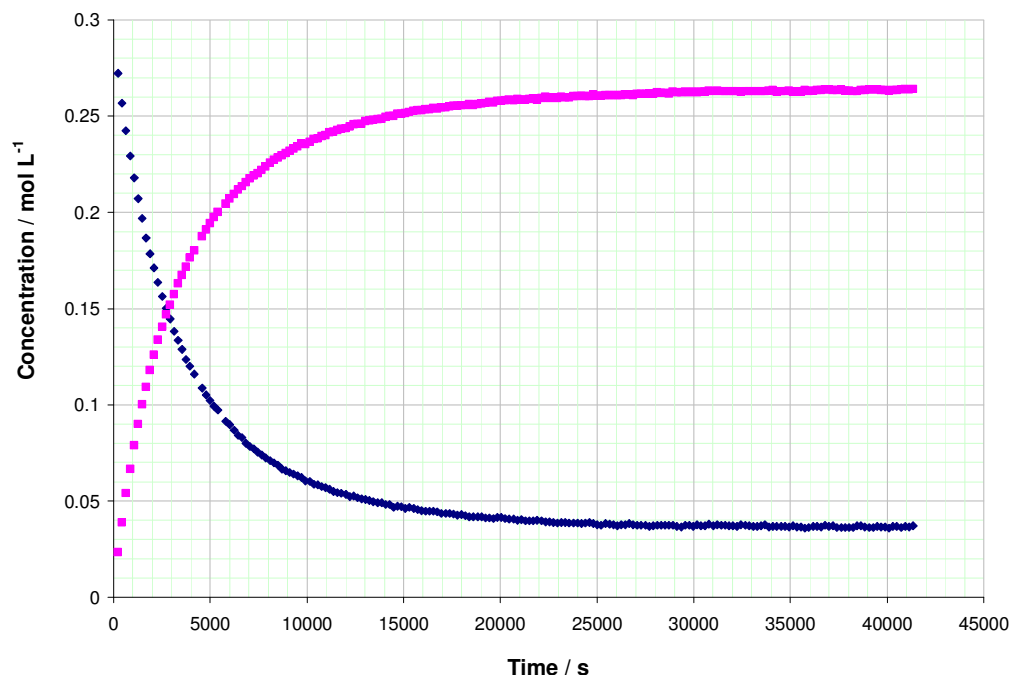


Figure 40 – Change in concentration over time of 2-adamantanone (\blacklozenge), and N-(tricyclo[3.3.1.1^{3,7}]dec-2-ylidene)ethanamine (\blacksquare), the imine product of reaction with ethylamine at 23 ± 3 °C.

3.3.4 Determination of observed rate constant.

To determine the rate constant for reactions the method of integration was adopted. The mechanism developed to describe imine formation and hydrolysis, on the basis of experimental observations, is in keeping with a second order reaction; first order with respect to each of the reactants^{139, 163}. For the reversible formation of imines from 2-adamantanone, the same order was assumed. The rate law describing consumption of 2-adamantanone could therefore be expressed as:

$$-\frac{d[Ad]}{dt} = k_f[Ad]^1[Am]^1 - k_r[Im]^1[H_2O]^1 \quad (15)$$

where k_f and k_r represent the forward and reverse rate constants and Ad, Am, Im and H_2O represent 2-adamantanone, amine, imine and water respectively. When 2-adamantanone and the amine reagent were present in the same initial concentration, expressing the rate law in terms of initial 2-adamantanone concentration a_0 and imine concentration x gives:

$$\frac{dx}{dt} = k_f(a_o - x)^2 - k_r x^2 \quad (16)$$

Upon integration subject to the boundary condition that $x = 0$ when $t = 0$ this equation becomes¹⁵²:

$$\frac{x_e}{2a_o(a_o - x_e)} \ln \frac{x(a_o - 2x_e) + a_o x_e}{a_o(x_e - x)} = k_f t \quad (17)$$

If plotting the expression on the left hand side of Equation 17 against time gives a linear plot the rate equation plotted is applicable to the system under study and the rate constant can be determined from the gradient of the linear data. The expression breaks down as the imine concentration approaches its equilibrium value and the bottom line in the \log_e term tends to zero. Figure 41 shows such a plot for the reaction of 2-adamantanone and ethylamine. After the reaction approaches equilibrium at around 25000 seconds the large scatter in the data is due to the break-down of the expression as highlighted above. In this example, the data obtained before the reaction reaches equilibrium conditions shows a slight curvature. This was not usually observed in similar plots for other experimental runs and may be due to experimental error such that the initial concentrations of 2-adamantanone and ethylamine differ slightly. The data can be described as linear over the first 10000 seconds by which time the reaction has proceeded to 90% conversion of reagents into the imine product. The rate constant could be reliably determined from the gradient of the linear data.

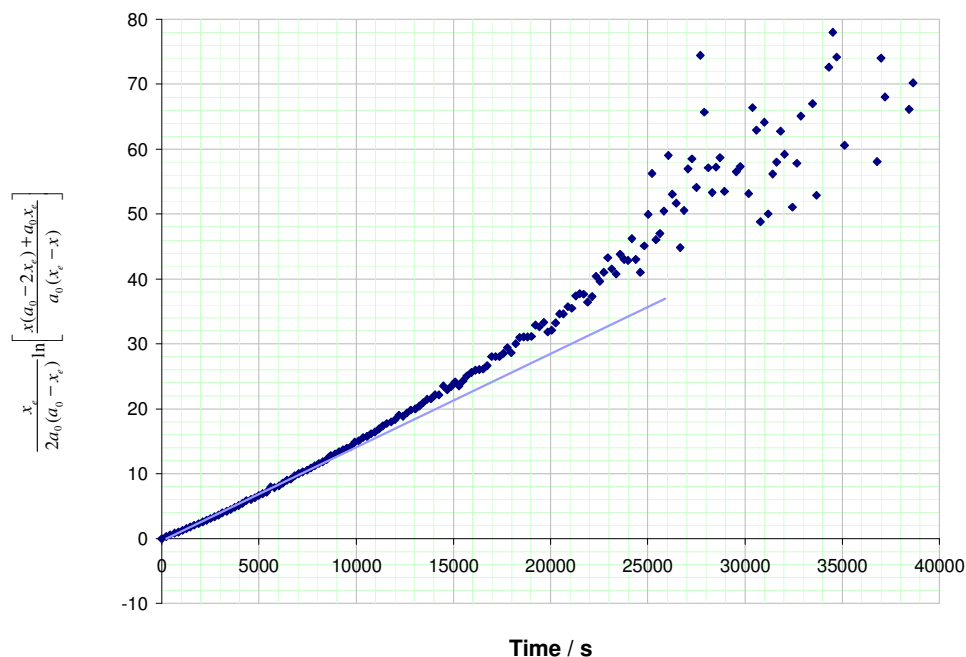


Figure 41 – Plot of integrated rate equation (17) for the reaction of 2-adamantanone and ethylamine $[\text{Ad}]_0 = [\text{Am}]_0 = 0.3 \text{ mol L}^{-1}$, $T = 23 \pm 3 \text{ }^\circ\text{C}$. The solid line (—) is shown to guide the eye.

Equation 16 described the system well but was only applicable when the initial concentrations of 2-adamantanone and amine were equal. It was desirable to be able to determine the rate constant for reactions where the initial concentrations were not equal.

The differential equation:

$$\frac{dx}{dt} = k(a_0 - x)(b_0 - x) \quad (18)$$

for a non-reversible reaction of two species of differing initial concentrations was adopted, where the initial concentration of 2-adamantanone is represented by a_0 and that of the amine reagent is b_0 . The integrated form becomes:

$$\frac{1}{(b_0 - a_0)} \ln \frac{a_0(b_0 - x)}{b_0(a_0 - x)} = k_f t \quad (19)$$

and can again be plotted graphically, as shown in Figure 42 again using experimental data obtained for the reaction of 2-adamantanone with ethylamine.

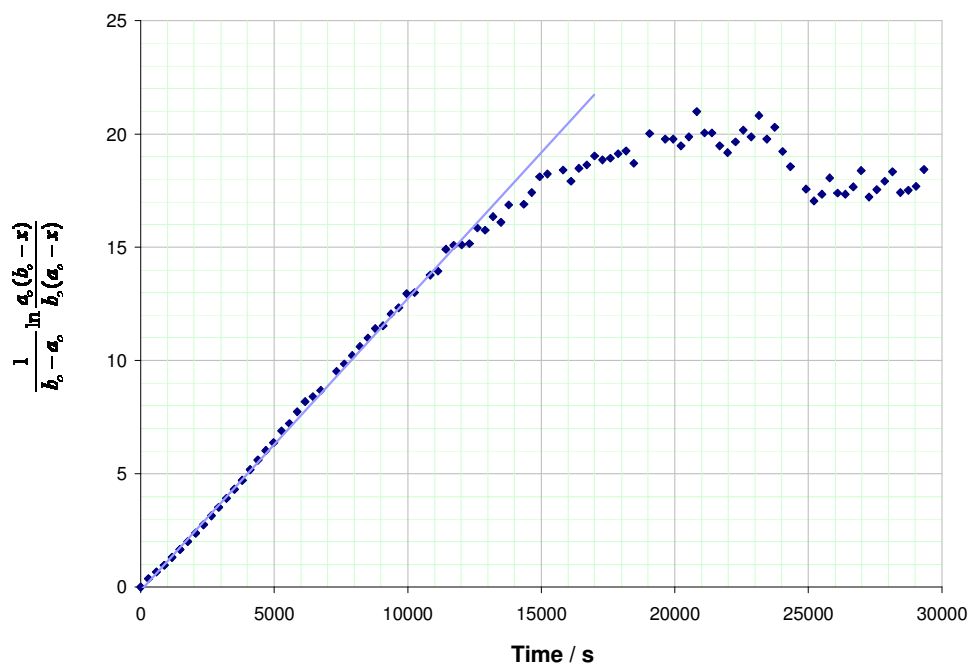


Figure 42 – Plot of integrated rate equation (19) for the reaction of 2-adamantanone and ethylamine. $[\text{Ad}]_0 = 0.45 \text{ mol L}^{-1}$, $[\text{Am}]_0 = 0.30 \text{ mol L}^{-1}$, $T = 23 \pm 3 \text{ }^\circ\text{C}$. The line (—) is shown to guide the eye.

Rate law (19) appears to describe the system well when the rate of the reverse reaction is negligible. The graph is linear up to around 12000 seconds by which time over 90% conversion has occurred. The observed rate constant for the reaction can be determined from the gradient of the linear section of the data. At later times when product concentrations become significant, this simple rate law no longer describes the mechanism, evidenced by the loss of linearity.

Good agreement was found between rate constants determined by the two different rate laws. Table 13 shows the rate constants determined from the data shown in Figure 41 and Figure 42 respectively. Rate constants, k_{obs} , were obtained from the slope of a best fit straight line determined by a least squares linear regression analysis. This analysis was carried out on the data in the linear region of integrated rate equation plots, where reactions had proceeded up to ~90% conversion. The line of best fit was determined over the largest number of data points for which a reasonable r^2 value (usually at least 0.995) could be obtained. The error in each rate constant was determined from the error in the best fit straight line. Where reactions were repeated average rate constants are quoted with errors representing the standard deviation, σ .

Initial concentration / mol L ⁻¹		Rate Law	k _{obs} / L mol ⁻¹ s ⁻¹
2-Adamantanone (a ₀)	Ethylamine (b ₀)		
0.30	0.30	Equation (17)	1.19 ± 0.01 x 10 ⁻³
0.45	0.30	Equation (19)	1.18 ± 0.02 x 10 ⁻³

Table 13 – Rate constants, at 23 ± 3 °C, determined from data shown in Figure 41 with initial reactant concentrations equal and data shown in Figure 42 when initial reactant concentrations were not equal.

3.3.5 Variation of rate with amine.

A series of six primary amines were selected for reaction with 2-adamantanone to investigate whether the structure of the amine had an effect on the rate of reaction. As the simplest amine, ammonia was studied as was ethylamine, benzylamine, 4-(trifluoromethyl)benzylamine, 3-phenylpropylamine and aniline. Ethylamine provided an example of a simple aliphatic amine. The other amines studied all contain an aromatic ring at increasing distance from the amino functionality. In aniline the amino group is bound to a carbon atom in the aryl ring, benzylamine has a single aliphatic carbon between the amino group and the ring whilst 3-phenylpropylamine has three such carbons. As a suitable candidate for analysing amine reactions on diamond surfaces (due to the sensitivity of X-ray photoelectron spectroscopy to fluorine) 4-(trifluoromethyl)benzylamine was studied to investigate its reactivity with 2-adamantanone. The forward reaction rate constants, k_{obs}, observed are shown in Table 14.

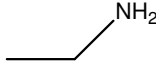
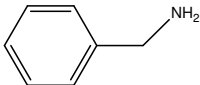
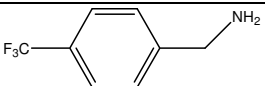
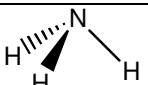
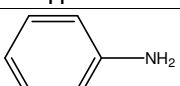
Amine	Structure	Runs averaged to determine k_{obs}	$k_{obs} / \text{L mol}^{-1} \text{s}^{-1}$
3-phenylpropylamine		3	$13.6 \pm 3.0 \times 10^{-4}$
Ethylamine		3	$11.3 \pm 1.0 \times 10^{-4}$
Benzylamine		2	$3.98 \pm 0.82 \times 10^{-4}$
4-(trifluoromethyl) benzylamine		4	$2.02 \pm 0.36 \times 10^{-4}$
Ammonia		4	$0.38 \pm 0.23 \times 10^{-4}$
Aniline		-	*

Table 14 – Observed rate constants of imine formation ($T = 23 \pm 3 \text{ }^\circ\text{C}$).

The reaction with aniline was extremely slow. To observe an appreciable drop in 2-adamantanone concentration required reaction times of several days. Over this time fluctuations appeared even in the normalised absorbance data, which appeared to correlate to the daytime rise and overnight fall of the spectrometer temperature due to ambient conditions. The rate constant, determined from a single experiment, with a poor r^2 value (0.83), was $< 0.03 \times 10^{-4} \text{ L mol}^{-1} \text{ s}^{-1}$. The reaction of aniline with 2-adamantanone was considerably slower than any of the other reactions studied.

The inability to compare the reaction rate of anilines with aliphatic amines at room temperature was disappointing. Structure-reactivity relationships are usually studied by reaction of aromatic molecules substituted with electron withdrawing and donating groups, for which the Hammett constants are well known. Increasing the reaction temperature from ambient was not possible since the experimental set-up lacked thermostatic temperature control.

3.3.6 Variation of rate with pH.

The effect of pH on the rate of reaction was studied for the reaction between 2-adamantanone and ethylamine. Without addition of acid or base the pH of reaction mixtures comprising ethylamine and 2-adamantanone in methanol was around 11.2. In alkaline solutions reaction was observed and rate constants are shown in Table 15. The rate constants quoted at pH 13.0 and 9.3 were determined from a single experiment at each pH and the relatively small errors quoted reflect the scatter in the data. Rate constants determined from several experiments at pH 11.2 gave a standard deviation of 10 – 20 % of the mean. The errors in the rate constants quoted at pH 13.0 and 9.3 are expected to be of this order.

pH	$k_{\text{obs}} / \text{L mol}^{-1} \text{s}^{-1}$
13.0	$12.0 \pm 0.1 \times 10^{-4}$
11.2	$11.3 \pm 1.0 \times 10^{-4}$
9.3	$4.97 \pm 0.67 \times 10^{-4}$
7.3	No reaction observed
4.0	No imine formation observed
2.8	No imine formation observed

Table 15 – Effect of pH on the rate constant of reaction between ethylamine and 2-adamantanone at 23 ± 3 °C.

In close to neutral solutions (pH = 7.3) no reaction was observed. The absorbance of the $\nu_s(\text{C}=\text{O})$ peak did not decrease with time and a $\nu_s(\text{C}=\text{N})$ peak was not observed. In acidic solutions the $\nu_s(\text{C}=\text{O})$ absorbance was observed to decrease over time. In contrast the $\nu_s(\text{C}=\text{N})$ peak did not emerge, indicating some process other than imine formation was consuming the 2-adamantanone. At pH < 7 the rate of decrease of the $\nu_s(\text{C}=\text{O})$ absorbance increased with decreasing pH.

In the absence of an amine, solutions of 2-adamantanone in acidified methanol also showed an identical decrease in the $\nu_s(\text{C}=\text{O})$ absorbance. This indicated that the amine was not participating at low pH. Electrospray mass spectrometry of a neutral solution

of 2-adamantanone in methanol showed a peak at m/z 151 corresponding to the molecular ion of 2-adamantanone²³. Solutions acidified to pH ~ 3 with methanolic HCl showed an additional peak at m/z 182. This corresponds to the molecular weight of the hemiacetal formed between 2-adamantanone and methanol. A peak was not observed at m/z = 196 which corresponds to the acetal.

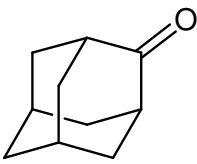
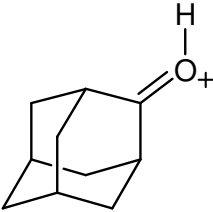
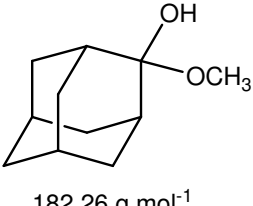
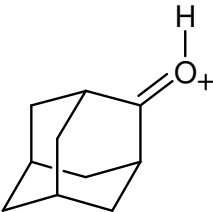
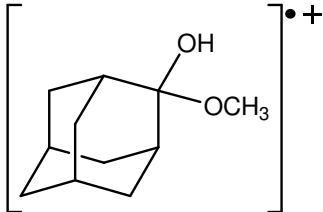
2-Adamantanone in methanol	Peak at m/z = 151.16	Peak at m/z = 182	Peak at m/z = 196
Neutral solution  $150.22 \text{ g mol}^{-1}$		None	None
Acidic solution  $182.26 \text{ g mol}^{-1}$			None

Table 16 – Significant peaks in electrospray mass spectra of 2-adamantanone in methanol at pH ~ 7 and pH ~ 3.

Hemiacetal formation occurs by nucleophilic attack of alcohol on the carbonyl group of an aldehyde or ketone¹³³. Reaction is generally slow at neutral pH, and no decrease in the $\nu_s(\text{C}=\text{O})$ absorbance was observed with time for solutions of 2-adamantanone in methanol at pH 7. Under acidic conditions acid catalysis occurs by protonation of the carbonyl oxygen atom to increase the electrophilicity of the carbon atom of the carbonyl functional group.

Since no change in the $\nu_s(\text{C}=\text{O})$ absorbance was observed with time at neutral pH the imine formation reaction was completely inhibited at ambient temperature. Hemiacetals were not formed at neutral pH so the implication is that they did not interfere with formation of the imine. An explanation for the lack of reaction is protonation of ethylamine, inhibiting its nucleophilicity. Jencks¹³⁹ observed that the reaction of

hydroxylamine ($pK_a = 5.94$) and acetone was inhibited by protonation of hydroxylamine at $pH \sim 2$. Under these conditions approximately one NH_2OH molecule in 1×10^4 is in the unprotonated form. For ethylamine ($pK_a = 10.70$) approximately one ethylamine molecule in 5×10^3 is in the unprotonated form at $pH 7$. It is proposed that the concentration of the reactive, unprotonated, nucleophile is simply too low for any significant reaction to occur under the experimental conditions adopted.

3.3.7 Effect of solvent on rate.

The reaction of 3-phenylpropylamine with 2-adamantanone was carried out in different solvents to investigate the effect of solvent on the reaction rate. Since most studies were carried out in polar protic methanol, for comparison polar aprotic dimethylsulphoxide and non-polar aprotic toluene were selected. The observed rates are tabulated in Table 17. The errors quoted in toluene and DMSO reflect the scatter of a single run. The more realistic error calculated from standard deviation of duplicate runs would be expected to be closer to the $\pm 20\%$ observed in methanol solution.

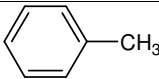
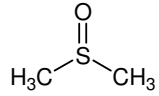
Solvent	Structure	Dielectric constant ¹⁶⁴ (T / °C)	$k_{obs} / L mol^{-1} s^{-1}$
Methanol	H_3C-OH	33.0 (20)	$13.6 \pm 3.0 \times 10^{-4}$
Toluene		2.4 (23)	$5.66 \pm 0.04 \times 10^{-4}$
DMSO		47.2 (20)	$1.87 \pm 0.02 \times 10^{-4}$

Table 17 – Rate constants for the reaction of 3-phenylpropylamine and 2-adamantanone in different solvents at 23 ± 3 °C.

To develop an understanding of solvent effects would require a far more detailed study than carried out here. It appears that reaction in toluene and DMSO are slower than reaction in methanol. As the only protic solvent studied the increased rate constant in methanol could be attributed to general acid catalysis. However, the unadjusted pH of 3-phenylpropylamine solutions was around 10 and therefore would not be catalysed by

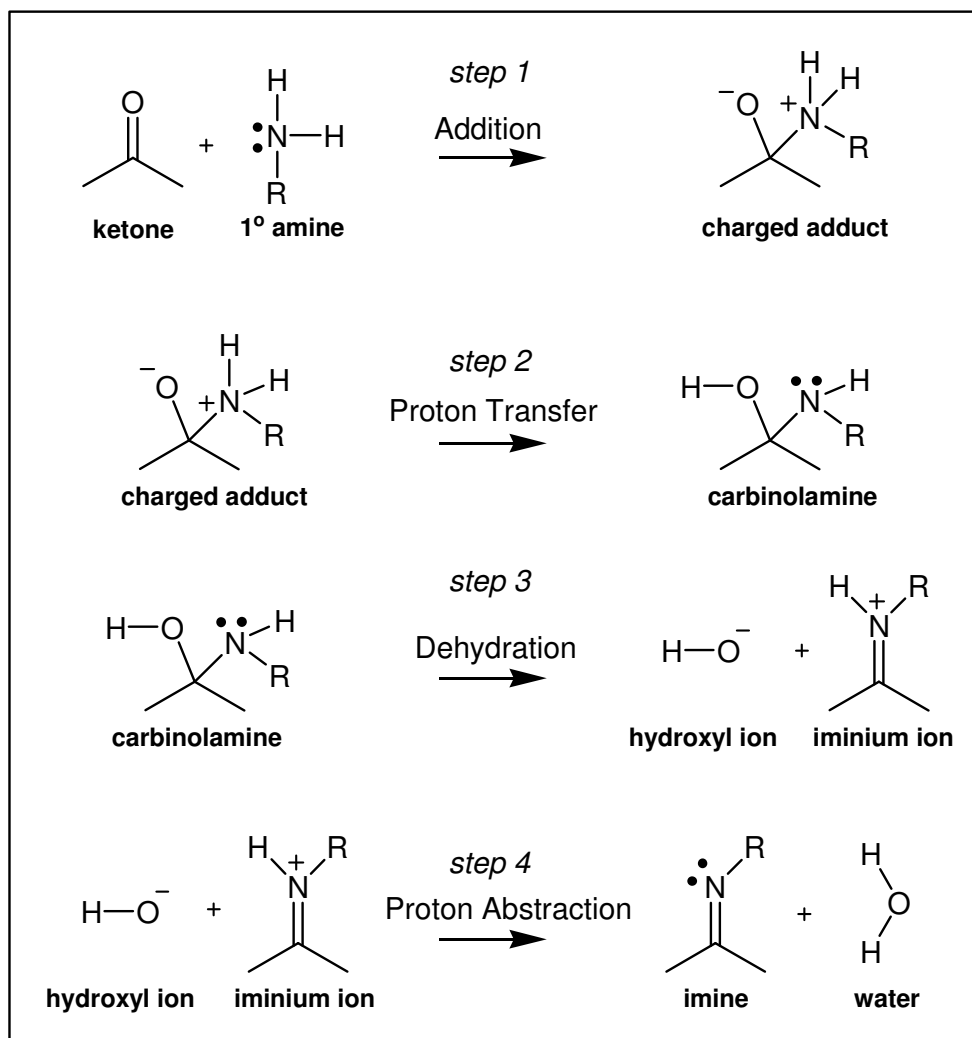
acid. The rate constants do not rank with dielectric constant of the solvent. The dielectric constant of a solvent is a measure of its polarity. The variation in rate constant cannot therefore be attributed to the polarity of each solvent. As the only solvent studied which is capable of hydrogen bonding, it seems more likely that methanol is better suited for solvation of the carbinolamine intermediate than the other solvents. This extra stabilization would promote carbinolamine formation, thus increasing the rate of amine addition.

3.3.8 Computational modelling.

To elucidate the mechanism of the reaction it was useful to be able to compare the experimental results obtained with kinetic modelling. The forward rate constants observed are necessarily that of the slowest, rate determining, step in the imine formation reaction. It has been shown^{139, 148, 163} that in the formation of imines from ketones other than 2-adamantanone the rate limiting step can either be addition or dehydration depending on the experimental conditions. Identification of the rate determining step is a key step in understanding a reaction mechanism. Kinetic modelling software was utilised to investigate the effect on reactant and product concentration when the experimentally determined rate constant was applied to the addition and dehydration steps in turn.

The experimental data from the reaction between 2-adamantanone and ethylamine, was used for comparison. Both reagents had initial concentrations of 0.3 mol L⁻¹ and the rate constant determined from this run was $11.9 \pm 0.1 \times 10^{-4}$ L mol⁻¹ s⁻¹ at 23 ± 3 °C. As stated above, ethylamine solutions exhibited a pH of around 10.7. Therefore, with reference to the published mechanism,¹⁴⁸ nucleophilic addition of ethylamine to 2-adamantanone without catalytic protonation of the carbonyl oxygen, followed by proton transfer and carbinolamine dehydration, as shown in Scheme 2, would be expected to occur. The mechanistic steps used for computational modelling are shown in Scheme 3. The proton transfer process, steps 2 and 3 in Scheme 1, in which protonation of the initial addition adduct occurs at the oxygen atom followed by loss of a proton adjacent to the nitrogen atom, was combined into one step, step 2 in Scheme 3. Proton transfer could occur as an intramolecular process and is expected to be fast compared to the bond formation or cleavage in the addition or dehydration steps, even under basic

conditions. The proton transfer and proton abstraction steps, steps 2 and 4 respectively in Scheme 3, were assigned forward rate constants $\sim 10^4$ times faster than the rate determining step.



Scheme 3 – Steps used to describe irreversible imine formation under basic conditions for computational modelling.

Whilst a limiting reverse rate constant could have been determined from:

$$K_{eq} = \frac{k_f}{k_r} \quad (20)$$

using the experimental equilibrium concentrations, assigning a rate determining step in the reverse reaction and assuming suitable rate constants for the other steps in the

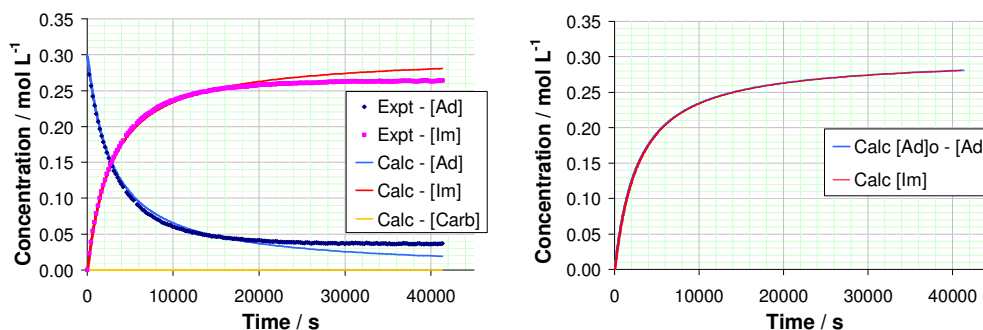
reverse reaction complicated the model considerably. It has already been shown that the reaction can be described as an irreversible process during early reaction times where product concentrations are small and the reverse reaction is negligible. The reaction was therefore modelled as an irreversible process.

The variation in 2-adamantanone and imine concentration with time was calculated for values of the addition and dehydration rate constants shown in Table 18. The results are overlaid on the experimental concentrations in Figure 43. The calculated concentration of carbinolamine over time is also plotted. Due to the approximation of an irreversible reaction the model gives equilibrium concentrations tending to complete reaction. At early reaction times, when the reverse reaction is negligible, the comparison between the calculated and experimental concentration data indicates how well the combination of rate constants used describes the experimental data. The amount of 2-adamantanone consumed is also plotted alongside the concentration of imine to allow comparison of the rate of formation of imine with the rate of 2-adamantanone loss.

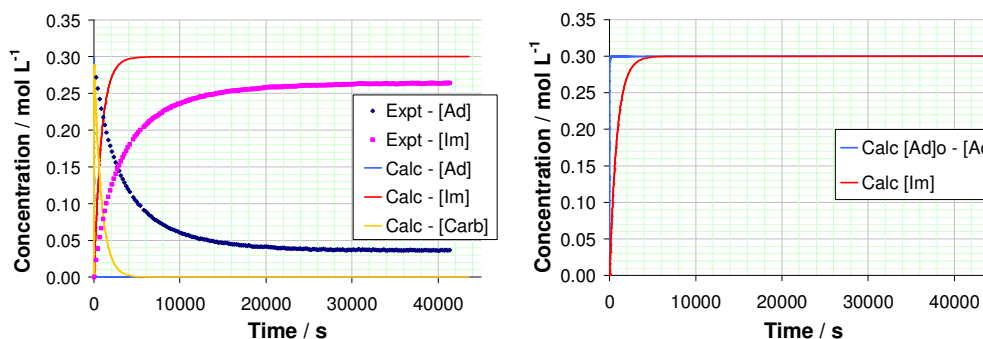
Data Set	Addition rate constant / L mol ⁻¹ s ⁻¹	Dehydration rate constant / L mol ⁻¹ s ⁻¹
A	1.19 x 10⁻³	10
B	10	1.19 x 10⁻³
C	1.19 x 10⁻³	2.38 x 10 ⁻³
D	2.38 x 10 ⁻³	1.19 x 10⁻³

Table 18 – Rate constants used for addition and dehydration steps in modelling calculations. Constants for the rate determining steps are given in bold. The resulting calculated concentration data is shown against time in Figure 43.

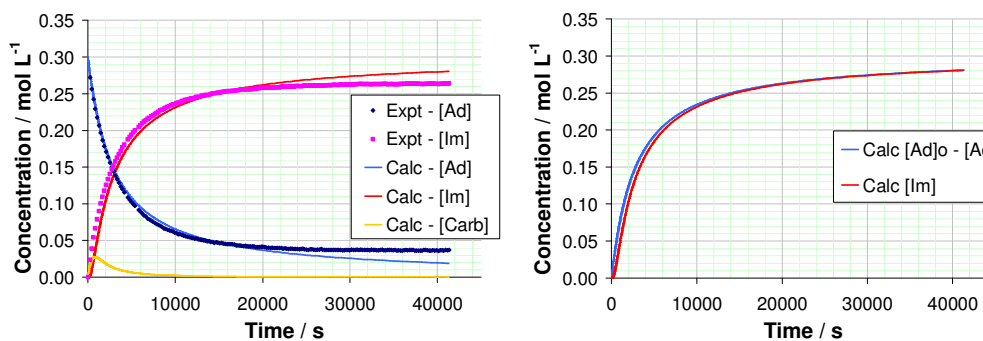
A – Addition $k_f = 1.19 \times 10^{-3} \text{ L mol}^{-1} \text{ s}^{-1}$, dehydration $k_r = 10 \text{ L mol}^{-1} \text{ s}^{-1}$



B – Addition $k_f = 10 \text{ L mol}^{-1} \text{ s}^{-1}$, dehydration $k_r = 1.19 \times 10^{-3} \text{ L mol}^{-1} \text{ s}^{-1}$



C – Addition $k_f = 1.19 \times 10^{-3} \text{ L mol}^{-1} \text{ s}^{-1}$, dehydration $k_r = 2.38 \times 10^{-3} \text{ L mol}^{-1} \text{ s}^{-1}$



D – Addition $k_f = 2.38 \times 10^{-3} \text{ L mol}^{-1} \text{ s}^{-1}$, dehydration $k_r = 1.19 \times 10^{-3} \text{ L mol}^{-1} \text{ s}^{-1}$

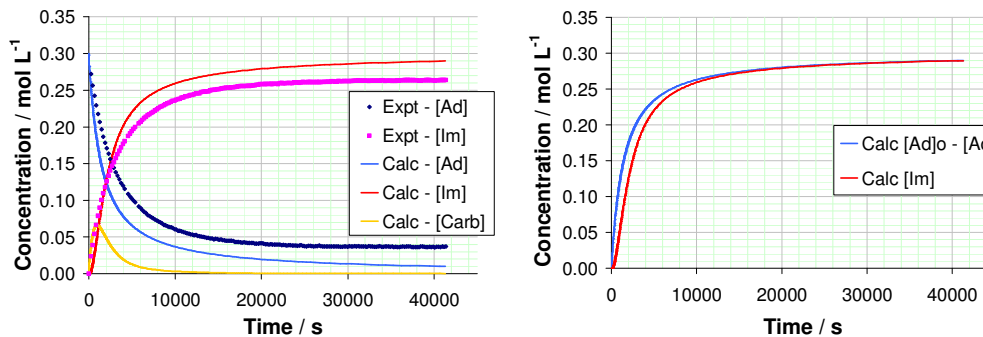


Figure 43 – Computed concentration vs time profiles using rate constants provided in Table 18. Left plot shows the evolution of 2-adamantanone, [Ad], and imine, [Im], concentration, compared to experiment, and carbinolamine concentration, [Carb]. Right hand plot shows the calculated imine concentration overlaid with the calculated amount of ketone consumed ($[\text{Ad}]_0 = \text{initial 2-adamantanone concentration}$).

The level of agreement between the calculated concentration profiles and experimental data, shown in Figure 43, provides information on which step in the mechanism is rate limiting. In Figure 43-A addition is rate determining and all other steps are several orders of magnitude faster. The computed reagent concentrations agree perfectly with the experimental data at early times. The rate of imine formation is exactly equal to that of ketone consumption. When dehydration is rate determining and several orders of magnitude slower than all other steps, as shown in Figure 43-B, calculation suggests equilibrium would be achieved at much shorter times than is experimentally observed. The model also demonstrates that 2-adamantanone would be completely consumed almost instantaneously to form a large concentration of carbinolamine. The rate of 2-adamantanone consumption is therefore very much faster than observed experimentally.

Figure 43-C and Figure 43-D demonstrate the computed concentrations if the rates of addition and dehydration are of the same order of magnitude. In Figure 43-C, where the addition step is rate determining and the rate constant of dehydration is twice that of addition, the computed 2-adamantanone concentration agrees well with experiment. However since a small carbinolamine concentration develops the concentration of imine over time does not match the experimental data perfectly. It can be seen that there is a slight difference between the rate of formation of imine and the rate of consumption of 2-adamantanone on adopting these rate constants. In Figure 43-D dehydration is rate determining with a rate constant half that of the addition step. The computed profiles again show a deviation from the experimental data and again the rate of imine formation is not equal to that of 2-adamantanone consumption. Similar calculations were carried out in which the addition and dehydration reactions were both given the experimentally determined rate constant. In this case, the computed concentrations showed deviation from the experimental results, similar to Figure 43-C and D.

The best agreement between experiment and calculation is shown in Figure 43-A and was obtained when the experimentally determined rate constant was applied to the addition step, step 1 in Scheme 3, with all other rate constants several orders of magnitude larger.

3.3.3 Rate of imine formation

Since kinetic modelling of the reaction indicated that comparison of the rate of imine formation and the rate of 2-adamantanone consumption could yield information on the rate determining step this was investigated further. The experimental data shown in Figure 40 for the reaction of 2-adamantanone with ethylamine were used to compare the experimental rates of imine formation and 2-adamantanone consumption in Figure 44. The pink points, as in Figure 40, show the imine concentration data. The black points overlaid on this show the amount of 2-adamantanone consumed throughout the reaction, calculated as the difference between the initial and current 2-adamantanone concentration at each time interval. It is clear from Figure 44 that the rate of imine formation from ethylamine is the same as the rate of loss of 2-adamantanone. The same excellent correlation was observed for all the other amines studied.

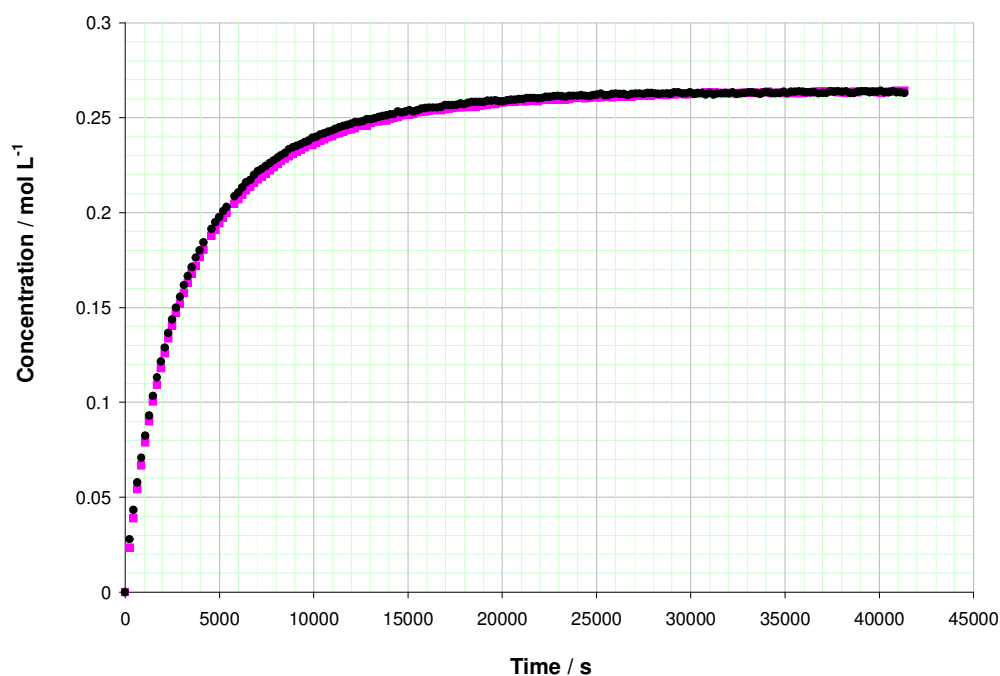


Figure 44 – Comparison of the experimentally determined change in imine concentration (■) with the concentration of 2-adamantanone consumed (●) for the reaction with ethylamine.

The calculated situation which shows the best agreement with the experimental data is that shown in Figure 43-A. In Figure 43-A the initial addition step, step 1 in Scheme 3, has been modelled with a limiting rate constant, all other rate constants are several

orders of magnitude larger, and it can be seen that the rate of imine formation and 2-adamantanone consumption are equal throughout the reaction.

The assumption made that the imine concentration at equilibrium is equal to the concentration of 2-adamantanone consumed between the start of the reaction and equilibrium would not be valid if the imine product reacted further to produce a secondary product or a concentration of carbinolamine intermediate existed at equilibrium. No evidence of imine polymerisation products was observed. Characterisation of the synthesised derivatives showed only the expected oxime and semicarbazide and no bands other than those corresponding to the starting materials and imine product were observed in the FTIR spectra. This is in-keeping with the published literature in which further reaction products of the imine have only been observed for low molecular weight aldehyde starting materials¹⁴²⁻¹⁴⁴.

If an equilibrium concentration of carbinolamine did exist the absolute values of imine concentration shown in Figure 44 may be incorrect but the shape of the curve would still be correct as the imine concentration at each point is deduced directly from the intensity of the $\nu_s(\text{C}=\text{N})$ peak in the FTIR spectra. The observation that the evolution of the imine concentration with time has exactly the same shape as the consumption of 2-adamantanone indicates that when carbinolamine intermediate is formed it must dehydrate immediately to yield the imine. If this was not true a concentration of carbinolamine would develop and there would necessarily be a delay in the onset of imine formation, giving a different shape to the rate of imine formation than that of 2-adamantanone consumption, as is observed in Figure 43 – C and D.

Since any carbinolamine is dehydrated to yield imine as soon as it is formed then the equilibrium concentration of carbinolamine must be negligible. The equilibrium imine concentration should therefore be equal to the concentration of 2-adamantanone consumed, validating the assumption made.

3.3.9 Discussion of imine formation from 2-adamantanone.

Investigations of imine formation from 2-adamantanone revealed that, for the examples studied, the rate of imine formation was equal to the rate of consumption of the 2-

adamantanone carbonyl group. This is demonstrated for the reaction of ethylamine in Figure 44. Since the C=O bond is consumed in the first step and the C=N bond not formed until the last steps in the mechanism, it seems intuitive that the interim steps must occur extremely quickly to allow the two processes to appear concurrent. This intuitive conclusion appears to be borne out by kinetic modelling of the reaction. Utilising the published mechanism¹⁴⁸ at alkaline pH where dehydration occurs by initial loss of hydroxyl ion, good agreement with the experimental data can only be achieved when the rate constant for addition of amine to ketone is several orders of magnitude less than that used for the rate constants of the other steps.

The conclusion that addition is rate limiting under basic conditions is different from the observations of Jencks et al^{87, 138, 139, 148, 163} in developing the accepted 'text-book' mechanism of imine formation. Addition is usually found to be rate limiting only under acidic conditions when the concentration of free amine becomes sufficiently small to reduce the rate of addition below that of dehydration. Investigating the variation in reaction rate with pH also revealed a situation quite different from the classic imine formation rate dependence on pH. Generally a rate maximum is observed corresponding to a transition from rate limiting addition at low pH to rate limiting dehydration at higher pH. A plot of the rate constant against pH for the imine formation reaction between ethylamine and 2-adamantanone is shown in Figure 45. There is no rate maximum corresponding to a switch in rate determining step. At high pH the rate appears to be independent of pH indicating a reaction uncatalysed by base. On lowering the pH the rate decreases due to ethylamine protonation. As less free amine is available to react the rate continues to drop until no reaction is observable at pH of approximately 7 under these conditions. Addition of free amine to the electrophilic carbonyl group of 2-adamantanone is the rate determining step throughout the pH range studied.

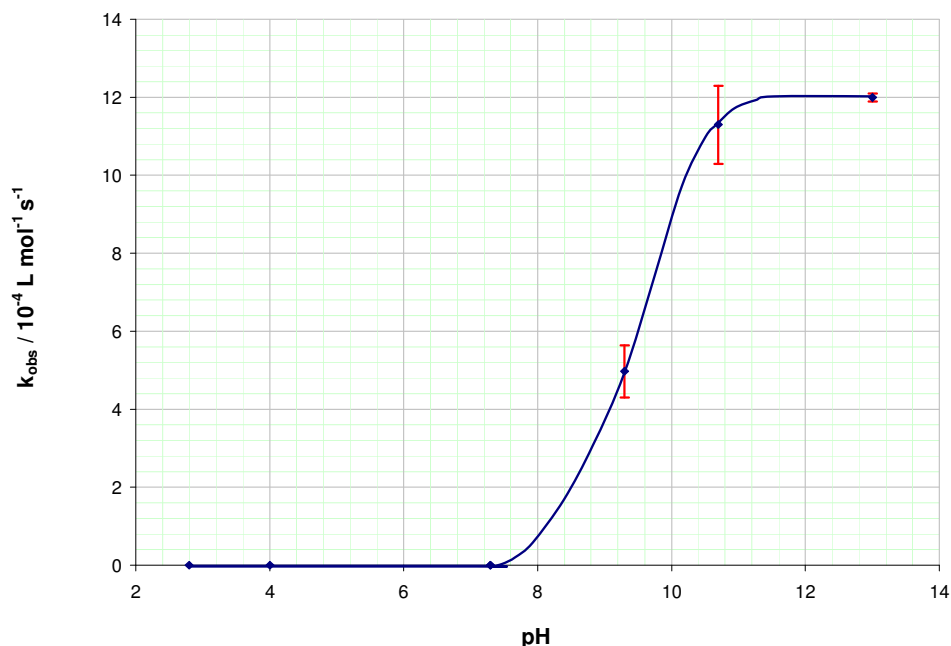


Figure 45 – Variation in rate constant with pH of imine formation reaction between ethylamine and 2-adamantanone. The line (—) is a guide to the eye.

In classic imine formation reactions, such as that between acetone and hydroxylamine¹³⁹, the rate constants of the addition and dehydration steps are finely balanced such that a change in conditions can bring about a switch in the rate determining step. In reactions with 2-adamantanone the rate constant of the addition step seems to be significantly less than that of dehydration, such that dehydration does not become rate limiting. This would suggest that 2-adamantanone either greatly facilitates dehydration of the carbinolamine derivative, increasing the rate constant for dehydration, or greatly hinders its ability to undergo nucleophilic attack, thus decreasing the rate constant for addition. The process of carbinolamine dehydration under basic conditions relies upon the rate of expulsion of hydroxide ion, assisted by nucleophilic action of the nitrogen lone pair from the amine. The product is a charged iminium ion. Facilitation of dehydration would require that 2-adamantanone stabilised the charged iminium ion more than other ketones, such as acetone. As 2-adamantanone is an aliphatic hydrocarbon without electronegative heteroatoms or assistance from aromatic delocalisation it is difficult to envisage why it should be particularly good at charge stabilisation. In contrast, due to its cage like structure, the rate of nucleophilic attack on 2-adamantanone is likely to be reduced relative to other aliphatic ketones.

Nucleophilic addition of an amine to a carbonyl group occurs by overlap of the σ highest occupied molecular orbital (HOMO) of the amine with the π^* lowest unoccupied molecular orbital (LUMO) of the carbonyl containing molecule. Figure 46 demonstrates the shape of A) the HOMO of ammonia and B) the LUMO of formaldehyde as exemplary compounds. The preferred angle of attack of nucleophiles on carbonyl groups, shown in Figure 46 C, is called the Bürgi-Dunitz trajectory after the researchers who identified it to be $105^\circ \pm 5^\circ$ by analysis of crystal structures of a range of materials¹⁶⁵. Computational modelling¹⁶⁶ supports the idea that this angle of approach is preferred as it maximises the required nucleophile HOMO – carbonyl LUMO interaction whilst minimising unfavourable molecular orbital interactions. 2-adamantanone's rigid cage structure means that four carbon – carbon bonds are fixed in space at the standard tetrahedral carbon angle of 109.5° to the carbonyl group. Particularly when the attacking nucleophile is bulky, the cage structure of 2-adamantanone is likely to hamper attack of nucleophiles along the Bürgi-Dunitz trajectory, forcing nucleophiles to approach the carbonyl group at lower angles to achieve successful reaction. Figure 46 D shows the structure of benzylamine and 2-adamantanone, and the steric bulk on each molecule which may prevent approach along the Bürgi-Dunitz trajectory. An additional orientation requirement would be expected to affect the pre-exponential factor in the Arrhenius equation, reducing the rate constant for nucleophilic attack on 2-adamantanone. Testing this hypothesis requires suitable experiments to place 2-adamantanone in a 'reactivity series' of ketones subject to nucleophilic attack. Unfortunately it is not possible to compare the rates determined in this work to reactions of other ketones as rates for addition can only be gleaned from other studies under strongly acidic conditions. In this case the rate is then dependant on the position of the acid base equilibrium of the amine. A reasonable comparison could be carried out by measuring the rate of reduction of 2-adamantanone by sodium borohydride to rank 2-adamantanone with the various ketones studied by Brown et al^{135, 136} (shown in Table 9).

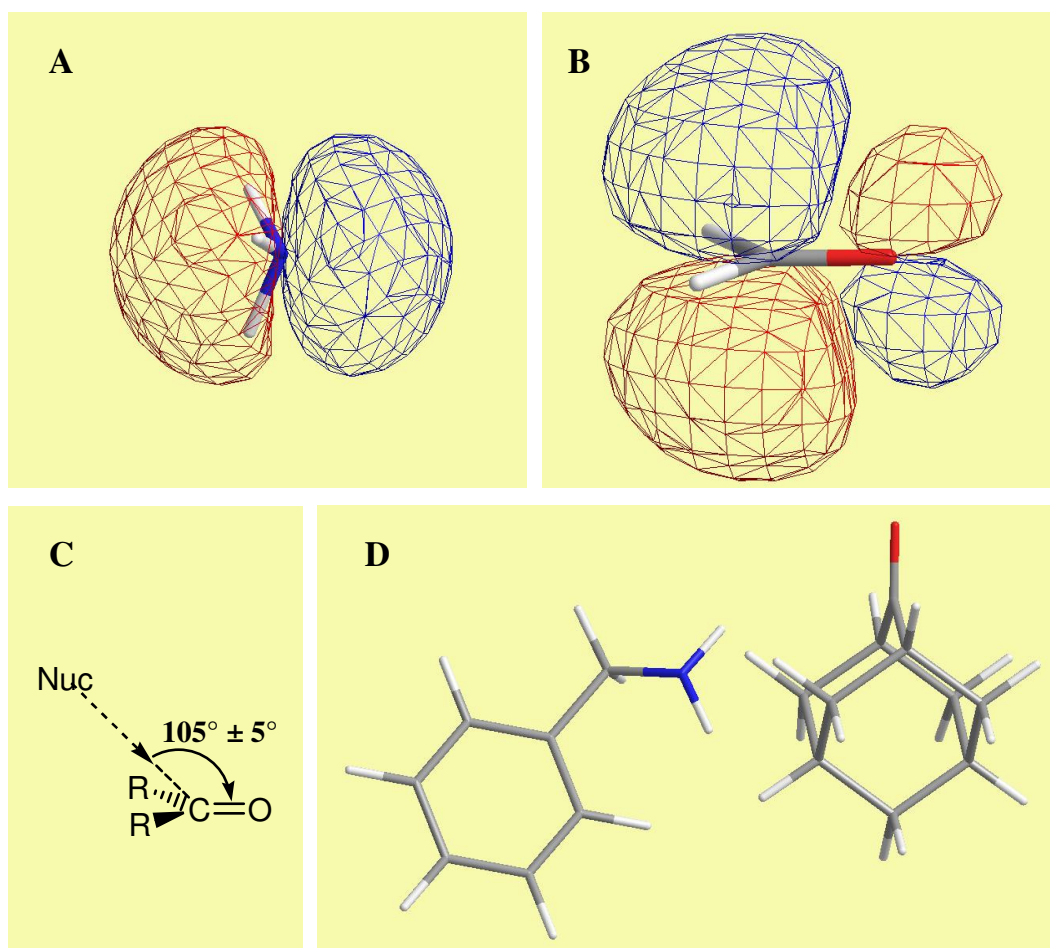


Figure 46 – A) the σ highest occupied molecular orbital (HOMO) of ammonia. B) The π^* lowest unoccupied molecular orbital (LUMO) of formaldehyde. C) Generalised representation of the preferred trajectory of attack (Bürgi-Dunitz trajectory) of a nucleophile on a carbonyl group D) The structures of 2-adamantanone and benzylamine to demonstrate the steric bulk on each molecule which may hinder nucleophilic attack.

Structure – reactivity relationships have been observed under conditions where the nucleophilic addition of amine to ketone is rate limiting¹⁶⁷. Unfortunately due to the slow reaction of aniline with 2-adamantanone it was not possible to carry out a structure – reactivity investigation with a variety of substituted anilines and produce a Hammett plot. However, there does seem to be some correlation of amine structure and rate constant. Within experimental error, tabulating the amines in order of their pK_a in aqueous solution, also ranks them in order of their reactivity with 2-adamantanone in methanol solution, as shown in Table 19.

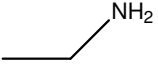
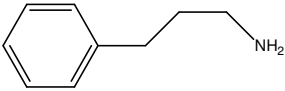
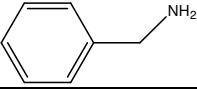
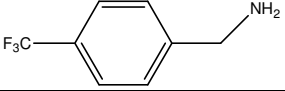
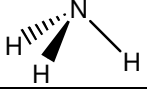
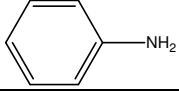
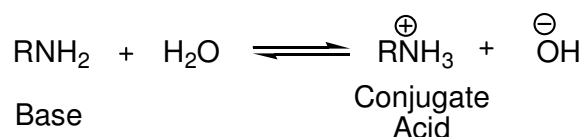
pK _a	Amine	Structure	k _{obs} / L mol ⁻¹ s ⁻¹
10.70	Ethylamine		11.3 ± 1.0 x 10 ⁻⁴
10.60	3-phenylpropylamine		13.6 ± 3.0 x 10 ⁻⁴
9.33	Benzylamine		3.98 ± 0.82 x 10 ⁻⁴
-	4-(trifluoromethyl) benzylamine		2.02 ± 0.36 x 10 ⁻⁴
9.25	Ammonia		0.38 ± 0.23 x 10 ⁻⁴
4.63	Aniline		~ 0.03 x 10 ⁻⁴

Table 19 – Rate constants for reaction of amines with 2-adamantanone at 23 ± 3 °C, tabulated by pK_a in aqueous solution.

The pK_a of an amine dictates the position of the equilibrium shown in Scheme 4 between the conjugate acid and the base. Stronger bases have a larger pK_a indicating that more of the base exists as the conjugate acid in solution.



Scheme 4 – The acid – base equilibrium of an amine in aqueous solution.

The availability of the amine lone pair for donation to a proton to form a quaternary ammonium ion is similar to its reactivity towards nucleophilic reaction with a carbonyl functional group. In aniline the nitrogen lone pair is stabilised by resonance with the aromatic ring and therefore is a weaker base and is less reactive towards imine formation. Conversely, the nitrogen lone pair in aliphatic nucleophiles such as ethylamine is not stabilised and acts as a strong base. Ethylamine and 3-phenylpropylamine show the fastest reaction with 2-adamantanone at room temperature. Whilst 3-phenylpropylamine contains an aromatic ring, it is separated from the amino functionality by three aliphatic carbon atoms and so does not stabilise the lone pair, as

reflected in its similar basicity to ethylamine. The pK_a of 4-(trifluoromethyl)benzylamine is expected to be similar but slightly less than that of benzylamine, due to the strongly electron withdrawing trifluoro group. In the absence of significant steric bulk, it seems that the pK_a of an amine may be used to give some guidance as to its relative rate of nucleophilic addition to 2-adamantanone.

3.3.10 Reductive amination.

Having observed that reaction of ethylamine and 2-adamantanone, in the presence of sodium cyanoborohydride, was capable of producing the reduced secondary amine *N*-ethyladamantan-2-amine, FTIR studies on simultaneous reductive amination reactions were carried out. It was observed that while the absorbance of the $\nu_s(\text{C}=\text{O})$ band decreased over time (as observed for imine formation), the $\nu_s(\text{C}=\text{N})$ band absorbance displayed classic intermediate behaviour, as shown in Figure 47. The imine concentration attained a maximum and then decreased as the reaction progressed. The loss of the $\text{C}=\text{N}$ stretching band was attributed to reduction of the $\text{C}=\text{N}$ double bond to a $\text{C}-\text{N}$ single bond, forming an amine.

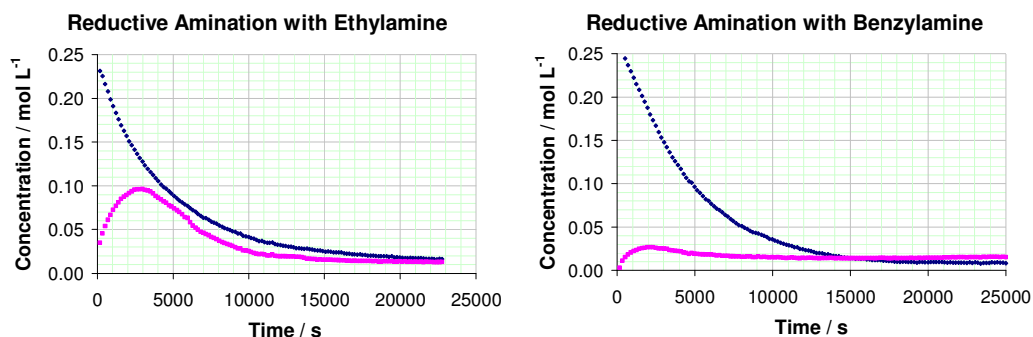


Figure 47 – Concentration of 2-adamantanone (◆) and imine product (■), during the reductive amination with sodium cyanoborohydride at $23 \pm 3^\circ\text{C}$.

The rate of imine reduction by sodium cyanoborohydride was indicated by the concentration of imine which developed prior to reduction to the amine. Ethylamine, which reacted relatively quickly with 2-adamantanone, developed a significant concentration of imine in the reductive amination experiment, as shown in Figure 47. Reductive amination with benzylamine, which reacted more slowly with 2-

adamantanone ($k_{\text{obs}} = 3.98 \pm 0.82 \times 10^{-4} \text{ L mol}^{-1} \text{ s}^{-1}$), developed a small concentration of imine, see Figure 47. 4-trifluoromethylbenzylamine, which reacted with 2-adamantanone more slowly than benzylamine ($k_{\text{obs}} = 2.02 \pm 0.36 \times 10^{-4} \text{ L mol}^{-1} \text{ s}^{-1}$), did not develop a detectable imine concentration during reductive amination experiments. The rate constant of imine reduction by sodium cyanoborohydride must be on the same order of magnitude as the rate constants measured for addition of amines to 2-adamantanone. If the rate constant for reduction was much faster than that of addition a concentration of imine would not be observed with any amine, if it was much smaller an intermediate concentration would always be observed. However further study would be required to confirm this tentative conclusion.

In reductive amination with ammonia a white solid was observed to form in solution. The solid was collected on filter paper, recrystallised from 50:50 chloroform and methanol and analysed by electron impact mass spectrometry, giving a molecular ion peak at $m/z = 283$. The expected product of the reductive amination reaction between ammonia and 2-adamantanone is adamantan-2-amine. However this primary amine (pK_a of 9.00¹⁶⁸) could react with a second molecule of 2-adamantanone to form *N*-(adamantyl)adamantan-2-imine, as shown in Figure 48. In the presence of sodium cyanoborohydride reduction to form *N*-(adamantyl)adamantan-2-amine could occur, also shown in Figure 48.

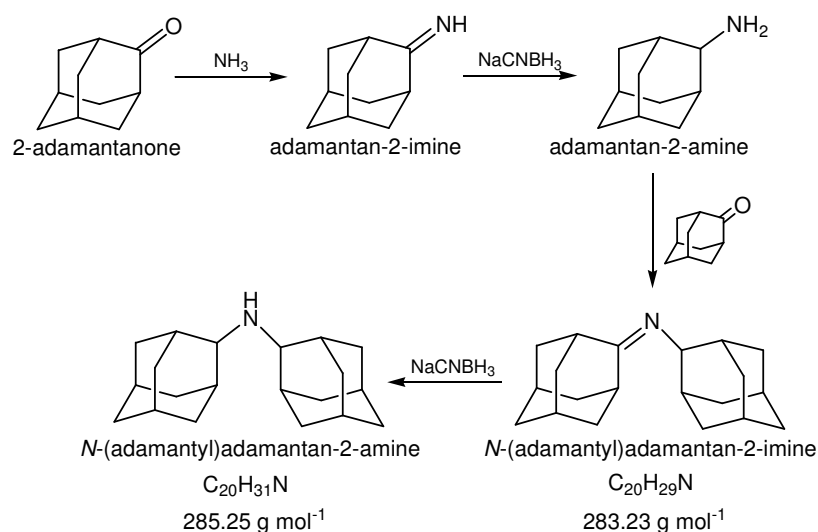


Figure 48 – Reaction scheme demonstrating the one-pot reaction in which adamantan-2-amine may undergo further reaction with 2-adamantanone to form *N*-(adamantyl)adamantan-2-imine. *N*-(adamantyl)adamantan-2-amine would result from subsequent reduction by sodium cyanoborohydride.

The molecular ion detected at $m/z = 283$ by mass spectrometry is consistent with the formation of the imine *N*-(adamantyl)adamantan-2-imine. Precipitation of this product would prevent it being reduced by sodium cyanoborohydride to the corresponding amine. The formation of this secondary imine product would undoubtedly complicate the kinetic analysis for the reductive amination of 2-adamantanone with ammonia. The rate of consumption of 2-adamantanone would be increased by its participation in the second reaction and two imines are formed, both of which would generate C=N stretching bands in the same region. Products from secondary reactions were not observed for the other amines studied. An analogous reaction would not be possible on a (100) diamond surface as the amine functionality would be bound to the surface and not free to undergo a second reaction with an adjacent carbonyl group. Solutions of 2-adamantanone and sodium cyanoborohydride in the absence of an amine did not show any decrease in $\nu_s(\text{C}=\text{O})$ absorbance with time. These studies suggest sodium cyanoborohydride is an ideal reagent for the selective reduction of hydrolysable imine bonds to amine bonds on diamondoid and possibly diamond structures.

3.4 Conclusions.

The ketone, 2-adamantanone, reacts with amines to form imines. The imine formation process can be accurately described by the rate law:

$$\text{Rate} = -\frac{d[Ad]}{dt} = k_f[Ad][Am] - k_r[Im][H_2O] \quad (15)$$

which is first order in each of the reagents. The imines formed can be subsequently reduced to adamantyl-amines by sodium cyanoborohydride.

For the amines studied, all of which were relatively strong bases, it was found that the rate at which the imine product was formed was equal to the rate at which the 2-adamantanone was consumed. In conjunction with simulated concentration profiles, this provided compelling evidence that nucleophilic addition of the amine to 2-adamantanone was the rate determining step in the reaction. Studies of the effect of pH

on the reaction between ethylamine and 2-adamantanone revealed that reaction was fastest under basic conditions. Below neutral pH the reaction was completely inhibited due to the protonation of free amine. The absence of a rate maximum with pH, as observed for imine formation from other ketones, suggests there is no change in which mechanistic step is rate determining and addition is rate limiting throughout the pH range studied.

Under acidic conditions in methanol solution (pH ~ 3), mass spectrometric evidence demonstrated that 2-adamantanone could form a hemiacetal, although there was no evidence for the presence of the acetal itself. The hemiacetal can be formed by nucleophilic attack of methanol on 2-adamantanone.

For a series of amines the rate of reaction with 2-adamantanone approximately follows the same trend as the pK_a values of the amines. This suggests pK_a may reflect the electronic ability of amines to undertake nucleophilic attack and, in the absence of steric effects, could be used to indicate the relative reaction rate of a particular amine with 2-adamantanone.

The solvent affected the rate of imine formation from 2-adamantanone. For the reaction of 3-phenylpropylamine with 2-adamantanone, the rate constant measured was lowest in dimethylsulphoxide, larger in toluene and greatest when methanol was used as the solvent. The rate constants measured did not rank with the dielectric constant of the solvents indicating the polarity of the solvent was not the critical affect. The ability of the solvent to stabilise the carbinolamine intermediate may, however, account for the different rate constants. Hydrogen bonding by methanol could stabilise the carbinolamine intermediate, promoting its formation and increasing the measured rate constant. Neither toluene or DMSO are capable of hydrogen bonding so would lack this ability to stabilise the intermediate. However further investigation is required to elucidate the role of solvent in the reaction.

It was found that the water-labile C=N bond in imines produced from 2-adamantanone can be reduced to a stable C-N bond by metal hydride reduction. Sodium cyanoborohydride is a suitably selective reagent for the reduction of imines in the presence of carbonyl groups. For the amines displaying fastest nucleophilic addition to 2-adamantanone a significant concentration of imine intermediate built up at early

reaction times. Imine molecules cannot be reduced as soon as they are formed and only once a significant imine concentration has developed does the rate of reduction overtake that of addition. In the case of benzylamine only a small concentration of imine was observed. No detectable imine concentrations were observed for amines, such as 4-trifluoromethylbenzylamine, displaying slower addition to 2-adamantanone than benzylamine. For no concentration of imine to develop imine molecules must be reduced as soon as they are formed. These observations suggest that the rate constant for hydride reduction is on the same order of magnitude as the rate constants measured for amine addition to 2-adamantanone.

2-adamantanone is potentially a molecular mimic of an oxidised (100) diamond surface. With the recent isolation of larger diamondoids¹²⁰ it would be informative to obtain a series of diamondoids of increasing size, each suitably oxidised to model a (100) diamond surface. The experiments in this study could be repeated on each diamondoid and any variation in results analysed from the perspective of the increasingly diamond-like nature of the substrate. Dry oxidation of a (100) diamond surface could introduce ether or carbonyl-like functionality, higher oxidation state groups such as carboxylic acid (RCOOH) or anhydride (R(CO)O(CO)R) cannot be formed while retaining the (100) character of the surface. Ether groups are generally unreactive and a diamond or diamondoid surface terminated with repeating ether groups would not be expected to be more reactive. When terminated with carbonyl groups a (100) diamond or diamondoid surface would have repeating 1,3 carbonyl groups. In organic chemistry, molecules with 1,3 carbonyl functionality are known as diketones. The reactivity of diketones is generally similar to that of ketones, varying only in that hydrogen atoms attached to the carbon at the 2- position are particularly acidic and proton transfer can occur of hydrogen atoms on the carbon atom at the two position to form an enol structure. On a (100) diamond or diamondoid surface there would be no hydrogen bound to the carbon atom at the 2- position as it would form two bonds into the carbon lattice structure. The reactivity of the carbonyl functionality would, therefore, not be expected to alter with increasing size of diamondoid substrate. It would be particularly interesting, however, to study the steric effects on the rate of the imine formation reaction for a series of increasing molecular weight diamondoids. The observation that, under all conditions studied, amine addition to 2-adamantanone is rate limiting suggests that the cage structure of 2-adamantanone may hinder attack of amines along the preferred Bürgi-Dunitz trajectory ($105^\circ \pm 5^\circ$). This would restrict their approach to lower angles where

orbital overlap is not as favourable, adversely affecting the rate constant for reaction due to a reduction in the pre-exponential factor in the Arrhenius equation. A range of carbonyl functional diamondoid molecules of increasing molecular weight would allow experiments to be carried out to probe whether the reaction rate decreases due to steric factors from the surface, as the area of the (100) surface increases.

In the absence of such a series of substrates the present results offer the best available guide towards the conditions required for nucleophilic attack on an oxidised diamond surface and to the mechanism of the process. With the extension from 2-adamantanone to an oxidised (100) diamond surface, the imine formation reaction would be expected to occur more slowly than observed with discrete molecules, not only due to increased steric inhibition of rate-determining nucleophilic attack but also because diffusion of the amine molecules to the reactive sites on the diamond surface may be required. Increasing the temperature would be expected to have a large effect on both the rate of diffusion of amine to the diamond surface and the rate of imine formation however it was not possible to study the effect of temperature on the kinetics of reactions involving 2-adamantanone due to limitations of the experimental set-up. Using a large concentration of a basic amine in methanolic solution at $\text{pH} > 10$ offers the best chance of achieving an acceptable reaction rate for imine formation with diamondoid molecules or (100) diamond surfaces. Addition of an acid catalyst is not required and would inhibit rather than facilitating reaction. Introduction of sodium cyanoborohydride offers the possibility of reducing water labile imine linkages to stable amine linkages as they are formed. In conclusion, the reaction of 2-adamantanone with amine reagents offers the prospect of functionalising carbonyl terminated oxidised (100) diamond surfaces with organic moieties.

4 – Introduction of an amine to oxidised (100) CVD diamond surfaces.

4.1 Introduction

A substrate material for devices such as microarrays and sensors requires a number of key properties. It must provide a solid, impermeable and flat support and be chemically stable in the service environment, which may require biocompatibility in biological environments. Thin film diamond technology has the capability to fulfil all of these requirements. An ideal substrate must also be capable of forming a robust interface with organic species which impart properties such as molecular recognition or electronics capability to the surface or which may passivate or protect the substrate, for example to prevent non-specific absorption of analyte species. A variety of approaches to functionalising diamond surfaces with organic species through stable covalent bonding have been reported and are briefly reviewed in this chapter. A good understanding of the chemistry taking place during any surface coupling reaction is necessary to optimise the process and maximise or control the surface coverage. Methods to functionalise both hydrogen and oxygen terminated diamond surfaces are needed to provide flexibility in device fabrication and access the capability of diamond to provide an electronically active substrate.

Carbonyl-like groups have been introduced to the (100) surface of single crystal diamond by thermal oxidation. The reaction of amines with the carbonyl group in 2-adamantanone, a molecular mimic of the carbonyl-terminated oxidised (100) surface, has been shown to link the species through a new covalent imine bond. Suitable conditions to undertake the reaction with a sterically hindered carbonyl group have been elucidated. In this chapter the imine formation reaction between a ketone and an amine nucleophile is extended to the carbonyl terminated oxidised (100) diamond surface. It is demonstrated that amine molecules can be introduced to the (100) diamond surface via a stable covalent linkage. The possibility for competing reactions or processes is minimised by the use of a well characterised carbonyl-terminated, oxidised single crystal (100) surface and the results are consistent with the formation of an imine bond on the diamond surface, which can be reduced, in situ, to a water stable amine linkage.

4.1.1 Reactions with radical species

A number of radical approaches have been adopted to alter the functionality of diamond surfaces or directly introduce organic species to the surface. Chlorinated diamond surfaces can be generated by photochemically activating chlorine gas over diamond substrates. Photochemical cleavage of Cl_2 forms chlorine radicals capable of abstracting hydrogen from C–H groups on the diamond surface and reacting with the carbon radicals formed to give a chlorine terminated surface. The chlorinated diamond surface is much more reactive than the hydrogenated one and can be used as a precursor to an amine functional surface¹⁶⁹ by reaction with ammonia under photochemical or thermal conditions. Thiol functional diamond surfaces can be achieved by a similar photochemical reaction of H_2S with either the hydrogenated or chlorinated diamond surface¹⁶⁹.

A chlorinated diamond surface can be achieved in solution in the presence of a radical initiator and sulfuryl chloride (SO_2Cl_2)^{170, 171} and was used to attach butyl groups to the diamond surface by reaction of the chlorinated diamond surface with butyllithium¹⁷¹. The chlorinated diamond surface is generally found to be sufficiently reactive to react with water under ambient conditions and result in an oxidised diamond surface. Despite this, however, Miller claimed a photochemically generated chlorinated diamond surface which was stable for several months¹⁶⁹. Termination of hydrogenated diamond surfaces with other halogens has also been demonstrated with both bromine¹⁷¹ and fluorine^{172, 173} with similar displacement of fluorine by amines and other nucleophiles claimed as observed for chlorinated diamond surfaces.

Hydrogenated polycrystalline diamond has been used as a substrate for a DNA chip fabricated by photochemical chlorination, then amination using ammonia¹⁷⁴. Further functional group conversions were necessary to carboxylate the diamond surface before binding an oligonucleotide to provide a suitable linker to tether large DNA molecules to the surface. In all seven steps were required to couple the DNA to the diamond surface.

Radical initiators such as peroxides^{175, 176} and diazo compounds have been shown to be capable of functionalising hydrogenated diamond surfaces. In a similar sequence to

chlorination, radical abstraction of hydrogen from the diamond surface produces surface carbon radicals which undergo combination with a second reagent radical, coupling it to the surface.

Benzoyl peroxide and lauroyl peroxide radicals can react directly with a hydrogenated diamond surface^{175, 176}. However, in the presence of other species with abstractable hydrogen atoms radical initiators can be used to facilitate the attachment of such organic molecules. In this way nitrile groups have been introduced to the surface via acetonitrile¹⁷⁷ and mono¹⁷⁸ and dicarboxylic¹⁷⁹ acids via suitable starting materials. In general the functionality introduced into the diamond surface by radical techniques is located on or close to the diamond surface. The use of dicarboxylic acids allowed one acid group to be involved in radical binding to the diamond surface whilst still providing a second acidic function on the end of an alkyl chain several atoms removed from the diamond surface which could be used for further reaction.

Perfluoroazooctane has been photolysed over diamond substrates and successfully introduced the perfluorooctyl radical to the surface¹⁸⁰. Electrochemical reduction of diazonium reagents provided a starting point for the immobilisation of DNA on boron doped single crystal diamond electrodes¹⁸¹. The nitrophenyl groups attached to the surface were subsequently reduced to aminophenyl groups prior to reaction with linker molecules and ultimately the DNA oligonucleotides.

Although some studies have been carried out on polycrystalline or diamond electrodes with defined faces, the vast majority of the published literature dealing with radical functionalisation of diamond surfaces has been carried out on diamond powder. The nature of such powders makes an understanding of the mechanism and surface processes problematical. The equipment and conditions required to safely undertake some of these reactions can also be onerous, in particular processing of substrates under chlorine and ammonia gas. Radical transformations have been shown to be a useful first step in attaching large molecules to the diamond surface but suffer from the drawback that many subsequent steps are often required involving further processing of the surface. Since it is unlikely that each reaction is 100% efficient each additional step may reduce the final areal density of molecules which can be coupled to the diamond surface.

4.1.2 Cycloaddition reactions

Under high vacuum bare (100) diamond surfaces exhibit a 2x1 reconstruction with the formation of rows of C-C dimers running parallel to the <110> direction. These dimers satisfy the two dangling bonds of an unreconstructed, bare carbon atom on a (100) diamond surface by formation of one σ and one π bond with an adjacent carbon atom. An analogy can be drawn between the dimers and alkene molecules, both comprising two carbon atoms sharing a double bond. In organic chemistry a variety of alkene reactions are known. A useful class of these for the formation of new carbon-carbon bonds are cycloaddition reactions in which two π bonded molecules react to form a cyclic structure containing two new σ bonds, with the consequent loss of two π bonds.

Cycloaddition reactions are classified by the number of π electrons in each reagent molecule. Therefore, a [2+2] addition involves two reagents with one double bond and hence two π electrons each. A [4+2] addition, also known as a Diels-Alder reaction, involves a diene with two conjugated double bonds (and hence 4 π -electrons) and an alkene with one double bond (2 π -electrons). In organic chemistry, cycloaddition reactions are governed by the Woodward – Hoffman rules, illustrated in Figure 49, which state that for a thermal process cycloadditions involving $4n$ π electrons are forbidden and those involving $4n+2$ π electrons are allowed by symmetry considerations. The Woodward Hoffman rules reflect the orbital interactions of the HOMO (highest occupied molecular orbital) and the LUMO (lowest unoccupied molecular orbital) of the two interacting species. For a thermal process in a [2+2] system the interacting HOMO and LUMO have an out-of-phase component and the reaction is therefore ‘forbidden’. In a thermally controlled process the HOMO – LUMO interaction of [4+2] systems is in-phase and reaction is said to be ‘allowed’ by the selection rules. The rules are reversed for systems under photochemical control.

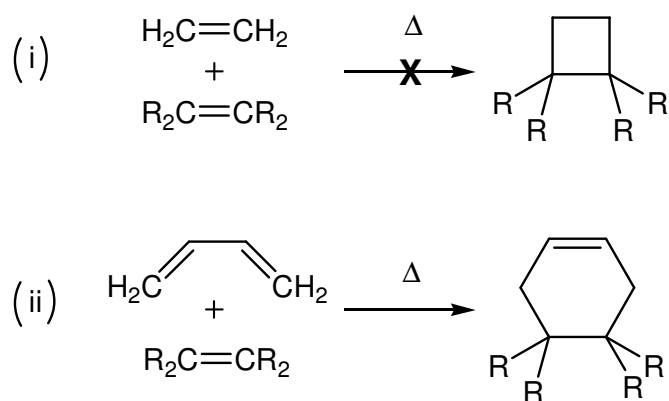


Figure 49 – Cycloaddition reactions under thermal control. (i) a [2+2] cycloaddition reaction ‘forbidden’ by the Woodward-Hoffman rules. (ii) a [4+2] cycloaddition or Diels-Alder reaction ‘allowed’ under the Woodward-Hoffman selection rules.

Supporting the analogy between alkenes and the surface dimers on clean (100) diamond surfaces, Diels-Alder reactions have been observed on the diamond (100)-2x1 surface. Reaction with butadiene formed a six membered ring on the diamond surface similar to that shown in Figure 49 (ii)¹. Further functionalisation of the surface could be attempted by reaction of the double bond present in the [4+2] cycloaddition product.

Some evidence for the occurrence of [2+2] additions on diamond surfaces has been observed, albeit as the minor product where a [4+2] reaction is also possible¹. [2+2] reaction products are observed in analogous reactions of silicon and germanium surfaces where the surface dimers are tilted and therefore circumvent the symmetry restrictions of the Woodward-Hoffman selection rules. Surface dimers on (100) diamond are symmetrical so this explanation does not apply. There is strain in each dimer as each atom has two bonds fixed into the diamond lattice and cannot therefore adopt the trigonal planar sp^2 configuration which exists in molecular alkenes. Relief of this strain may provide an explanation for the occurrence of ‘forbidden’ [2+2] reactions on (100) diamond.

Cycloaddition reactions provide a useful method of functionalising the (100) diamond surface. However, to produce a bare diamond surface and allow the 2x1 reconstruction to take place requires the (100) diamond surface to be treated under high vacuum or temperature to produce a chemically reactive dimer double bond. This fact limits the coupling reagents to those which can be suitably handled under these conditions.

4.1.3 Attachment of alkenes to hydrogenated diamond

In recent years the method of attaching organic molecules to diamond surfaces that has attracted the greatest attention is the photochemical attachment of alkenes to hydrogenated diamond surfaces.

Using fluorinated molecules as markers for XPS analysis, Strother et al.¹⁶ demonstrated in 2002 that when a hydrogenated polycrystalline diamond surface covered with a film of fluoroalkene was exposed to ultraviolet light an F 1s signal became detectable in the XPS spectrum of the diamond surface. Moreover the signal remained after washing. Control experiments demonstrated that attachment did not occur without exposure to the UV light and that only very limited attachment was observed if alkanes were used in place of alkenes. In one specific example, the quantity of the trifluoroethyl ester of ω -undecenoic acid present on the diamond surface plateaued after around 15 hours exposure with a coverage estimated at 10% of a monolayer.

Carboxylic acid and amino functional alkenes were targeted as being particularly useful initial linkers for tethering biomolecules onto diamond surfaces. The reagents used were, therefore, ω -functional alkenes, i.e. molecules with the alkene function at the 1 position and another functional group located at the extreme other end of the molecule. It was, however, observed that attachment of carboxylic acid and amine functional alkenes directly resulted in much lower attachment densities and it was necessary to protect the ω -functional group prior to attachment and deprotect once the molecule was immobilised on the diamond surface to achieve good coverage¹⁶.

This chemistry has been used to prepare poly and nanocrystalline diamond substrates with tethered amino linker molecules from protected amino-alkenes. Reaction of the amino group with a bi-functional cross-linker allowed tethering of thiol modified DNA strands^{18, 19}. The bound DNA strands could be hybridised with complementary DNA segments and showed good selectivity by not binding to non-complementary strands. This method of binding DNA to diamond involves the formation of covalent bonds at each stage and showed superior stability over many hybridisation and denaturation cycles than is generally observed on other substrates such as silicon, glass or gold.

Photochemical attachment of alkenes to hydrogenated diamond surfaces provides a stable and reproducible method of attaching linker molecules to diamond surfaces. Once bound to diamond, end-functional linker molecules of around ten carbon atoms in length have proved a suitable means of coupling further linker molecules and hence biomolecules by standard solution phase reactions^{18, 21}. This technology has been used to advance greatly what can be achieved by a diamond substrate, particularly for biosensor applications. For example, Hartl et al. have demonstrated that large proteins and enzymes can be covalently tethered to a nanocrystalline diamond substrate and still retain their functionality²¹. Utilising the surface conductivity of hydrogen terminated diamond they were able to measure a direct electrochemical interaction between the nanocrystalline diamond electrode and the redox centre of the enzyme. Exposure of the enzyme to hydrogen peroxide caused an increased current to be detected, due to the redox reaction occurring as the enzyme splits hydrogen peroxide to water and oxygen. This is an example of a true diamond based biosensor for the detection of hydrogen peroxide. Such a method of diamond functionalisation currently seems the most likely approach to realise diamond based sensors and chips for a range of applications. There are, however, issues to be overcome. For example; efforts have been made to minimise non-specific binding of proteins²² and it has been stated that more efficient and flexible immobilisation chemistries would be desirable¹⁸². A complementary attachment chemistry to oxidised diamond would provide more flexibility in device manufacture.

4.1.4 Reaction with silane coupling agents

Organo-functional alkoxy silane molecules, such as aminopropyltriethoxysilane shown in Figure 50, have long been the staple linker molecule utilised to fabricate microarrays of biomolecules on glass substrates. In theory, hydroxyl groups on the glass surface displace alkoxy groups on the silane liberating alcohol molecules and binding the linker molecule to the glass substrate at up to three sites.

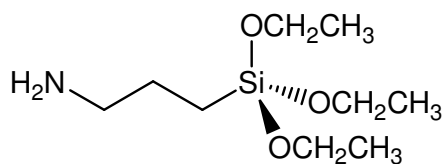


Figure 50 – Aminopropyltriethoxysilane (APTES) an example of a silane coupling agent

In practice the reactions taking place can be complex. The amine group catalyses hydrolysis of the alkoxy groups. If traces of water are present this can cause polymerisation of silane molecules rather than coupling to the surface. Significant hydrogen bonding can also occur between the various groups either on the surface or in solution. Whilst such systems tend to be represented schematically as an ordered monolayer of individual silane molecules coupled to a substrate the reality is likely to be much more complex and may involve polymerisation of a polysiloxane like film over the substrate, only covalently bound to the substrate at a few locations.

Despite the potential drawbacks, the ability to produce hydroxyl functional diamond surfaces means silane coupling agents could offer an approach to functionalising diamond substrates. Tsubota et al.¹⁸³ demonstrated that diamond powders oxidised in sulphuric or sulphuric/nitric acid mixtures and subsequently heated in solutions of silane coupling agents demonstrated IR peaks attributable to the silane coupling agents even after repeated washing. The authors acknowledge the potential for formation of a polymer network structure by the silane reagents and that their results cannot distinguish between individually coupled molecules and a polymerised film on the diamond surface.

4.1.5 Reactions analogous to synthetic organic procedures

In seeking to devise new attachment methodologies to diamond surfaces, the field of organic chemistry provides a plethora of reactions which can be considered. The ability to routinely and reliably functionalise diamond surfaces in solution and under the relatively mild conditions used for many reactions of small organic molecules would offer great advantages in terms of ease of processing. In order to undertake the surface

analogue of a solution phase reaction one or more suitable functional groups must be present on the diamond surface. Despite the utilisation of hydrogenated diamond in the radical procedures described above, the surfaces are generally chemically inert, similar to analogous hydrocarbon molecules. The ability to attach a range of oxygen functional groups to the diamond surface make an oxidised diamond surface a much more likely starting point for molecular tethering via functional group chemistry analogous to synthetic organic procedures carried out in solution.

A range of chemistries with a clear analogue in synthetic organic chemistry have been utilised to functionalise oxidised diamond surfaces. DNA was immobilised on diamond powders by Ushizawa et al.¹⁸⁴. Following oxidation in sulphuric and nitric acids to generate a mixture of surface oxides, the powders were reacted with thionyl chloride in order to convert surface carboxylic acid groups to acid chloride functions. Reaction of the acid chloride groups with hydroxyl groups on a thymidine linker molecule, immobilised thymidine on the surface and allowed subsequent coupling of DNA to the surface. Krysinski et al.¹⁸⁵ utilised the chemistry of acid chlorides to functionalise boron doped diamond electrodes (crystallographic face not specified) which had been oxidised in 'piranha' solution. In this case hydroxyl groups on the diamond surface underwent an alcoholysis reaction with one end of bifunctional acid chloride molecules to bind them to the surface of the diamond via an ester linkage. The remaining acid chloride groups on the di-acid chloride linker underwent reaction with an amine to immobilise it on the diamond surface. When a target molecule is bound to a surface in a number of steps the final yield of target molecule on the surface is dependant on the efficiency of each intermediate step. In their work Krysinski et al.¹⁸⁵ measured the final amine coverage on the surface at 0.5% of a monolayer. This was at least an order of magnitude less than they had achieved on alternative electrode materials such as silica, indium-doped tin oxide and gold by a similar method utilising hydroxyl functionality. They highlighted the small number of hydroxyl groups introduced to the diamond surface by their oxidation treatment.

Boron-doped polycrystalline diamond electrodes were oxidised electrochemically by Delabouglise et al.¹⁸⁶ introducing mainly hydroxyl groups to the surface. Direct esterification was then carried out by reacting carboxylic acid functional biotin with the hydroxylated surface. The presence of biotin was demonstrated by binding fluorescent streptavidin, for which biotin has a strong affinity. It was found that varying the

oxidation conditions varied the quantity of streptavidin which could be detected from the surface and that non-oxidised and non-biotin functionalised surfaces gave no signal from streptavidin.

Reactions analogous to those known in synthetic organic chemistry can be carried out on diamond surfaces if the correct functionality is present on the surface and the correct conditions are used. Detailed mechanistic information about the surface reactions described above has not been published, so it cannot yet be established whether the surface reaction mechanisms are the same as those of small molecules in solution or whether the nature of the surface affects the reaction kinetics or mechanism.

4.1.6 Imine formation

The reaction of primary amines with ketones is well known in synthetic organic chemistry and results in formation of an imine with the expulsion of water.

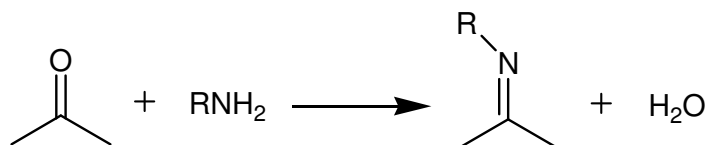


Figure 51 – Reaction of a ketone with a primary amine yields an imine and water

CVD polycrystalline diamond nanopowders have been thermally oxidised and subsequently functionalised by reaction with a fluorinated amine¹⁸⁷. Washing experiments and high resolution XPS analysis, shown in Figure 52, suggested that the covalent attachment occurred via an imine bond. Despite the high surface area of the diamond nanopowders, the surfaces were not well defined (100) crystallographic faces. Therefore the concentration of carbonyl-like oxygen functional groups on the surface, and hence immobilised amine molecules, may have been relatively low. Also, since other crystallographic faces and grain boundaries were present immobilisation of fluoroamine by some unintended adsorption process cannot be entirely ruled out.

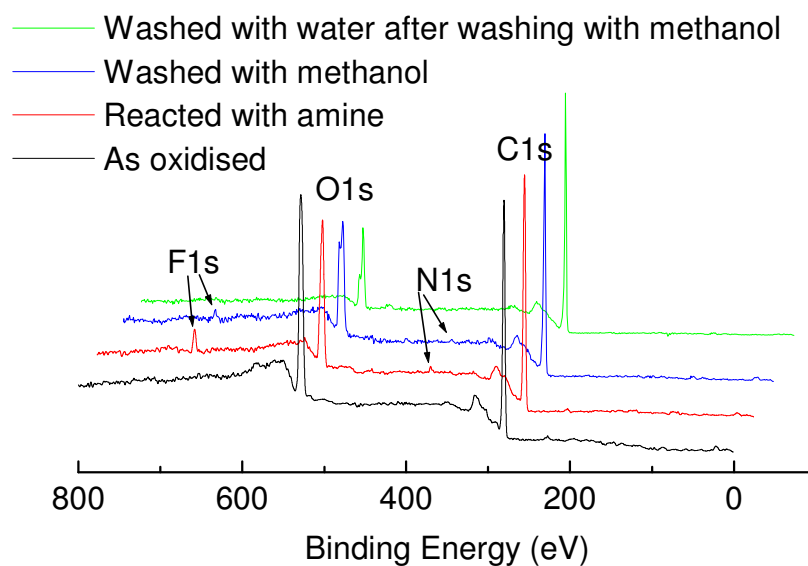


Figure 52 – Wide area XPS scans of oxidised polycrystalline diamond nanopowders. Following reaction with a fluorinated amine, F and N 1s signals are detectable on the diamond surface. These are reduced but not removed following washing in methanol but disappear completely on washing in water.

The work presented in this chapter seeks to utilise the reaction of primary amines with carbonyl groups to allow molecular attachment to oxidised diamond surfaces. The work utilises a fluorinated mono-functional amine to investigate the applicability of the approach. Di-functional amines would provide suitable linker molecules to which subsequent molecules could be tethered, for example by reaction with carboxylic acid functional groups to form the amide bond ubiquitous in chemical biology. Use of well-defined (100) single-crystal diamond substrates means the quantity of carbonyl-like oxygen on the diamond surface can be maximised and the likelihood of unintended binding between the amine molecule and non-(100) facets or grain boundaries reduced. By optimising the conditions towards one attachment chemistry and observing if attachment occurs, and if it does, at what rate and to what extent; the opportunity is presented to begin to develop an understanding of reactions occurring on diamond surfaces and potentially their mechanisms. A greater understanding of diamond surface reactions can only be beneficial in the drive to utilise diamond as a substrate for a whole range of sensor applications. In preparing sensors from diamond it is likely that both conducting hydrogenated regions and insulating oxidised regions will be required. Complementary methods of functionalising both areas, for example to allow binding of an analyte in one region and prevent non-specific binding in another, offer chemists,

materials scientists and engineers an expanding ‘tool-box’ of techniques which can be used to tailor diamond substrates and maximise their potential as sensor materials.

In Chapter 2 it was demonstrated that thermal oxidation introduced oxygen to (100) single-crystal surfaces in the form of carbonyl and ether groups. The majority of the oxygen was introduced as carbonyl functionality. In Chapter 3 2-adamantanone, a molecular mimic of the carbonyl functional (100) diamond surface, was reacted with a number of amines under a range of conditions to demonstrate the amine-ketone reaction and elucidate the mechanism by which the reaction occurred when a hindered cage-like ketone was used. The steric hindrance of the 2-adamantanone cage affected the rate of amine nucleophilic attack upon the carbonyl group; but still resulted in the expected covalently bound imine products. In this chapter, the reaction between 4-trifluoromethylbenzylamine and a thermally oxidised diamond single-crystal (100) surface is described.

4.2 Experimental

The results presented in the following section relied on X-ray photoelectron spectroscopic analysis of the two Apollo Diamond Inc. (100) single crystal diamond samples described previously. The experiments carried out can be categorised as:

- Surface attachment and washings – oxidised (100) diamond was immersed in a solution of 4-trifluoromethylbenzylamine in methanol to introduce amine to the surface. The nature of the bonding between the amine and surface was investigated by attempts to remove the amine by evaporation and washing in methanol and water.
- Room temperature immersion – two experiments were carried out to investigate the quantity of amine present on the oxidised (100) diamond surface as a function of immersion time.
- Elevated temperature immersion – two experiments were carried out to investigate the quantity of amine present on the oxidised (100) diamond surface as a function of immersion time at elevated temperature.
- Reductive amination and washings – oxidised (100) diamond was immersed in a solution of 4-trifluoromethylbenzylamine and sodium cyanoborohydride reducing agent to attempt to reduce the product imine, in situ, to a water stable amine bond. The nature of the bonding between the amine and surface was investigated by washing the diamond in methanol and water.
- Control experiments – An oxidised (100) diamond surface was immersed in methanol only. Hydrogen terminated (100) diamond was immersed in solutions of 4-trifluoromethylbenzylamine in methanol and subsequently washed in methanol and water to allow comparison of oxidised and non-oxidised surfaces.

The X-ray photoelectron spectrometer is located in the National Centre for Electron Spectroscopy and Surface Analysis laboratory in Daresbury some distance from Heriot-Watt University, where the oxidation and hydrogen plasma apparatus were located. It was therefore not always possible to generate a freshly oxidised or hydrogenated diamond (100) surface prior to each set of experiments, as would have been the ideal. For this reason the experiments in which (100) diamond underwent elevated

temperature immersion were not carried out on freshly oxidised (100) surfaces but on a diamond surface which had first been used to carry out a room temperature immersion experiment. The surface was washed thoroughly in water between experiments in an attempt to regenerate the 'as-oxidised' surface. This will be discussed in more detail in the following section. The other experiments were carried out on oxygen or hydrogen terminated (100) diamond surfaces which had not been exposed to any solutions since their generation in the relevant apparatus.

4.2.1 X-ray Photoelectron Spectroscopy (XPS)

X-ray photoelectron spectroscopy was carried out at the National Centre for Electron Spectroscopy and Surface Analysis (NCESS) on the Scienta ESCA300 instrument described previously.

The set-up detailed in a previous chapter for XPS analysis of (100) diamond samples was followed. 4 x 4 mm square (100) diamond plates were mounted on sample stubs (VG ESCALAB Mk II) and held in place by a metal retaining clip. As far as possible, samples were aligned such that the 6 x 0.5 mm X-ray beam would span the sample diagonal, maximising the signal from the sample. Electron take-off angles of 15 – 90 degrees were used. The hemispherical electron analyser was used at a constant pass energy of 150 eV which, with a slit width of 0.8 mm on the slit-aperture pair preceding the hemispherical analyser, resulted in a spectrometer resolution limited by the X-ray line width (~0.26 eV). Regular use was made of the electron flood gun (VSW EG2) to compensate for charging of insulating oxidised diamond samples.

4.2.2 Hydrogen termination

To hydrogenate the surface of a (100) diamond plate the hydrogen plasma etching treatment fully described in a previous chapter was used. The sample was mounted in the 1kW microwave plasma enhanced chemical vapour deposition (MPECVD) apparatus at Heriot-Watt University and exposed to a hydrogen plasma for 6 hours. Hydrogen gas (Linde, 99.999 %) pressure was 35 torr with a flow of 999 sccm. Microwave power of 500 W and the platen heater operating at 70 % of its full power resulted in a temperature, measured by two – wavelength pyrometry, of 710 ± 50 °C.

Upon termination of the plasma treatment the diamond sample was allowed to cool to room temperature under hydrogen (22 torr) before being removed to ambient conditions and stored in a glass container.

4.2.3 Thermal oxidation

The (100) diamond samples were thermally oxidised in the stainless steel vacuum chamber with a resistively heated block described in detail elsewhere. Samples were heated under a static fill of dried oxygen (BOC 99.6 %) to around 600°C and oxidised for a period of time under approximately 1 atmosphere of oxygen. Exact oxidation conditions used to treat samples prior to exposure to amine solutions and XPS analysis are detailed below. Hot oxygen was pumped away and the sample cooled under vacuum to ‘freeze-in’ the oxygen configuration imparted at high temperature. Upon cooling to room temperature the chamber was vented with air and the sample removed.

4.2.4 Surface attachment and washing experiments

A single crystal (100) diamond plate was exposed to 910 mbar of oxygen at a substrate temperature of 560°C for 10 minutes prior to immersion in a 0.2 mol L⁻¹ 4-trifluoromethylbenzylamine solution in methanol for several hours. Upon removal droplets of solution present on the sample surface were allowed to dry by evaporation in air. After evaporation of the droplets white stains were visible on the diamond surface. The sample was loaded into the X-ray photoelectron spectrometer without any further treatment. As the diamond sample was transferred to the analysis chamber it was exposed to the vacuum of the preparation chamber (1×10^{-8} mbar) for several minutes, after which the white stains on the surface were no longer visible. The pressure in the analysis chamber did not noticeably increase by the removal of the white material. Normally the analysis chamber pressure was around 5×10^{-9} mbar on transfer of the sample from the preparation chamber and dropped to a base pressure of 1.5×10^{-9} after about 1 hour.

Over the course of around 7.5 hours the sample remained in the spectrometer and was analysed at a number of electron take-off angles (TOA). In order of collection these

were -30° , 90° , 15° , 45° and 60° . On completion the sample was removed and returned to 0.2 mol L^{-1} 4-trifluoromethylbenzylamine solution overnight.

A series of washing experiments were carried out to investigate the bonding between 4-trifluoromethylbenzylamine and the (100) diamond surface. The sample was initially removed from 0.2 mol L^{-1} 4-trifluoromethylbenzylamine solution, allowed to dry in air and the surface composition measured by XPS. The (100) diamond sample was subsequently removed from the spectrometer, subjected to 1 washing step, allowed to dry in air and returned to the spectrometer for further XPS analysis and this process repeated. The washing steps were, in turn; dipping for 2 seconds in methanol (SigmaAldrich, anhydrous, $<0.002\%$ water), dipping for 2 seconds in deionised water, dipping for a further 4 seconds in deionised water and dipping for a final 5 seconds in deionised water. The same (100) face of the single crystal diamond plate was interrogated in each XPS analysis.

4.2.5 Room temperature immersion experiments

Room temperature immersion 1:

A single crystal (100) diamond plate was oxidised at 620°C for 6 minutes in 940 mbar of oxygen. After XPS analysis of the as-oxidised (100) diamond surface, the plate was immersed in 0.2 mol L^{-1} 4-trifluoromethylbenzylamine solution in methanol at room temperature for 20 hours and periodically removed and analysed by XPS to investigate the quantity of fluorinated amine present on the surface. The upper and lower faces of the (100) diamond substrate could not be visually differentiated at this time so care was taken to try to ensure the same (100) face of the diamond crystal was analysed each time, however this could not be guaranteed. When removed from the 4-trifluoromethylbenzylamine solution to collect the XPS data after 0.5, 1, 2 and 4 hours the (100) diamond sample was washed by dipping in methanol (SigmaAldrich, anhydrous, $<0.002\%$ water) for several seconds and allowed to dry prior to loading in the spectrometer. The XPS analysis, carried out on the sample after 6 to 20 hours immersion at room temperature, was performed on the untreated sample, i.e. the diamond substrate was removed from the 4-trifluoromethylbenzylamine solution, allowed to dry in air and mounted directly into the spectrometer.

Room temperature immersion 2:

The single crystal (100) diamond plate was oxidised in 970 mbar of oxygen with a substrate temperature of 625°C for 9 minutes. The as-oxidised surface was analysed by XPS prior to immersion of the sample in 0.1 mol L⁻¹ 4-trifluoromethylbenzylamine solution in methanol for 58 hours. The sample was periodically removed from the 4-trifluoromethylbenzylamine solution, allowed to dry in air and analysed by XPS to investigate the quantity of fluoroamine present on the (100) diamond surface. The upper and lower (100) faces of this diamond sample could be differentiated so it is known that the same (100) face was interrogated by XPS on each occasion.

4.2.6 Elevated temperature immersion experiments

The higher temperature treatment of oxidised (100) diamond to 0.1 mol L⁻¹ 4-trifluoromethylbenzylamine in methanol was not undertaken with a freshly oxidised (100) diamond surface. Following oxidation the sample was used for the second room temperature immersion experiment described above then washed and immersed overnight in methanol as described below in Section 4.3.8 before being exposed to 4-trifluorobenzylamine solution at elevated temperature.

The (100) diamond sample was immersed in a methanol solution of 0.1 mol L⁻¹ 4-trifluoromethylbenzylamine in a round bottomed flask fitted with reflux condenser and heated with a heating mantle until the methanol refluxed (boiling point of methanol is 65°C). Initially the diamond sample was removed from the hot solution after 6 and 8 hours for interrogation by XPS. Any solution remaining on the sample on removal evaporated quickly and the dry sample was mounted in the spectrometer without washing. After the 8 hour analysis the sample was returned to the hot solution and left to react overnight. At some time overnight the water pressure to the condenser dropped and the safety latch cut the power to the heating mantle. The sample was therefore immersed in 4-trifluoromethylbenzylamine for a further 10 hours but the time the solution was at elevated temperature is unknown. The sample was interrogated by XPS at this point to determine the level of fluoroamine on the surface after 8+x hours

immersion at elevated temperature. The solution was heated to reflux and the diamond plate immersed in hot solution for a further 2 hours before being analysed by XPS to give the level of fluoroamine present on the surface after immersion for 10+x hours at elevated temperature. At this point the sample was retained, under vacuum, within the spectrometer and XPS analysis carried out to investigate the effect of the vacuum on the level of fluoroamine present on the (100) diamond surface. The sample was then subject to washing in methanol and water, with XPS analysis carried out after each treatment.

Further washing of the sample in methanol and water and mechanical wiping were carried out to completely remove the fluoroamine from the (100) diamond surface and the elevated temperature immersion experiment repeated with a fresh solution of 0.1 mol L⁻¹ 4-trifluoromethylbenzylamine in methanol. The (100) diamond sample was removed from the hot solution after 1, 2.5, 4, 5.25 and 6.33 hours and interrogated by XPS. The same (100) diamond face was measured by each XPS analysis.

4.2.7 Reductive amination and washing experiment

A single crystal (100) diamond plate was exposed to 930 mbar oxygen at a substrate temperature of 640°C for 8 minutes. Following XPS analysis to characterise the oxidised surface, the sample was immersed in a solution of 0.1 sodium cyanoborohydride and 0.1 mol L⁻¹ 4-trifluoromethylbenzylamine in methanol for 14 hours and analysed by XPS. The sample was subsequently subjected to washing in methanol for 10 seconds, water for 5 seconds and water for 10 seconds with XPS analysis of the surface between each washing step.

4.2.8 Control experiments on oxidised (100) diamond surfaces

The effect of immersing an oxidised (100) diamond surface in methanol for extended periods (in the absence of 4-trifluoromethylbenzylamine) was investigated. This study was carried out following the second room temperature immersion experiment described above. It was not possible to generate a freshly oxidised (100) diamond surface by thermal oxidation between experiments. Instead the (100) diamond surface

was washed with methanol (SigmaAldrich, anhydrous, <0.002% water), copiously washed with deionised water and mechanically wiped. XPS analysis of the surface ensured the fluorine, introduced to the surface by its previous immersion in fluoroamine solution, had been suitably removed and investigated the effect of these washing treatments on the (100) diamond surface. The sample was then immersed in methanol (SigmaAldrich, anhydrous, <0.002% water) for 10 hours, allowed to dry and analysed by XPS.

4.2.9 Control experiments on hydrogenated (100) diamond surfaces

The hydrogenated (100) diamond surface, described in Section 4.2.2, was first analysed 'as-hydrogenated' and then analysed following a number of treatments. The treatments were designed to provide data to compare with the tests carried out on oxidised (100) diamond. They therefore comprised i) immersion in methanol only ii) immersion in fluoroamine solution with evaporation and washings to investigate the nature of the bonding present between the amine and the surface and finally iii) analysis of the surface as a function of immersion time at room temperature in the fluoroamine solution.

The sample was immersed in methanol (SigmaAldrich, anhydrous, <0.002% water) for 2 hours and analysed before immersion in a 0.1 mol L⁻¹ methanol solution of 4-trifluoromethylbenzylamine with analysis after 2 hours and 12 hours immersion. After 12 hours immersion the sample was analysed several times to investigate whether the fluoroamine signal from the surface reduced with the length of time the sample was retained within the high vacuum of the spectrometer. Next the sample was washed in methanol for 1, 3 and 30 seconds then deionised water for 3 and 30 seconds with XPS analysis after each washing. The sample was mechanically wiped and exposed to fresh 0.1 mol L⁻¹ solution with analysis after 1 hour, 1 hour 5 minutes, 2 hours, 2 hours 5 minutes, 2 hours 30 minutes and 3 hours 40 minutes to investigate how the surface fluoroamine signal changed with immersion time.

4.3 Results and discussion

4.3.1 Introduction of a fluorinated amine to (100) CVD diamond surfaces

The XPS spectrum resulting from a thermally oxidised (100) diamond sample, shown in Figure 53, indicates that only carbon and oxygen atoms were detected at the surface.

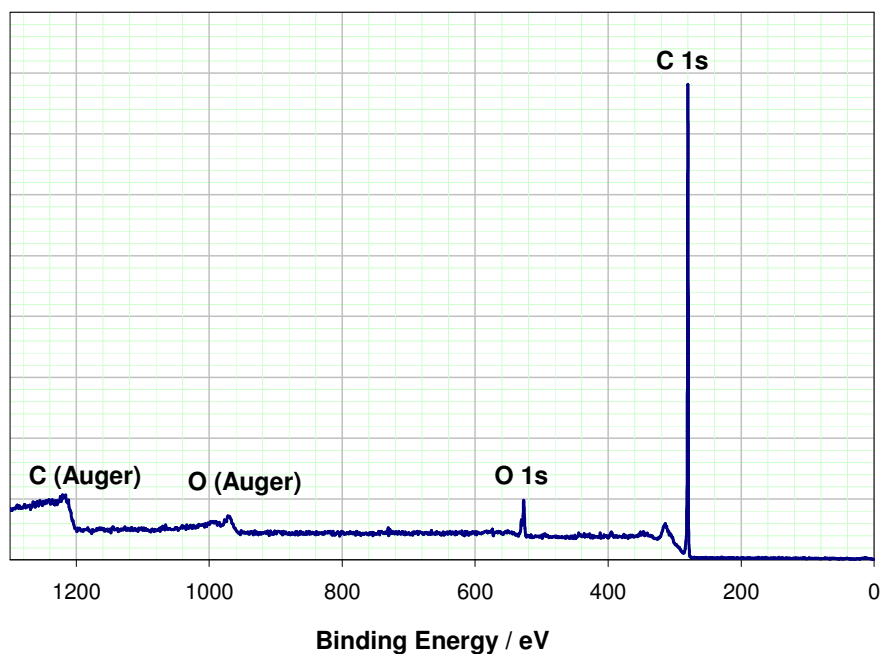


Figure 53 – XPS survey spectrum collected (at TOA = 90°) from a thermally oxidised (100) diamond sample demonstrating that only carbon and oxygen atoms can be detected at the surface.

Following immersion of the oxidised (100) diamond sample in a methanol solution of 4-trifluoromethylbenzylamine, the XPS spectrum shown in Figure 54 demonstrates that fluorine and nitrogen atoms were also detected on the surface.

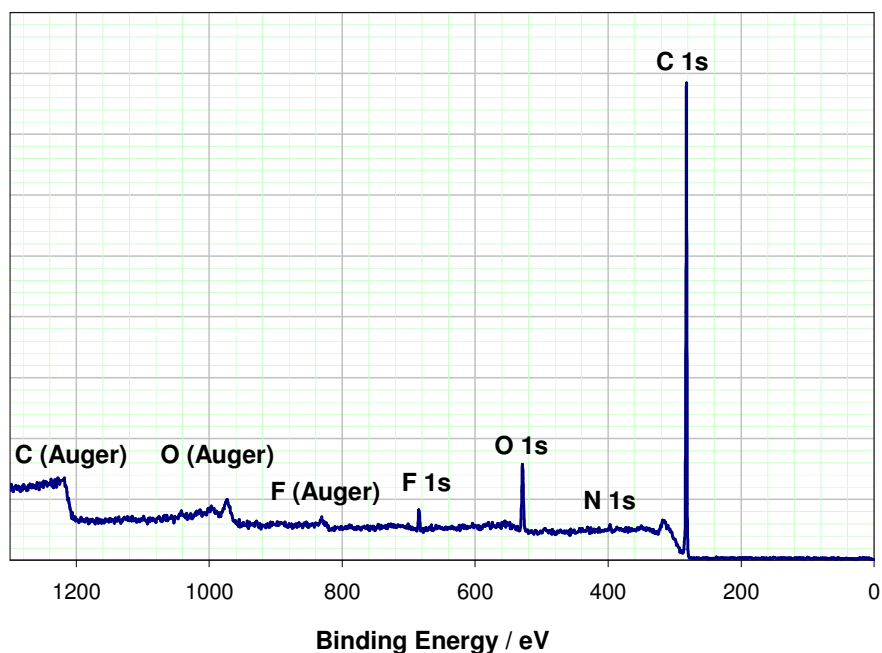


Figure 54 – XPS survey spectrum collected (at TOA = 90°) from an oxidised (100) diamond as removed from a solution of 4-trifluoromethylbenzylamine in methanol after a period of immersion. In addition to carbon and oxygen, nitrogen and fluorine was detected at the surface.

In a control experiment oxidised (100) diamond was immersed for 10 hours in methanol which, as expected, did not yield fluorine or nitrogen XPS peaks indicating that they are produced only in the presence of the fluoroamine. 4-trifluoromethylbenzylamine has the chemical structure shown in Figure 55.

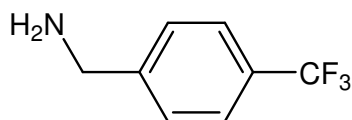


Figure 55 – The chemical structure of 4-trifluoromethylbenzylamine

When present as an overlayer on an oxidised (100) diamond surface 4-trifluoromethylbenzylamine will make a small contribution to the C 1s signal and give rise to N 1s and F 1s peaks in the XPS spectrum. In this study, N 1s and F 1s signals can be used as markers indicative of the presence of 4-trifluoromethylbenzylamine on exposed (100) diamond surfaces. A fluorinated amine was intentionally selected as F 1s electrons provide a particularly intense XPS response making identification of small

concentrations of fluoroamine on the surface easier. This is demonstrated in Figure 54 where the N 1s signal is barely visible in the XPS survey spectrum whereas the F 1s signal is clearly visible.

High resolution XPS scans, carried out over energy ranges within which C 1s, O 1s, N 1s and F 1s peaks occur, allowed high resolution spectra and accurate peak shapes to be determined. After correction for the relative sensitivity of XPS to electrons from different atoms and orbitals, the area under each peak is proportional to the concentration of that element within the analysis depth. Relative sensitivity factors for carbon, oxygen, nitrogen and fluorine 1s photoelectrons, determined on the NCESS Scienta ESCA300 used in this study, are provided in Table 20.

Photoelectron	Relative sensitivity factor (RSF)
Carbon 1s	1.00
Oxygen 1s	2.80
Nitrogen 1s	1.73
Fluorine 1s	5.10

Table 20 – Relative sensitivity factors for carbon, oxygen, nitrogen and fluorine 1s photoelectrons, determined on the NCESS Scienta ESCA300 X-ray photoelectron spectrometer

To demonstrate the presence of 4-trifluoromethylbenzylamine on the surface of the (100) diamond substrate, XPS analysis was carried out at a variety of electron take-off angles. Reducing the electron take-off angle increases the surface sensitivity of XPS and therefore any surface overlayer makes a greater contribution to the total XPS signal. If a material was distributed evenly through the bulk of the substrate no change in the relative signal intensities would be observed on varying the analysis angle. Using the F 1s signal as indicative of the presence of 4-trifluoromethylbenzylamine, and the C 1s signal from the diamond substrate, Figure 56 demonstrates the analysis angle dependence of the intensity of the F 1s signal. The result that fluoroamine is introduced to the surface of a (100) diamond, and not somehow incorporated into the bulk, is what would be expected following immersion of the diamond in a solution of the fluoroamine.

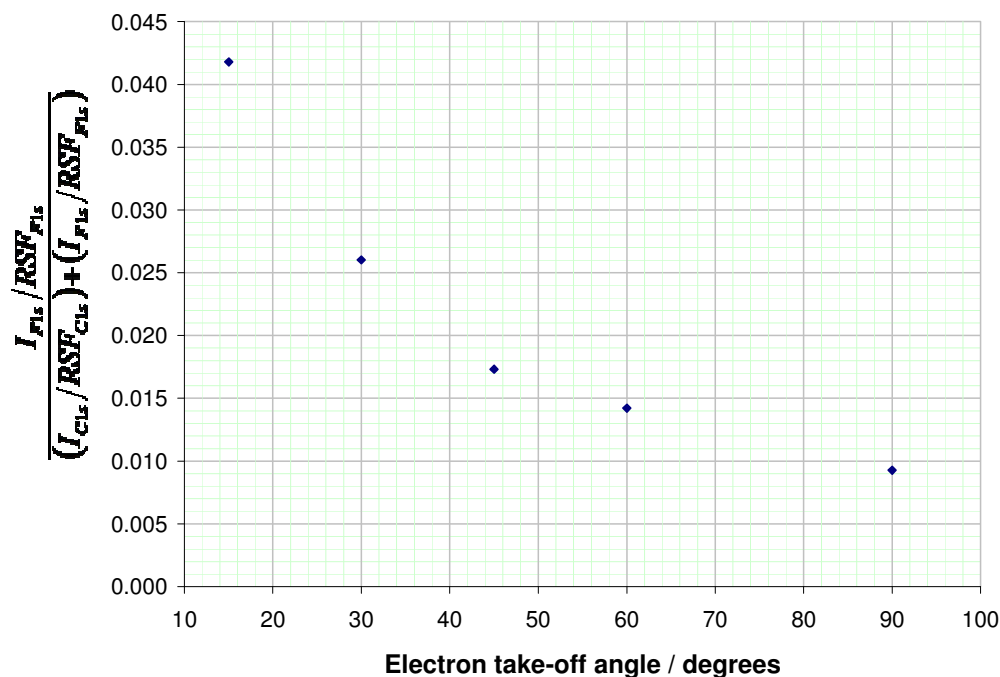


Figure 56 – The relative ratio of the F 1s signal, from 4-trifluoromethylbenzylamine, to the C 1s signal, from the diamond bulk, as a function of electron take-off angle, demonstrating the presence of the fluoroamine as an overlayer on the surface of the diamond substrate.

4.3.2 Quantifying the level of fluorinated amine on (100) diamond surfaces

Quantifying the level of 4-trifluoromethylbenzylamine introduced to oxidised (100) diamond surfaces is not trivial⁹⁵. The approach followed in Chapter 2 for the quantification of surface oxygen assumed that the oxygen monolayer did not attenuate the XPS signal since the monolayer thickness was much less than the electron attenuation length. The 4-trifluoromethylbenzylamine molecule (shown in Figure 55) is much more bulky than an individual oxygen atom and the same assumption cannot necessarily be made.

The XPS signal due to a fractional monolayer of material on a substrate is given by¹⁰¹:

$$I_{ov}^d = \Phi_{ov} I_{ov}^\infty \left\{ 1 - e^{\left(\frac{-d_{ov}}{\lambda_{ov}(E_{ov}) \cos \theta} \right)} \right\} \quad (21)$$

whilst the signal from the substrate is given by¹⁰¹:

$$I_{sub}^d = I_{sub}^\infty \left\{ 1 - \Phi_{ov} + \Phi_{ov} e^{\left(\frac{-d_{ov}}{\lambda_{ov}(E_{sub}) \cos \theta} \right)} \right\} \quad (22)$$

where:

Φ_{ov} is the monolayer fraction present.

d is the depth of the overlayer.

θ is the analysis angle relative to the surface normal ($\theta = 90^\circ - \text{TOA}$).

λ_{ov} is the electron attenuation length in the overlayer. The attenuation length is the distance, in nanometres, that the average electron ejected from the overlayer (of energy E_{ov}) or from the substrate (of energy E_{sub}) can travel through the overlayer before inelastic scattering occurs.

I_{ov}^∞ is the theoretical signal obtained from an infinitely thick overlayer.

I_{sub}^∞ is the theoretical signal obtained from an infinitely thick substrate with no overlayer present. Relative sensitivity factors, measured on the same instrument as used in the study can be taken as I^∞ values¹⁰¹.

From equations (21) and (22), the fractional monolayer coverage is related to the experimentally measured XPS signal from the overlayer, I_{ov} , and substrate, I_{sub} , by:

$$\frac{\Phi_{ov} \left\{ 1 - e^{\left[\frac{-d}{\lambda_{ov}(E_{ov}) \cos \theta} \right]} \right\}}{1 - \Phi_{ov} \left\{ 1 - e^{\left[\frac{-d}{\lambda_{ov}(E_{sub}) \cos \theta} \right]} \right\}} = \frac{I_{ov} / RSF_{ov}}{I_{sub} / RSF_{sub}} \quad (23)$$

If the overlayer thickness is small compared to the electron attenuation length, i.e. d/λ is small, then photoelectrons can travel many times the thickness of the overlayer before being inelastically scattered. Attenuation of the substrate signal by the overlayer is therefore small. Under these conditions the following simplifications to equation (23) can be adopted⁹⁵:

$$\Phi_{ov} \left\{ 1 - e^{\left[\frac{-d}{\lambda_{ov}(E_{ov}) \cos \theta} \right]} \right\} \approx \Phi_{ov} \left(\frac{d}{\lambda_{ov}(E_{ov}) \cos \theta} \right) \quad (24)$$

$$1 - \Phi_{ov} \left\{ 1 - e^{\left[\frac{-d}{\lambda_{ov}(E_{sub}) \cos \theta} \right]} \right\} \approx 1 \quad (25)$$

When these approximations apply equation (23) simplifies and rearranges to¹⁰¹:

$$\Phi_{ov} = \frac{\lambda_{ov}(E_{ov}) \cos \theta}{d} \frac{I_{ov}/RSF_{ov}}{I_{sub}/RSF_{sub}} \quad (26)$$

Ideally, application of equation (23) or (26) to analysis of an overlayer of 4-trifluoromethylbenzylamine on a (100) diamond surface requires measurement of the total XPS signal due to the 4-trifluoromethylbenzylamine overlayer (I_{ov}) and the signal due only to the diamond substrate (I_{sub}). Deconvolution of the contribution made to the C 1s signal by 4-trifluoromethylbenzylamine is not possible and so the total fluoroamine and diamond signals can not be separated out. Instead, the area under the F 1s peak, indicative of the concentration of fluoroamine present, has been used to provide values of I_{ov} and the area under the C 1s peak has been used to provide values of I_{sub} . This provides a consistent approach which can be used to determine how the quantity of fluoroamine on the surface varied between different spectra. However, the absolute values of fluoroamine concentration (in monolayers) calculated in this way will always be smaller than the true value since using only the area under the F 1s peak underestimates the total signal from the fluoroamine overlayer and, since a component of the area under the C 1s peak is due to the fluoroamine, the signal from the diamond substrate will always be slightly overestimated.

To calculate the fractional monolayer coverage of 4-trifluoromethylbenzylamine on a (100) diamond substrate by equations (23) or (26) requires suitable values for the overlayer thickness (d) and electron attenuation length in the overlayer ($\lambda_{ov}(E_{ov})$). The ‘thickness’ of a single monolayer of 4-trifluoromethylbenzylamine, shown in Figure 55,

will depend on the orientation it adopts on the (100) diamond surface. Lying flat on the diamond surface 4-trifluoromethylbenzylamine could provide a layer around one atom thick in places, with the molecule standing upright the monolayer thickness would become several atoms thick. In XPS quantification, the monolayer thickness (in metres) of organic molecules has been calculated from^{96, 101}

$$(d)^3 = \frac{M}{1000n\rho N_a} \quad (27)$$

where:

M is the molecular weight

n is the number of atoms per molecule

N_a is Avogadro's number

ρ is the matrix density in kg.m⁻³

For 4-trifluoromethylbenzylamine the monolayer thickness, d, is therefore:

$$(d)^3 = \frac{175.10}{1000 \times 20 \times 1229 \times 6.0221 \times 10^{23}}$$

$$d = 2.28 \times 10^{-10} \text{ m} \quad (28)$$

$$\underline{d = 0.228 \text{ nm}}$$

The attenuation length of F 1s electrons in 4-trifluoromethylbenzylamine has not been measured directly. However it can be estimated by the empirical relation for inelastic mean free paths (IMFP) of electrons in organic compounds proposed by Seah and Dench^{96, 101}.

$$\lambda = 49E^{-2} + 0.11E^{0.5} \text{ mg/m}^2 \quad (29)$$

where:

λ = Electron inelastic mean free path in mg/m². Dividing by 10⁻³ρ converts to λ in nm.

E = The electron kinetic energy (= X-ray energy – Electron binding energy). For a F 1s electron = 1486.7 – 686 = 800.7 eV

Evaluating expression (29) with the relevant values returns an inelastic mean free path length for an F 1s electron in 4-trifluoromethylbenzylamine of 2.53 nm. Tanuma et al.

used experimental data to calculate IMFP lengths of electrons in 14 organic materials, ranging from small molecules to polymers⁹⁷. At 800 eV (the energy of an F 1s electron) the average IMFP value across the 14 materials is 2.58 ± 0.23 nm. The value predicted by Seah and Dench's relation for 4-trifluoromethylbenzylamine is in very good agreement with the experimentally determined values for other materials which provides confidence in the approach.

Equation (26) can be used to determine the fractional monolayer coverage of 4-trifluoromethylbenzylamine on (100) diamond if d/λ is small and therefore simplifications (24) and (25) apply⁹⁵. For the case of 4-trifluoromethylbenzylamine on (100) diamond where $d = 0.228$ nm and $\lambda = 2.53$ nm, $d/\lambda = 0.09$. This means that the overlayer thickness is less than one tenth of the distance an electron can travel before it is attenuated. Signal attenuation by the overlayer will therefore be small and simplifications (24) and (25) can be applied, if it is accepted that they introduce an error to the calculated monolayer fraction of up to 10% for analysis carried out at an electron take-off-angle of 90° and an error of up to 30% when analysis is carried out at a 15° take off angle.

Application of equation (26) to the angle resolved experimental data shown in Figure 56 allows the fractional monolayer coverage to be calculated at each take off angle employed. The results are shown below in Table 21. The standard deviation of the results indicates a variation of 15% due to experimental error or issues with applying baselines under peaks consistently. The error introduced by the simplifications in the derivation of equation (26) could be as large as 30% therefore the quantity of 4-trifluoromethylbenzylamine present on this oxidised (100) diamond surface is more properly described as 0.13 ± 0.04 monolayers. As discussed earlier, this value represents a systematic underestimation of the true 4-trifluoromethylbenzylamine concentration since only the area under the F 1s peak was used as I_{ov} , the total signal from the fluoroamine overlayer, and the total area under the C 1s peak was used as I_{sub} , the signal from the diamond substrate, when in fact the fluoroamine also contributes to the C 1s signal.

TOA / °	Φ / monolayers	Time under vacuum
90	0.10	2 hr 45 min
60	0.14	7 hr 30 min
45	0.14	6 hr 00 min
30	0.15	0 hr 45min
15	0.13	4 hr 30 min
Average \pm Standard deviation = 0.13 \pm 0.02 monolayers		

Table 21 – Values of the fractional monolayer coverage (Φ) of 4-trifluoromethylbenzylamine present on an oxidised (100) diamond surface, determined from XPS data collected at various electron take-off angles. The average value and standard deviation are also shown.

The method described above has been used to quantify the fractional monolayer coverage of 4-trifluoromethylbenzylamine on (100) diamond substrates in the discussion which follows. Where values are quoted or represented in graphs they are the absolute values calculated from the areas under F 1s and C 1s peaks, with appropriate baselines, from one XPS experiment. The largest error introduced by the simplifying assumptions in the quantification procedure (30% at 15 degrees take-off angle) is greater than the standard deviation of the repeated measurements made in the angle resolved study above (15%). An error of $\pm 30\%$ may, therefore, be taken as representative of the uncertainty in any quoted value of 4-trifluoromethylbenzylamine coverage which follows.

4.3.3 Nature of the bonding between 4-trifluoromethylbenzylamine and (100) diamond

Having demonstrated the presence of fluorinated amine on the surface of oxidised (100) diamond it was necessary to probe the nature of the bonding between the fluorinated amine and the diamond surface. The solution phase condensation reaction of small organic amines and ketones to form a covalent imine bond is well known. The imine bond is stable and prevents the imine reverting to the starting materials except in the presence of water which reverses the reaction by hydrolysing the imine bond. The rationale of these experiments was to probe the proposition that a primary amine could

react with carbonyl-like $>C=O$ groups on the surface of an oxidised (100) diamond surface to form a surface bound imine: a reaction analogous to imine formation by molecular ketones in solution.

Oxidised (100) diamond surfaces

Several possible outcomes could result from the presence of small polar amines near an oxidised (100) diamond surface. Molecules could become weakly associated with the diamond surface via a physical effect such as hydrogen bonding. Reversible imine formation, analogous to the solution phase reaction, could occur. Unexpected reactions could occur between functional groups present on the oxidised (100) diamond and the amine molecule which may covalently bind the molecule to the surface.

Following immersion of an oxidised (100) diamond sample in a methanol solution of 4-trifluoromethylbenzylamine for several hours, the angle resolved data, shown in Figure 56 and Table 21, indicated that fluoroamine was associated with the diamond surface. When the diamond sample was first removed from the 4-trifluoromethylbenzylamine solution, and the residues allowed to evaporate to dryness, white drying stains appeared on the diamond substrate. These disappeared under the vacuum of the spectrometer preparation and analysis chamber (10^{-8} - 10^{-9} mbar) in the few minutes required to load the sample and transfer it into the analysis position. In order to interrogate the surface at various electron take-off angles the sample was present in the analysis chamber of the spectrometer, and exposed to the high vacuum, for over seven hours. As can be seen from the results in Table 21 no systematic decrease in the quantity of fluoroamine detected was observed over time. The chemical nature of the material which caused the white stains was not determined. However the bond to the oxidised (100) diamond substrate was evidently sufficiently weak to allow the material to evaporate within the spectrometer. Clearly, 4-trifluoromethylbenzylamine was sufficiently strongly bound to the oxidised (100) diamond surface to remain attached over several hours whilst the angle resolved analysis was carried out.

Washing experiments were carried out to investigate their effect on the quantity of 4-trifluoromethylbenzylamine present on an oxidised (100) diamond surface. Figure 57 shows the F 1s peaks (offset for clarity) collected following immersion in fluoroamine, washing in methanol solvent and then 3 subsequent washes in water. The peaks shown

in Figure 57 are from wide area survey scans of the surface and in each case the intensity of the C 1s peak was adjusted to the same intensity to allow an objective comparison of the F 1s peak heights.

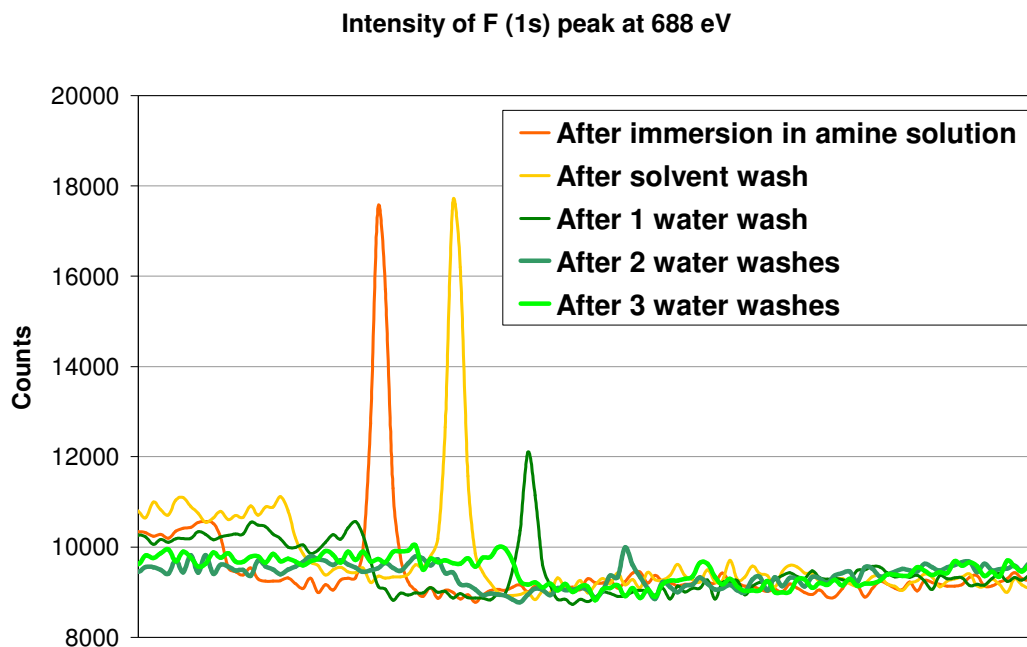


Figure 57 – The F 1s peaks at 688 eV, offset for clarity, from XPS survey scans of an oxidised (100) diamond surface which has been in turn; exposed to 4-trifluoromethylbenzylamine solution, dipped for 2s in methanol, dipped for 2s in water, dipped for a further 4s in water and finally dipped for a further 5s in water.

Figure 57 indicates that briefly washing an oxidised (100) diamond substrate, which has been immersed in 4-trifluoromethylbenzylamine, with methanol solvent has little or no effect on the quantity of fluoroamine present on the surface. A similarly brief wash in water however causes a marked reduction in the concentration of fluoroamine present on the diamond surface. Further washes in water further reduced the fluoroamine quantity present until the F 1s signal was barely detectable above the spectral noise.

High resolution narrow XPS scans were carried out over the C 1s and F 1s regions after immersion in fluoroamine, washing in methanol and after the first and third water wash. After applying a suitable baseline to each peak these could be used to quantify the concentration of fluoroamine present by the method described in the previous section. The results of this treatment are shown in Figure 58.

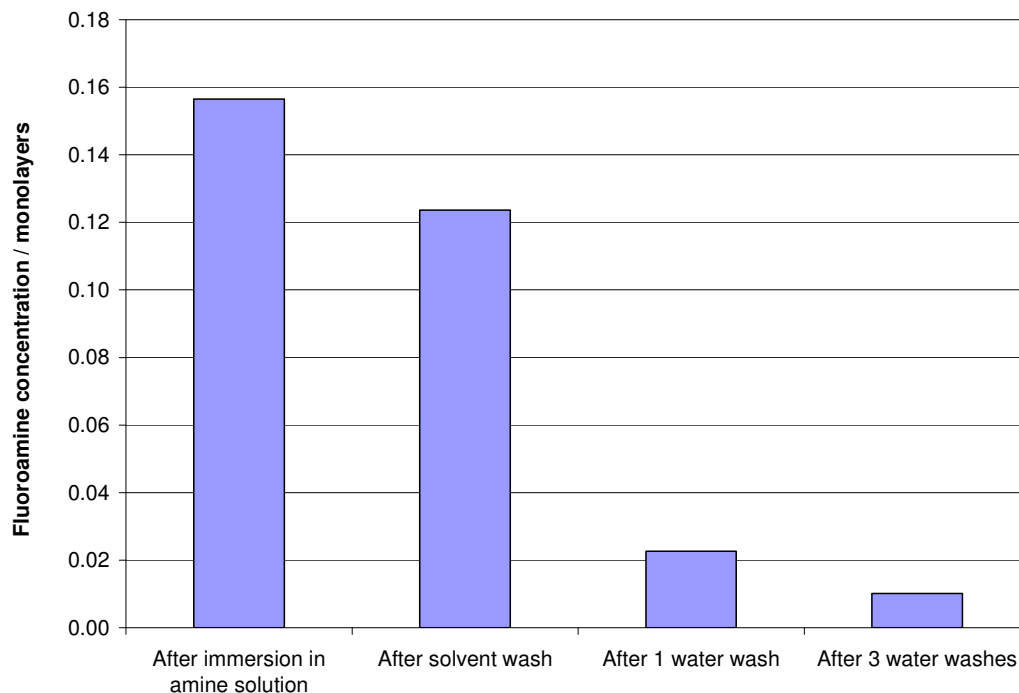


Figure 58 – Quantitative values of the fluoroamine concentration (in monolayers) on the oxidised (100) diamond surface before and after several washing treatments.

The quantitative results in Figure 58 generally agree with the observations made from direct comparison of the spectra in Figure 57. Washing in water causes a very marked reduction in the amount of 4-trifluoromethylbenzylamine present on the oxidised (100) diamond surface. A brief two second wash in water reduces the fluoroamine present from around 15% of a monolayer to less than 3% of a monolayer. Further washes in water continue to reduce the fluoroamine signal. However the signal was not reduced entirely to zero after 10 seconds of washing in water. Figure 58 reveals that washing the diamond surface with methanol solvent slightly reduced the quantity of 4-trifluoromethylbenzylamine detectable on the surface, by around 3% of a monolayer. Unfortunately further methanol washes were not carried out to test if this decrease continued regularly until all of the fluoroamine was removed or whether the concentration reached a plateau. Although anhydrous methanol was used to carry out the washing, the methanol had to be opened to air for decanting and prior to carrying out the washing itself. Since methanol is a very polar protic solvent in which water dissolves easily, it is conceivable that a sufficient concentration of water existed in the methanol solvent to cause the loss of fluoroamine observed when washing in methanol.

The vapour pressure of 4-trifluoromethylbenzylamine is not published although values for benzylamine¹⁸⁸ and methylbenzylamine¹⁸⁹ are around 0.5 mbar at 20°C. The vapour pressure of 4-trifluoromethylbenzylamine can be expected to be of the same order of magnitude. When exposed to external pressures less than their vapour pressure liquids boil and solids sublime. When exposed to pressures of 10^{-8} – 10^{-9} mbar in the XPS spectrometer 4-trifluoromethylbenzylamine can be expected to evaporate¹⁹⁰. White drying residues, observed on the oxidised (100) diamond surface following evaporation of fluoroamine solution droplets at ambient, disappeared once the sample was mounted in the spectrometer. The material forming these stains could not have been strongly bound to the diamond surface. It seems probable that these stains were formed by excess 4-trifluoromethylbenzylamine physisorbed onto the oxidised (100) diamond surface. That no decrease in fluoroamine concentration was observed during analysis of the diamond surface while it was exposed to the spectrometer vacuum for several hours (Table 21) suggests that physisorbed material evaporated rapidly and the remaining fluoroamine was strongly bound to the oxidised (100) diamond surface. Formation of a covalent bond would provide a suitably strong attachment between the fluoroamine and (100) diamond surface.

Formation of an imine bond between 4-trifluoromethylbenzylamine and the oxidised (100) diamond surface is supported by the results of the washing experiment. The sharp loss of fluoroamine from the surface on washing in water, evident in Figure 58, is entirely consistent with hydrolysis of a water-labile imine bond. Since the imine bond is only susceptible to water, washing in methanol was not expected to decrease the concentration of fluoroamine on the surface. The loss of a small quantity of fluoroamine on washing in methanol is attributed to water present in the methanol used for washing which results in hydrolysing a fraction of the surface attached imine.

Hydrogenated (100) diamond surfaces

To investigate how crucial the oxygen functional groups present on the oxidised (100) diamond surface were in covalently attaching amines, hydrogenated (100) diamond surfaces were exposed to methanol solutions of 4-trifluoromethylbenzylamine. No

covalent bonds were expected to form between the amine and the hydrogenated surface. Following immersion in methanol solutions of 4-trifluoromethylbenzylamine, the hydrogenated (100) diamond surface was interrogated following periods of exposure to the high vacuum of the XPS spectrometer and after washing in methanol and water. The concentration of fluoroamine present on the surface after each of these treatments was quantified by the method described in the preceding section utilizing the area under the F 1s and C 1s peaks. Figure 59 shows the quantity of fluoroamine present on the hydrogenated (100) diamond surface after each treatment.

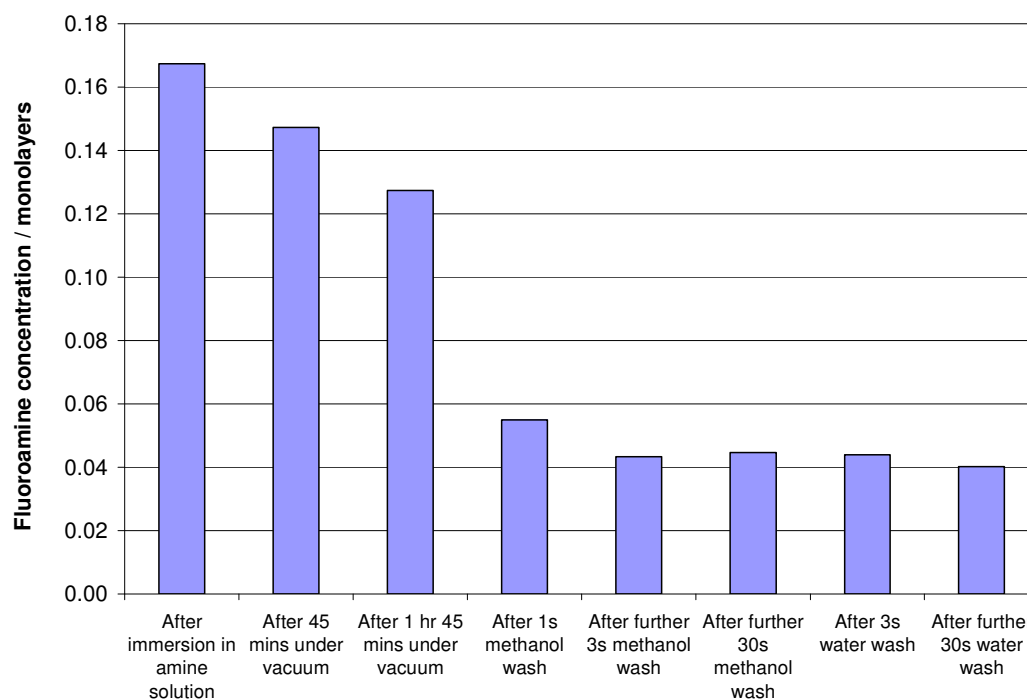


Figure 59 – Quantified values of fluoroamine concentration (in monolayers) on a hydrogen terminated (100) diamond surface following exposure to 4-trifluoromethylbenzylamine solution and subsequent residence under high vacuum in the XPS spectrometer and washings.

Immersion of a hydrogenated (100) diamond sample in 4-trifluoromethylbenzylamine solution introduces fluorinated amine to the diamond surface, as can be seen in Figure 59. A control experiment immersing hydrogen terminated (100) diamond only in methanol confirmed that the introduction of fluorine and nitrogen peaks to the diamond surface occurred only in the presence of the fluorinated amine. The level of fluoroamine on the hydrogenated surface clearly decreases with time exposed to the high vacuum of the spectrometer. After less than 2 hours exposed to the vacuum the

quantity of fluoroamine detected on the surface has dropped by 4% of a monolayer. The decrease appears to occur at a regular rate of around 2% per hour. In contrast, on the oxidised (100) diamond surface visual observations suggested some physisorbed material was lost into the vacuum but this occurred rapidly and no further loss of fluoroamine was detected over 7 hours analysis time exposed to the spectrometer vacuum. It appears that 4-trifluoromethylbenzylamine is not bound to the oxidised surface in the same way as the hydrogenated surface.

Figure 59 demonstrates that washing very briefly in methanol solvent removed a significant quantity of 4-trifluoromethylbenzylamine from the surface of hydrogenated (100) diamond. This contrasts with the oxidised (100) surface where methanol removed only a relatively small proportion of the fluoroamine present. On the hydrogenated surface, further washes in methanol did not significantly reduce the signal from 4-trifluoromethylbenzylamine further, suggesting that all of the fluoroamine capable of removal by washing in methanol was removed by one short wash. Unlike the oxidised surface, subsequent washing of the hydrogenated (100) diamond surface with water did not reduce the fluoroamine level present. After the first wash in methanol, a small but non-zero level of fluoroamine (~5% of a monolayer) remained on the surface and appeared to be unaffected by further washes in methanol or water. It appears that the bulk of the fluoroamine introduced to hydrogenated (100) diamond surfaces is weakly bound and can be removed by evaporation under the vacuum of the spectrometer or by washing in methanol solvent. A small quantity of material appears to become sufficiently strongly bound to the notionally hydrogenated (100) surface that it cannot be removed by washing in methanol or water. This material may be covalently bound but the washing experiments rule out attachment by a hydrolysable imine bond.

The above XPS data may be explained by concluding that on both hydrogenated and oxidised (100) diamond 4-trifluoromethylbenzylamine is capable of binding via two processes, physisorption and chemisorption. The nature of the bonding of physisorbed fluoroamine is clearly different between the oxidised and hydrogenated surfaces. On oxidised (100) diamond surfaces any physisorbed 4-trifluoromethylbenzylamine is very weakly bound and evaporates before it can be detected by XPS. On hydrogenated (100) diamond surfaces physisorbed 4-trifluoromethylbenzylamine is more strongly bound and is lost over the course of hours under vacuum. Initially, the observation of stronger physisorption on hydrogenated (100) diamond surfaces seems counter-intuitive. A

diamond surface, terminated by carbon-hydrogen bonds, is less polar than an oxidised one, terminated by carbon-oxygen bonds, and would be expected to interact less strongly with the polar amine and CF₃ groups on 4-trifluoromethylbenzylamine, shown in Figure 55. The surface transfer doping mechanism of hydrogen terminated diamond, which gives rise to its unusual surface conductivity, may offer an explanation. At a very simple level, the negative electron affinity of hydrogenated diamond means that when its surface is covered by a layer of adsorbate with an unoccupied orbital of suitable energy; electrons can transfer from the diamond to the adsorbate, leaving holes at the diamond surface which are responsible for conduction¹⁵. Such charge transfer between hydrogenated diamond and a surface adsorbate will result in electrostatic attraction between the two which would be significantly stronger than any polar attractions which may exist between the adsorbate and an oxidised diamond surface. Suitable adsorbates to allow surface transfer doping require a relatively high electron affinity of around 4 eV to overcome the ionisation potential of hydrogenated diamond¹⁵. Electron affinities of isolated molecular atmospheric molecules are usually too low to allow transfer doping to occur and whilst those of halogenated molecules are generally higher it is probably unlikely that 4-trifluoromethylbenzylamine happens to have a suitably high electron affinity to allow transfer doping by itself. It has however been suggested that solvated ions within a thin wetting layer can act as redox couple to allow surface transfer doping to occur¹⁵. One example from a number of possible options is transfer of electrons from hydrogenated diamond to hydronium ions in equilibrium with molecular hydrogen and water. As this work was carried out in methanol, a very polar, protic solvent, it is very possible that some suitable species, such as hydronium ions, were present on the hydrogenated (100) diamond surface and allowed charge transfer to occur. Once conductive 'holes' existed at the hydrogenated diamond surface, even if the charge transfer did not directly involve 4-trifluoromethylbenzylamine, the lone pair on the amino group would become attracted to the positive holes and cause a strong physical bond which could explain the slow disappearance of fluoroamine from the hydrogenated (100) diamond surface under the high vacuum of the XPS spectrometer.

The fluorinated amine 4-trifluoromethylbenzylamine interacts with oxidised (100) diamond surfaces in such a way that some fluoroamine becomes strongly bound. In a previous chapter it was demonstrated that the oxidised diamond surfaces contained a significant concentration of carbonyl-like >C=O moieties on their surface. The data

presented here is consistent with the formation of an imine bond between the amine and carbonyl groups on the diamond surface, providing a linkage stable to washing in dry solvent but susceptible to hydrolysis by water. When the fluorinated amine is introduced to a hydrogen terminated (100) diamond surface a similar reaction cannot occur as there is not a suitable concentration of carbonyl-like moieties on the diamond surface. Instead most of the fluoroamine introduced to the hydrogenated surface is only physisorbed and can be removed by evaporation under high vacuum or by briefly washing in solvent. A small quantity (~5% of a monolayer) of fluoroamine appears to become strongly attached to the hydrogenated surface and persists despite washing in methanol and water. The nature of this association has not been investigated further as part of this work.

4.3.4 Kinetics of attachment at room temperature

Two experiments, carried out at ambient temperature, were performed to investigate the quantity of fluoroamine present on the surface of oxidised (100) diamond as a function of immersion time in 4-trifluoromethylbenzylamine solution. In the first experiment an oxidised (100) single crystal diamond plate was immersed in 0.2 mol L⁻¹ 4-trifluoromethylbenzylamine solution for 20 hours. The upper and lower (100) faces of this plate were indistinguishable. In the second experiment an oxidised single crystal (100) diamond plate was immersed in 0.1 mol L⁻¹ 4-trifluoromethylbenzylamine solution for up to 58 hours. This plate had distinguishing marks which allowed the same face to be reliably identified for analysis after each immersion period.

After each period of immersion, high resolution XPS scans were collected over the C 1s and F 1s regions. After applying a baseline to each peak, the peak areas were used to quantify the level of 4-trifluoromethylbenzylamine by the method described previously in this chapter. Figure 60 shows how the level of fluoroamine varied as a function of time in each experiment.

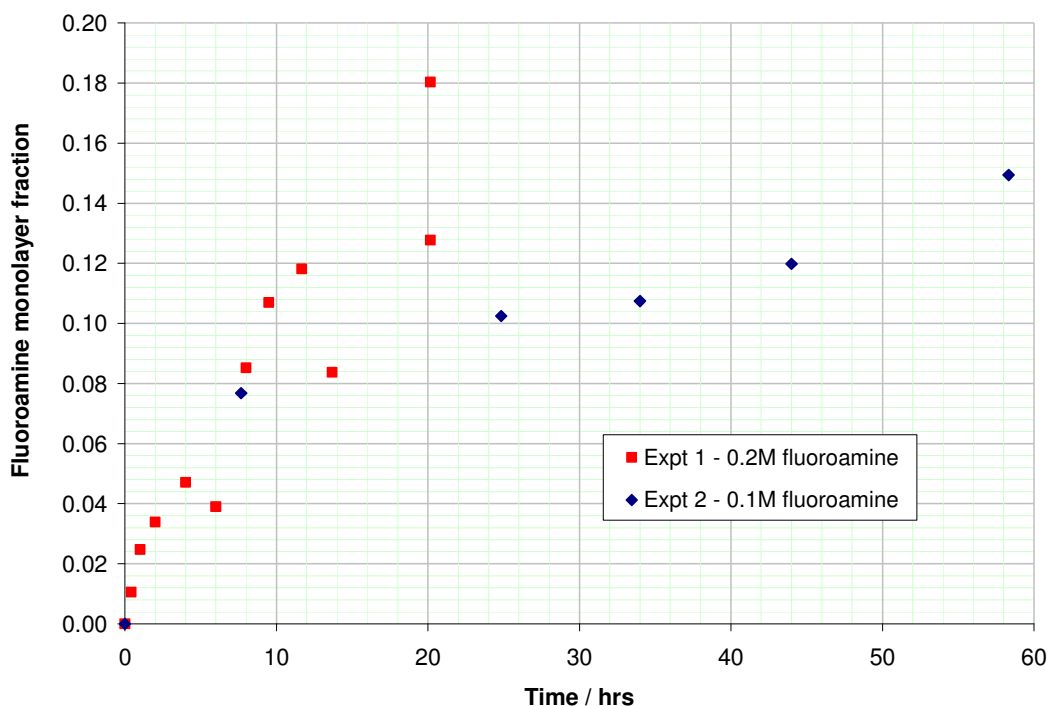


Figure 60 – 4-trifluoromethylbenzylamine concentration (in monolayers) on the surface of oxidised (100) diamond as a function of time immersed in; Experiment 1 (■) 0.2 mol L⁻¹ and Experiment 2 (◆) 0.1 mol L⁻¹ 4-trifluoromethylbenzylamine in methanol.

Figure 60 demonstrates that the quantity of fluoroamine present on an oxidised (100) diamond surface increases with immersion time in the fluoroamine solution. Over the timescale of the experiments the increase appears to be linear, within the experimental error, indicating that the rate of attachment is constant. Neither set of data produces a limiting coverage indicating that the attachment reaction has not reached equilibrium and a maximal quantity of 4-trifluoromethylbenzylamine has not been introduced to the oxidised (100) diamond surface in either experiment.

In Experiment 1, the coverage measured after 6 and 12 hours immersion does not lie on the same line as the rest of the data. After 20 hours immersion the quantity of 4-trifluoromethylbenzylamine detectable from both indistinguishable (100) faces of the diamond plate was measured. One (100) face gave data in line with the coverage measured after 6 and 12 hours whilst the other gave a result in-keeping with the coverage measured at all other times. Efforts were made to consistently analyse the same face of the diamond substrate after each immersion period. However it is possible that the measurements made at 6 and 12 hours and the lower coverage measured after

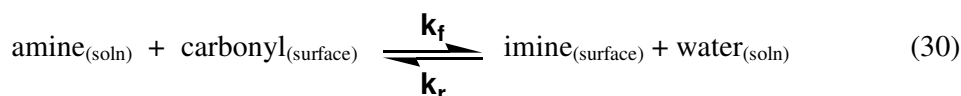
20 hours were measured on one (100) face of the diamond plate whilst the other data was measured from the other face. Alternatively, the apparent variation may be due to errors in each measurement associated with the surface of the diamond after each reaction period and the errors of the XPS measurements. In Experiment 2, as the (100) diamond faces could be differentiated, the same face was interrogated after each immersion period.

A straight-line fit through the data from Experiment 2 would not pass through the origin. This could either be due to experimental error in the XPS measurements and analysis or could indicate a real change in reaction rate from a faster rate over the first 8 hours immersion to a slower rate after 8 hours. One explanation for a decrease in rate would be if an amine depletion zone was formed in the solution near the diamond surface, after around 8 hours, and subsequent diffusion of amine molecules into this zone was required to allow further reaction to take place. There is no evidence of such a change in rate in the Experiment 1 data where the amine concentration was twice that used in Experiment 2. There are around 1.6×10^{15} surface carbon atoms per cm^2 on a (100) diamond surface and hence theoretically of the order of 2.5×10^{14} possible carbonyl functional groups on the 16 mm^2 (100) single crystal diamond plates used in this study. In Experiment 2 the diamond plate was immersed in 5 ml of 0.1 mol L^{-1} fluoroamine solution. The number of amine molecules present in this solution is of the order of 3.0×10^{20} . The amine molecules are therefore in excess of the carbonyl functions by a factor of 10^6 . With such an excess, there is negligible reduction in the amine concentration due to reaction with the surface and it is unlikely that a depletion zone forms in the amine solution. The variation in the Experiment 2 data is therefore attributed to experimental error.

A significant barrier to a detailed kinetic analysis of the XPS results shown in Figure 60 is the lack of an accurate knowledge of, and control over, the exact number of carbonyl functionalities on the (100) diamond surface. Ideally, by controlling the initial concentration of 4-trifluoromethylbenzylamine and the number of carbonyl functional groups on the (100) diamond surface the order of reaction with respect to each reactant would be determined. By using a large excess of fluoroamine, the experiments carried out here have, in effect, utilised the isolation method to investigate the effect on the initial rate of the concentration of carbonyl groups. Figure 60 suggests attachment occurred at different initial rates in the two experiments; this may be due to different

initial concentrations of carbonyl groups on the oxidised (100) diamond surface in each experiment, introduced by slightly different oxidation conditions. Unfortunately to determine the rate constant for the reaction by the initial rate method the initial concentration of carbonyl groups would have to be known to a greater accuracy than was possible from the XPS analysis described in a previous chapter.

Assuming that the surface reaction, like the solution formation of an imine from a ketone and amine, is second order; the form of the rate law can be postulated by following the derivation of the Langmuir isotherm, modifying it to account for adsorption of solution phase molecules instead of gaseous ones. Assuming that; i) a maximum of one monolayer of fluoroamine can adsorb (consistent with chemisorption), ii) all surface sites are energetically equivalent so reaction is equally likely at all sites and iii) that the ability of reaction to occur at a given site is independent of whether adjacent sites are occupied or not, a simple model of adsorption can be adopted. For the reaction shown in (30) the rate at which a fractional monolayer (θ) of imine is built up (31) is proportional to the amine concentration ($[amine]$), and number of vacant sites $N(1 - \theta)$, where N is the total number of surface sites. The rate of loss of imine groups from the surface (32) is proportional to the water concentration ($[water]$) and the number of sites where reaction has occurred to form imine bonds ($N\theta$). The rate law for the overall reaction is therefore postulated to be of the form shown in (33).



$$\frac{d\theta}{dt} = k_f [amine] N(1 - \theta) \quad (31)$$

$$\frac{d\theta}{dt} = -k_r [water] N\theta \quad (32)$$

$$\frac{d\theta}{dt} = k_f [amine] N(1 - \theta) - k_r [water] N\theta \quad (33)$$

The Langmuir isotherm, which describes how the equilibrium fractional monolayer coverage of an adsorbed gas varies with the partial pressure of that gas at a given temperature, recognises that the rates of the forward and reverse reaction are equal at equilibrium and that $k_f/k_r = K$ (the equilibrium constant). A similar treatment of

equation (33) results in (34) which relates the equilibrium fractional monolayer coverage of imine on a surface to the equilibrium concentrations of amine and water. Unfortunately neither experiment, carried out to immobilise fluoroamine on the (100) diamond surface at room temperature, reached equilibrium to allow this analysis to be probed.

$$\theta_{eq} = \frac{K[amine]_{eq}}{[water]_{eq} + K[amine]_{eq}} \quad (34)$$

The rate constant for a given reaction can be explained in terms of collision theory by the Arrhenius equation. Chemisorption on a surface can be explained in terms of collision theory by equation (35), analogous to the Arrhenius equation. The rate of chemisorption of amine molecules on an oxidised (100) diamond surface is dependant on the activation energy of the reaction (E_a). Higher activation energy leads to a slower rate of reaction as fewer collisions have sufficient energy to surmount the energy barrier to reaction. In place of the standard pre-exponential factor, on a surface the number of collisions potentially leading to reaction is governed by the number of collisions per unit area of surface in unit time (Z) and the sticking coefficient (σ). The sticking coefficient reflects the fraction of collisions which lead to adsorption.

$$k = \sigma Z e^{\left(\frac{-E_a}{RT}\right)} \quad (35)$$

The number of collisions per unit surface area per unit time (Z) occurring between fluoroamine molecules and a (100) diamond surface is proportional to the concentration of fluoroamine in the solution in which the diamond sample is immersed. The sticking coefficient (σ) of molecules of 4-trifluoromethylbenzylamine on an oxidised (100) diamond surface is not known, neither is the activation energy for the reaction between 4-trifluoromethylbenzylamine and carbonyl groups on the surface of (100) diamond. Measurement of the rate constant (k) at a number of temperatures could allow determination of values for the pre-exponential terms and activation energy to be determined. Unfortunately, as explained above, it was not possible to determine values of the rate constant from the experiments reported here.

4.3.5 Attachment at elevated temperature

The quantity of fluoroamine present on the (100) diamond surface had not reached a limiting coverage after 60 hours immersion at room temperature, indicating that the attachment reaction had not reached equilibrium. In an attempt to increase the rate of reaction and allow equilibrium to be reached oxidised (100) diamond was immersed in 4-trifluoromethylbenzylamine solution at elevated temperature (refluxing methanol at 65°C). Figure 61 demonstrates that the quantity of fluoroamine, detected by XPS, present on the oxidised (100) diamond surface showed a general increase with immersion time in the hot amine solution. The maximum quantity of fluoroamine introduced to the surface approached half a monolayer after around 8 hours. The amount is much greater than that achieved at room temperature where the maximum quantity of fluoroamine detected was 0.18 monolayers. However after extended exposure to the vacuum and washing in solvent the level of fluoroamine detectable from the (100) diamond surface decreased, as shown in Figure 62, indicating that the detected material was not chemically bound to the surface.

Increasing the reaction temperature may affect the position of equilibrium as well as the reaction rate. It was previously found that the reaction between 2-adamantanone and 3-phenylpropylamine was endothermic and therefore the equilibrium shifted towards the reactants with increasing temperature²³. The same may be true of the reaction between carbonyl groups on the surface of (100) diamond and 4-trifluoromethylbenzylamine. In Figure 61, fluoroamine covalently bound to the (100) diamond surface may make some contribution to each F 1s signal but cannot be identified as it is masked by the signal from physisorbed material. Figure 62 demonstrates that washing the surface with methanol reduced the F 1s signal from the surface, with continued washing the F 1s signal may have reached a plateau indicating that all physisorbed material had been removed and reflecting the level of chemisorbed fluoroamine. Physisorbed material on the diamond surface persisted for longer following these experiments than it did following room temperature immersion experiments, where no decrease in F 1s intensity was observed over 7 hours exposure of the sample to high vacuum.

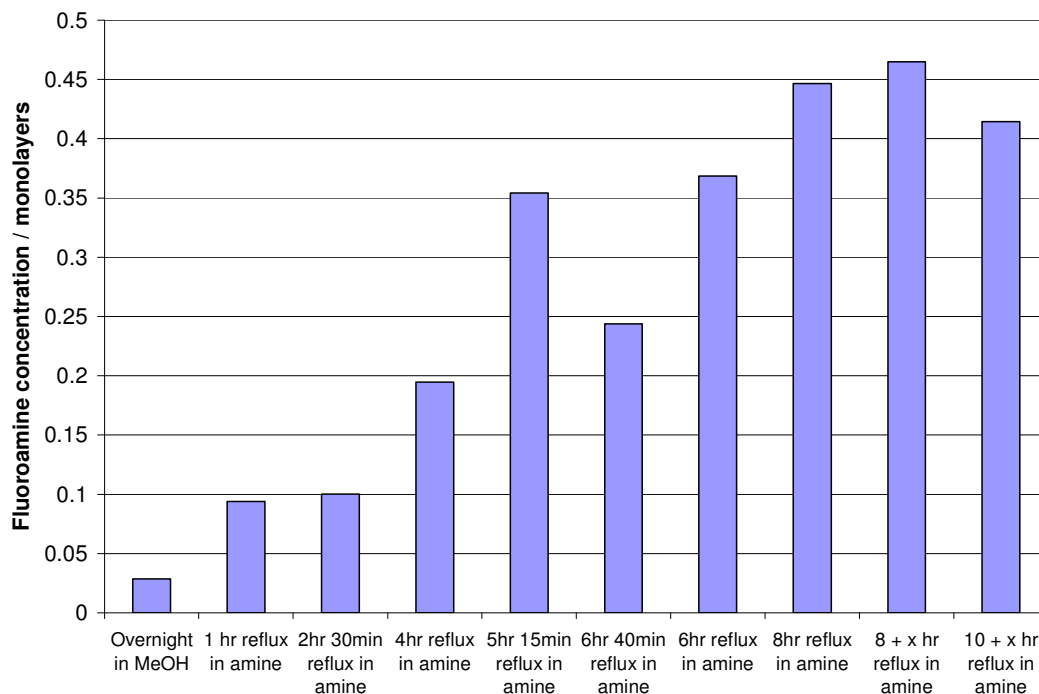


Figure 61 – Quantified values of the fluoroamine concentration (in monolayers) on an oxidised (100) diamond surface after periods of immersion in 4-trifluoromethylbenzylamine solution at elevated temperature.

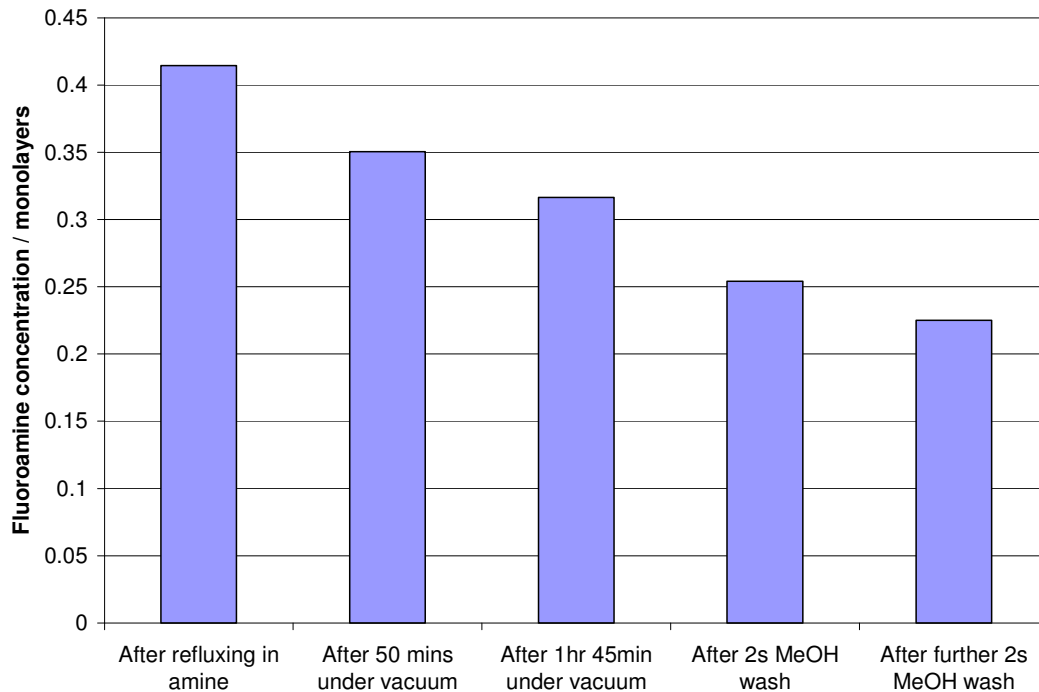


Figure 62 - Quantified values of fluoroamine concentration (in monolayers) on an oxidised (100) diamond surface following exposure to 4-trifluoromethylbenzylamine solution at elevated temperature, after extended residence under high vacuum in the XPS spectrometer and subsequent washings

The elevated temperature immersion experiments were not carried out on freshly prepared oxidised (100) diamond surfaces. This was not possible due to the separation of the oxidation equipment in Heriot-Watt University and the XPS instrument at NCESS, Daresbury and the limitations of time and access to the XPS. Instead, based on the known reversibility of the imine formation reaction in solution, it was attempted to regenerate the carbonyl terminated (100) diamond surface by washing the (100) diamond substrate in water. Figure 63 i) shows the XPS data collected from the (100) diamond surface prior to washing in water (to hydrolyse the imine bonds and regenerate the carbonyl terminated surface). Figure 63 ii) shows the spectrum from the surface after washing in water and demonstrates that the F 1s signal from bound fluoroamine has been almost completely removed but also that contamination of the surface has occurred as significant signals from silicon can be detected. The O 1s signal also appears increased suggesting that the contamination introduced to the surface may be some silicone related material. The (100) diamond surface was immersed overnight in methanol, as a control experiment, to ensure the methanol caused no unexpected XPS signals to appear. It can be seen in Figure 63 iii) that this introduced some additional sodium contamination to the substrate surface in addition to the silicone contamination. Figure 63 iv) shows the signals detectable from the (100) diamond surface following the first 6 hours of immersion in 4-trifluoromethylbenzylamine solution at elevated temperature. It can be seen that whilst this has introduced F 1s and N 1s signals from the fluoroamine the silicon and sodium contaminant peaks remain.

Unfortunately it was not possible to demonstrate chemisorption of 4-trifluoromethylbenzylamine to oxidised (100) diamond at elevated temperatures. Detection of the F 1s signal by XPS indicated that fluoroamine was present on the diamond surface. However, reduction of the F 1s signal by evaporation of fluoroamine into the vacuum and on washing the diamond surface in methanol indicated that at least some of this material was physisorbed.

One explanation for fluoroamine becoming physisorbed in the elevated temperature experiments is that the washing carried out to regenerate a carbonyl terminated (100) diamond surface may not have achieved the desired surface. Imine hydrolysis could occur by a different mechanism on a (100) diamond surface than the reversible reconversion to carbonyl functional reactants which occurs with small ketone molecules in solution. Hydrolysis of surface imine bonds may not regenerate carbonyl-like

functionality on the (100) diamond surface. It has to be admitted that these are unlikely propositions.

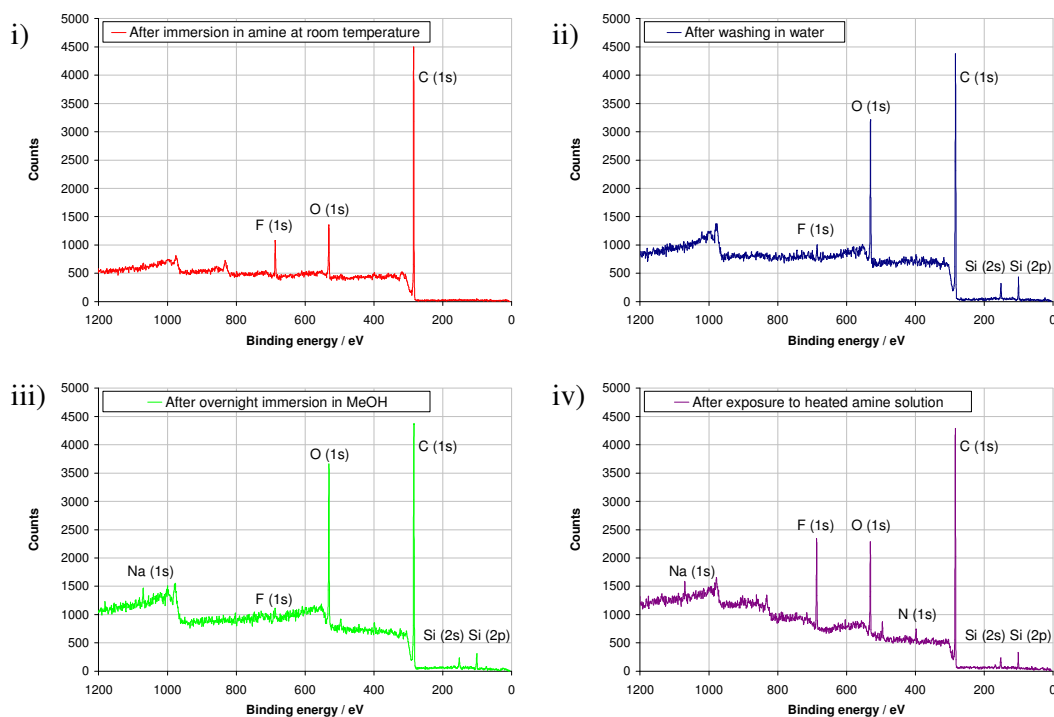


Figure 63 – XPS wide area survey spectra showing the elements detectable from the oxidised (100) diamond surface after; i) room temperature immersion in fluorinated amine solution, ii) subsequent washing in water, iii) immersion overnight in methanol solvent, iv) 6 hours immersion in fluorinated amine solution at elevated temperature.

If the reaction of 4-trifluoromethylbenzylamine with carbonyl groups on the oxidised (100) diamond surface follows the model reaction of 3-phenylpropylamine with 2-adamantanone then the position of equilibrium may lie further towards the reactants with increasing temperature. The quantity of covalently bound imine present on diamond surface would be lower at elevated temperature than at room temperature. Chemisorbed fluoroamine may contribute to the F 1s signal detected following elevated temperature immersion but be masked by the presence of physisorbed material. Introduction of a film of contamination on the diamond surface is likely to affect the interaction of reagents with the surface. The XPS data suggests that washing the (100) diamond surface in water introduced significant and unexpected contamination, particularly from a silicone material. Physical interaction of the fluoroamine with surface contamination could explain the observation that physisorbed fluoroamine took some time to desorb from the contaminated surface, and was detected by XPS, whereas

desorption of physisorbed material from the clean oxidised (100) surface, used in the room temperature immersion experiments, occurred quickly, before it could be detected.

4.3.6 Reductive amination

Imines can be reduced to water-stable amines in the presence of a reducing agent such as sodium cyanoborohydride¹⁵¹. When imine formation and reduction are carried out in one-pot the process is termed reductive amination¹⁵¹. Reductive amination was attempted on the surface of oxidised (100) diamond. Following immersion in a solution of 4-trifluoromethylbenzylamine and sodium cyanoborohydride for several hours the diamond surface was washed in methanol solvent twice and water twice. XPS analysis was carried out after each wash and the quantity of fluoroamine present on the surface calculated. The results are shown in Figure 64 and compared to those obtained from oxidised (100) diamond which had been immersed in 4-trifluoromethylbenzylamine with no sodium cyanoborohydride present.

Figure 64 shows that, following immersion of an oxidised (100) diamond surface in 4-trifluoromethylbenzylamine in the presence of sodium cyanoborohydride, the quantity of bound fluoroamine present on the surface was not reduced by washing in either methanol or in water. This differs from the observation that fluoroamine bound to the surface of oxidised (100) diamond surfaces by exposure to 4-trifluoromethylbenzylamine, in the absence of sodium cyanoborohydride, was stable to washing in methanol but could be removed by washing in water (data originally shown in Figure 58 and reproduced in Figure 64). These observations are consistent with sodium cyanoborohydride reduction of the hydrolysable imine bond to a water stable amine linkage between the fluoroamine molecule and the (100) diamond substrate, as shown schematically in Figure 65. In the two experiments represented in Figure 64 the exposure time of the (100) diamond substrates to the fluoroamine solution was different in each experiment, hence the reason the quantity of fluoroamine present on the surface after the first wash in methanol is different in each case.

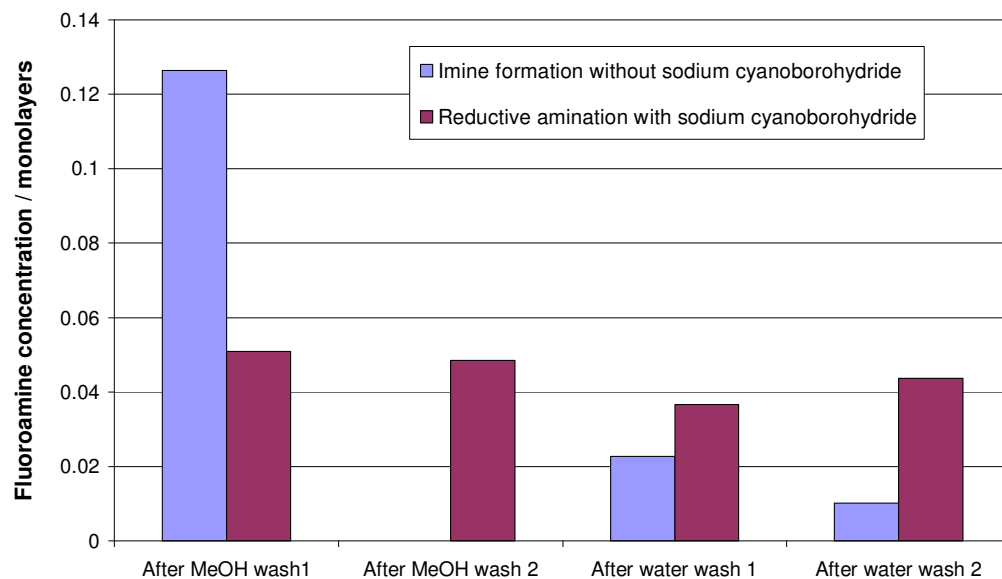


Figure 64 - Quantified values of fluoroamine concentration (in monolayers) on an oxidised (100) diamond surface after washes in methanol and water. (■) Reproduced data from Figure 58 following exposure of the diamond surface to a methanol solution of only 4-trifluoromethylbenzylamine. (■) Fluoroamine concentration following exposure of the diamond surface to a solution of 4-trifluoromethylbenzylamine and sodium cyanoborohydride in methanol.

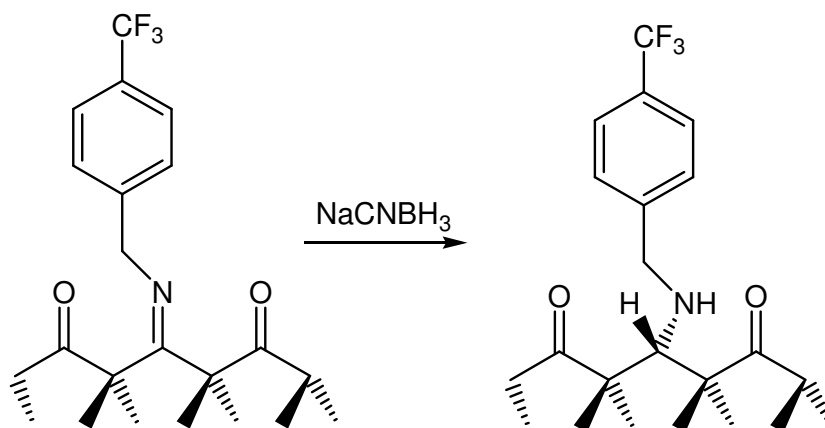


Figure 65 – Idealised depiction of an oxidised (100) diamond surface to which a molecule of 4-trifluoromethylbenzylamine has chemisorbed via a hydrolysable imine bond and the conversion of this to a water-stable amine bond by reduction with sodium cyanoborohydride.

4.4 Conclusions

Following immersion of oxidised (100) diamond in methanol solutions of the fluorinated amine 4-trifluoromethylbenzylamine at room temperature for several hours, the presence of 4-trifluoromethylbenzylamine has been detected by the appearance of F 1s and N 1s peaks in X-ray photoelectron spectra. Angle resolved studies demonstrated that 4-trifluoromethylbenzylamine is localised on the surface of the diamond and not distributed throughout the bulk.

A consistent approach to quantifying the level of 4-trifluoromethylbenzylamine present on the (100) diamond surface has been adopted based on published equations for quantifying overlayers on substrates¹⁰¹. In theory this was based on the ratio of the total signal from the fluoroamine overlayer to the signal from the diamond substrate but in practice used the intensity of the F 1s peak to the C 1s peak. As such this results in a systematic under-estimation of the quantity of fluoroamine present. Simplifying assumptions (equations (24) and (25)) used in the calculations may introduce an error of up to 30% in the resulting fractional monolayer coverage value. Therefore, $\pm 30\%$ represented an estimation of the error in any calculated coverage value. This consistent approach allowed comparison of 4-trifluoromethylbenzylamine quantities between spectra and allowed conclusions on the effects of surface treatments such as washings or immersion time to be made.

Hydrogenated (100) diamond was immersed in 4-trifluoromethylbenzylamine solution and interrogated by XPS as a control experiment. A measurable level of 4-trifluoromethylbenzylamine could initially be detected from the surface. With increasing exposure time to the high vacuum of the XPS instrument, the quantity of fluoroamine detectable on the surface decreased. One short wash in methanol solvent reduced the level of fluoroamine detectable to a small but non-zero level. This level remained constant despite further washes in methanol and water. These observations are consistent with the majority of 4-trifluoromethylbenzylamine introduced to hydrogenated (100) diamond surfaces by immersion being physisorbed and removed by exposure to the spectrometer vacuum or by washing in solvent. The presence of a small quantity of fluoroamine on the hydrogenated (100) diamond surface which could not be

removed by washing in solvent or water was unexpected. The nature of this binding was not investigated.

Samples of (100) diamond which had been freshly oxidised prior to immersion in 4-trifluoromethylbenzylamine solution demonstrated a constant level of fluoroamine on the oxidised diamond surface by XPS despite exposure to the spectrometer vacuum for several hours. Upon washing in methanol the level of fluoroamine detectable from the surface was only slightly reduced. This suggests the fluoroamine was strongly bound to the diamond surface, consistent with formation of a covalent bond between 4-trifluoromethylbenzylamine and the oxidised (100) diamond surface. On washing in water the level of fluoroamine detectable from the (100) diamond surface was markedly reduced. Such evidence that 4-trifluoromethylbenzylamine present on oxidised (100) diamond surfaces is stable except on exposure to water provides a strong argument for formation of hydrolysable imine bonds between 4-trifluoromethylbenzylamine molecules and carbonyl-like $>C=O$ groups on the surface of oxidised (100) diamond. Evidence of physisorbed material was observed in the form of white drying stains which were formed on the surface of some oxidised (100) diamond samples on their removal from fluoroamine solution. However, these disappeared within few minutes on exposure to the spectrometer vacuum and no XPS evidence for physisorbed material was observed despite repeated interrogation of the surface. Physisorbed material appeared to be lost to the spectrometer vacuum very quickly from these oxidised (100) diamond surfaces.

The quantity of 4-trifluoromethylbenzylamine present on oxidised (100) diamond surfaces increased with immersion time in fluoroamine solution at room temperature. Within experimental error the increase appeared to be linear but did not reach a limiting coverage in the duration of the experiment. The rate of attachment was different in the two experiments carried out. 4-trifluoromethylbenzylamine was present in excess of the maximum number of carbonyl groups theoretically possible on the 4 x 4 mm diamond surface by a factor of 10^6 . The difference in rate was most likely due to a difference in the number of carbonyl-like groups introduced to the (100) diamond surface by slightly different oxidation conditions. XPS results presented in an earlier chapter were consistent with the introduction of one complete monolayer of oxygen to the (100) diamond surface by thermal oxidation. However, determining the proportion of this present in carbonyl and ether-like form relied on peak fitting of high resolution spectra

introducing a degree of uncertainty and making the method unsuitable for the detection of small changes in the ratio of carbonyl to ether groups. The lack of a definitive measure of the number of carbonyl groups present on the oxidised (100) diamond surface limited the kinetic analysis which could be undertaken to understand imine formation on oxidised (100) diamond surfaces by 4-trifluoromethylbenzylamine.

Oxidised (100) diamond was immersed in 4-trifluoromethylbenzylamine solution at elevated temperature in an attempt to increase the reaction rate and achieve a limiting imine coverage on the (100) diamond surface. XPS analysis of surfaces exposed to fluoroamine solution at elevated temperature did not provide conclusive proof of covalent attachment. The presence of an intense F 1s signal indicated that 4-trifluoromethylbenzylamine was present on the (100) diamond surface following immersion at elevated temperature. However decreases in the detected F 1s intensity, as material evaporated into the spectrometer vacuum or was lost on washing in methanol, suggested that at least some of the 4-trifluoromethylbenzylamine was physisorbed, not chemisorbed, to the diamond surface. Increasing the reaction temperature will affect the position of equilibrium as well as the reaction rate. In model studies on 2-adamantanone²³ it has been demonstrated that increasing temperature drives the position of equilibrium towards the reactants. If the position of equilibrium lies far towards the reactants under these conditions it may well be that a quantity of fluoroamine has been covalently bound to the (100) diamond surface. More extensive washing of the surface, to remove the physisorbed material and allow detection of the F 1s signal from chemisorbed fluoroamine only, would have been required to probe this theory.

XPS analysis of freshly oxidised (100) diamond surfaces immersed in fluoroamine solution at room temperature did not detect the presence of physisorbed material. Physisorbed material was present on the surface of (100) diamond, immersed at elevated temperature, during XPS analysis. The presence of physisorbed material could have a number of explanations. The (100) diamond surface had not been freshly oxidised prior to exposure to 4-trifluoromethylbenzylamine solution at elevated temperature. Following initial oxidation, the (100) diamond surface had first been used for room temperature immersion experiments. After the room temperature immersion experiments it was attempted to regenerate a carbonyl terminated oxidised (100) diamond surface, based on the reversibility of imine formation by small molecules in solution, by washing the diamond copiously in water. Washing the surface in water

may not have regenerated carbonyl groups by hydrolysis of surface imines. If this was the case it would suggest imine formation on an oxidised (100) diamond surface was not analogous to the reversible reaction of small molecules in solution. Alternatively, it seems more likely that the presence of contamination may have affected the interactions occurring on the diamond surface. After washing, silicon and increased oxygen peaks in the XPS spectra indicated the presence of silicone material on the (100) diamond surface. The presence of contamination may have prevented the 4-trifluoromethylbenzylamine being able to bind to surface carbonyl groups on immersion at elevated temperature. A physical interaction of 4-trifluoromethylbenzylamine with the silicone could explain why physisorbed material took some time to desorb from the surface. A definitive explanation cannot be concluded from the present results.

Reductive amination in which a hydrolysable imine is reduced, in situ, to a water stable amine was attempted by immersing a freshly oxidised (100) diamond substrate in a solution of 4-trifluoromethylbenzylamine and sodium cyanoborohydride. When carried out without sodium cyanoborohydride present the surface imine groups formed were stable to washing in methanol but hydrolysed during washing in water. When sodium cyanoborohydride reducing agent was present in the reagent solution the quantity of fluoroamine detected from the (100) diamond surface was not reduced by contact with water. This result indicated that it was possible to bind amine molecules to the surface of an oxidised (100) diamond substrate via a stable linkage by immersing the diamond surface in a solution containing the amine and sodium cyanoborohydride reducing agent. The experimental observations are entirely consistent with the formation of an imine by reaction of the fluoroamine reagent with the diamond surface and subsequent reduction of the imine bond to a water-stable amine.

The experiments undertaken here have utilised a small fluorinated amine in order to demonstrate the applicability of the approach. Covalent attachment of larger linker diamine molecules could be undertaken by this approach and, following further coupling steps, allow the use of oxidised (100) diamond surfaces for array and sensing applications.

5 – Summary and conclusions

The oxidised (100) surface of single crystal diamond has been functionalised with a fluorinated amine via a stable, covalent bond. The use of well characterised high quality (100) single crystal diamond allowed the oxygen functionality present on the diamond surface to be identified and therefore was instrumental in allowing study of the proposed coupling reaction. The data collected is consistent with reaction of the amine nucleophile with carbonyl groups on the (100) diamond surface, analogous to the well-studied reversible reaction undertaken by ketones to form imines in organic synthetic chemistry. A simple fluorinated amine has been used to demonstrate the applicability of the approach. The use of di-functional amine linker molecules would allow further reaction to introduce larger molecules to the surface, providing a method for the functionalisation of oxidised diamond complementary to existing methods for functionalising hydrogenated diamond.

The faces of a purchased single crystal diamond substrate were characterised as (100) faces by XRD. Lacking supporting documentation, a novel XRD experiment was devised which determined that the main (100) face was misoriented from (100) by $0^\circ \pm 1^\circ$. Hydrogen plasma treatment was employed to reduce the surface roughness and improve the quality and perfection of the (100) surface. After 8 – 12 hours hydrogen plasma exposure the surface roughness (R_a) measured by AFM fell to a limit of around 1 nm and the AFM images collected were rather featureless. Given the resolution of the AFM instrument, the observed value ($R_a \sim 1$ nm) represents an upper limit of the surface roughness achievable by maximising the extent of the (100) terraces. While the intention was to maximise the terrace coverage by anisotropic hydrogen plasma etching of steps, the presence of carbon species in the plasma chamber, detected by mass spectrometry, meant smoothing due to step-growth could not be ruled out.

Oxidation of the smooth, high quality (100) single crystal diamond substrate at 640°C under 930 mbar of O_2 for 8 minutes was evidenced by angle resolved XPS. Quantitative analysis of the XPS data, based on the relative areas under C 1s and O 1s peaks indicated there was 1.07 ± 0.26 monolayers of oxygen present on the (100)

diamond surface. High resolution scans of the C 1s peak identified detail in the core line envelope, attributed to carbon atoms in different chemical environments. Peak fitting to the C 1s peak using published fitting parameters⁸⁸ and chemical shifts, in line with those previously published for diamond, identified that over 60% of the oxygen present on the oxidised (100) surface was double bonded to carbon in a carbonyl-like configuration while the rest was present in an ether-like form. High resolution scans of the O 1s peak revealed two partially resolved peaks. Lacking prior published data of O 1s peak deconvolution on diamond, these were tentatively assigned to carbonyl and ether like oxygen based on published XPS polymer spectra. Quantitative analysis based on the peak areas confirmed that the majority of the oxygen was present in a carbonyl configuration.

Exposure of (100) diamond single crystals to thermal oxidation for extended periods resulted in morphological changes identified by AFM and optical microscopy. After 10 minutes exposure, ridge features were visible in AFM images which became visible by optical microscopy after around 50 minutes exposure. After several hours oxidation these ridges broke up to give the surface a 'brick-work' appearance in optical images. The surface roughness increased so significantly that high quality AFM images could not be obtained as severe wear was caused to the AFM tip. Material removal by etching was evident from the increase in dimension of surface features, such as polishing grooves. These observations were attributed to anisotropic step etching by oxygen of a surface with two small, but differently sized orthogonal miscuts from (100). In the direction with the larger miscut more step edges exist on the surface. As oxidative etching of steps occurs, step pinning causes step bunching to occur. The height of bunched steps will increase more quickly in the direction of the larger miscut due to the greater number of steps and become visible, first by AFM and later by optical microscopy, as macro-bunched steps. As further etching takes place step pinning in the direction with the lower miscut will eventually also create macro-bunched steps, forming terraces bounded on two adjacent sides by steps in the step-up direction and, on the other two sides, by steps in the step-down direction, which become visible by optical microscopy.

The molecular ketone, 2-adamantanone, based on the smallest diamondoid molecule adamantane and containing a carbonyl functional group, was adopted as a molecular mimic of the carbonyl terminated, oxidised (100) diamond surface. Derivatisation

reactions of 2-adamantanone with amine functional species resulted in the expected imine products. Sodium cyanoborohydride was shown to be capable of reducing the imine bond to a stable amine product by reductive amination. FTIR allowed kinetic analysis of the reactions and, for a range of amines and reaction conditions, rate constants were calculated allowing an insight into the reaction mechanism. The mechanism of imine formation involves two main stages, addition of amine to the carbonyl group to form a carbinolamine intermediate and subsequent dehydration of the carbinolamine. Literature reports of imine formation from ketones other than 2-adamantanone^{87, 138, 139, 148, 163} describe rate limiting dehydration at alkaline and neutral pH. At slightly acidic pH the carbonyl group can become protonated, and therefore more electrophilic, causing an acid catalysed rate maximum to occur. At increasingly acid pH however the amine nucleophile becomes protonated, reducing the rate of amine addition such that it is rate limiting. In the reaction of 2-adamantanone with ethylamine, imine formation was not observed at neutral and acidic pH, attributed to protonation of the amine nucleophile. At alkaline pH however, unlike other ketones, amine addition was rate limiting. This unusual observation is an interesting twist on the established mechanism of imine formation and was attributed to the cage-like structure of 2-adamantanone creating steric hindrance to the attacking amine and reducing the rate of amine addition below that of dehydration. An amine attacking carbonyl groups on an oxidised (100) diamond surface can be expected to encounter significant steric hindrance and the use of this molecular model of a small section of the diamond surface suggests how the standard solution phase mechanism of imine formation may be modified on a (100) diamond surface.

Thermally oxidised (100) diamond was immersed in solutions of the fluorinated amine 4-trifluoromethylbenzylamine, under the conditions elucidated from the work with 2-adamantanone. Angle resolved XPS analysis demonstrated the presence of fluorine and nitrogen in the diamond surface. A consistent approach to quantifying the level of 4-trifluoromethylbenzylamine on the (100) diamond surface was adopted based on the area under the F 1s peak, from the fluoroamine, and the area under the C 1s peak, assumed to be due only to the diamond substrate. Assumptions in the derivation of the quantification expression resulted in a systematic underestimation of the quantity of 4-trifluoromethylbenzylamine present on the (100) diamond surface, but this approach allowed a reasonable comparison of the quantity of 4-trifluoromethylbenzylamine present between the various spectra. The quantity of 4-trifluoromethylbenzylamine

present on freshly oxidised (100) diamond surfaces did not decrease during several hours exposure to high vacuum. Subsequent washing of the surface in methanol did not significantly reduce the level of 4-trifluoromethylbenzylamine present on the surface, but washing in water quickly removed almost all of the amine. In contrast, immersion of a hydrogen terminated (100) diamond sample, under the same conditions, introduced 4-trifluoromethylbenzylamine to the surface but the quantity decreased under vacuum and was markedly reduced by washing in methanol. These results are consistent with the formation of a covalent imine bond between oxidised (100) diamond and the fluorinated amine, which provided a covalent linkage which is hydrolysed by water. On a hydrogenated diamond surface no such linkage could be created and the bulk of the 4-trifluoromethylbenzylamine appeared to be physisorbed. Unexpectedly, a small quantity of 4-trifluoromethylbenzylamine could not be removed from the hydrogenated (100) diamond surface by washing in methanol and was unaffected by water. The nature of the bond between this material and the hydrogenated surface was not investigated further.

The quantity of 4-trifluoromethylbenzylamine attached to freshly oxidised (100) diamond surfaces increased regularly with immersion time in amine solution at room temperature. The rate of attachment differed between two experiments, one achieving 0.18 monolayers coverage after 20 hours, the other 0.15 monolayers after 58 hours immersion although neither attained a limiting coverage. Since the amine was present in a 10^6 -fold excess in each experiment the difference in rate was believed to be due to a difference in the concentration of carbonyl-like moieties on the oxidised (100) diamond surfaces created by slightly different oxidation conditions. The rate of 4-trifluoromethylbenzylamine uptake is expected to be acutely dependant on the concentration of carbonyl groups on the surface. Unfortunately, the deconvolution of high resolution C 1s peak shapes and peak fitting to determine relative concentrations of oxygen functional groups on a (100) diamond surface is not a sufficiently robust method to accurately differentiate small differences in the concentration of surface moieties. Accurate knowledge of the starting concentration of carbonyl groups on each oxidised (100) diamond surface would have allowed a more comprehensive kinetic analysis of these results to be explored.

In experiments intended to investigate the rate of 4-trifluoromethylbenzylamine uptake on (100) diamond at elevated temperature, chemisorption to the diamond surface could

not be unequivocally demonstrated. The level of 4-trifluoromethylbenzylamine detected on the (100) diamond surface decreased over time exposed to vacuum and was reduced by washing in methanol. The data were consistent with physisorption. Based on model studies on 2-adamantanone²³, the equilibrium position of the attachment reaction may shift towards free amine and the carbonyl terminated surface on increasing the reaction temperature. It is possible that a concentration of covalently bound fluoroamine existed on the (100) diamond surface but could not be differentiated from physisorbed fluoroamine by XPS. The diamond surface used in this experiment had not been freshly oxidised prior to immersion in the amine solution but, instead, had been used for room temperature attachment experiments. Attempting to hydrolyse the imine formed at room temperature, the surface was washed copiously in water in an attempt to regenerate the surface carbonyl groups. XPS revealed that washing had significantly reduced the F 1s signal but unfortunately had introduced silicone contamination to the (100) diamond surface in these series of experiments. The contamination layer is likely to have interfered with the processes occurring on the diamond surface. It may have inhibited chemical reaction of the fluoroamine to form surface bound imines while interacting physically with the fluoroamine which would explain the observation that physisorbed fluoroamine took some time to desorb from the contaminated surface in the elevated temperature experiments.

Reductive amination was attempted on a freshly oxidised (100) diamond surface by immersion in a solution of 4-trifluoromethylbenzylamine and sodium cyanoborohydride. The quantity of surface bound 4-trifluoromethylbenzylamine was not reduced upon washing in methanol or in water. This is consistent with imine formation between 4-trifluoromethylbenzylamine and the oxidised (100) diamond surface with *in-situ* borohydride reduction of the imine bond to a water-stable amine linkage.

6 – Future work

This work has demonstrated that organic molecules can be immobilised on an oxidised (100) diamond surface via a stable covalent linkage. Use of suitable di-functional linker molecules such as α , ω -carboxylic acid-amines or di-amines would provide suitable additional reactivity that, once tethered to the diamond surface, the linker molecule could react further with bio- or other molecules. Where the molecule of interest contains a primary amine group, common in biological molecules, direct coupling to the (100) diamond surface by this method could be attempted. To discern whether this route could truly provide an attachment chemistry to oxidised diamond, complementary to existing routes for hydrogenated diamond, molecules of specific interest, such as DNA for sensing arrays and ethylene glycol oligomers to prevent non-specific binding²², should be covalently coupled to the surface and fluorescence imaging hybridisation studies carried out.

To be useful in device fabrication, optimisation of the attachment route in terms of reaction rate and surface coverage would be required. By utilising a well characterised surface and demonstrating analogous reactions garnered from the chemistry of the carbonyl group, this work provides an understanding of the chemical reactions that take place on a diamond surface. A deep understanding of the kinetics and thermodynamics is central to optimising the attachment process. Further work should be pursued, such as investigating whether carbonyl groups on the (100) diamond surface are regenerated upon reaction of imine functional groups with water, in order to fully elucidate the reaction mechanism on the diamond surface. To this end, it would be informative to study the reaction of a series of suitably oxidised diamondoid molecules of increasing molecular weight, to mimic sections of the oxidised (100) diamond surface. This would allow a true progression in the chemistry to be studied from the standpoint of an isolated organic molecule, 2-adamantanone, to an extended oxidised (100) diamond surface. Notwithstanding the availability of suitable quantities of diamondoids, the difficulty of selective oxidation to mimic the equivalent diamond surface makes this task a significant challenge for the future.

Critical to optimising the process is a precise and accurate measure of the number of carbonyl groups present on the oxidised (100) diamond surface and a suitable technique

for this should be strongly pursued. Atomic scale AFM imaging is desirable to study the extent to which the diamond surface can be smoothed and the proportion of (100) terraces maximised. Complementary work would involve investigating how the morphology is affected by thermal oxidation on the atomic scale.

Far from being limited to one attachment chemistry, the approach adopted in this study could be extended to investigate organic functionalisation of diamond surfaces by a range of different chemical approaches. Understanding the nature of the chemical functional groups present on well defined single crystal diamond surfaces is a prerequisite to utilise advances in organic chemistry which provide a plethora of covalent bond forming reactions. Successful extension of these to diamond surfaces would result in a range of organic functionalisation routes and provide the flexibility required for successful manufacture of diamond thin film devices for a range of technological applications.

References

1. S. F. Bent. "Organic functionalization of group IV semiconductor surfaces: principles, examples, applications and prospects" *Surface Science* (2002) **500**, 879 - 903.
2. S. Bhattacharyya, O. Auciello, J. Birrell, J. A. Carlisle, L. A. Curtiss, A. N. Goyette, D. M. Gruen, A. R. Krauss, J. Schlueter, A. Sumant, P. Zapol. "Synthesis and characterisation of highly-conducting nitrogen-doped ultrananocrystalline diamond films" *Applied Physics Letters* (2001) **79**, 1441 - 1443.
3. H. Yoshikawa, H. Morel, Y. Koga. "Synthesis of nanocrystalline diamond films using microwave plasma CVD" *Diamond and Related Materials* (2001) **10**, 1588 - 1591.
4. D. K. Milne, P. G. Roberts, P. John, M. G. Jubber, M. Liehr, J. I. B. Wilson. "Epitaxy of diamond on silicon" *Diamond and Related Materials* (1995) **4**, 394 - 400.
5. C. J. Tang, A. J. Neves, A. J. S. Fernandes. "Influence of nucleation density on film quality, growth rate and morphology of thick CVD diamond films" *Diamond and Related Materials* (2003) **12**, 1488 - 1494.
6. A. Tallaire, A. T. Collins, D. Charles, J. Achard, R. Sussmann, A. Gicquel, M. E. Newton, A. M. Edmonds, R. J. Cruddace. "Characterisation of high-quality thick single-crystal diamond grown by CVD with a low nitrogen addition" *Diamond and Related Materials* (2006) **15**, 1700 - 1707.
7. Y. Mokuno, A. Chayahara, Y. Soda, Y. Horino, N. Fujimori. "Synthesizing single-crystal diamond by repetition of high rate homoepitaxial growth by microwave plasma CVD" *Diamond and Related Materials* (2005) **14**, 1743 - 1746.
8. J. Isberg, J. Hammersberg, E. Johansson, T. Wikstrom, D. J. Twitchen, A. J. Whitehead, S. E. Coe, G. A. Scarsbrook. "High carrier mobility in single-crystal plasma-deposited diamond" *Science* (2002) **297**, 1670 - 1672.
9. A. M. Schrand, H. Huang, C. Carlson, J. J. Schlager, E. Osawa, S. M. Hussain, L. Dai. "Are diamond nanoparticles cytotoxic?" *Journal of Physical Chemistry B* (2007) **111**, 2 - 7.
10. L. Tang, C. Tsai, W. W. Gerberich, L. Kruckeberg, D. R. Kania. "Biocompatibility of chemical-vapour-deposited diamond" *Biomaterials* (1995) **16**, 483 - 488.
11. L. Nordsletten, A. K. M. Hogasen, Y. T. Kontinen, S. Santavirta, P. Aspenberg, A. O. Aasen. "Human monocytes stimulation by particles of hydroxyapatite,

silicon carbide and diamond: *in vitro* studies of new prosthesis coatings " *Biomaterials* (1996) **17**, 1521 - 1527.

12. H. J. Looi, L. Y. S. Pang, A. B. Molloy, F. Jones, J. S. Foord, R. B. Jackman. "An insight into the mechanism of surface conductivity in thin film diamond" *Diamond and Related Materials* (1998) **7**, 550 - 555.
13. F. Maier, M. Riedel, B. Mantel, J. Ristein, L. Ley. "Origin of surface conductivity in diamond" *Physical Review Letters* (2000) **85**, 3472 - 3475.
14. P. Strobel, M. Riedel, J. Ristein, L. Ley, O. Boltalina. "Surface transfer doping of diamond by fullerene" *Diamond and Related Materials* (2005) **14**, 451 - 458.
15. J. Ristein. "Surface science of diamond: familiar and amazing" *Surface Science* (2006) **600**, 3677 - 3689.
16. T. Strother, T. Knickerbocker, J. R. Russell Jr, J. E. Butler, L. M. Smith, R. J. Hamers. "Photochemical functionalisation of diamond films" *Langmuir* (2002) **18**, 968 - 971.
17. D. Shin, B. Rezek, N. Tokuda, D. Takeuchi, H. Watanabe, T. Nakamura, T. Yamamoto, C. E. Nebel. "Photo- and electrochemical bonding of DNA to single crystalline CVD diamond" *Physica Status Solidi (a)* (2006) **203**, 3245 - 3272.
18. T. Knickerbocker, T. Strother, M. P. Schwartz, J. R. Russell Jr, J. E. Butler, L. M. Smith, R. J. Hamers. "DNA-modified diamond surfaces" *Langmuir* (2003) **19**, 1938 - 1942.
19. W. Yang, O. Auciello, J. E. Butler, W. Cai, J. A. Carlisle, J. E. Gerbi, D. M. Gruen, T. Knickerbocker, T. L. Lasseter, J. R. Russell Jr, L. M. Smith, R. J. Hamers. "DNA-modified nanocrystalline diamond thin-films as stable, biologically active substrates" *Nature Materials* (2002) **1**, 253 - 257.
20. M. Lu, T. Knickerbocker, W. Cai, W. Yang, R. J. Hamers, L. M. Smith. "Invasive cleavage reactions on DNA-modified diamond surfaces" *Biopolymers* (2004) **73**, 606 - 613.
21. A. Hartl, E. Schmich, J. A. Garrido, J. Hernando, S. C. R. Catharino, S. Walter, P. Feulner, A. Kromka, D. Steinmuller, M. Stutzmann. "Protein-modified nanocrystalline diamond thin films for biosensor applications" *Nature Materials* (2004) **3**, 736 - 742.
22. T. L. Lasseter, B. H. Clare, N. L. Abbott, R. J. Hamers. "Covalently modified silicon and diamond surfaces: Resistance to nonspecific protein absorption and optimisation for biosensing" *Journal of the American Chemical Society - Communications* (2004) **126**, 10220 - 10221.
23. N. Polwart. "Modification of diamond (100) surfaces" Ph.D. Thesis - Heriot-Watt University, Edinburgh. (2003)

24. A. J. Mayne, D. Riedel, G. Comtet, G. Dujardin. "Atomic-scale studies of hydrogenated semiconductor surfaces" *Progress in Surface Science* (2006) **81**, 1-51.
25. W. J. P. van Enckevort, F. K. de Theije, Etching of diamond In *Properties, growth and applications of Diamond*. M. H. Nazare, A. J. Neves, eds., pp. 115-124. INSPEC, The Institute of Electrical Engineers, London (2000).
26. K. Hayashi, S. Yamanaka, H. Watanabe, T. Sekiguchi, H. Okushi, K. Kajimura. "Atomic force microscopy of atomically flat (001) diamond surfaces treated with hydrogen plasma" *Applied Surface Science* (1998) **125**, 120 - 124.
27. Y. Xia, T. Sekiguchi, W. Zhang, X. Jiang, W. Wu, T. Yao. "Effects of hydrogen ion bombardment and boron doping on (001) polycrystalline diamond films" *Journal of Crystal Growth* (2000) **213**, 328 - 333.
28. N. Lee, A. Badzian. "A study on surface morphologies of (001) homoepitaxial diamond films" *Diamond and Related Materials* (1997) **6**, 130-145.
29. N. Lee, A. Badzian. "Effect of misorientation angles on the surface morphologies of (001) homoepitaxial diamond thin films" *Applied Physics Letters* (1995) **66**, 2203 - 2205.
30. X. Jiang, C. Rickers. "Defect examination of diamond crystals by surface hydrogen-plasma etching" *Applied Physics Letters* (1999) **75**, 3935 - 3937.
31. R. E. Stallcup, Y. Mo, T. W. Scharf, J. M. Perez. "Formation of nanometer-size high-density pits on epitaxial diamond (100) films" *Diamond and Related Materials* (2007) **16**, 1727-1731.
32. R. Sung-Gi, H. Watanabe, M. Ogura, D. Takeuchi, S. Yamasaki, H. Okushi. "Hydrogen plasma etching mechanism on (001) diamond" *Journal of Crystal Growth* (2006) **293**, 311-317.
33. H. Okushi, H. Watanabe, S. Ri, S. Yamanaka, D. Takeuchi. "Device-grade homoepitaxial diamond film growth" *Journal of Crystal Growth* (2002) **237 - 239**, 1269 - 1276.
34. R. Sung-Gi, H. Yoshida, S. Yamanaka, H. Watanabe, D. Takeuchi, H. Okushi. "Misorientation angle dependance of surface morphology in homoepitaxial diamond film growth at low CH₄/H₂ ratio" *Journal of Crystal Growth* (2002) **235**, 300-306.
35. C. Battaile, D. Srolovitz, I. Oleinik, D. Pettifor, A. Sutton, S. Harris, J. E. Butler. "Etching effects during the chemical vapour deposition of (100) diamond" *Journal of Chemical Physics* (1999) **111**, 4291 - 4299.
36. R. Rawles, S. Komarov, R. Gat, W. Morris, J. Hudson, M. P. D'Evelyn. "Mechanism of surface smoothing of diamond by a hydrogen plasma" *Diamond and Related Materials* (1997) **6**, 791 - 795.

37. R. E. Stallcup, J. M. Perez. "Scanning tunneling microscopy studies of temperature-dependent etching of diamond (100) by atomic hydrogen" *Physical Review Letters* (2001) **86**, 3368 - 3371.
38. D. Takeuchi, H. Watanabe, S. Yamanaka, H. Okushi, K. Kajimura. "Homoepitaxial diamond films grown by step-flow mode in various misorientation angles of diamond substrates" *Diamond and Related Materials* (2000) **9**, 231-235.
39. F. K. de Theije, J. J. Schermer, W. J. P. van Enkevort. "Effects of nitrogen impurities on the CVD growth of diamond: step bunching in theory and experiment" *Diamond and Related Materials* (2000) **9**, 1439 - 1449.
40. F. C. Frank, On the kinematic theory of crystal growth and dissolution processes In *Growth and Perfection of Crystals*. R. H. Doremus, B. W. Roberts, D. Turnbull, eds., pp. 411-419. Wiley, New York (1958).
41. D. Kandel, J. D. Weeks. "Theory of impurity-induced step bunching" *Physical Review B* (1994) **49**, 5554-5564.
42. D. Kandel, J. D. Weeks. "Kinetics of surface steps in the presence of impurities: patterns and instabilities" *Physical Review B* (1995) **52**, 2154 - 2164.
43. S. Jin, T. D. Moustakas. "Effect of nitrogen on the growth of diamond films" *Applied Physics Letters* (1994) **65**, 403 - 405.
44. G. Z. Cao, J. J. Schermer, W. J. P. v. Enkevort, W. A. L. M. Elst, L. J. Giling. "Growth of {100} textured diamond films by the addition of nitrogen" *Journal of Applied Physics* (1996) **79**, 1357 - 1364.
45. S. Bohr, R. Haubner, B. Lux. "Influence of nitrogen additions on hot-filament chemical vapor deposition of diamond" *Applied Physics Letters* (1996) **68**, 1075 - 1077.
46. A. Afzal, C. A. Rego, W. Ahmed, R. I. Cherry. "HFCVD diamond grown with added nitrogen: film characterization and gas-phase composition studies" *Diamond and Related Materials* (1998) **7**, 1033 - 1038.
47. T. Frauenheim, G. Jungnickel, P. Stich, M. Kaukonen, F. Weich, J. Widany, D. Porezag. "A molecular dynamics study of N-incorporation into carbon systems: doping, diamond growth and nitride formation" *Diamond and Related Materials* (1998) **7**, 348 - 355.
48. J. J. Schermer, F. K. d. Theije. "Nitrogen addition during flame deposition of diamond: a study of nitrogen-enhanced growth, texturing and luminescence" *Diamond and Related Materials* (1999) **8**, 2127 - 2139.
49. K. Larsson, H. Bjorkman, K. Hjort. "Role of water and oxygen in wet and dry oxidation of diamond" *Journal of Applied Physics* (2001) **90**, 1026 - 1034.
50. J. S. Foord, C. H. Goeting. "Electrochemically controlled modification of CVD diamond surfaces" *Diamond and Related Materials* (2004) **13**, 1054 - 1058.

51. H. Notsu, I. Yagi, T. Tatsuma, D. A. Tryk, A. Fujishima. "Surface carbonyl groups on oxidised diamond electrodes" *Journal of Electroanalytical Chemistry* (2000) **492**, 31 - 37.
52. M. Tachiki, T. Fukuda, K. Sugata, H. Seo, H. Umezawa, H. Kawarada. "Control of adsorbates and conduction on CVD-grown diamond surface, using scanning probe microscopy" *Applied Surface Science* (2000) **159 - 160**, 578 - 582.
53. T. Kondo, M. Yanagisawa, L. Jiang, D. A. Tryk, A. Fujishima. "Nanolithographic modification of diamond" *Diamond and Related Materials* (2002) **11**, 1788-1796.
54. Y. Kaibara, K. Sugata, M. Tachiki, H. Umezawa, H. Kawarada. "Control wettability of the hydrogen-terminated diamond surface and the oxidised diamond surface using an atomic force microscope" *Diamond and Related Materials* (2003) **12**, 560 - 564.
55. M. Tachiki, Y. Kaibara, Y. Sumikawa, M. Shigeno, H. Kanazawa, H. Kawarada. "Characterization of locally modified diamond surface using Kelvin probe force microscope" *Surface Science* (2005) **581**, 207 - 212.
56. W. Deferme, K. Haenen, G. Tanasa, C. F. J. Filipse, M. Nesladek. "Compositional and electrical characterisation of the hydrogen-oxygen terminated diamond (100) surface" *Physica Status Solidi* (2006) **203**, 3114-3120.
57. M. Yamamoto, T. Teraji, T. Ito. "Improvement in the crystalline quality of homoepitaxial diamond films by the oxygen plasma etching of mirror-polished diamond substrates" *Journal of Crystal Growth* (2005) **285**, 130 - 136.
58. M. Bernard, A. Deneuve, L. Ortega, K. Ayadi, P. Muret. "Electron cyclotron resonance oxygen plasma etching of diamond" *Diamond and Related Materials* (2004) **13**, 287 - 291.
59. D. S. Hwang, T. Saito, N. Fujimori. "New etching process for device fabrication using diamond" *Diamond and Related Materials* (2004) **13**, 2207 - 2210.
60. G. F. Ding, H. P. Mao, Y. L. Cai, Y. H. Zhang, X. Yao, X. L. Zhao. "Micromachining of CVD diamond by RIE of MEMS applications" *Diamond and Related Materials* (2005) **14**, 1543 - 1548.
61. I. Bello, M. K. Fung, W. J. Zhang, K. H. Lai, Y. M. Wnag, Z. F. Zhou, R. K. W. Yu, C. S. Lee, S. T. Lee. "Effects at reactive ion etching of CVD diamond" *Thin Solid Films* (2000) **368**, 222 - 226.
62. W. J. P. van Enkevort, F. K. de Theije, Etching of diamond In *Properties, growth and applications of Diamond*. M. H. Nazare, A. J. Neves, eds., pp. 115-124. INSPEC, The Institute of Electrical Engineers, London (2001).
63. P. E. Pehrsson, T. W. Mercer. "Oxidation of the hydrogenated diamond (100) surface" *Surface Science* (2000) **460**, 49 - 66.

64. P. E. Pehrsson, T. W. Mercer. "Oxidation of heated diamond C(100):H surfaces" *Surface Science* (2000) **460**, 74 - 90.
65. J. S. Foord, L. C. Hian, R. B. Jackman. "An investigation of the surface reactivity of diamond cathodes with molecular and atomic oxygen" *Diamond and Related Materials* (2001) **10**, 710 - 714.
66. A. Laikhtman, A. Lafosse, Y. Le Coat, R. Azria. "Clarification of oxygen bonding on diamond surfaces by low energy electron stimulated desorption and high resolution electron energy loss spectroscopy" *Journal of Chemical Physics* (2003) **119**, 1794 - 1799.
67. F. K. de Theije. "Diamond surfaces - growth and etching mechanisms" Ph. D. Thesis - Department of solid state chemistry, University of Nijmegen, Nijmegen. (2001)
68. F. K. de Theije, N. J. van der Laag, M. Plomp, W. J. P. van Enkevort. "A surface topographic investigation of {100} diamond surfaces etched in oxygen" *Philosophical Magazine A* (2000) **80**, 725 - 745.
69. F. K. de Theije, O. Roy, N. J. van der Laag, W. J. P. van Enkevort. "Oxidative etching of diamond" *Diamond and Related Materials* (2000) **9**, 929 - 934.
70. P. E. Pehrsson, T. W. Mercer, J. A. Chaney. "Thermal oxidation of the hydrogenated diamond (100) surface" *Surface Science* (2002) **497**, 13 - 28.
71. M. Yokoyama, T. Ito. "Dependance on the electron affinity of homoepitaxially grown CVD diamond on the amount of surface oxygen" *Applied Surface Science* (2000) **162 - 163**, 457 - 463.
72. P. John, N. Polwart, C. E. Troupe, J. I. B. Wilson. "The oxidation of (100) textured diamond" *Diamond and Related Materials* (2002) **11**, 861 - 866.
73. T. Ando, K. Yamamoto, M. Ishii, M. Kamo, Y. Sato. "Vapour-phase oxidation of diamond surfaces in O₂ studied by diffuse reflectance fourier-transform infrared and temperature-programmed desorption spectroscopy" *Journal of the Chemical Society. Faraday Transactions* (1993) **89**, 3635 - 3640.
74. J. Nakamura, T. Ito. "Oxidation process of CVD diamond (100):H 2 x 1 surfaces" *Applied Surface Science* (2005) **244**, 301 - 304.
75. Y. M. Wang, K. W. Wong, S. T. Lee, M. Nishitani-Gamo, I. Sakaguchi, K. P. Loh, T. Ando. "Recent studies on diamond surfaces" *Diamond and Related Materials* (2000) **9**, 1582 - 1590.
76. P. John, N. Polwart, C. E. Troupe, J. I. B. Wilson. "The oxidation of diamond: the geometry and stretching frequency of carbonyl on the (100) surface" *Journal of the American Chemical Society* (2003) **125**, 6600 - 6601.
77. S. J. Sque, R. Jones, P. R. Briddon. "Structure, electronics and interaction of hydrogen and oxygen on diamond surfaces" *Physical Review B* (2006) **73**, 085313-085311 - 085313-085315.

78. S. Skokov, B. Weiner, M. Frenklach. "Molecular-dynamics study of oxygenated (100) diamond surfaces" *Physical Review B* (1994) **49**, 11374 - 11382.
79. H. Tamura, H. Zhou, K. Sugisako, Y. Yokoi, S. Takami, M. Kubo, K. Teraishi, A. Miyamoto, A. Imamura, M. N.Gamo, T. Ando. "Periodic density-functional study on oxidation of diamond (100) surfaces" *Physical Review B* (2000) **61**, 11025 - 11033.
80. L. D. Madsen, R. Charavel, J. Birch, E. B. Svederg. "Assessment of MgO (100) and (111) substrate quality by X-ray diffraction" *Journal of Crystal Growth* (2000) **209**, 91-101.
81. S. E. G. Slusky, A. T. Macrander. "Measurement of the miscut angle of crystal surfaces vicinal to major crystal planes by X-ray diffractometry at glancing incidence" *Applied Physics Letters* (1988) **53**, 2042-2043.
82. M. Gailhanou. "Accurate monocrystal miscut angle determination by X-ray diffraction on a wedge" *Applied Physics Letters* (1993) **63**, 458 - 460.
83. "The Cambridge Crystallographic Data Centre".
<http://www.ccdc.cam.ac.uk/products/csd/>. 2006
84. T. Yamanaka, S. Morimoto. "Isotope effect on anharmonic thermal atomic vibration and kappa refinement of C-12 and C-13 diamond" *Acta Crystallographica Section B - Structural Science* (1996) **52**, 232 - 238.
85. D. N. Batchelder, R. O. Simmons. "Lattice constants and thermal expansivities of silicon and of calcium fluoride between 6° and 322° K" *Journal of Chemical Physics* (1964) **41**, 2324.
86. M. G. Jubber, J. I. B. Wilson, I. C. Drummond, P. John, D. K. Milne. "Design of a UHV reactor for microwave plasma deposition of diamond films" *Vacuum* (1994) **45**, 499 - 506.
87. B. M. Anderson, W. P. Jencks. "The effect of structure on reactivity in semicarbazone formation" *Journal of the American Chemical Society* (1960) **82**, 1773 - 1777.
88. G. Beamson, D. Briggs. *High Resolution XPS of Organic Polymers - the Scienta ESCA300 Database*. John Wiley & Sons (1992).
89. J. E. Field, Wear and abrasion of diamond surfaces In *Properties, growth and applications of diamond*. M. H. Nazare, A. J. Neves, eds., pp. 105 - 107. INSPEC, The Institute of Electrical Engineers, London (2001).
90. F. M. van Bouwelen. "Diamond polishing from different angles" *Diamond and Related Materials* (2000) **9**, 925 - 928.
91. F. M. van Bouwelen, W. J. P. van Enckevort. "A simple model to describe the anisotropy of diamond polishing" *Diamond and Related Materials* (1999) **8**, 840 - 844.

92. B. Rezek, C. E. Nebel. "Electronic properties of plasma hydrogenated diamond surfaces: A microscopic study" *Diamond and Related Materials* (2006) **15**, 1374 - 1377.
93. W. J. P. van Enkevort, G. Janssen, J. J. Schermer, L. J. Giling. "Step-related growth phenomena on exact and misoriented {001} surfaces of CVD-grown single-crystal diamonds" *Diamond and Related Materials* (1995) **4**, 250-255.
94. H. Watanabe, D. Takeuchi, S. Yamanaka, H. Okushi, K. Kajimura, T. Sekiguchi. "Homoepitaxial diamond film with an atomically flat surface over a large area" *Diamond and Related Materials* (1999) **8**, 1272-1276.
95. G. Beamson, Personal Communication (2009).
96. M. P. Seah, W. A. Dench. "Quantitative electron spectroscopy of surfaces: a standard data base for electron inelastic mean free paths in solids" *Surface and Interface Analysis* (1979) **1**, 2 - 11.
97. S. Tanuma, C. J. Powell, D. R. Penn. "Calculations of electron inelastic mean free paths. 5. Data for 14 organic-compounds over the 50 - 2000 eV range" *Surface and Interface Analysis* (1994) **21**, 165 - 176.
98. W. H. Gries. "A universal predictive equation for the inelastic mean free pathlengths of x-ray photoelectrons and Auger electrons " *Surface and Interface Analysis* (1996) **24**, 38 - 50.
99. S. Tanuma, C. J. Powell, D. R. Penn. "Calculation of electron inelastic mean free paths. VIII. Data for 15 elemental solids over the 50 - 2000 eV range" *Surface and Interface Analysis* (2004) **36**, 1 - 14.
100. J. Zemek, J. Potmesil, M. Vanecek, B. Lesiak, A. Jablonski. "Inelastic mean-free path of electrons at nanocrystalline diamond surfaces" *Applied Physics Letters* (2005) **87**, 1 - 2.
101. M. P. Seah, Quantification of AES and XPS In *Practical Surface Analysis. Volume 1 - Auger and X-ray Photoelectron Spectroscopy*. D. Briggs, M. P. Seah, eds., Second Edition. pp. 201 - 255. John Wiley & Sons (1990).
102. C. J. Powell, A. Jablonski. *NIST Electron Inelastic-Mean-Free-Path Database - Version 1.1*. National Institute of Standards and Technology, Gaithersburg (2000).
103. D. Briggs, J. C. Riviere, Spectral interpretation In *Practical Surface Analysis. Volume 1 - Auger and X-ray Photoelectron Spectroscopy*. D. Briggs, M. P. Seah, eds., Second Edition. pp. 85 - 141. John Wiley & Sons Ltd (1990).
104. D. B. Ratner, D. G. Castner, Electron spectroscopy for chemical analysis In *Surface Analysis - The Principal Techniques*. J. C. Vickerman, ed., pp. 43 - 98. John Wiley & Sons Ltd (1997).
105. Scienta. *WinESCA Users Manual*. Scienta, Upsalla, Sweden.

106. *Practical Surface Analysis. Volume 1: Auger and X-ray Photoelectron Spectroscopy*. 2nd Edition. John Wiley & Sons Ltd (1990).
107. S. Mahl, M. Neumann, V. Schlett, A. Baalman. "Some aspects of the fitting of XPS core spectra of polymers" *Surface and Interface Analysis* (1998) **26**, 204-212.
108. D. Briggs, N. Fairley. "XPS of chemically modified low-density polyethylene surfaces: observations on curve-fitting the C 1s spectrum" *Surface and Interface Analysis* (2002) **33**, 283 - 290.
109. D. Briggs, G. Beamson. "Primary and secondary oxygen-induced C 1s binding energy shifts in X-ray photoelectron spectroscopy of polymers" *Analytical Chemistry* (1992) **64**, 1729 - 1736.
110. G. Beamson, D. Briggs. "High resolution monochromated X-ray photoelectron spectroscopy of organic polymers: A comparison between solid state data for organic polymers and gas phase data for small molecules" *Molecular Physics* (1992) **76**, 919 - 936.
111. R. Graupner, F. Maier, J. Ristein, L. Ley, C. Jung. "High-resolution surface-sensitive C 1s core-level spectra of clean and hydrogen-terminated diamond (100) and (111) surfaces" *Physical Review B* (1998) **57**, 12397 - 12409.
112. L. Ley, R. Graupner, J. B. Cui, J. Ristein. "Electronic properties of single crystalline diamond surfaces" *Carbon* (1999) **37**, 793 - 799.
113. J. I. B. Wilson, J. S. Walton, G. Beamson. "Analysis of chemical vapour deposited diamond films by X-ray photoelectron spectroscopy" *Journal of Electron Spectroscopy and Related Phenomena* (2001) **121**, 183 - 201.
114. C. H. Goeting, F. Marken, A. Gutierrez-Sosa, R. G. Compton, J. S. Foord. "Electrochemically induced surface modifications of boron-doped diamond electrodes: an X-ray photoelectron spectroscopic study" *Diamond and Related Materials* (2000) **9**, 390 - 396.
115. S. R. Haines, K. H. Williams, N. Almond, M. Schwitters, D. S. Martin, J. E. Butler, P. Weightman. "The initial stages of graphite formation on the diamond (100) 2 x 1 surface" *Journal of Electron Spectroscopy and Related Phenomena* (2006) **152**, 33 - 36.
116. T. Sugino, T. Itagaki, J. Shirafuji. "Formation of pn junctions by bonding of GaAs layer onto diamond" *Diamond and Related Materials* (1996) **5**, 714 - 717.
117. Z. R. Yue, W. Jiang, L. Wang, S. D. Gardner, C. U. Pittman Jr. "Surface characterisation of electrochemically oxidised carbon fibres" *Carbon* (1999) **37**, 1785 - 1796.
118. C. Hontoria-Lucas, A. J. Lopez-Peinado, J. d. D. Lopez-Gonzalez, M. L. Rojas-Cervantes, R. M. Martin-Aranda. "Study of oxygen-containing groups in a series

- of graphite oxides: physical and chemical characterisation" *Carbon* (1995) **33**, 1585 - 1592.
119. W. J. P. van Enkevort, Morphology of diamond surfaces In *Properties, Growth and Applications of Diamond*. M. H. Nazare, A. J. Neves, eds., pp. 95 - 101. INSPEC, The Institute of Electrical Engineers, London (2000).
 120. J. E. Dahl, S. G. Liu, R. M. K. Carlson. "Isolation and structure of higher diamondoids, nanometer-sized diamond molecules" *Science* (2003) **299**, 96 - 99.
 121. P. v. R. Schleyer, My thirty years in hydrocarbon cages: from adamantane to dodecahedrane In *Cage Hydrocarbons*. G. A. Olah, ed., 1st Ed. pp. 1 - 38. Wiley - Interscience (1990).
 122. W. Burns, T. R. B. Mitchell, M. A. McKervey, J. J. Rooney. "Gas-phase reactions on platinum. Synthesis and crystal structure of anti-tetramantane, a large diamondoid fragment" *Journal of the Chemical Society. Chemical Communications* (1976), 893 - 895.
 123. M. A. McKervey, J. J. Rooney, Catalytic routes to adamantane and its homologues In *Cage Hydrocarbons*. G. A. Olah, ed., pp. 39 - 64. Wiley - Interscience (1990).
 124. G. A. Olah, Carbocations and electrophilic reactions of cage hydrocarbons In *Cage Hydrocarbons*. G. A. Olah, ed., pp. 103 - 153. Wiley - Interscience (1990).
 125. A. P. Marchand. "Polycyclic cage compounds: reagents, substrates, and materials for the 21st century" *Aldrichimica Acta* (1995) **28**, 95 - 104.
 126. "MolecularDiamond Technologies". <http://moleculardiamond.chevron.com/>. Chevron Corporation. 2005
 127. G. C. McIntosh, M. Yoon, S. Berber, D. Tomanek. "Diamond fragments as building blocks of functional nanostructures" *Physical Review B* (2004) **70**, 045401.
 128. T. M. Willey, C. Bostedt, T. v. Buuren, J. E. Dahl, S. G. Liu, R. M. K. Carlson, R. W. Meulenberg, E. J. Nelson, L. J. Terminello. "Observation of quantum confinement in the occupied states of diamond clusters" *Physical Review B* (2006) **74**, 205432.
 129. J. Filik, J. N. Harvey, N. L. Allan, P. W. May, J. E. P. Dahl, S. Liu, R. M. K. Carlson. "Raman spectroscopy of nanocrystalline diamond: An ab initio approach" *Physical Review B* (2006) **74**, 035423.
 130. J. Oomens, N. Polfer, O. Pirali, Y. Ueno, R. Maboudian, P. W. May, J. Filik, J. E. Dahl, S. Liu, R. M. K. Carlson. "Infrared spectroscopic investigation of higher diamondoids" *Journal of Molecular Spectroscopy* (2006) **238**, 158 - 167.

131. L. Bisticic, G. Baranovic, K. Mlinaric-Majerski. "Vibrational analysis of 2-adamantanone and its deuterated isotopomers" *Spectrochimica Acta Part A* (1998) **54**, 1961-1986.
132. T. H. Lowry, K. S. Richardson. *Mechanism and Theory in Organic Chemistry*. 3rd Ed. Harper & Row, New York (1987).
133. J. McMurray. *Organic Chemistry*. 4th Ed. Brooks/Cole Publishing Company (1996).
134. A. Finiels, P. Geneste. "Correlation of the reactivity of ketones relative to different nucleophiles" *Journal of Organic Chemistry* (1979) **44**, 1577 - 1578.
135. H. C. Brown, O. H. Wheeler, K. Ichikawa. "Chemical effects of steric strains - XIII. Kinetics of the reaction of sodium borohydride with carbonyl groups - a convenient tool for investigating the reactivities of aldehydes and ketones" *Tetrahedron* (1957) **1**, 214 - 220.
136. H. C. Brown, K. Ichikawa. "Chemical effects of steric strains - XIV. The effect of ring size on the rate of reaction of the cyclanones with sodium borohydride." *Tetrahedron* (1957) **1**, 221 - 230.
137. J. Stubbe. "Session 1: The nature of chemical and biological diversity". www.nature.com/horizon/chemicalspace/kq/1_stubbe.html. 2003
138. E. H. Cordes, W. P. Jencks. "General acid catalysis of semicarbazone formation" *Journal of the American Chemical Society* (1962) **84**, 4319 - 4328.
139. W. P. Jencks. "Studies on the mechanism of oxime and semicarbazone formation" *Journal of the American Chemical Society* (1959) **81**, 475 - 481.
140. J. M. Sayer, B. Pinsky, A. Schonbrunn, W. Washtien. "Mechanism of carbinolamine formation" *Journal of the American Chemical Society* (1974) **96**, 7998 - 8009.
141. F. H. Westheimer. "Semicarbazone formation in sixty per cent methyl cellosolve" *Journal of the American Chemical Society* (1962) **56**, 1962 - 1965.
142. M. M. Sprung. "A summary of the reactions of aldehydes with amines" *Chemical Reviews* (1940) **26**, 297 - 338.
143. W. E. Hull, B. D. Sykes, B. M. Babior. "A proton nuclear resonance study of the aqueous chemistry of acetaldehyde and ammonia. The formation of 2,4,6-trimethylhexahydro-s-triazine" *Journal of Organic Chemistry* (1973) **38**, 2931 - 2939.
144. J. A. Chudek, R. Foster, D. Young. "¹³C Nuclear Magnetic Resonance studies of the products of reaction of acetaldehyde and of simple ketones in liquid ammonia, in hydrazine hydrate and in some substituted hydrazine solutions " *Journal of the Chemical Society. Perkin Transactions II* (1985), 1285-1289.

145. F. Hibbert, M. A. Malana. "Cyclic imine formation by intramolecular nucleophilic addition and elimination between an amino group and amide carbonyl; rate - pH profile for the reaction of 1-amino-8-trifluoroacetylaminonaphthalene to 2-trifluoromethylperimidine" *Journal of the Chemical Society. Perkin Transactions II* (1992), 1067 - 1070.
146. S. Rosenberg, S. M. Silver, J. M. Sayer, W. P. Jencks. "Evidence for two concurrent mechanisms and a kinetically significant proton transfer process in acid-catalyzed O-methyloxime formation" *Journal of the American Chemical Society* (1974) **96**, 7986 - 7997.
147. D. R. Lide, ed. *CRC Handbook of Chemistry and Physics*. 76th Edition. CRC Press (1995).
148. E. H. Cordes, W. P. Jencks. "The mechanism of hydrolysis of schiff bases derived from aliphatic amines" *Journal of the American Chemical Society* (1963) **85**, 2843 - 2848.
149. F. A. Carey, R. J. Sundberg. *Advanced Organic Chemistry - Part A: Structure and Mechanisms*. 3rd Ed. Plenum Press, New York (1990).
150. D. H. McDaniel, H. C. Brown. "An extended table of Hammett substituent constants based on the ionization of substituted benzoic acids" *Journal of Organic Chemistry* (1958) **23**, 420 - 427.
151. R. F. Borch, M. D. Bernstein, H. D. Durst. "The cyanohydridoborate anion as a selective reducing agent" *Journal of the American Chemical Society* (1971) **93**, 2897-2904
152. K. J. Laidler. *Chemical Kinetics*. 2nd Ed. McGraw - Hill Book Company (1965).
153. W. Kemp. *Qualitative Organic Analysis, Spectrochemical Techniques*. 2nd Ed. McGraw-Hill (1986).
154. "IBM CKS". http://almaden.ibm.com/st/computational_science/ck/msim/. IBM Almaden Research Center. 2006
155. M. A. Fox, J. K. Whitesell. *Organic Chemistry*. Jones and Bartlett Publishers (1994).
156. S. Berger, K.-P. Zeller. "Two and three bond ^{13}C - ^{13}C spin coupling constants in adamantane derivatives" *Journal of the Chemical Society. Chemical Communications* (1976), 649 - 650.
157. E. Antoniadou-Vyza, N. Avramidis, A. Kourounakis, L. Hadjipetrou. "Anti-inflammatory properties of new adamantane derivatives. Design, synthesis and biological evaluation" *Archiv Der Pharmazie* (1998) **331**, 72-78.
158. T. Sasaki, S. Eguchi, T. Okano. "Synthesis of adamantane derivatives; 48. Synthesis of some novel 1,2-fused adamantane azaheterocycles via 2-oxoadamant-1-yl isocyanate" *Synthesis* (1980) **6**, 472-475

159. T. I. Pekhk, E. T. Lippmaa, L. N. Lavrova, N. N. Vinogradova, N. V. Klimova, M. I. Shmar'yan, A. P. Skoldinov. "Use of ^{13}C NMR spectroscopy for analysis of stereoisomeric 2,5-disubstituted derivatives of adamantane" *Journal of Organic Chemistry USSR* (1978) **14**, 1526-1531.
160. H. W. Geluk, V. G. Keizer. "Adamantanone" *Organic Syntheses Collective* (1988) **6**, 48 - 50.
161. S. Y. Venyaminov, F. G. Prendergast. "Water (H_2O and D_2O) molar absorptivity in the 1000-4000 cm^{-1} range and quantitative infrared spectroscopy of aqueous solutions" *Analytical Biochemistry* (1997) **248**, 234-245.
162. P. R. Dave, M. Ferraro. "Synthesis of 2,2,4,4-tetranitroadamantane" *Journal of Organic Chemistry* (1990) **55**, 4459-4461.
163. E. H. Cordes, W. P. Jencks. "On the mechanism of schiff base formation and hydrolysis" *Journal of the American Chemical Society* (1962) **84**, 832 - 837.
164. D. R. Lide, ed. *CRC Handbook of Chemistry and Physics*. 86th Edition. CRC Press (2005).
165. H. B. Bürgi, J. D. Dunitz, E. Shefter. "Geometrical reaction coordinates. II. Nucleophilic addition to a carbonyl group" *Journal of the American Chemical Society* (1973) **95**, 5056-5067.
166. C. L. Liotta, E. M. Burgess, W. H. Eberhardt. "Trajectory analysis. Theoretical model for nucleophilic attack at π -systems. The stabilizing and destabilizing orbital terms." *Journal of the American Chemical Society* (1984) **106**, 4849 - 4852.
167. E. F. Pratt, M. J. Kamlet. "Reaction rates by distillation IX. The condensation of anilines with benzaldehydes" *Journal of Organic Chemistry* (1961) **26**, 4029 - 4031.
168. R. Spector. "Transport of amantadine and rimantadine through the blood-brain barrier." *Journal of Pharmacology and Experimental Therapeutics Online* (1988) **244**, 516 - 519.
169. J. B. Miller. "Amines and thiols on diamond surfaces" *Surface Science* (1999) **439**, 21-33.
170. T. Tsubota, K. Urabe, S. Egawa, H. Tagaki, K. Kusakabe, S. Morooka, H. Maeda. "Surface modification of hydrogenated diamond powder by radical reactions in chloroform solutions" *Diamond and Related Materials* (2000) **9**, 219-223.
171. Y. Ikeda, T. Saito, K. Kusakabe, S. Morooka, H. Maeda, Y. Taniguchi, Y. Fujiwara. "Halogenation and butylation of diamond surfaces by reactions in organic solvents" *Diamond and Related Materials* (1998) **7**, 830 - 834.

172. V. S. Smentkowski, J. T. Yates Jr, X. Chen, W. A. Goddard III. "Fluorination of diamond - C₄F₉I and CF₃I photochemistry on diamond (100)" *Surface Science* (1997) **370**, 209 - 231.
173. Y. Liu, V. N. Khabashesku, N. J. Halas. "Fluorinated nanodiamond as a wet chemistry precursor for diamond coatings covalently bonded to glass surface" *Journal of the American Chemical Society - Communications* (2005) **127**, 3712 - 3713.
174. K. Takahashi, M. Tanga, O. Takai, H. Okmura. "DNA preservation using diamond chips" *Diamond and Related Materials* (2003) **12**, 572 - 576.
175. S. Ida, T. Tsubota, O. Hirabayashi, M. Nagata, Y. Matsumoto, A. Fujishima. "Chemical reaction of hydrogenated diamond surface with peroxide radical initiators" *Diamond and Related Materials* (2003) **12**, 601 - 605.
176. T. Tsubota, O. Hirabayashi, S. Ida, S. Nagaoka, M. Nagata, Y. Matsumoto. "Chemical modification of hydrogenated diamond surface using benzoyl peroxides" *Physical Chemistry Chemical Physics* (2002) **4**, 806 - 811.
177. T. Tsubota, S. Ida, O. Hirabayashi, S. Nagaoka, M. Nagata, Y. Matsumoto. "Chemical modification of diamond surface using a diacyl peroxide as radical initiator and CN group-containing compounds for the introduction of the CN group" *Physical Chemistry Chemical Physics* (2002) **4**, 3881 - 3886.
178. T. Tsubota, S. Tanii, S. Ida, M. Nagata, Y. Matsumoto. "Chemical modification of diamond surface with CH₃(CH₂)_nCOOH using benzoyl peroxide" *Physical Chemistry Chemical Physics* (2003) **5**, 1474 - 1480.
179. S. Ida, T. Tsubota, S. Tanii, M. Nagata, Y. Matsumoto. "Chemical modification of the diamond surface using benzoyl peroxide and dicarboxylic acids" *Langmuir* (2003) **19**, 9693 - 9698.
180. T. Nakamura, M. Ishihara, T. Ohana, Y. Koga. "Chemical modification of diamond powder using photolysis of perfluoroazooctane" *Chemical Communications* (2003), 900 - 901.
181. D. Shin, N. Tokuda, B. Rezek, C. E. Nebel. "Periodically arranged benzene-linker molecules on boron-doped single-crystalline diamond films for DNA sensing" *Electrochemistry Communications* (2006) **8**, 844 - 850.
182. J. A. Carlisle. "Diamond films - precious biosensors" *Nature Materials* (2004) **3**, 668 - 669.
183. T. Tsubota, S. Ida, O. Hirabayashi, S. Nagaoka, S. Nagayama, M. Nagata, Y. Matsumoto. "Surface reforming of the oxidised diamond surface with silane coupling agents" *Journal of the Ceramic Society of Japan* (2002) **110**, 904 - 910.
184. K. Ushizawa, Y. Sato, T. Mitsumori, T. Machinami, T. Ueda, T. Ando. "Covalent immobilisation of DNA on diamond and its verification by diffuse reflectance infrared spectroscopy" *Chemical Physics Letters* (2002) **351**, 105 - 108.

185. P. Krysinski, Y. Show, J. Stotter, G. J. Blanchard. "Covalent adlayer growth on a diamond thin film surface" *Journal of the American Chemical Society - Communications* (2003) **125**, 12726 - 12728.
186. D. Delabouglise, B. Marcus, M. Mermoux, P. Bouvier, J. Chane-Tune, J. Petit, P. Mailley, T. Livache. "Biotin grafting on boron-doped diamond" *Chemical Communications* (2003), 2698 - 2699.
187. J.-K. Lee, M. W. Anderson, F. A. Gray, P. John, J.-Y. Lee. "Reactions of amines with CVD diamond nanopowders" *Diamond and Related Materials* (2005) **14**, 675 - 678.
188. "Materials safety data sheet - Benzylamine". <https://securesearch.acros.com/msds?for=acros&sup=acros&lang=UK&search=105850050>. Acros Organics. 2008
189. "Materials safety data sheet - D-alpha-methylbenzylamine". http://worldaccount.basf.com/wa/NAFTA~en_US/Catalog/ChemicalsNAFTA/doc4/BASF/PRD/30037125/.pdf?title=&asset_type=msds/pdf&language=EN&validArea=US&urn=urn:documentum:ProductBase_EU:09007af8800a73cf.pdf. BASF. 2006
190. P. Kirby. "The variation of boiling point with pressure". <http://www-jmg.ch.cam.ac.uk/tools/magnus/boil.html>. University of Cambridge. 2000